A Study of Protein–Protein Interactions Involving Type 4 Phosphodiesterase

Matthew Brian Beard

B.Sc. Hons. Biochemistry

A thesis submitted to the University of Glasgow for the degree of Doctor of Philosophy in the Faculty of Science

Department of Biochemistry and Molecular Biology

Institute of Biomedical and Life Sciences

University of Glasgow

September 1999

ProQuest LLC.
789 East Eisenhower Parkway
P.O. Box 1346
Ann Arbor, MI 48106 – 1346

This thesis is dedicated to my parents

Abstract

The cyclic adenosine monophosphate (cAMP) signalling pathway is centrally involved in the regulation of cell function by many extracellular messengers. Signalling through the cAMP pathway is involved in the acute regulation of numerous metabolic processes including glucose and lipid metabolism, neurotransmission and membrane trafficking. The cAMP pathway also functions to affect gene expression and can thereby mediate the long term control of processes such as cell growth and differentiation.

Every stage in the cAMP signalling pathway is mediated by a family of enzymes. This provides opportunities for cell type and developmental stage specific variations in the control of the cAMP signalling, dependant upon the particular isoforms of each of the components of the cAMP pathway that are expressed in a given cell. In addition, each stage in the cAMP pathway is able to interact with components of other intracellular signalling pathways and this allows for a cell to modulate its response to any one stimuli depending upon the other stimulatory inputs that it receives.

An important aspect of intracellular signalling is the spatial organisation of the components of the various pathways within the 3 dimensional cell interior. The paradigm for the spatial organisation of signalling proteins as a regulatory factor arose with the identification of protein domains that mediated the rapid clustering of tyrosine kinases around activated insulin receptors. It has since become apparent that the regulated targeting of a wide variety of signalling proteins to specific subcellular locations is an essential feature of much of the signalling that occurs within eukaryotic cells.

In chapter 3 of this thesis I have shown that the type 4 phosphodiesterase (PDE4) splice variant PDE4D4 can interact specifically with Src homology 3 (SH3) domains *in vitro*. HSPDE4D4 showed a selectivity for the SH3 domains that it could interact with and bound most strongly to the SH3 domains of the tyrosyl kinases Src, Lyn, Fyn and Abl and also the SH3 domain of the cytoskeletal protein fodrin. In contrast it did not bind to a number of other SH3 domains that were tested.

In chapter 4 of this thesis I have shown for the first time that it is possible to express both full length HSPDE4D4 and also the unique, alternatively spliced, amino terminal 166 amino acids of HSPDE4D4 in *E.coli* as fusion proteins with maltose binding protein (MBP) and to purify these species to near homogeneity by affinity chromatography. I used these purified fusion proteins to demonstrate a direct protein–protein interaction between the alternatively spliced, amino terminal region of HSPDE4D4 and the SH3 domain of Lyn kinase.

By engineering a recognition site for a high fidelity viral protease (TEV) into the MBP-HSPDE4D4 fusion protein, I was able to separate proteolytically the MBP and the HSPDE4D4 moieties and, for the first time, to perform a limited characterisation of highly purified, full length HSPDE4D4. This species migrated on SDS-PAGE with and apparent Mw of 121kDa and catalysed the hydrolysis of cAMP with a Km of 2.3μM and an apparent Vmax of 3490μmol/min/mg.

In chapter 5 of this thesis I have mapped sub-regions within the amino terminal of RNPDE4A5 that are involved in the interaction with SH3 domains, in the subcellular targeting and in the regulation of the catalytic activity of this isoform. My data suggest that the extreme amino terminal region, residues 1–10, of RNPDE4A5 are important in the interaction of this isoform with the SH3 domain of Lyn kinase. The region between residues 218–259 of RNPDE4A5 appears to be involved in both the subcellular targeting and the regulation of the catalytic activity of this enzyme.

In chapter 6 of this thesis I have shown that 2 highly conserved regions of sequence called Upstream Conserved Regions 1 and 2 (UCR1 and UCR2) that characterise the amino terminal regions of all long PDE4 isoforms can bind to one another. I have shown that this interaction is stabilised by electrostatic bonds between specific residues located in the carboxyl terminal portion of UCR1 and the amino terminal portion of UCR2. This interaction can be regulated by the phosphorylation of a serine residue that lies within the amino terminal region of UCR1 and forms a consensus recognition site for protein kinase A (PKA).

Acknowledgements

I am very much indebted to Prof. Miles Houslay for the excellent supervision, help and support that he has given to me during my time in his laboratory.

I acknowledge my colleagues in the Gardiner laboratory whose friendship I value and whose technical assistance I could not have done without.

I also acknowledge my family and my friends for their company and support.

Table of contents

List of tables

List of figures

Abbreviations

AC	adenylyl cyclase
AKAP	A kinase anchoring protein
ATP	adenosine trisphosphate
Ca /CaM	calcium/calmodulin
cAMP	cyclic 3'5' adenosine mono phosphate
CAT	chloramphenicol acetyltransferase
cGMP	cyclic guanosine mono phosphate
cDNA	complementary DNA
DEAE	diethyl aminoethyl
DEPC	diethyl pyrocarbonate
DMEM	Dulbecco's modification of Eagle's Medium
DMSO	dimethylsulphoxide
DNA	deoxyribonucleic acid
dNTP	deoxynucleotide trisphosphate
DTT	dithiothreitol
EC_{50}	effector concentration 50
ECL	enhanced chemiluminescence
EDTA	diaminoethanetetra-acetic acid
EGF	epidermal growth factor
EGTA	ethylene glycol-bis(β-aminoethyl ether)-N,N,N',N'-tetraacetic acid
ELISA	enzyme linked immunosorbent assay
EU	enzyme units
FCS	foetal calf serum
GPCR	G-protein coupled receptor
G-protein	guanine nucleotide binding regulatory protein
GRK	G-protein coupled receptor kinase
GST	glutathione S-transferase
GTP	guanosine triphosphate
HEPES	N-2-Hydroxyethylpiperazine-N'-2-ethanesulfonic acid
IC_{50}	inhibitor concentration 50

IBMX	isobutylmethylxanthine
IPTG	isopropyl-ß-D-thiogalactopyranoside
KHEM	potassium (K), HEPES, EGTA, Magnesium
Km	Michaelis-Menten constant (mathematically equivalent to the concentration of substrate at which the initial reaction rate is half of Vmax)
LB	Luria-Bertoni
LR	linker region
MAP kinase	mitogen activated protein kinase
MBP	maltose binding protein
mRNA	messenger RNA
ORF	open reading frame
PBS	phosphate buffered saline
PCR	polymerase chain reaction
PDE	phosphodiesterase
PI 3-kinase	Phosphatidyl inositol 3-kinase
PKA	protein kinase A
PKC	protein kinase C
PPII helix	polyproline type II helix
RNA	ribonucleic acid
ROM	reactive oxygen metabolite
RT	reverse transcription
SDS	sodium dodecyl sulphate
SH2 domain	Src homology 2 domain
SH3 domain	Src homology 3 domain
TAE	tris/acetate/EDTA
TBS	tris buffered saline
TE	tris/EDTA
TEA	triethanolamine
TEMED	N,N,N',N'-Tetramethyl-ethylenediamine
UCR	upstream conserved region
Vmax	The maximum initial rate of an enzyme catalysed reaction under defined conditions

1. Introduction

1.1 Cyclic nucleotide signalling pathways

The cyclic nucleotides 3',5' cyclic adenosine monophosphate (cAMP) and 3',5' cyclic guanosine monophosphate (cGMP) are ubiquitous second messengers in mammalian cells. They are both small, stable molecules that are well suited to their roles in intracellular signalling.

The precursors of each of these molecules, adenosine triphosphate (ATP) and guanosine triphosphate (GTP) for cAMP and cGMP respectively, are important molecules within cells where their hydrolysis provides free energy to drive anabolic reactions and, in the case of GTP, also serves as a timing mechanism for many processes. Due to the importance of their roles, the intracellular concentrations of these precursor molecules are kept constantly high by homeostatic mechanisms within cells. Due to the high levels of ATP and GTP, in normal cells, the cyclases that generate cAMP and cGMP can always operate at Vmax when activated. This means that a cells responsiveness to signalling through these pathways is not directly dependent on the availability of nucleotide triphosphate.

Unlike their precursor molecules, neither cAMP nor cGMP are themselves substrates in any major metabolic pathways. This allows for their concentrations to be independently controlled within cells.

1.1.1 The cAMP signalling pathway

Many hormones and growth factors act through the cAMP signalling pathway to regulate a diverse range of physiological processes in their target cells. These include both acute regulation of various metabolic processes such as glucose and lipid metabolism, neurotransmission, membrane trafficking and also the long term control of processes such as cell growth and differentiation (37, 44).

1.1.1.1 Overview of the cAMP signalling pathway

The cAMP signalling pathway can be thought of as beginning at the cell surface, with the binding of an extracellular signalling molecule to a specific, transmembrane receptor protein, expressed on the plasma membrane of a target cell. The signal is transmitted across the membrane as a conformational change in the receptor protein that allows a heterotrimeric guanine nucleotide binding regulatory protein (G-protein) to associate with the cytoplasmic domain of the receptor. This G-protein is in its guanosine diphosphate (GDP) bound (inactive) state but, upon its interaction with an activated receptor it exchanges its bound GDP for a molecule of GTP. This exchange results in the disassociation of the G-protein from the receptor and also of the GTP bound α subunit from the $\beta\gamma$ dimer of the G-protein. Both the GTP bound α subunit and the $\beta\gamma$ dimer of the G-protein are active signalling molecules and interact with downstream elements in the pathway. An important example of such a downstream element is adenylyl cyclase, a membrane-bound enzyme that catalyses the synthesis of the second messenger, cAMP. All known adenylyl cyclases are activated by GTP bound α subunits of Gs G-proteins (see section 1.1.1.2). The major action of cAMP in a cell is to bind to and activate protein kinase A (PKA) which, in turn, phosphorylates downstream proteins and thereby regulates their function. The degradation and inactivation of cAMP is catalysed by 3'5' cyclic nucleotide phosphodiesterase (PDE) activity which catalyses the hydrolysis of cAMP to AMP (*Figure 1.1*).

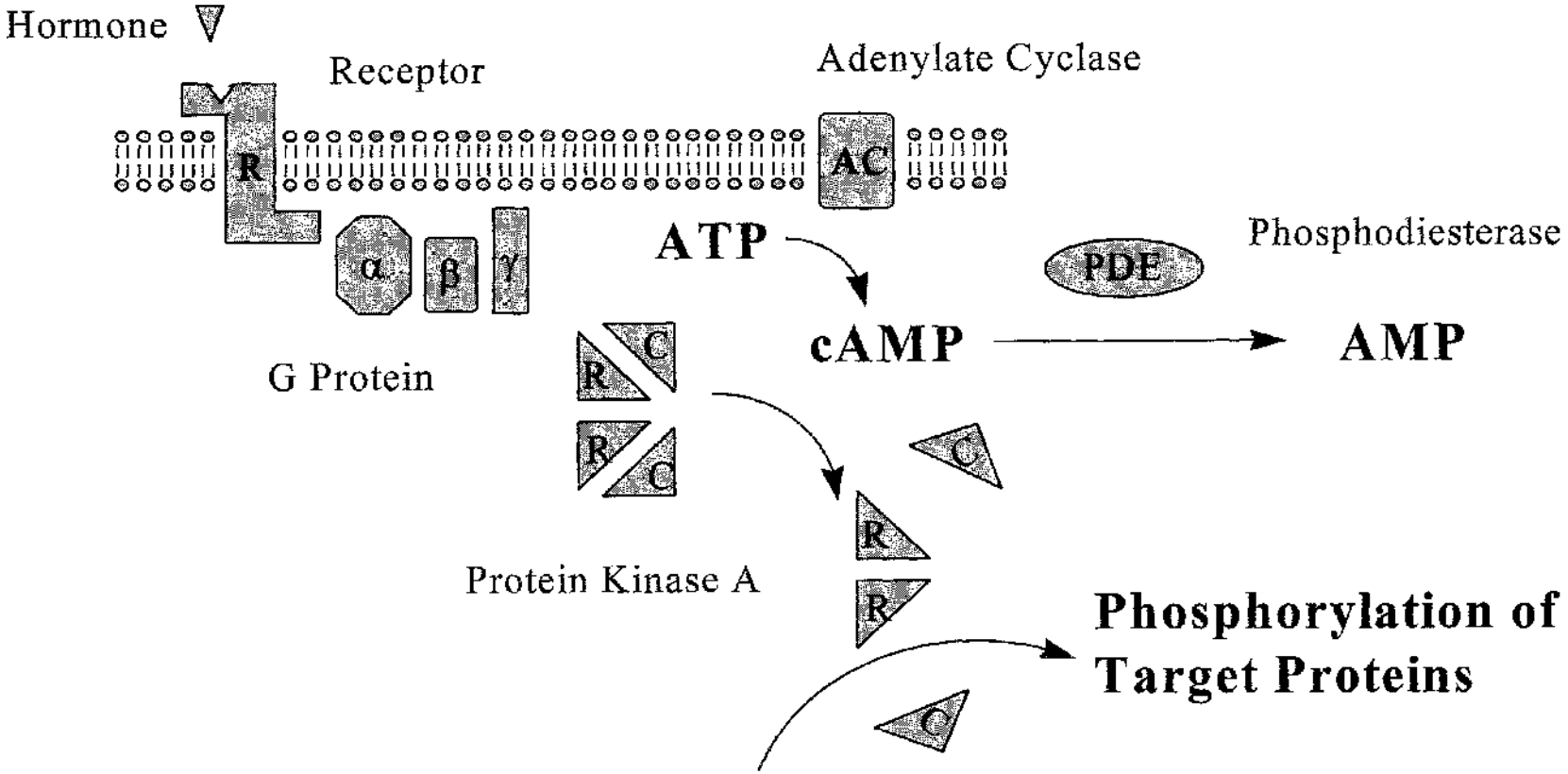
Hormone
Receptor
Adenylate Cyclase
R
AC
α
β
γ
G Protein
ATP
cAMP
PDE
Phosphodiesterase
AMP
R
C
R
C
C
R
R
C
Protein Kinase A
Phosphorylation of
Target Proteins

Figure 1.1: Classical model for the cAMP signalling pathway

The figure is a diagram to show the classical cAMP signalling pathway. The binding of an extracellular ligand activates a transmembrane receptor protein, expressed on the cell surface. The signal is transmitted across the membrane as a conformational change in the receptor protein that allows a G-protein in its GDP bound (inactive) state to associate with the cytoplasmic domain of the receptor. Upon its interaction with the activated receptor the G-protein exchanges its bound GDP for a molecule of GTP. This exchange results in the disassociation of the G-protein from the receptor and also of the GTP bound α subunit from the βγ dimer of the G-protein. The released, GTP bound α subunit of Gs G-proteins interacts with adenylyl cyclase, a membrane-bound enzyme that catalyses the synthesis of the second messenger, cAMP. The major action of cAMP in a cell is to bind to and activate PKA which, in turn, phosphorylates downstream proteins and thereby regulates their function. The degradation and inactivation of cAMP is catalysed by 3'5' cyclic nucleotide phosphodiesterase (PDE) activity which catalyses the hydrolysis of cAMP to AMP.
Abbreviations: ***R*** *G-protein coupled receptor, α G-protein alpha subunit, β G-protein beta subunit, γ G-protein gamma subunit,* ***AC*** *adenylate cyclase,* ***ATP*** *adenosine trisphosphate,* ***cAMP*** *cyclic adenosine monophosphate,* ***AMP*** *adenosine monophosphate,* ***PDE*** *phosphodiesterase,* ***R (in triangle)*** *protein kinase A regulatory subunit,* ***C*** *protein kinase A catalytic subunit*

1.1.1.2 Agonist stimulation of G-protein coupled, heptahelical receptors

A large family of G-protein coupled receptors (GPCRs) transmit signals from many different extracellular messengers across the plasma membrane to G-proteins (196, 243). This family of receptors all display a high degree of structural similarity and of membrane topology. The primary sequence of each member contains 7 putative membrane spanning domains of 22--28 hydrophobic residues, connected by a series of extracellular and cytoplasmic loops. The amino terminal region of these receptors is located on the extracellular side of the membrane, is of variable length and can be glycosolated. The carboxyl terminal region is intracellular and is often a substrate for phosphorylation and regulation by kinases such as PKA, protein kinase C (PKC) and G-protein coupled receptor kinases (GRKs) (67, 97).

Activation of this class of receptor causes a conformational change that is transmitted across the plasma membrane to the intracellular domain of the receptor. This allows the cytoplasmic region of the receptor to bind to a G-protein. The receptor bound G-protein then undergoes a conformational change that serves to allow the exchange of a molecule of GDP, bound to the α subunit of the G-protein, for GTP. The primary site on the GPCR that interacts with G-proteins has been mapped to the third cytoplasmic loop (163) although the carboxyl tail region of the GPCR is also of major importance in regulating the coupling of G-proteins to GPCRs. It has recently been suggested that GPCRs may adopt multiple, ligand specific, conformations that interact with G-proteins differently depending on which extracellular messenger activated the receptor (195).

Persistent stimulation of cells leads to receptor desensitisation. This occurs by numerous mechanisms that operate at the transcriptional, translational and protein levels (113). Classically these processes have been regarded as mechanisms to dampen a cells responsiveness to strong or persistent stimulations and thereby to increase the range over which changes in the intensity of stimulation can be detected. Recent evidence, however, suggests that the mechanisms which operate at the protein level may function as "pathway switching" as well as "pathway desensitising" mechanisms (113).

Both PKA, activated by Gs coupled receptors, and PKC, activated by Gq coupled receptors, can phosphorylate GPCRs (113). Phosphorylation by either one of these kinases can lead to a conformational change in the receptor that alters its ability to interact with G-proteins. Usually the effect of such phosphorylation is to inhibit the interaction between the receptor and the G-protein and thereby to dampen (desensitise) signalling through that receptor. In at least one case, however, this type of phosphorylation leads to a change in the class of coupled G-protein rather than to a simple desensitisation or the receptor (43).

When expressed in HEK 293 (human embryonic kidney) cells, β2-adrenergic receptors (β2-AR) can activate ERK1 and ERK2 by a G-protein (Gi) βγ subunit, Ras dependent pathway (43). This activation of MAP kinase signalling is, however, also dependent on the activation of PKA as H89, an inhibitor of PKA, can block the activation of MAP kinase signalling in this system. The reason that PKA activation is necessary for the activation of MAP kinase signalling in this system seems to be that PKA regulates the class of G-protein that the β2-AR receptor preferentially couples to. Phosphorylation of a PKA site within the third cytoplasmic loop of the receptor increases its interaction with the Gi class of G-proteins and decreases its interaction with the Gs class of G-proteins. For the β2-AR receptor to activate MAP kinase signalling downstream of the activated Gi G-protein βγ subunit dimer then, it must first activate, and be phosphorylated by, PKA. It therefore appears that, in this system, signalling from the β2-AR can be switched from a Gs G-protein coupled cAMP, PKA pathway to a Gi G-protein coupled MAP kinase pathway. This is achieved by the PKA dependent phosphorylation of the receptor (43).

Another major, protein level mechanism for the desensitisation of GPCRs is a 2-step process that begins with the phosphorylation of the receptor by a G-protein receptor specific kinase (GRK). This modification increases the affinity of the GPCR for a class of binding proteins called arrestins (113). The binding of an arrestin to the carboxyl terminal region of the GPCR sterically inhibits receptor interaction with G-proteins, thereby causing desensitisation. The bound arrestin also leads to receptor internalisation by clathrin coated vesicles (113). The internalisation of receptors by this mechanism is necessary both for their resensitisation, which is achieved by

receptor dephosphorylation and also for the activation of ERK1 and ERK2 by the GPCRs that couple to this pathway (130). The latter appears to involve the formation of a multi-protein signalling complex around the internalised receptor. The assembly of multi-protein signalling complexes around internalised GPCRs can be considered as being analogous to the complexes that form around activated tyrosine kinase receptors in the more classical tyrosine kinase signalling pathways.

It appears that, as with every other step in the cAMP signalling pathway, the activated receptor provides opportunities for crosstalk between a variety of signalling pathways. It is easy to imagine the exquisite control of cell function that could be achieved by the temporally co-ordinated activation and desensitisation of a number of different pathways that even this single stage of the complete cAMP signalling pathway alone can allow for.

1.1.1.3 heterotrimeric G-proteins

The heterotrimeric G-proteins are a subset of a larger family of GTP binding proteins. They are composed of an α subunit (40–50kDa) that can reversibly associate with a $\beta\gamma$ subunit dimer (35 and 8kDa for β and γ respectively). At least 20 different isoforms of the α subunit, 5 of the β subunit and 7 of the γ subunit are known to exist. This allows for a potential 700 or more distinct G-protein trimers. In fact, however, certain combinations of subunits seem to be preferred and only a fraction of the theoretically possible trimers have been shown to occur (155).

The α subunit of the heterotrimeric G-proteins contains the both the guanine nucleotide binding site and the site that defines the specificity of interaction between the individual G-protein and receptor proteins. Indeed G-protein holoenzymes are most often thought of as being defined by their α subunit. The interaction between a G-protein heterotrimer and an activated receptor catalyses the exchange of a bound molecule of GDP on the α subunit of the G-protein for GTP. This exchange promotes the disassociation of the α subunit from both the receptor and from the $\beta\gamma$ subunit dimer. Both of these released species are active in signalling. The released $\beta\gamma$ subunits of G-proteins can variously interact with certain isoforms of adenylyl

cyclase, with ras and with phospholipase C. The GTP-bound α subunits variously interact with adenylyl cyclases, with phospholipase C and with certain ion channels. Thus, for example, Gs α shows specificity for adenylyl cyclase activation and Gq α shows specificity for PLC activation (242).

In addition to their actions on downstream signalling molecules all G-protein α subunits have measurable GTPase activity in *vitro* and catalyse the gradual hydrolysis of the bound GTP to GDP (242). Free α subunits in the GDP-bound state are not themselves active as signalling molecules. They do, however, serve to sequester and inactivate free βγ dimers thus reforming the holoenzyme. The hydrolysis of GTP by the G-protein α subunit therefore serves as a "timing mechanism" for the activation of the G-protein. In the case of the Gi, and possibly other classes of, G-proteins the rate of GTP hydrolysis by the released α subunit is regulated by a class of binding proteins called regulators of G-protein signalling (RGS) (52).

1.1.1.4 Adenylyl cyclases

Adenylyl cyclases are a family of membrane bound enzymes that catalyse the conversion of ATP into cAMP. Nine different mammalian genes encoding adenylyl cyclases (classes I–IX) have so far been cloned and there is some evidence for alternative splicing within these forms (91, 242). The protein sequences of these forms all share homology with one another (approximately 50%) and suggest a conserved structure composed of 2 transmembrane regions (M1 and M2) that each comprise 6 membrane spanning helices connected by short loops. The M1 and M2 regions are separated from one another by a much larger cytoplasmic loop (C1). The carboxyl terminal tail of these proteins (C2) is also cytoplasmic and is well conserved between the forms (91).

The transmembrane regions of adenylyl cyclase are topologically similar to certain ion channels and ATP dependent transporters (85, 109). This has lead to the speculation that these regions of the protein may themselves have some transporter or ion channel activity . Indeed the adenylyl cyclase of *Paramecium* does function as a

voltage dependent K^+ channel when reconstituted into artificial bilayers (192), however no conclusive evidence to support any such activity of a mammalian adenylyl cyclase has yet been reported.

The large cytoplasmic regions of mammalian adenylyl cyclases show much higher sequence conservation than do the membrane spanning regions (approximately 90% homology at the amino acid level). These regions of the protein can be further subdivided into C1a, C1b, C2a and C2b. Of these subregions C1a and C2a are homologous to one another and contain the catalytic site of the enzyme (91). The C1b subregion is large, poorly conserved between different cyclases, and contains, isoform specific regulatory sites. The C2b region of adenylyl cyclases does not have an identified function and is extremely short in several of the isoforms.

As yet no 3 dimensional structure for an intact adenylyl cyclase has been reported. The active sites of these enzymes are, however, entirely contained within the intracellular domains C1a and C2a. Soluble, regulated, adenylyl cyclase activity can be reconstituted by expressing either a tethered C1a–C2a species or by expressing C1a and C2a individually and then mixing them. The C2a region alone also exhibits some forskolin stimulated cyclase activity although this is greatly reduced compared to that of either the C1a–C2a heterodimer or to the native enzyme (253).

Crystal structures for both the C2a homodimer and the C1a–C2a heterodimer have been reported (230, 253). These species each form similar, wreath like structures in which the catalytic residues line a central cleft. The residues that are involved in both substrate binding and in the catalysis are shared between the C1a and the C2a moieties of the heterodimer. This fact is important in understanding the regulation of adenylyl cyclases. Its significance is that any agent that affects the relative orientation of these 2 domains is a potential regulator of their activity (91). An important example of such a regulatory molecule is forskolin; which strongly activates all mammalian adenylyl cyclases except for type IX. Forskolin binds to a hydrophobic pocket at one end of the central cleft that contains the catalytic site of the enzyme and causes activation by moving the elements of the active site together (91). The forskolin binding site is very strongly conserved between adenylyl cyclase

types I–VIII and this has lead to speculation that a forskolin-like, physiological regulator of adenylyl cyclase activity may exist.

The characteristics and regulatory properties of the various mammalian adenylyl cyclases differ. All of the isoforms so far identified are activated by the α subunit of Gs G-proteins. In contrast to this there is a deal of variation in the regulation of these isoforms by Gi, Go, Gz α subunits, by G-protein $\beta\gamma$ dimers and by other regulators such as Ca^{2+} calmodulin and PKC (*Table 1.1.1*).

			Effect of regulators				
Adenylyl cyclase	**Splice variants**	**Chromosome location**	**Ca2+**	**G-protein βγ subunits**	**Gi G-protein α subunit**	**PKC**	**PKA**
AC-I		7p12-7p13	activates	inhibits	inhibits	activates	unknown
AC-II		5p15.3	no change	activates (+αGs)	no change	activates	unknown
AC-III*		2p22-2p24	activates (+αGs)	no change	unknown	activates	unknown
AC-IV		14q11.2	no change	activates (+αGs)	no change	no change /inhibits	unknown
AC-V	2	3q13.2-3q21	inhibits	no change	inhibits	no change /activates	inhibits
AC-VI	2	12q12-12q13	inhibits	no change	inhibits	no change /activates	inhibits
AC-VII		16q12-16q13	no change	activates	unknown	unknown (activates)	unknown
AC-IIX		8q24.2	activates	inhibits	inhibits	unknown	unknown
AC-IX			inhibits	no change	unknown	unknown	unknown

Table 1.1.1:Differential regulation of the multiple forms of adenylyl cyclase

*The table summarises the modes of regulation of the known forms of adenylyl cyclase. * AC-III is inhibited by phosphorylation by CAMK-II*
Table adapted from (85).

1.1.1.5 Inactivation of intracellular cAMP

The major mechanism for the inactivation of cAMP within cells is provided by members of the cyclic nucleotide phosphodiesterase (PDE) superfamily of enzymes. These enzymes catalyse the hydrolysis of the internal cyclic phosphodiester bond of a cyclic nucleotide to generate the cognate 5' nucleotide monophosphate. Within this enzyme superfamily members of the PDE1, PDE2, PDE3, PDE4, PDE7, PDE8 and PDE10 enzyme families have cAMP phosphodiesterase. Most of these families are composed of the products from more than a single gene and additional diversity arises from alternative splicing. The various cAMP PDEs are expressed in a cell and developmental stage specific fashion; also the total cAMP hydrolytic capacity of any one cell invariably represents the combined activities of a number of different PDEs. This allows for very fine control of the degradation of cAMP. The properties if the various PDEs are discussed in detail in sections 1.2 and 1.3.

In addition to inactivation by PDEs, intracellular cAMP and cGMP can be exported from certain cell types. This has been shown to be able to occur by facilitated diffusion across the plasma membrane of human erythrocytes and also by a hormonally regulated, energy dependent transport system that is known to operate in pigeon erythrocytes, rat C6 glioma cells, human fibroblasts (normal and transformed), human astrocytoma cells, MDCK (dog kidney epithelial) cells and rat reticulocytes (23, 77-79, 246). There is, however, little published research on this aspect of cyclic nucleotide regulation and the importance of cyclic nucleotide export in the regulation of intracellular signalling remains unclear.

1.1.1.6 Protein kinase A

The major intracellular sensor of cAMP in eukaryotic cells is PKA. The inactive, holoenzyme form of this protein kinase is a heterotetramer (R_2C_2) that is composed of 2 catalytic (C) subunits that are bound to a regulatory (R) subunit dimer. Multiple forms of both the C and the R subunits occur and these are differentially expressed in tissues.

Three isoforms of C subunit have been identified: α β and γ. These share homology with one another (93% homology between Cα and Cβ, 83% homology between Cα and Cγ, 79% between Cβ and Cγ at the amino acid level) and also with the catalytic subunits of all other eukaryotic protein kinases (240). The various forms of C subunit are differentially expressed between tissues. The Cα and Cβ forms each have a broad tissue distribution. Cα is ubiquitously expresses and is the most abundant of the C subunit isoforms. Cβ is generally expressed at lower levels than Cα but is enriched in neuronal tissue (191). The Cγ form has a much more restricted distribution and is only readily detected in primate testis (9). The substrate specificities of the Cα and Cβ isoforms, as defined by in *vitro* phosphorylation assays, are identical to each another and are very similar to that of Cγ. The relevance of the multiplicity and the differential expression of these C subunit isoforms to the regulation of signal transduction is therefore unclear.

Four isoforms of R subunit have been identified, these are further subdivided into 2 classes (RI and RII): RIα, RIβ, RIIα and RIIβ. The classification of PKA holoenzymes (into types I and II) is defined by the class of R subunit dimer to which the C subunits are bound. All of the R subunits share homology with one other. They occur in normal tissues as stable homodimers that form via a dimerisation domain located within the amino terminal of these subunits (184). In addition to the dimerisation domain each R subunit contains 2 cAMP binding sites that are located within the carboxyl terminal third of the polypepeptide and a pseudosubstrate, regulatory region that binds to and inhibits the active site of a C subunit in the holoenzyme. The binding of a molecule of cAMP to each of the 4 cAMP binding sites on the R subunit dimer of the PKA holoenzyme causes a conformational change in the protein that results in the dissociation and activation of the 2 bound C subunits.

The various isoforms of R subunit show tissue specific patterns of expression and have distinct subcellular localisations. The RI class of R subunits are predominantly located in the cytosolic compartment of cells. RIα is expressed in almost all tissues whereas RIβ is predominantly expressed in brain, testis and placenta. The RII class of R subunits are predominantly located to the particulate fractions of cells. The targeting of these isoforms is mediated by their specific binding to members of

the A kinase anchoring protein (AKAP) class of binding proteins (see section 1.4.2.1). RIIα has a broad tissue distribution whilst RIIβ is detected predominantly in brain, testis and placenta (129).

In addition to the cAMP regulated pool of PKA holoenzyme another, cAMP independent, pool of PKA C subunit has been identified in rabbit lung cytosol (256). This pool of C subunit is maintained in an inactive state by binding to IκB-α or IκB-β in a multiprotein complex comprising the transcription factor NFκB, its regulatory protein IκB and the PKA C subunit. The activation and, translocation to the nucleus, of NFκB is regulated by signalling pathways that lead to the phosphorylation, ubiquitination and degradation of IκB. This results in the release of both NFκB and of active PKA C subunit. The released PKA C subunit then phosphorylates and activates the transcriptional activation activity of NFκB.

1.1.1.7 PKA independent signalling through cAMP

Although most of the effects of cAMP on cell function are downstream of activated PKA, several examples of signalling through cAMP that are independent of PKA mediated phosphorylation have been reported.

The RIIβ subunit dimer of PKA, in its cAMP bound state, can bind directly to the cAMP responsive element (CRE) in the promoter region of cAMP responsive genes and can activate transcription independently of the classical CREB/ATF class of CRE binding transcription factors (219).

Cyclic AMP can bind to and directly regulate members of the cyclic nucleotide gated class of ion channels; examples of this form of signalling by cAMP include olfactory adaptation (110) and the modulation of cardiac pacemaker activity (51). Cyclic AMP can also bind to and directly regulate the activity of GLUT4 glucose transporters in transfected Chinese hamster ovary (CHO) cells (170). Another protein that is directly regulated by cAMP in this manner is the guanine nucleotide exchange factor Epac (exchange protein directly activated by cAMP) (181). Guanine nucleotide exchange factors are a family of enzymes that catalyse the exchange of GDP for GTP on G-

proteins. In the cAMP bound state Epac can activate the small, Ras like GTPase Rap1 by catalysing the exchange of bound GDP for GTP on Rap1. In its GTP bound (active) state Rap-1 can interact with downstream molecules such as B-raf and so feed into the mitogen activated kinase (MAP/ERK) signalling pathway (20).

1.2 The 3'5' cyclic nucleotide phosphodiesterase (PDE) superfamily

The 3'5' cyclic nucleotide phosphodiesterases (PDEs) compose a large and complex enzyme superfamily. On the basis of sequence homology this superfamily can be broadly divided into 2 distinct classes. Class I PDEs all contain a conserved region of approximately 250 residues, normally located towards the carboxyl terminal end of the molecule. This region contains the catalytic site of the enzyme and is the only region of sequence that is common to all class I PDEs. All known mammalian PDEs are members of class I. Class II PDEs do not contain any single identifiable conserved unit such as the 250 residue region that is present in the class I enzymes. Rather they share homology with one another throughout the entire length of the molecule. Members of this class of PDE include the yeast PDE I gene product and the *Dictyostelium discoideum* phosphodiesterase.

At present mammalian PDEs are classified into 10 enzyme families each of which comprises the products from up to 4 related but distinct genes. Many of these genes have of multiple start sites for transcription that are controlled by distinct (possibly tissue specific) promoters and therefore encode multiple, alternatively spliced, mRNAs (83, 238). This generates a further level complexity in the classification of this enzyme family (*Table 1.1.2*).

A standardised nomenclature for describing mammalian PDEs has been devised (8). The name of each isoenzyme is constructed from: (a) 2 letters indicating the source species (HS - *Homo sapiens* or RN - *Rattus norvegicus* for example); (b) PDE for cyclic nucleotide phosphodiesterase; (c) an arabic numeral for the gene family; (d) a single letter for the gene; (e) an arabic number for the splice variant; (f) a single letter for the report.

The classification of mammalian PDEs is, nowadays, based primarily on sequence homology. Before the widespread availability of sequence information for PDE isoenzymes, however, PDE activities were classified according to their biochemical and pharmacological characteristics. These were each assigned a descriptive name and a roman numeral that alluded to their order of elution from ion exchange chromatography columns (87). These various classes of PDE activities roughly correspond to individual gene families, as defined by their sequence homology. Many authors continue to use both the formal and the descriptive nomenclature when referring to a PDE family (the cAMP specific, rolipram sensitive PDE4 gene family or the Ca2+ calmodulin dependent PDE1 gene family, for example).

Family	Descriptive Name	Substrate	Selective Inhibitor	Number of Genes	Splice Variants
PDE1	Ca^{2+} Calmodulin Dependent	cAMP cGMP	Vinopocetine	3	9+
PDE2	cGMP Stimulated	cAMP cGMP	MEP1 (EHNA)	1	3
PDE3	cGMP Inhibited	cAMP (cGMP)	Cilostimide, Milirione	2	3
PDE4	Rolipram sensitive, cAMP Specific	cAMP	Rolipram, Ro 20-1724	4	19(+)
PDE5	cGMP Specific	cGMP	Zaprinast, Sildenafil, Dipyridamole	2	2
PDE6	Photoreceptor	cGMP	Dipyridamole, M&B 22 984	3	3
PDE7	Rolipram Insensitive, cAMP Specific	cAMP		1	2
PDE8	IBMX Insensitive, cAMP Specific	cAMP	Dipyridamole	2(+)	3(+)
PDE9	IBMX Insensitive, cGMP Specific	cGMP	Zaprinast	1	2
PDE10	Putatively cAMP Inhibited	(cAMP) cGMP		1	1

Table 1.1.2: Mammailian PDE isoenzyme familys

The table summarises the current classification of class I PDEs into 10 isoenzyme families. This classification is based primarily on sequence homology however different enzyme families often display distinctive pharmacological and biochemical properties such as substrate preference and sensitivity to certain inhibitors and effectors. These differences are reflected in the descriptive names assigned to each of the isoenzyme families.

1.2.1 The PDE1 enzyme family

The PDE1 enzyme family is composed of the products from 3 homologous genes (A, B and C). There is evidence for alternative splicing of the mRNA from each of these genes. Three splice variants of PDE1A (128, 213, 214) and 5 splice variants of PDE1C (128, 248, 249) have been characterised. RNase protection assays suggest the presence of alternatively spliced PDE1B species (10).

The pattern of splicing of the forms PDE1C4 and PDE1C5 is especially interesting because this deviates from the 5' domain swaps usually seen for other PDE splice variants. The open reading frames (ORFs) of the PDE1C4 and PDE1C5 complementary DNA (cDNA) sequences are identical with the differences being confined to their 3' untranslated regions. These differences may be important in the post transcriptional regulation of these mRNAs (248).

The various PDE1 isoenzymes are differentially expressed in tissues. For instance PDE1A1, PDE1B1 and PDEs 1C1-5 all show distinct patterns of expression in brain whilst PDE1A2 is enriched in heart and lung (128, 248, 249).

1.2.1.1 Regulation of PDE1

PDE1 isoforms can catalyse the hydrolysis of both cAMP and cGMP at physiological concentrations. The PDE1A and PDE1B forms each exhibit a Km for cAMP that is approximately 10 fold higher than that for cGMP whereas the Km of PDE1C isoenzymes for cAMP and cGMP are approximately equivalent (7).

All PDE1 enzymes are stimulated by Ca^{2+}/calmodulin binding to one or more regulatory calmodulin binding domains located within the amino terminal of the protein. The PDE1 family of enzymes therefore represents an obvious point of crosstalk between the cyclic nucleotide and the Ca^{2+} signalling pathways. The catalytic activity of PDE1 is stimulated at least 10 fold by the binding of calmodulin and this is due, almost exclusively, to an increase in Vmax with little change in Km (7). The mechanism of activation seems to be that calmodulin binding relieves

inhibition of the catalytic site of the enzyme by an inhibitory domain that is located near to the calmodulin binding domain in the amino terminal of PDE1 (214).

The splice variant PDE1A2 exhibits a higher affinity for Ca^{2+}/calmodulin than do the other PDE1 isoenzymes. This is because this splice variant contains a second calmodulin binding domain within an alternatively spliced region at its amino terminal (214).

PDE1 enzymes are subject to regulation by phosphorylation. PDE1A1, PDE1A2 and PDE1B are all substrates for phosphorylation by PKA (202). PDE1B can also be phosphorylated by CaM kinase II (75). Phosphorylation of these isoforms appears to reduce their affinity for Ca^{2+}/calmodulun and therefore reduces their activity. The phosphorylation of PDE1 by PKA therefore has the potential to form a positive feedback loop in which cAMP activates PKA which then phosphorylates PDE1 reducing its activity and leading to an increase in the level of cAMP. An increase in the level of intracellular Ca^{2+} could terminate this feedback loop by increasing the concentration of Ca^{2+}/calmodulin. It has been suggested that such a positive feedback loop may operate in post synaptic terminals to amplify signals that cause a small increase in intracellular cAMP (7). Nevertheless, the state of phosphorylation and regulation in intact cells remains to be established

The dephosphorylation of PDE1 isoforms is mediated by the Ca^{2+}/calmodulin dependent phosphatase (calcineurin) (7, 202).

Evidence for the transcriptional regulation of PDE1 comes from studies that investigated the induction of this class of PDE in CHO cells. No PDE1 activity is detectable in unstimulated CHO cells, however, stimulation with the phorbol ester phorbol 12-myristate 13-acetate (PMA); stimulation with agonists for endogenous P2-purinoceptors, for lysophosphatidic acid receptors or for thrombin receptors leads to the transient induction of a PDE1 that has been identified by reverse transcriptase polymerase chain reaction (RT-PCR) analysis as PDE1B. This induction then seems to depend upon PKC activation. Consistent with this the transient transfection of CHO cells to overexpress specific isoforms of protein kinase C (PKC), PKCα or

PKCε but not PKCβ1 nor PKCγ leads to the transient induction of PDE1B (217, 218).

1.2.2 The PDE2 enzyme family

Members of the PDE2 enzyme family catalyse the hydrolysis of both cAMP and cGMP. The catalytic activity of these enzymes is stimulated by low (sub μM) concentrations of cGMP. This is an allosteric regulation, mediated by a cGMP binding site that is located within the amino terminal region of the protein. The stimulation is due to an increase in Vmax with little change in Km. That the allosteric, cGMP binding site is distinct from the catalytic site of the enzyme can be demonstrated by its separation from the catalytic site by limited proteolysis of the enzyme (220). The catalytic region of PDE2 can also bind cGMP, although with lower affinity than can the allosteric binding site.

In addition to their regulation by cGMP there is evidence that PDE2 may be regulated by phosphorylation. A PDE2 associated with the Golgi-endosomal fraction of rat liver is rapidly and transiently activated downstream of PKCα following stimulation with PMA (66).

Only 1 gene encoding PDE2 has so far been identified (212). Alternative splicing of mRNA from this gene gives rise to at least 3 splice variants (PDE2A1, PDE2A2 and PDE2A3) that diverge in their amino terminal regions (182). Both soluble and membrane-associated forms of PDE2 activity have been identified and it is likely that the individual splice variants have different subcellular localisations.

Members of the PDE2 enzyme family have been implicated in the control of the basal Ca^{2+} current in human although not rat cardiomyocytes (177); in signalling within a subset of olfactory neurones (101); in the regulation of human platelet aggregation, by antagonising the accumulation of cAMP and hence the inhibition of aggregation that follows inhibition of PDE3 by intracellular cGMP, (50).

1.2.3 The PDE3 enzyme family

Members of the PDE3 enzyme family can catalyse the hydrolysis of both cAMP and cGMP. These enzymes have high affinity for both of these cyclic nucleotides; Km values for the hydrolysis of both cAMP and cGMP are in the range 0.1–0.8μM. The value of Vmax for the hydrolysis of cAMP by PDE3 is, however, approximately 10 fold higher than that for the hydrolysis of cGMP. For this reason, the PDE3 family of enzymes are considered to function as cAMP specific PDEs (48, 134).

1.2.3.1 Regulation of PDE3 by cGMP

Although cGMP is not considered to be a physiological substrate for PDE3, the high affinity with which it binds to these enzymes means that it acts as a competitive inhibitor of cAMP hydrolysis by PDE3. For this reason the PDE3 enzyme family is also referred to as the cGMP inhibited PDE family. Several of the physiological effects of cGMP arise at, least in part, from its ability to inhibit PDE3 and thereby to increase intracellular levels of cAMP. Examples of this include the stimulation of renin secretion downstream of nitric oxide (NO) in kidney (111) and the synergistic effects on the inhibition of platelet aggregation by agents that increase cAMP and those that increase cGMP (50). The latter example is especially interesting because PDE2, as well as PDE3, is present in platelets. In this system the actions of these 2 classes of PDE in response to cGMP appear to antagonise one another with PDE2 limiting the accumulation of cAMP that follows the inhibition of PDE3.

1.2.3.2 Structure of PDE3

Two separate genes encoding PDE3 have been identified and, localised, in humans, to chromosomes 12 and 11 for PDE3A and PDE3B respectively (143). There is evidence for alternative splicing of the PDE3A gene. This appears to generate 2 forms of the protein, the shorter of which is a truncated version of the longer (103).

The organisation of the primary structures of PDE3 follows a pattern typical for members of the PDE superfamily. The catalytic region, that is conserved between all mammalian PDE classes, is located towards the carboxyl terminal end of the

molecule and the amino terminal region of the molecules is involved in the subcellular targeting and the regulation of the protein.

Uniquely amongst PDEs the catalytic region of PDE3 contains a 44 amino acid insert region that is not present in other classes of PDE. Furthermore, although this insert is present in both PDE3A and PDE3B proteins, the sequence of this region is poorly conserved between the 2 genes. Although deletion of the 44 amino acid insert in PDE3 increases the homology of the catalytic region to those of other PDE classes, mutants of PDE3A in which this insert was deleted were found to be catalytically inactive (33, 229). The mutation of putative β turn forming residues that at the beginning and the end of this 44 amino acid insert also reduced the catalytic activity of the enzyme (229). These results suggest that the PDE3 specific insert region is important in maintaining the structure of the catalytic site of PDE3 enzymes.

The amino terminal regions of both PDE3A and PDE3B contain a hydrophobic region of sequence that, based upon hydrophobicity plots and secondary structure predictions, may contain several transmembrane, helical regions (48). It has been suggested that this region of the protein may constitute a membrane association domain that is involved in the membrane association of PDE3 (103, 115). Recent work in the laboratory of M. Houslay, using mutated forms of PDE3B in which this putative membrane association domain was deleted suggest, however, that this region is not necessary for the association of PDE3 with the particulate fraction of transfected COS-7 cells. Rather, it seems, sequence within the region that links this hydrophobic region to the catalytic domain of PDE3 (residues 267–613 in PDE3B) is involved in the membrane association of this enzyme [G. Rena personal communication].

1.2.3.3 The acute regulation of PDE3 by phosphorylation

PDE3 can be acutely activated by hormones in a number of systems (174). These activations seem to be due to phosphorylation of the PDE on serine. The in *vivo* site of phosphorylation has been mapped to Ser_{302} (in PDE3B). This residue is located within a PKA consensus motif in the amino terminal of PDE3. Interestingly, although this serine appears to be the in *vivo* site of phosphorylation both by PKA

and by an unidentified insulin stimulated kinase (see below) it is not the site that is most efficiently phosphorylated by PKA in *vitro* (175). In these assays Ser_{427} of solubilised, rat adipocyte PDE3B was most efficiently phosphorylated by PKA. This residue does not, however, become modified in intact cells (174). This discrepancy may reflect a conformational change in the PDE upon its association with membranes of perhaps differences between the interaction of PDE3 with additional regulatory factors in intact and in broken cells.

The stimulation of intact adipocytes, hepatocytes or platelets with agents that activate adenylyl cyclase and increase intracellular cAMP leads to the rapid phosphorylation and activation of PDE3 (134). This activation appears to be due to the direct phosphorylation of PDE3 by PKA and probably functions as a negative feedback loop that limits the accumulation of cAMP.

In addition to PKA this serine in PDE3 is also a substrate for an insulin stimulated kinase that lies downstream of phosphatidylinositol 3 kinase (PI3K) in adipocytes, platelets and liver (127, 203, 204). The pathway appears to be a major mechanism by which insulin reduces the intracellular cAMP concentration in these cells to antagonise the effects of agents that promote lipolysis and glycogenolysis. A similar pathway, downstream of activated insulin like growth factor 1 (IGF1) receptors, also operates in pancreatic islet β cells to attenuate insulin secretion (255). This forms an elegant negative feedback loop in which insulin secreted by β cells stimulates the release of IGF1 by the liver that then activates IGF1 receptors on the β cells and inhibits insulin secretion.

It seems likely that PDE3 is also acutely regulated by phosphorylation on residues other than Ser_{302}. It has been proposed that at least 2, interacting sites of phosphorylation exist in the rat liver dense vesicle associated PDE3. Phosphorylation at one of these sites results in an activation of the enzyme whereas phosphorylation at the other site does not activate the enzyme but can prevent modification of the activating site (105). Also, a membrane associated PDE3 present in frog ventricle cells is inactivated, downstream of activated glucagon receptors via a pertussis toxin sensitive G-protein (21).

1.2.4 The PDE4 enzyme family

The PDE4 enzyme family was initially identified as a PDE activity, resolved by ion exchange chromatography that specifically hydrolysed cAMP but not cGMP (87). This family of enzymes are potently and specifically inhibited by the antidepressant drug, rolipram. Indeed endogenous PDE4 activity is frequently defined as "that cAMP PDE activity which is inhibited by 10μM rolipram".

The PDE4 gene family is composed of the products from 4 homologous genes (A, B, C and D) that are located on 3 chromosomes (4A and 4C on chromosome 19, 4B on chromosome 1 and 4D on chromosome 5 in humans) (83, 86). Distinct transcriptional start sites coupled with the alternative splicing of mRNAs leads to the production of multiple splice variants from each of these genes. The splicing of all known, active PDE4s follows the typical pattern for PDE splicing and takes the form of 5' domain swaps. This results in splice variants from each PDE4 gene that all share an identical primary structure within the catalytic region and the carboxyl terminal end of the proteins but that diverge in their amino termini. There is considerable evidence that the various PDE4 isoenzymes are differentially expressed (15-17, 83, 87, 140, 225).

An exception to the usual pattern of splicing is the human PDE4A splice variant HSPDE4A8A (2EL). This species is alternatively spliced at 2 points to produce an mRNA that has a unique 5' end and that also contains a 34bp insert within the region that would otherwise encode the catalytic region of the protein. The 34bp insert causes a shift in the reading frame of the sequence, relative to those of other PDE4As. This results in the occurrence of an in frame stop codon just downstream of the insert and leads to the production of a truncated, catalytically inactive protein (83).

1.2.4.1 The dunce PDE of Drosophila melanogaster

The mammalian PDE4s are highly homologous to the dunce PDE of *Drosophila melanogaster*. This gene was the first PDE to be cloned from any species and was

used as a probe to isolate the first mammalian PDE4 cDNA in a screen of a rat brain cDNA library (47).

Insights into the functions of mammalian PDE4s have been gained from studies of the *Drosophila dunce* PDE. Flies that are deficient in the *dunce* PDE exhibit deficiencies in learning and memory and are also sterile, suggesting a role for the *dunce* PDE in these functions (46). These deficiencies in *dunce*- flies can be rescued by the expression of a mammalian PDE4 (45). This is consistent with the notion that cAMP signalling and, specifically, the actions of the *dunce* PDE are involved in regulating processes such as long term potentiation and synaptic plasticity. Furthermore it seems likely that at least some of these functions will be conserved in mammalian PDE4s.

Despite the high degree of homology between the *dunce* PDE and mammalian PDE4s, the PDE4 specific inhibitors rolipram and RO-20-1724 do not inhibit the dunce PDE. Another PDE4 specific inhibitor, denbufylline, does inhibit the dunce PDE, although with a lower potency than with which it inhibits mammalian PDE4s (IC_{50} values of 1–3μM and of 0.1–0.22μM for the inhibition of *Drosophila* and of mammalian PDE4 respectively) (13). The structural differences in the catalytic regions of these enzymes that account for these differences in inhibitor specificity are unclear. It is perhaps significant, however, that the conformation of the active site of PDE4 can be post translationally modulated by PKA action and that this modulation can be detected as a change in sensitivity to inhibition by rolipram (82). Certain other specific inhibitors of PDE4, such as RS-25344 and RS-33793, also interact differently with the different forms of the enzyme (2). Other specific PDE4 inhibitors, such as SB207499 and trequinsin, seemingly do not differentiate between these different forms of the enzyme (see section 1.3.6) (2, 141).

1.2.5 The PDE5 enzyme family

To date only 1 PDE5 gene has been identified. This, however, appears to encodes 2 splice variants (42, 138, 251). The PDE5 enzyme family has recently been the focus of much attention because it is the molecular target of sildenafil, the active ingredient of the anti erectile dysfunction drug, Viagra™ (see section 1.2.5.1).

PDE5 exists as a homodimer. It is highly specific for cGMP, the hydrolysis of which it catalyses approximately 100 times more efficiently than it does that of cAMP. Each subunit of the PDE5 holoenzyme contains 2 allosteric cGMP binding sites that are located within the amino terminal region of the protein. These are distinct from the catalytic region of the protein and they share homology with the allosteric cGMP binding sites in PDE2, PDE6 and PDE10 (231).

The binding of cGMP to the allosteric sites of PDE5 is a necessary prerequisite for the phosphorylation of the protein by PKG on Ser^{92}. This phosphorylation stimulates the catalytic activity of PDE5 and may represent a negative feedback loop that regulates cGMP levels (24, 25). The same site in PDE5 is also a substrate for phosphorylation by PKA in *vitro* (42). It is, however, unclear whether or not PDE5 is an in *vivo* substrate of PKA as, for Ser^{92} to be available to be modified, cGMP must be bound to the allosteric sites on PDE5. Under these conditions one would expect PKG to be active.

It is also unclear whether or not the binding of cGMP to the allosteric sites in PDE5 has a direct effect on the conformation of the catalytic site of the enzyme. The binding of cGMP analogues that are specific for the catalytic site to PDE5 stimulates the binding of cGMP to the allosteric sites (42). This shows that the conformation of the PDE5 active site can affect the conformation of the allosteric cGMP binding sites. It therefore seems likely that ligand at the allosteric site may be able to influence the conformation of the catalytic site.

The catalytic region of PDE5 contains 2 putative Zn^{2+} binding sequences of the form $HX_3HX_n(E/D)$ and bound Zn^{2+} is necessary for the catalytic activity of PDE5. These putative Zn^{2+} binding motifs are conserved in all known mammalian PDEs and are homologous to the single Zn^{2+} binding motif of metalloproteases.

1.2.5.1 PDE5 as the target of sildenafil

The PDE5 enzyme family has recently received much attention because it is the molecular target of sildenafil, the active ingredient of Pfizer's anti erectile dysfunction drug, Viagra™. Sildenafil is potent and highly specific inhibitor of PDE5

(236). It has long been appreciated that elevation of intracellular cGMP causes relaxation of vascular smooth muscle. It was therefore envisaged that compounds, such as PDE5 inhibitors, that could increase levels of cGMP would be of potential therapeutic value in the treatment of conditions such as hypertension and angina. Indeed, the effects of sildenafil on penile erectility were first noticed during a clinical trial conducted to determine its efficacy as a treatment for angina (42). The reason that sildenafil acts more specifically on penile erectile smooth muscle compared to smooth muscle that controls general circulation is not well understood.

1.2.6 The PDE6 enzyme family

The PDE6 enzyme family are the photoreceptor PDEs. This is a cGMP specific family of PDEs that are expressed in photoreceptor rod and cone cells. The inactive, holoenzyme form of PDE6 is a heterotetramer composed of 2 catalytic and 2 regulatory subunits. In rod cells the 2 large, homologous catalytic subunits (α and β) and 1 inhibitory subunit (γ) are expressed (65, 70). Usually these subunits assemble into a $\alpha\beta\gamma_2$ heterotetramer although $\alpha_2\gamma_2$ and $\beta_2\gamma_2$ heterotetrameric forms have also recently been demonstrated. In cone cells the heterotetramer is composed of 2 identical catalytic subunits (α') complexed with 2 inhibitory subunits (γ). The cone cell α', catalytic subunit is the product of a homologous but distinct gene from the rod cell α and β catalytic subunits (118, 123).

PDE6 enzymes are predominantly peripherally membrane associated enzymes. This association is due to methylation or isoprenylation of a site within the carboxyl terminal region of the catalytic subunits (11, 117). A fraction of the PDE6 in both rod and in cone cells is, however, present in the soluble fraction. This fraction of the PDE6 is associated with a 17kDa polypepeptide that has been called the PDE6 δ subunit (117). This subunit does not effect the catalytic activity of the PDE but it prevents membrane association by directly interacting with the modified carboxyl terminal. The physiological significance of the partial solubilisation of PDE6 is unclear. It has, however, been suggested that this may function as some sort of a desensitisation mechanism by removing the PDE6 catalytic subunits from their site of action (64).

Each catalytic subunit of PDE6 contains 2 noncatalytic, allosteric cGMP binding sites that are located amino terminally to the catalytic region of the PDE (123). These sites are homologous to the noncatalytic cGMP binding sites of PDE2, PDE5 and PDE10. The binding of cGMP at these allosteric sites may affect the interaction of the catalytic subunits with the inhibitory γ subunits. Certainly the interaction of γ subunits with the catalytic subunits affects interaction between cGMP and its allosteric binding sites (71). It is therefore possible that the function of the allosteric cGMP binding sites on PDE6 is to regulate the activation of the PDE by transducin.

1.2.6.1 The role of PDE6 in photoreception

PDE6 functions as a major effector enzyme in the photodetection cascade in both rod and cone cells. The light receptor in these cells is rhodopsin, a member of the heptahelical, G protein coupled, transmembrane class of receptor proteins. Rhodopsin contains the chromophore 11-*cis*-Retinal as a prosthetic group. When it absorbs a photon of light the chromophore isomorises to all-*trans*-Retinal and this causes a conformational change in the protein. This conformational change allows rhodopsin to catalyse the exchange of GDP for GTP on a heterotrimeric G protein (transducin). The GTP bound transducin α subunit, in turn, binds to the inhibitory γ subunits of PDE6, causing their dissociation from the holoenzyme and the activation of the PDE6 catalytic subiunits. This activation of PDE6 causes a reduction in intracellular cGMP concentration and consequently the closure of cGMP gated Na^+ channels in the cell membrane. This results in a hyperpolarisation of the plasma membrane (221). It is interesting that photosensitive cells, unlike other excitable cell types, convert the initial stimulation into a hyperpolarisation rather than a depolarisation of the plasma membrane.

1.2.7 The PDE7 enzyme family

The existence of a PDE7 enzyme family was originally suggested by the detection of a novel, cAMP specific PDE activity present in preparations of hepatocytes and liver that was insensitive to any of the known PDE inhibitors including IBMX, a broad range PDE inhibitor (112). Since that time 2 IBMX insensitive, cAMP PDE enzyme

families (PDE7 and PDE8) have been identified. The activity resolved by Lavan *et al* was most similar to the PDE enzyme family that is now designated PDE8.

To date 1 gene that encodes 2 splice variants of PDE7 (PDE7A1 and PDE7A2) has been identified in humans and in mice. These enzymes have a high affinity for cAMP (Km 0.1-0.2μM), do not hydrolyse cGMP and are insensitive to known effectors of other PDE enzyme families. Notably PDE7 is insensitive to rolipram and to RO-20-1724, inhibitors of the cAMP specific PDE4 family. It also shows a relatively low sensitivity to IBMX (IC_{50} 30μM).

The first of the PDE7 splice variants to be cloned, HSPDE7A1, was isolated from a human glioblastoma cDNA library by its ability to rescue a PDE deficient strain of yeast from heat shock (142). Subsequently this cDNA was used to probe cDNA libraries to isolate the murine MMPDE7A2 enzyme from mouse then the human HSPDE7A2 enzyme from skeletal muscle (12, 72).

The 2 splice variants of HSPDE7A differ from each other only in their amino terminal regions. The kinetic characteristics of these 2 splice variants are very similar to one another but their subcellular localisations differ markedly. HSPDE7A1 partitions between the particulate and the soluble fractions of cells whereas HSPDE7A2 is exclusively located in the particulate fraction (72). The subcellular targeting of HSPDE7A2 is mediated by the hydrophobic character and modifications of its 20 residue, alternatively spliced amino terminus.

A functional role of HSPDE7A1 in regulating T cell activation has recently been identified (116). The full activation of CD4 and possibly of other classes of T cells requires stimulation of both the T cell receptor CD3 complex (TCR-CD3) and also the CD28 costimulatory receptor. One effect of this costimulation is that the steady state protein levels of HSPDE7A1 in these cells are increased. This increase in HSPDE7A1 is necessary for the activation as antisense oligonucleotides that specifically inhibit HSPDE7A1 expression also prevent T cell activation. The increase in HSPDE7A1 levels seems to allow proliferation by suppressing intracellular levels of cAMP. This prevents the activation of PKA activation that occurs downstream of TCR-CD3 receptor stimulation in the absence of CD28

receptor costimulation. Stimulation of the TCR-CD3 receptor in the absence of CD28 receptor stimulation promotes T cell anergy or apotosis (96). This seems to result from the antiproliferative effects of activated PKA.

1.2.8 The PDE8 enzyme family

The PDE8 enzyme family was identified in the modern way, by searching expressed sequence tag (EST) databases for sequences with homology to known PDE sequences. The identified EST clones were then sequenced in their entirety and assembled into single sequences. The open reading frames (ORFs) generated by this strategy were all open at their 5' ends so the technique of rapid amplification of cDNA ends (5' RACE) was used to extend the sequences. The existence of the deduced sequences was then confirmed by RT-PCR of the entire ORF from tissues (63, 76, 208).

At least 2, possibly 3, distinct genes encode PDE8 and there is evidence for alternative splicing within the 5' region of at least one of these genes (HSPDE8A) (63). The members of this PDE enzyme family are high affinity, cAMP specific PDEs with a sub μM Km for cAMP. The Vmax of PDE8 isoforms is approximately 10-fold lower than that of PDE4 isoforms. These characteristics of high affinity for substrate together with relatively low Vmax values suggest that PDE8 may function to maintain low background cAMP levels whilst PDE4 may serve to rapidly reverse transient increases in cAMP concentration that occur during signalling.

The PDE8 enzyme family is pharmacologically distinct from other PDE enzyme families. This family of enzymes is insensitive to most known effectors of other PDE families including rolipram, RO-20-1724, cGMP and IBMX (208). Surprisingly, however, PDE8 is sensitive to dipyridamole (IC_{50} 4.5μM), which was previously considered to be an inhibitor of cGMP but not cAMP specific PDEs.

1.2.9 The PDE9 enzyme family

The PDE9 enzyme family was identified by searching EST databases for sequences homologous to known PDE sequences. To date 1 gene encoding PDE9 has been

identified in both mouse and in humans. The presence of a 60 residue insert within the amino terminal region of the human PDE9 clone (HSPDE9A2) that is not conserved in the mouse sequence (MMPDE9A1) suggests that there may be at least 2 splice variants from this gene (62, 209).

The PDE9 enzyme family specifically hydrolyses cGMP with very high affinity (Km 70-170nM) this is the highest affinity for cGMP of any PDE identified to date. The Vmax of the reaction catalysed by PDE9 is also high, being approximately 2 fold higher than that for the hydrolysis of cAMP by PDE4. PDE9 does not catalyse the hydrolysis of cAMP at physiological concentrations (Km 230μM) and it is insensitive to many known inhibitors of other PDE families including rolipram, vinpocetine, sildenafil and IBMX. It is, however sensitive to the PDE5 inhibitor zaprinast (IC_{50} 35μM). Unlike the other known cGMP specific PDE families (PDE2, PDE5 and PDE6), the putative regulatory, amino terminal region of PDE9 does not contain allosteric cGMP binding sites (62, 209).

1.2.10 The PDE10 enzyme family

As in the identification of the PDE8 and the PDE9 enzyme families, the PDE10 enzyme family was identified by screening an EST database (210). To date only 1 cDNA encoding a murine PDE10 (MMPDE10A) has been cloned. This cDNA contains the a complete OFR and is predicted to encode a 779 residue protein. Northern blot analysis reveals that PDE10 RNA is most prevalent in testis and in brain (210).

When expressed in Sf9 cells, MMPDE10A has the characteristics of a dual specificity PDE that hydrolyses cAMP with a Km of 0.05μM and cGMP with a Km of 3μM. The cGMP:cAMP Vmax ratio of this enzyme is 4.7. It is therefore possible that PDE10 may function in *vivo* to regulate cGMP signalling. Indeed it is possible that PDE10 could be regulated by cAMP acting as a competitive inhibitor of cGMP hydrolysis in a manner analogous to the regulation of cAMP hydrolysis by PDE3 by cGMP (210). Unlike PDE8 and PDE9, PDE10 is sensitive to inhibition by the broad range PDE inhibitor IBMX (IC_{50} 2.6μM).

The amino terminal region of PDE10 contains 2 regions homologous to the allosteric cGMP binding sites present in PDE2, PDE5 and PDE6. These motifs in MMPDE10A are, however, imperfectly conserved and binding assays suggest that the affinity of the noncatalytic cGMP binding motifs in PDE10 is lower than that of these motifs in the other cGMP specific PDE enzyme families (210).

1.3 Molecular biology and biochemistry of the PDE4 enzyme family

The PDE4 enzyme family is composed of 4 distinct but related genes each of which encodes multiple splice variants. At least 18 distinct splice variants of PDE4 exist (14, 85, 87). Splicing of PDE4 mRNAs predominantly takes the form of 5' domain swaps and leads to the production of isoenzymes that have distinct amino termini but share identical primary structures within their carboxyl termini. The spliced amino termini of PDE4 isoenzymes appear to function as regulatory domains of the proteins. Effects on both the conformation and the activity of the catalytic region (82, 140, 197, 200) and on the subcellular targeting and protein–protein interactions of the PDE (162, 194, 252) have been demonstrated.

1.3.1 The primary structure of PDE4

Sequence alignments of the deduced primary structures for the active PDE4 isoenzymes reveal that these proteins share a common overall structure (*Figure 1.2*). The catalytic region of the enzyme, that is conserved between all class I PDEs, is located towards the carboxyl terminal end of the molecule. In addition to the catalytic region there are 2 other regions of sequence that are highly conserved between all of the mammalian PDE4 gene families and the *dunce* PDE of *Drosophila;* these regions are located amino terminal to the catalytic region and are called Upstream Conserved Regions 1 and 2 (UCR1 and UCR2) (see section 6.1) (14). The regions of sequence that lie between UCR1 and UCR2 and between UCR2 and the catalytic region appear to be hypervariable. They are not conserved between the 4 PDE4 genes and nor are they well conserved between homologous PDE4 genes in different species. These regions have been called Linker Regions 1 and 2 (LR1 and LR2) respectively (141).

The regions of sequence that lie carboxyl terminal to the catalytic regions of PDE4s are poorly conserved between the PDE4 gene families but they are invariant between the active splice variants within each gene family. This region of PDE4s contains sequences that have been suggested to be involved in dimerisation of PDE4 isoforms (108). It is possible that sequences contained within the extreme carboxyl terminal regions of PDE4s may confer, as yet unidentified, gene family specific properties on the enzymes.

The sequences at the extreme amino termini of PDE4 isoforms are extremely divergent between the 4 gene families and also between different isoenzymes within a single gene family. The amino terminal regions of individual PDE4 isoenzymes are involved in regulating the activity of the catalytic region (140, 201), in defining the subcellular localisation of the enzyme (194) and in mediating protein–protein interactions (162, 252).

There are 2 major points of alternative mRNA splicing within mammalian PDE4s. The position of the first (most 5') of the splice points in mammalian PDE4s corresponds to the 5' end of the third exon of the *dunce* gene of *Drosophila*, where it is also the site of extensive alternative splicing. The coding sequence at this splice junction corresponds to the consensus F(E/D)(A/V)(E/D)NG. The second major splice junction lies at the 5' end of the sequence that encodes UCR2. The consensus protein sequence at this point is EE(A/S/T)(G/C/Y)(L/Q)(Q/K)LA (14). There are 2 cases in which the splicing of PDE4s diverges from this pattern. The first of these is the PDE4A isoform PDE4A1, in which splicing occurs 3' to the second of the major splice junctions, at the beginning of the second of the 3 exons that encode UCR2 of PDE4A. The second example of isoenzymes that diverge from the usual pattern of splicing are PDE4D1 and PDE4D2. The splicing of these isoforms occurs 5' to the second of the major PDE4A splice junctions (14).

The positions of the splice junctions in relation to the conserved regions, UCR1 and UCR2, in PDE4 isoforms allows for the informal classification of these isoenzymes into so called long and short forms. Thus long form splice variants contain both UCR1 and UCR2 whereas short form splice variants that contain only UCR2. In the cases of the short form splice variants PDE4A1 and PDE4D2 not only do these

isoforms lack UCR1 but also the amino terminal portion of UCR2 (*Figure 1.2 and Figure 1.3*).

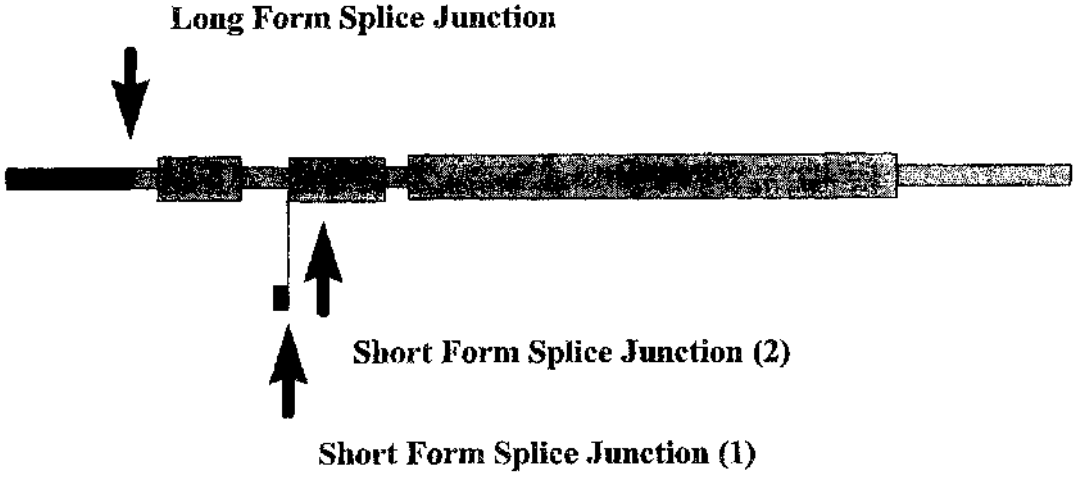

Figure 1.2: The domain structure of a typical mammalian PDE4

The figure shows a diagrammatic representation of the typical domain structure of PDE4 isoenzymes. Within each PDE4 enzyme family multiple splice variants arise through the alternative splicing of mRNA. Typically the alternative splicing takes the form of 5' domain swaps. This results in splice variants form each PDE4 gene that share a common catalytic region and extreme carboxyl terminus but that diverge in their amino termini. The positions of the major points of splicing in PDE4s are indicated by arrows. Also shown are regions of sequence that are highly conserved between each of the mammalian PDE4 enzyme families and the Dunce PDE of Drosophila. These are upstream conserved regions 1 and 2 (UCR1 and UCR2) and the catalytic region (catalytic).

```
  1                                                                  50
  ........er s...s..... .g.......p khlwrqprtp iriqqrgysd
A MEPPTVPSER SLSLSLPGPR EGQATLKPPP QHLWRQPRTP IRIQQRGYSD
B .....MKKSR SVMTVMADDN VKDYFECSLS KSYSSSSNTL GIDLWRGRRC
C .MENLGVGEG AEACSRLSRS RGRHSMTRAP KHLWRQPRRP IRIQQRFYSD
D .......... .......... .......... .......... ..........

  51                                                                 100
  ....a..... .......ar. .d.s...... ....swp.s. ..t...s...
A SAERAERERQ PHRPIERADA MDTSDRPGLR TTRMSWPSSF HGTGTGSGGA
B CSGNLQLPPL SQRQSERART PEGDG..... ...ISRPTTL PLTTLPSIAI
C PDKSAG.... .......CRE RDLSPRPELR KSRLSWPVS. ..........
D .......... .......... .......... .......... .MMHVNNFPF

                                                          UCR1
  101                                                                150
  ...S.r.Fdv eNG..pSpGR spLDpqaSpg .Gl.l.A.fp .hSQRRESFL
A GGGSSRRFEA ENGPTPSPGR SPLDSQASP. .GLVLHAG.A ATSQRRESFL
B TTVSQECFDV ENG..PSPGR SPLDPQASSS AGLVLHATFP GHSQRRESFL
C ...SCRRFDL ENGL..SCGR RALDPQSSPG LGRIMQAPVP .HSQRRESFL
D RRHSWICFDV DNG..TSAGR SPLDPMTSPG SGLILQANF. VHSQRRESFL

                                    UCR1
  151                                                                200
  YRSDSDYdlS PKaMSRNSSv aS..Hg.DlI VTPFAQVLAS LR.VR.Nfaa
A YRSDSDYDMS PKTMSRNSSV TSEAHAEDLI VTPFAQVLAS LRSVRSNFSL
B YRSDSDYDLS PKAMSRNSSL PSEQHGDDLI VTPFAQVLAS LRSVRNNFTI
C YRSDSDYELS PKAMSRNSSV ASDLHGEDMI VTPFAQVLAS LRTVRSNVAA
D YRSDSDYDLS PKSMSRNSSI ASDIHGDDLI VTPFAQVLAS LRTVRNNFAA

                         LR1                  UCR2
  201                                                                250
  Ltnlq...sn KrsP.gn.p. vnkatp.Eet yQkLA.ETLe ELDWCLdQLE
A LTNVPV.PSN KRSPLGGPTP VCKATLSEET CQQLARETLE ELDWCLEQLE
B LTNLHG.TSN KRSPAASQPP VSRVNPQEES YQKLAMETLE ELDWCLDQLE
C LARQQCLGAA KQGPVGNPSS SNQLPPAEDT GQKLALETLD ELDWCLDQLE
D LTNLQDRAPS KRSPMCNQPS INKATITEEA YQKLASETLE ELDWCLDQLE

                                    UCR2
  251                                                                300
  TlQT..SVsE MASnKFKRmL NRELTHLSEm SRSGNQVSEy ISnTFLDkQn
A TMQTYRSVSE MASHKFKRML NRELTHLSEM SRSGNQVSEY ISTTFLDKQN
B TIQTYRSVSE MASNKFKRML NRELTHLSEM SRSGNQVSEY ISNTFLDKQN
C TLQTRHSVGE MASNKFKRIL NRELTHLSET SRSGNQVSEY ISRTFLDQQT
D TLQTRHSVSE MASNKFKRML NRELTHLSEM SRSGNQVSEF ISNTFLDKQH

                               LR2                Catalytic
  301                                                                350
  eVEiPspTqk erekkk.p.. .......... ...qpMsqIs G.kkLmHSsS
A EVEIPSPTMK EREKQQAPRP RPSQPPPPPV PHLQPMSQIT GLKKLMHSNS
B DVEIPSPTQK DREKKKKQ.. .......... ...QLMTQIS GVKKLMHSSS
C EVELPKVTAE EAP....... .......... ...QPMSRIS GLHGLCHSAS
D EVEIPSPTQK EKEKKKRP.. .......... .....MSQIS GVKKLMHSSS
```

Catalytic

```
  351                                                        400
    LnnssipRFG VkT.qE..LA kELEdlNKWG Ln.F.vadys gnRpLTcImy
A LNNSNIPRFG VKTDQEELLA QELENLNKWG LNIFCVSDYA GGRSLTCIMY
B LNNTSISRFG VNTENEDHLA KELEDLNKWG LNIFNVAGYS HNRPLTCIMY
C LSSATVPRFG VQTDQEEQLA KELEDTNKWG LDVFKVADVS GNRPLTAIIF
D LTNSSIPRFG VKTEQEDVLA KELEDVNKWG LHVFRIAELS GNRPLTVIMH
```

Catalytic

```
  401                                                        450
    .IFQERDLLK tFrIpvDTli TY..tLEdHY HadVAYHNsl HAADVaQSTH
A MIFQERDLLK KFRIPVDTMV TYMLTLEDHY HADVAYHNSL HAADVLQSTH
B AIFQERDLLK TFRISSDTFI TYMMTLEDHY HSDVAYHNSL HAADVAQSTH
C SIFQERDLLK TFQIPADTLA TYLLMLEGHY HANVAYHNSL HAADVAQSTH
D TIFQERDLLK TFKIPVDTLI TYLMTLEDHY HADVAYHNNI HAADVVQSTH
```

Catalytic

```
  451                                                        500
    VLL.TPAL.A VFTDLEILAA .FA.AIHDVD HPGVSNQFLI NTNSelALMY
A VLLATPALDA VFTDLEILAA LFAAAIHDVD HPGVSNQFLI NTNSELALMY
B VLLSTPALDA VFTDLEILAA IFAAAIHDVD HPGVSNQFLI NTNSELALMY
C VLLATPALEA VFTDLEILAA LFASAIHDVD HPGVSNQFLI NTNSDVALMY
D VLLSTPALEA VFTDLEILAA IFASAIHDVD HPGVSNQFLI NTNSELALMY
```

Catalytic

```
  501                                                        550
    NDeSVLENHH LAVGFKLLQe enCDIFqNL. kkQRqsLRkM VIDmVLATDM
A NDESVLENHH LAVGFKLLQE DNCDIFQNLS KRQRQSLRKM VIDMVLATDM
B NDESVLENHH LAVGFKLLQE EHCDIFMNLT KKQRQTLRKM VIDMVLATDM
C NDASVLENHH LAVGFKLLQA ENCDIFQNLS AKQRLSLRRM VIDMVLATDM
D NDSSVLENHH LAVGFKLLQE ENCDIFQNLT KKQRQSLRKM VIDIVLATDM
```

Catalytic

```
  551                                                        600
    SKHMnLLADL KTMVETKKVT SsGVLLLDNY sDRIQVL.Nm VHCADLSNPT
A SKHMTLLADL KTMVETKKVT SSGVLLLDNY SDRIQVLRNM VHCADLSNPT
B SKHMSLLADL KTMVETKKVT SSGVLLLDNY TDRIQVLRNM VHCADLSNPT
C SKHMNLLADL KTMVETKKVT SLGVLLLDNY SDRIQVLQNL VHCADLSNPT
D SKHMNLLADL KTMVETKKVT SSGVLLLDNY SDRIQVLQNM VHCADLSNPT
```

Catalytic

```
  601                                                        650
    KpLeLYRQWT DRIM.EFFqQ GDrERErGme ISPMCDKHtA SVEKSQVGFI
A KPLELYRQWT DRIMAEFFQQ GDRERERGME ISPMCDKHTA SVEKSQVGFI
B KSLELYRQWT DRIMEEFFQQ GDKERERGME ISPMCDKHTA SVEKSQVGFI
C KPLPLYRQWT DRIMAEFFQQ GDRERESGLD ISPMCDKHTA SVEKSQVGFI
D KPLQLYRQWT DRIMEEFFRQ GDRERERGME ISPMCDKHNA SVEKSQVGFI
```

Catalytic

```
  651                                                        700
    DYIvHPLWET WADLVhPDAQ diLDTLEDNR eWYqS.IpqS PSpppdee.r
A DYIVHPLWET WADLVHPDAQ EILDTLEDNR DWYYSAIRQS PSPPPEEESR
B DYIVHPLWET WADLVQPDAQ DILDTLEDNR NWYQSMIPQS PSPPLDEQNR
C DYIAHPLWET WADLVHPDAQ DLLDTLEDNR EWYQSKIPRS PSDLTNPERD
D DYIVHPLWET WADLVHPDAQ DILDTLEDNR EWYQSTIPQS PSPAPDDPEE
```

```
                                Catalytic
   701                                                              750
   ..g.gglp.k FQFELTLeEe eeed.e.... .......... ...k...e..
A GPGHPPLPDK FQFELTLEEE EEEEISMAQI PCTAQEALTA QGLSGVEEAL
B ..DCQGLMEK FQFELTLDEE DSEGPE.... .......... ...KEG....
C G......PDR FQFELTLEEA EEEDEE.... .......... .......EEE
D ..GRQGQTEK FQFELTLEED GESDTE.... .......... ...KDSGSQV

   751                                                              800
   eg....sask .l...d.e.. e..le.d.e. ..l.....s. ..a.......
A DATIAWEASP AQESLEVMAQ EASLEAELEA VYLTQQAQST GSAPVAPDEF
B EGHSYFSSTK TLCVIDPENR DSLGETDID. ..IATEDKSP VDT.......
C EGEETALAKE ALELPDTELL SPEAGPDPGD LPLDNQRT.. ..........
D EEDTSCSDSK TLCTQDSEST EIPLDEQVEE EAVGEEEESQ PEACVIDDRS

   801                                                              850
   .......... .......... .......... .......... ..........
A SSREEFVVAV SHSSPSALAL QSPLLPAWRT LSVSEHAPGL PGLPSTAAEV
B .......... .......... .......... .......... ..........
C .......... .......... .......... .......... ..........
D PDT....... .......... .......... .......... ..........

   851                                                  890
   .......... .......... .......... ..........
A EAQREHQAAK RACSACAGTF GEDTSALPAP GGGGSGGDPT
B .......... .......... .......... ..........
C .......... .......... .......... ..........
D .......... .......... .......... ..........
```

Figure 1.3: Alignment of the deduced amino acid sequences of cDNAs for the 4 human PDE4 genes

The figure shows an alignment, made using the GCG PILEUP multiple alignment software, of the PDE4 isoforms HSPDE4A4, HSPDE4B1, HSPDE4C1 and HSPDE4D3. The regions of sequence coloured in green are regions conserved between all PDE4s and the Dunce PDE of Drosophila. These are UCR1(residues 141-200 in HSPDE4A4B), UCR2 (residues 224–302 in HSPDE4A4B) and the catalytic region (residues 332–688 in HSPDE4A4B). The positions of the hypervariable regions LR1 (residues 201–223 in HSPDE4A4B) and LR2 (residues 303–331 in HSPDE4A4B are also shown.

1.3.2 The PDE4A enzyme family

There are currently thought to be at least 6 different, endogenously occurring splice variants of PDE4A. In the cases of a number of these splice variants their expression has been detected in one of either the rat or humans but not in both. This may be due either to genuine species differences between these organisms or it may simply reflect the fact that the homologous isoenzyme in the other species has not yet been cloned.

The human PDE4A gene locus has been characterised and finely mapped to a region of chromosome 19 p13.2 between the genes encoding TYK2 and the low density lipoprotein receptor. The HSPDE4A gene spans 50kb and is composed of at least 17 exons. The upstream conserved regions UCR1 and UCR2 are each encoded by 3 exons (exons 2, 3 and 4 and exons 6, 7 and 8 respectively). The hypervariable regions LR1 and LR2 are encoded by 2 and 1 exons (exons 4 and 5 and exon 8 respectively). The catalytic region of the enzyme is primarily encoded by 5 exons (exons 10, 11, 12, 13 and 14) with some additional contribution from exon 15 (225).

1.3.2.1 PDE4A1

The first cDNA encoding a mammalian PDE4 to be cloned was the rat PDE4A splice variant RNPDE4A1. This clone was isolated from a rat brain cDNA library. It encodes for a protein of 610 amino acids with a predicted Mw of 68kDa (47). Antibodies raised against deduced amino acid sequences contained within the carboxyl terminal region of RNPDE4A1 detect a 73kDa immunoreactive species that is expressed endogenously in cerebellum (201) and also in other regions of brain (140). This 73kDa endogenous species migrates with a slightly higher apparent Mw than that predicted from the deduced protein sequence of RNPDE4A1. It is likely, however, to represent native RNPDE4A1 as it co migrates exactly with the novel immunoreactive species that is present in COS cells transiently transfected to express recombinant RNPDE4A1. Indeed, anomalous migration on SDS–PAGE is a common feature of PDE4 isoforms (16, 87, 108). This may be attributable to stretches of negatively charged amino acids that lie within the catalytic region of PDE4 enzymes and that may affect the ratio of SDS binding to these proteins (87).

Northern blot analysis suggests that the endogenous expression of RNPDE4A1 is confined to brain(201). Immunological analysis show that within brain RNPDE4A1 is expressed in the brain stem, the cerebellum, the hippocampus, the striatum, the cortex, the midbrain and the hypothalamus (140). RNPDE4A1 is the only PDE4A species detected in cerebellum (140, 201).

The subcellular localisation of RNPDE4A1 has been studied in brain and also in a number of transfected, model systems using both biochemical and confocal microscopic analyses. In all of the systems investigated full length RNPDE4A1 exists as a membrane-bound protein that is associated predominantly with the cytosolic faces of the plasma membrane and the Golgi (possibly endocytotic) apparatus (171, 200, 201). The association of RNPDE4A1 with these membranous structures is not disrupted by washing with buffers containing high concentrations of salt. It is, however, disrupted by washing with buffers containing even very low concentrations of the non-ionic detergent triton X-100 (200, 201). This suggests that the interaction of RNPDE4A1 with these structures may be predominantly hydrophobic in nature.

The alternatively spliced amino terminal 23 amino acids of RNPDE4A1 are both necessary and sufficient for the regulated, subcellular targeting of this protein. That this region of RNPDE4A1 is necessary for its subcellular targeting was shown by examining the localisation of the engineered species Met^{26}RD1. This species, a truncation of RNPDE4A1 that lacks the first 25 amino acids of the full length protein, has an entirely cytosolic subcellular localisation in transfected COS-1 and COS-7 cells (200). That the spliced, amino terminal region of RNPDE4A1 is sufficient for its subcellular targeting was shown by examining the subcellular localisation of chimeric constructs between the alternatively spliced, amino terminal region of RNPDE4A1 and the normally cytosolic, bacterial protein chloramphenicol acetyltransferase (CAT). Constructs in which the extreme amino terminal 25 residues of RNPDE4A1 were expressed as an amino terminal fusion protein with CAT were associated with the particulate fractions of transfected COS cells. This is in marked contrast to the entirely cytosolic subcellular localisation of native CAT and of regions of RNPDE4A1, other than that between residues 1–25, expressed as fusion proteins with CAT (194).

The 3 dimensional structure of a 25 residue peptide corresponding to the alternatively spliced, amino terminal region of RNPDE4A1 has been determined by nuclear magnetic resonance (NMR) (207). This peptide folds into 2 well ordered regions that are separated by a mobile hinge region. The most amino terminal of the 2 ordered regions is formed by the residues Leu^{3}–Cys^{11}. These residues fold into a amphipathic α helix in which the non polar residues (Leu^{3}, Ala^{4}, Phe^{6}, and Phe^{7}) are concentrated along one edge. The region Cys^{11}–Pro^{14} appears to be highly mobile implying that it forms a hinge region in the structure. The region Pro^{14}–Lys^{24} forms the second of the 2 ordered regions of the peptide and can itself be resolved into 2 identifiable domains. The residues Pro^{14}–Trp^{20} fold into a compact, globular structure formed principally from large, hydrophobic residues. The folding of this region forces the hydrophobic residue Val17 out into the solvent. This exposed residue has the potential to help stabilise specific interactions with other molecules. The residues Asp^{21}–Arg^{25} form a polar helix and it is likely that in the intact protein this helical region may extend further downstream.

There are no features obvious from either the amino acid sequence or the NMR structure of the spliced amino terminal region of RNPDE4A5 that would be expected to insert into the phospholipid bilayer of a membrane. Neither is there any evidence that this region of RNPDE4A1 is modified by palmitoylation or by myristolyation (201). The mechanism by which this protein sequence can specifically target proteins to membranous structures within cells is likely therefore to involve its binding to some unidentified anchoring molecule. At present it seems more likely that this anchoring molecule is a specific phospholipid than a protein. This is because in *vitro* translated RNPDE4A1 is still able to associate with a membrane fraction from COS-7 cells even after the membrane fraction has been treated with proteases or has been boiled [Scotland and others, manuscript in preparation].

1.3.2.2 HSPDE4A4 (RNPDE4A5)

The human PDE4A splice variant HSPDE4A4B and its homologue in the rat RNPDE4A5 are long PDE4A isoforms. As such they contain both UCR1 and UCR2. These isoforms each have an alternatively spliced region of approximately 110 unique residues at their extreme amino terminus. This region is the only sequence

that is unique to this PDE4A splice variant and it is likely to be responsible for the isoenzyme specific properties of these forms.

Immunological analysis shows that RNPDE4A5 is differentially expressed in various regions of rat brain. It is detected in the hippocampus, the striatum, the cortex, the midbrain and the hypothalamus but not in the brain stem, the pituitary gland nor the cerebellum (140). Both endogenously in brain and in a number of different transfected cell lines (COS-1, COS-7, HEK and Rat-1 cells), RNPDE4A5 partitions between the soluble and the particulate cell fractions (140). This subcellular distribution is also seen with the human homologue, HSPDE4A4B in transfected, model systems (93).

The particulate fractions of these proteins are not solubilised by repeated washing with buffers containing high concentrations of salt, the non-ionic detergent triton X-100 nor both salt and this detergent. This has lead to the speculation that these isoenzymes may interact with some element of the cytoskeleton (86, 93, 140). This hypothesis is further supported by immunofluoresent confocal microscopic analysis of the subcellular distributions of RNPDE4A5 and HSPDE4A4B in transfected cells. These analyses show that a high concentration of these proteins are localised into foci (ruffles) at the cell margins. This distribution is reminiscent of those seen for the actin associated, cytoskeletal proteins fodrin and cortactin (86, 93).

The alternatively spliced, amino terminal regions of RNPDE4A5 and of HSPDE4A4B are rich in proline and arginine residues and each contains 3 identifiable motifs that conform to the PxxP consensus sequence for interaction with SH3 domains (see section 1.5.1.1). Both RNPDE4A5 and HSPDE4A4B are able to specifically interact, in *vitro*, with certain SH3 domains expressed as fusion proteins with glutathione S-transferase (GST). Furthermore co-immunoprecipitation experiments show that RNPDE4A5 and HSPDE4A4B can interact with full length Src and Lyn kinases (141, 162).

The interaction between RNPDE4A5 and SH3 domains has an absolute requirement for the alternatively spliced, amino terminal region of the protein; other rat PDE4A splice variants and amino terminal truncations of RNPDE4A5 that do not contain the

unique, amino terminal region do not interact with SH3 domains (see section 5.2.2) (162). It is likely that the most amino terminal of the 3 PxxP motifs present in this splice variant is directly involved in mediating the interaction between RNPDE4A5 and SH3 domains (see section 5.2.2).

The alternatively spliced, extreme amino terminal region of HSPDE4A4B is also able to interact with SH3 domains (141). The interaction of HSPDE4A4B with SH3 domains appears to be more complicated than that of the rat isoform RNPDE4A5. This is because, in addition to the 3 putative SH3 domain binding motifs that are present within the alternatively spliced region of these proteins, there is another proline and arginine rich stretch of sequence within LR2 of the human but not of the rat isoenzyme that can interact with SH3 domains. The interaction between LR2 of HSPDE4A4B and an SH3 domain in *vitro* causes a change in the conformation of the catalytic site of HSPDE4A4B that can be detected by a change in its sensitivity to inhibition by rolipram. It has been suggested that a similar, in *vivo* interaction between HSPDE4A4B and an SH3 domain may function as a regulatory mechanism for this PDE and as a point of crosstalk between cAMP and tyrosine kinase signalling pathways (141).

The alternatively spliced, amino terminal region of RNPDE4A5 can be proteolytically cleaved from the enzyme during apoptosis in both the rat-1 fibroblast and the PC12 cell lines [Huston and others, manuscript in preparation]. This is due to the specific proteolysis of RNPDE4A5 by caspase-3, a downstream effector of appopotsis. The site of cleavage conforms to the consensus recognition motif for caspase-3 and lies at the carboxyl terminal end of the alternatively spliced unique, amino terminal region of RNPDE4A5. Cleavage of RNPDE4A5 at this site abolishes its ability to interact with SH3 domains and, truncations that mimic the cleaved product have a different subcellular distribution from full length RNPDE4A5 as assessed by confocal microscopy [Huston and others, manuscript in preparation].

A functional role for the murine homologue of RNPDE4A5, MMRNPDE4A5 in regulating differentiation of the 3T3-F442A fibroblast cell line has been identified (132). Stimulation by growth hormone (GH) is an essential prerequisite for the differentiation of 3T3-F442A fibroblasts into adipocytes. The activated GH receptor

interacts with the cytosolic tyrosine kinase JAK-2 to initiate a number of signalling cascades. This results in the cells exiting from the cell cycle and becoming primed for differentiation. Elevated levels of intracellular cAMP are then important for the subsequent differentiation of the primed cells. In addition to priming 3T3-F442A fibroblasts for differentiation stimulation by growth hormone also causes an acute activation of MMPDE4A5 in these cells. This antagonises subsequent increases in intracellular cAMP levels and so antagonises the differentiation process. This stimulation of MMPDE4A5 in 3T3-F442A fibroblasts is downstream of JAK-2 and of p70S6 kinase and it appears to involve a post translatational modification, probably phosphorylation, of this PDE form (132).

1.3.2.3 RNPDE4A8

The splice variant RNPDE4A8 is a long PDE4A isoform that was initially cloned from a rat testes cDNA library. The cDNA encodes for a 763 amino acid protein that includes an alternatively spliced, extreme amino terminal region of 21 residues that is not conserved in any other splice variant (16). When expressed in heterologous systems (COS-7 and MA-10 cells), RNPDE4A8 migrates on SDS-PAGE as a single band of 98±1.4kDa (16, 152). RNAse protection analysis suggests that RNPDE4A8 may be exclusively expressed in testis and immunoblotting of this tissue with antisera specific for PDE4A demonstrates the presence of a 97±2kDa immunoreactive species that is likely to be endogenous RNPDE4A8 (16). A similar immunoreactive species is also present in extracts from human ejaculated spermatozoa suggesting that a human homologue of RNPDE4A8 is also expressed in this tissue (152).

The expression of RNPDE4A8 is restricted to the testis and is developmentally regulated in maturing spermatozoa. A number of other components of the cAMP signalling pathway also have testis specific isoforms that are differentially expressed during the differentiation of spermatozoa. This suggests that the cAMP signalling pathway may regulate some tissue specific function in these cells (152).

1.3.2.4 HSPDE4A10 (Olf RD1), rPDE66 and TM3

There is evidence for the existence of 3 further long form splice variants from the PDE4A gene.

The splice variant PDE4A10 is the full length sequence represented by a partial cDNA clone (Olf-RD1) that was first isolated from rat olfactory bulb RNA. This sequence has recently been cloned [G. Rena and others, manuscript in preparation] but the protein has not yet been fully characterised.

The cDNA rPDE66 was isolated form a rat lung cDNA library. A preliminary characterisation of protein product from this cDNA expressed in COS-7 cells has been undertaken [J. O'Donnell and others, manuscript in preparation]. The endogenous expression of this splice variant, however, has not yet been demonstrated.

A human PDE4A cDNA, called TM3 (HSPDE4A5) that is distinct from other PDE4A sequences has also been cloned (13). This cDNA appeared to encode for a novel long form PDE4A splice variant in that it contains sequences for UCR1 and UCR2. The sequence at the extreme 3' end of the TM3 cDNA clone, however, bears no homology to any known PDE. Rather, it has been suggested that, the 3' region of this clone is the inverted 3' end of a cDNA derived form another gene and that these 2 cDNAs became inappropriately ligated during the cloning process (225). The existence of a unique 5' exon, that encodes for novel sequence found in the TM3 cDNA clone, in PDE4A genomic sequence suggests however that a cDNA closely resembling TM3 may nevertheless be transcribed (225).

1.3.2.5 HSPDE4A8 (2EL)

The cDNA encoding HSPDE4A8 (2EL) was cloned from a human T-cell Jurkat cDNA library. This clone contains 2 regions of sequence that are not found in other PDE4A isoforms. These are a novel 5' end and also a 34bp insert within the region that encodes the catalytic region of other PDE4A isoforms. The 34bp insert causes a frame shift in the ORF of the cDNA, compared to those of other PDE4A splice

variants, and brings a downstream stop codon into frame. This can be expected to cause the premature termination of the expressed protein and to result in a catalytically inactive species (83). Exons that encode both of the novel regions of sequence present in the HSPDE4A8 clone have been identified within the human PDE4A gene locus. This supports the hypothesis that HSPDE4A8 is a genuine PDE4A splice variant (225).

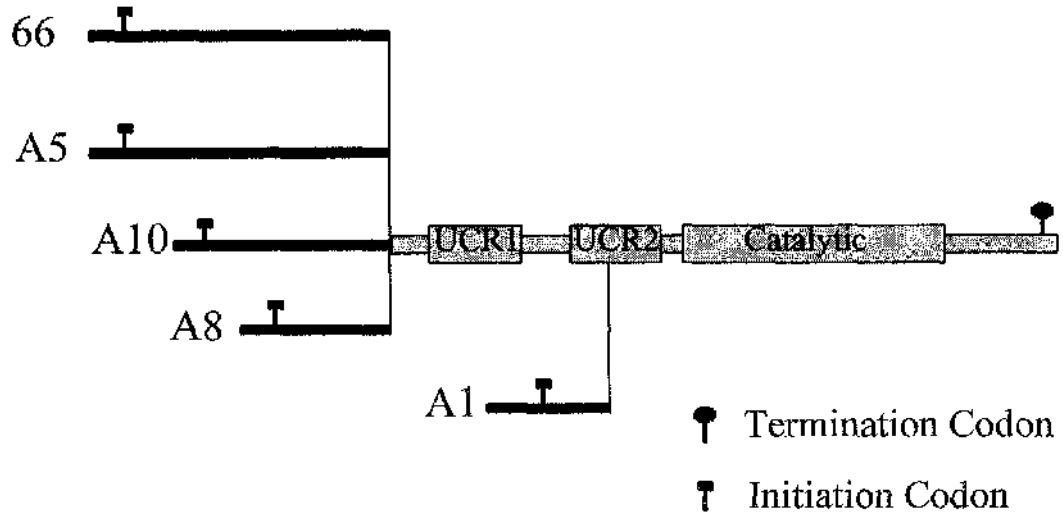

Figure 1.4: Rat PDE4A mRNA splice variants

The figure shows a diagrammatic representation of the mRNAs that are known to be encoded by the rat PDE4A gene. Regions of sequence that are conserved between all mammalian PDE4 genes and the dunce PDE of Drosophila (UCR1, UCR2 and the catalytic region) are shown as boxes. Regions of alternatively spliced sequence that are unique to each splice variant are shown as dark bars. The splice variants shown are: 66, the recently cloned rPDE66; A5, RNPDE4A5A (accession number L27057); A10, RNPDE4A10 (Olf RD1); A8, RNPDE4A8A (accession number L36467); A1, RNPDE4A1A (accession number M26715).
NB. This diagram is not drawn to scale.

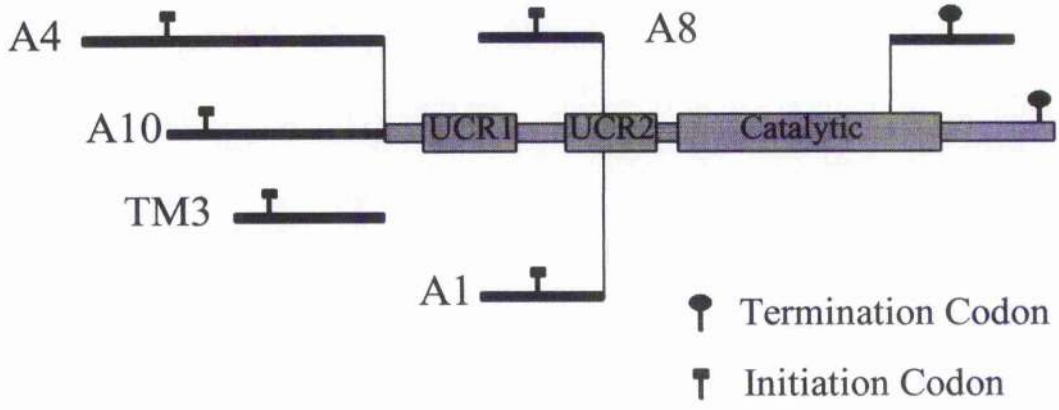

Figure 1.5: Human PDE4A mRNA splice variants

The figure shows a diagrammatic representation of the mRNAs that are known to be encoded by the human PDE4A gene. Regions of sequence that are conserved between all mammalian PDE4 genes and the dunce PDE of Drosophila (UCR1, UCR2 and the catalytic region) are shown as boxes. Regions of alternatively spliced sequence that are unique to each splice variant are shown as dark bars. The splice variants shown are: A4, HSPDE4A4B (accession number L20965); A10 the recently cloned HSPDE4A10, TM3, HSPDE4A5 (TM3, accession number L20967); A1, HSPDE4A1 (accession number NM_006202); A8, HSPDE4A8 (2EL accession number U18088).
NB. This diagram is not drawn to scale.

1.3.3 The PDE4B enzyme family

To date 4 splice variants from the PDE4B gene have been identified. Each of these has been cloned from either or both the human and the rat. There are 2 long form splice variants PDE4B1 (human clone TM72, rat clone DPD) (13, 38) and PDE4B3 (rat clone rPDE74) (92); and 2 short form splice variants PDE4B2 (human clones PDE32 and HPB106, rat clones ratPDE4 and RPDE18) (13, 17, 139, 160, 228) and PDE4B4 (human clone HBP102) (160). There is evidence that different PDE4B splice variants are differentially expressed between brain regions (126).

The recombinant PDE4B splice variants HSPDE4B1, HSPDE4B2 and HSPDE4B3 have each been expressed and characterised in COS-7 cells. In this system these enzymes all have broadly similar kinetic characteristics that are typical of members of the PDE4 enzyme. There are, however, several differences in specific characteristics, such as the Vmax and the sensitivity to inhibition by rolipram between these isoforms. There are also differences between the cytosolic and the particulate populations of individual splice variants. Such differences are likely to be related to specific functions of these isoenzymes (92).

The subcellular localisations of the splice variants HSPDE4B1, HSPDE4B2 and HSPDE4B3 were examined in transfected COS-7 cells. In this system all of these splice variants were found to partition between the particulate and the soluble cell fractions, with 30–40% of each splice variant present in the particulate fractions. The mode of association of each of these splice variants with particulate cell fractions, however, appears to be quite different as each showed very different susceptibility to solubilisation by buffers containing either or both the detergent Triton X-100 and high concentrations of NaCl. Furthermore the populations of each individual splice variant that were associated with the low speed (P1) and the high speed (P2) pellet fractions also showed different susceptibility to solubilisation by the various buffers (92).

1.3.3.1 Phosphorylation of PDE4B

The short form PDE4B splice variant HSPDE4B2 is phosphorylated on 2 serine residues (Ser^{487} and Ser^{489}) when expressed in Sf9 cells or in yeast but not when expressed in *E.coli* (114). This region of the protein is conserved between all of the known PDE4B splice variants and it is likely that these too are similarly modified. These serine residues lie within consensus motifs for phosphorylation by mitogen activated protein kinase (MAPK/ERK) and by casein kinase II respectively. A truncated form of HSPDE4B2B expressed in and purified form *E.coli* is a substrate for phosphorylation by MAPK in *vitro* (114). This purified HSPDE4B2B species was phosphorylated by MAPK on Ser^{487}. No effects of this phosphorylation on the kinetic characteristics of the enzyme were reported, however, this was not rigorously investigated and the function of phosphorylation, by MAPK, at this site is, as yet, unclear (114).

1.3.4 The PDE4C enzyme family

The PDE4C gene family is the least well characterised of all the PDE4 gene families. To date there is evidence for 3 PDE4C splice variants (58, 165). The best characterised of these is the human PDE4C splice variant HSPDE4C2 that was isolated from the U87 glioblastoma cell line by 5'RACE and RT-PCR. This cDNA clone encodes a predicted protein of 605 amino acids that migrates with an apparent Mw of 80kDa when expressed in COS-1 cells or yeast. The interaction of this splice variant with rolipram differed between the 2 expression systems, with high affinity binding of rolipram being detected for the COS-1 cell but not for the yeast expressed enzyme (165). This indicates that the enzyme can adopt more than one active conformation, which are distinguished by their interaction with rolipram (see section 1.3.6).

No endogenous PDE4C isoform has yet been detected at the protein level but RT-PCR has been used to detect the expression of PDE4C message in a number of cell and tissue types including rat parotid gland (94) and heart (107). The levels of PDE4C message in heart appeared to be altered following treatment of the animals

with 7-oxo-prostacyclin (107). This suggests that the expression of PDE4C may be hormonally regulated in this tissue.

1.3.5 The PDE4D enzyme family

To date 5 distinct splice variants from the PDE4D gene have been identified (*Figure 1.6*). There are 2 short form splice variants, PDE4D1 (159, 226) and PDE4D2 (99, 159). In addition there are 3 long form splice variants, PDE4D3 (199), PDE4D4 (14, 15, 98) and PDE4D5 (15). These splice variants have all been identified both in humans and in the rat. The cDNA sequence for the rat form of PDE4D5, however, has not yet been cloned and the evidence for the existence of this isoenzyme is solely immunological.

1.3.5.1 Short form PDE4D splice variants, PDE4D1 and PDE4D2

The primary structures of the 2 short form splice variants from the PDE4D gene, PDE4D1 and PDE4D2 are very similar to one another, the only difference being a 78 residue extension at the extreme amino terminal of PDE4D1 that is not present in PDE4D2. Each of these splice variants has been extensively characterised in transfected COS-7 cells. In this model system these splice variants each exhibit kinetic characteristics typical of PDE4 isoforms: a low Km for cAMP, an insensitivity to cGMP or to Ca^{2+} calmodulin and a sensitivity to inhibition by rolipram (15, 227). The 2 proteins both have a predominantly cytosolic subcellular localisation in transfected COS-7 cells, approximately 94% of the protein fractionating with the S2 cell fraction and also in FRTL-5 thyroid cells (98). Both HSPDE4D1 and HSPDE4D2 migrate on SDS–PAGE with similar apparent Mw's of 68±1kDa (15).

The mRNAs that encode PDE4D1 and PDE4D2 are transcribed from the same start site and their expression is controlled by the same promoter (146, 238). The promoter that controls the expression of these 2 splice variants contains cAMP responsive elements and is regulated by hormones that act through the cAMP signalling pathway in a number of different cell types including Sertoli cells (227) and the FRTL-5

thyroid cell line (238). The induction of these splice variants in response to hormonal stimulation appears to be involved in the long term desensitisation of the cells (98).

1.3.5.2 Long form PDE4D splice variants PDE4D3, PDE4D4 and PDE4D5

The primary structures of the long form PDE4D splice variants, PDE4D3, PDE4D4 and PDE4D5, differ from one another only in their alternatively spliced amino-terminal regions (*Figure 1.6*). These splice variants have been expressed and characterised in transfected COS-7 cells (15). As with the short form PDE4D splice variants each has catalytic characteristics typical for a member of the PDE4 superfamily. All of the long PDE4D isoforms partition between the cytosolic and the particulate fractions of transfected COS-7 cells (15) and a similar distribution has also been observed for endogenous, long PDE4D splice variants in FRTL-5 thyroid cells (98).

1.3.5.3 Phosphorylation of PDE4D3 by PKA

The long form PDE4D splice variant PDE4D3 is a substrate for phosphorylation by PKA in *vitro* (2, 197). This isoform also becomes phosphorylated and activated in response to agents that act to increase intracellular cAMP and activate PKA in *vivo* in FRTL-5 thyroid cells (122, 197), COS-1 cells (82), U937 promonocyte cells (2) and vascular smooth muscle cells (124).

The phosphorylation of PDE3D3 by PKA produces an approximately 3 fold increase in activity that is due to a change in Vmax but not in Km of the enzyme. This phosphorylation also generates an increase in affinity for Mg^{2+} and a change in sensitivity to inhibition by rolipram (82, 197).

Two residues in PDE4D3 (Ser^{13} and Ser^{54}) become phosphorylated by PKA (197). Mutational analysis has shown that phosphorylation at Ser^{54}, in the absence of phosphorylation at Ser^{13}, is sufficient to engender activation of the enzyme and the changes in sensitivity to both Mg^{2+} and to rolipram (82, 197). A model in which modification at Ser^{54} disrupts at least 2 distinct intramolecular bonds to cause both

the activation of and the change in sensitivity to rolipram of PDE4D3 has been proposed on the basis of mutational analysis (82).

This model proposes that Ser^{54} and the adjacent Glu^{53} are each involved in making bonds that influence the structure of the catalytic site of the enzyme. It has been suggested that Glu^{53} is involved in forming an ion pair that constrains the activity of the enzyme and that the introduction of a negative charge by the phosphorylation of Ser^{54} would disrupt this interaction and cause an activation (82). In addition to this Ser^{54} has been suggested to be involved in forming a hydrogen bond with another, unidentified residue in the protein (82). The disruption of this hydrogen bond has been suggested not to affect the catalytic activity of the enzyme but to influence the conformation of the active site in such a way that can be detected by a change in affinity for rolipram (82).

The functional consequences of phosphorylation at Ser^{13} are not known. A change in the electrophoretic mobility of HSPDE4D3 on SDS–PAGE that occurs upon its phosphorylation by PKA has, however, been linked to the phosphorylation of PDE4D3 in certain cells (98) but not observed in others (82).

1.3.5.4 Phosphorylation of PDE4D3 by ERK

The PDE4 isoforms PDE4D3 and PDE4D5 have been shown to be substrates for phosphorylation and regulation by the MAP kinase ERK2 (81). These proteins are phosphorylated by ERK2 both in *vitro* and in *vivo* on a single serine residue (Ser^{579} in HSPDE4D3) that is located within the carboxyl terminal region of the molecule and lies within a consensus motif of the form PXn(S/T)P for phosphorylation by ERKs

The phosphorylation of PDE4D3 by ERK2 causes an inactivation of the enzyme that can be reversed either by dephosphorylation by PP1 or by a further phosphorylation at the PKA site located within UCR1 (Ser^{54} in HSPDE4D3) (81). It has been suggested that the PKA phosphorylation may provide a negative feedback loop whereby activation of ERK2 causes an inhibition of long form PDE4s, leading to an increase in intracellular cAMP, the activation of PKA and the subsequent phosphorylation and reactivation of the PDEs (81).

1.3.5.5 PDE4D4

The long form PDE4D splice variant HSPDE4D4 was initially isolated from a human fetal brain cDNA library as an incomplete cDNA that was open at its 5' end (13). Full length cDNA sequences for PDE4D4 have subsequently been cloned from both humans and the rat (15, 98). This splice variant differs, at the level of primary structure, from the other long PDE4D splice variants solely in its alternatively spliced, amino terminal region (*Figure 1.6*). The expression of this splice variant appears to be largely restricted to brain (15) although mRNA encoding RNPDE4D4 has been detected by RT-PCR in the FRTL-5 thyroid cell line (98).

The alternatively spliced, amino terminal region of PDE4D4 comprises 152 amino acids. This region of HSPDE4D4 contains long stretches of extremely proline rich sequence that might be expected to fold into a left handed PPII helical structure. This region of the protein is also unusually rich in histidine residues. The primary structure of this region of HSPDE4D4 is somewhat reminiscent of sequences that participate in specific protein–protein interactions and, in this thesis, I present evidence that PDE4D4 can interact, at least *in vitro*, with specific SH3 domains (see chapter 3).

1.3.5.6 Interaction of PDE4D5 with RACK

The long form PDE4D splice variant HSPDE4D5 differs, at the level of primary structure, from the other long PDE4D splice variants solely in its alternatively spliced, amino terminal region.

A yeast 2 hybrid screen that used the unique, alternatively spliced region of HSPDE4D5 as a bait identified a potential interaction between HSPDE4D5 and protein called, receptor for activated C kinase 1 (RACK1) (252). The interaction between RACK1 and HSPDE4D5 was subsequently confirmed as being a genuine protein–protein interaction that occurs both *in vitro* and *in vivo* (252).

RACK 1 is a 36kDa protein which was first identified as one of several proteins, present in the detergent insoluble fraction of heart and brain that can bind to activated

protein kinase C (PKC) (145). This protein was cloned from a rat brain cDNA library and found to belong to the superfamily of WD40 motif containing proteins (180). The structure of another WD40 motif protein (the G protein β subunit) has been solved; the G protein β subunit has a propeller like structure in which the blades of the propeller are formed by the repeating WD40 motifs. Other WD40 motif proteins such as RACK 1 are presumed to adopt a similar conformation (211). In both RACK 1 and the G protein β subunit the WD40 motifs are involved in mediating protein–protein interactions.

The interaction between PDE4D5 and RACK1 is due to a specific, high affinity, direct binding of these 2 proteins and not due to each protein binding to a third bridging protein. A short stretch of sequence found within amino acids 19–50 and that is contained within the alternatively spliced amino-terminal region of PDE4D5 is necessary for the interaction of PDE4D5 with RACK 1. The mutation of any 1 of 4 amino acids (N22, P23, W24 or N26) within this region to alanine is sufficient to completely abolish the interaction with RACK 1. This suggests that this region is the major site of interaction between the 2 proteins (252).

In addition to PDE4D5 and PKC, RACK1 can interact with the cytoplasmic domain of the integrin β subunit(121) and with Src kinase (30). In the cases of PKC and the integrin β subunit interaction with RACK 1 is not constitutive but requires activation by phosphatidylserine and Ca^{2+} in the case of PKC and by stimulation of the cells by phorbol esters (which would also be expected to activate PKC) in the case of the integrin β subunit. In the cases of PDE4D5 and of Src kinase the interaction with RACK 1 appears to be constitutive.

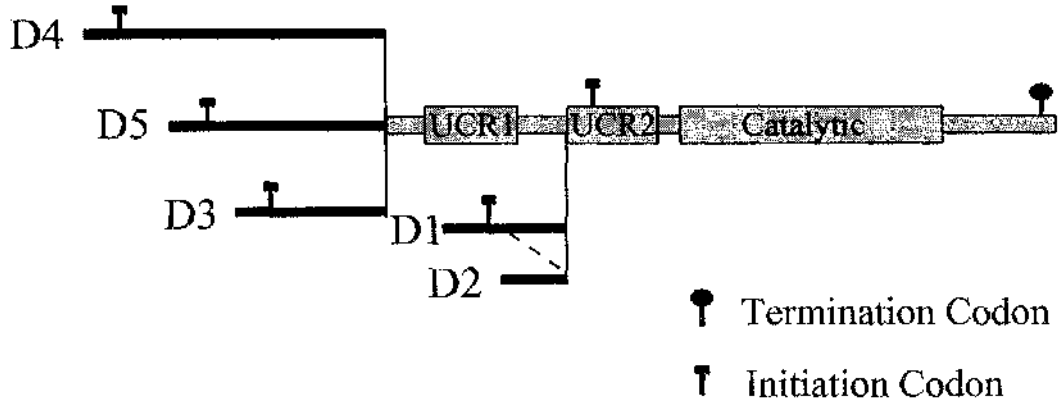

Figure 1.6: Mammalian PDE4D mRNA splice variants

The figure shows a diagrammatic representation of the mRNAs that are known to be encoded by the mammalian PDE4A gene. Regions of sequence that are conserved between all mammalian PDE4 genes and the dunce PDE of Drosophila (UCR1, UCR2 and the catalytic region) are shown as boxes. Regions of alternatively spliced sequence that are unique to each splice variant are shown as dark bars. The dashed line indicates a region of sequence that is absent from the PDE4D2 mRNA. The splice variants shown are:D1, PDE4D1 (accession numbers U79571 and L27060 for the human and rat sequences respectively); D2 PDE4D2 (accession numbers S:1059275 and U09456 for the human and rat sequences respectively); D3, PDE4D3 (accession numbers L20970 and U09457for the human and rat sequences respectively); D4, PDE4D4 (accession numbers L20962 and AF031373 for the human and rat sequences respectively); D5, PDE4D5 (accession number S:1059276 for the human sequence).
NB. This diagram is not drawn to scale.

1.3.6 Inhibition of PDE4 isoforms by rolipram: evidence for distinct conformational states

The antidepressant drug, rolipram (4-[3-(cyclopentoxyl)-4-methoxyphenyl]2-pyrrolidone) is a specific inhibitor of the PDE4 enzyme family (158). The structural similarities between rolipram and cAMP, together with the kinetic characteristics of the inhibition suggest that rolipram binds at or near to the catalytic site of PDE4 isoenzymes and functions as a competitive inhibitor. Rolipram is widely considered to be the archetypal PDE4 specific inhibitor; indeed PDE4 activity is often defined as the PDE enzyme activity within a preparation that is inhibited by 10μM rolipram. Rolipram has been tested in clinical trials as an antidepressant drug but its adverse side effects, which include emesis and nausea, limit its therapeutic utility.

Despite its limited therapeutic utility the interaction between rolipram and PDE4 continues to receive considerable attention. This is largely because certain discrepancies between a model of simple competitive inhibition and the data obtained for the effect of rolipram on various preparations of PDE4 suggest that specific long form PDE4 isoenzymes may be able to adopt more than 1 conformational state and that these can be distinguished by differences in their interaction with rolipram (6, 141, 215, 233).

A high affinity (low nM) rolipram binding site is present in preparations of brain and certain, although by no means all, other tissues. There is good evidence that this high affinity rolipram binding site is a property of the PDE4 enzyme as high affinity rolipram binding is co expressed with recombinant PDE4 in yeast (234). The high affinity rolipram binding shows marked sterioselectivity with a 20 fold greater affinity for the R-(-) enantiomer than for the S-(+) enantiomer of rolipram. In contrast to this the inhibitory potency of rolipram against PDE4 usually lies in the 0.1–2.0μM range and little stereosclectivity between the R-(-) and S-(+) enantiomers of rolipram is apparent (215, 216). Furthermore many peripheral tissues that are rich in PDE4 activity do not display high affinity rolipram binding (87).

Despite the apparent differences between the high affinity binding and the inhibitory action of rolipram on PDE4 a number of lines of evidence suggest there is only a

single rolipram binding site on each PDE4 subunit. Firstly, as rolipram is structurally similar to cAMP, one might expect that any additional rolipram binding site within a PDE4 molecule would be contained in a domain of a similar size and with some homology to the catalytic domain. In PDE2, PDE5, PDE6 and PDE10, for instance, the allosteric cGMP binding site is clearly identifiable as sharing homology with the catalytic domain (87). There are, however, no regions of sequence outside of the catalytic region of PDE4s that are obvious candidates for forming an additional rolipram binding site. Secondly, rolipram binding assays performed using HSPDE4B2 purified to homogeneity show that the stochiometry of binding does not exceed 1mol rolipram per mol of PDE. This supports the hypothesis of a single rolipram binding site on PDE4 (178, 179).

A number of different models have been proposed that could account for the discrepancies between the binding of and the inhibition by rolipram of PDE4 (87, 215). Most of these models involve the existence of at least 2 distinct conformational states of the PDE, each of which exhibits a different affinity for rolipram. An attractive hypothesis is that the interconversion between possible conformers may be controlled by some type of molecular switch, such as a phosphorylation or by a protein-protein interaction. This notion is consistent with the observations that vanadyl-glutathione complexes can cause an activation of and an increase in the affinity for rolipram of PDE4 from guinea pig eosinophil membranes (104). It is plausible that these effects are due to a thiol group modification of either the PDE or an associated protein that triggers a conformational change in the PDE and results in the accumulation of a conformer exhibiting high affinity rolipram binding (87). Also PDE4D3, expressed in either Sf9 cells or MA10 cells, appears to exist as 2 distinct conformers each of which has a different sensitivity to inhibition by rolipram. The interconversion of the enzyme between these conformational states appears to be regulated in some way as phosphorylation by PKA specifically activates high affinity rolipram binding form but does not perturb the amount of the low rolipram affinity conformer (2). Finally the between a proline and arginine rich motif, located within LR2 of HSPDE4A4B, and the SH3 domain of a Src family tyrosyl kinase (Src or Lyn kinase) causes a change in the sensitivity of this PDE to inhibition by rolipram (141).

There is evidence to suggest that different conformers of PDE4 may have distinct physiological functions (215). This raises the possibility of developing conformer specific PDE4 inhibitors that might be expected to have a more specific action (fewer side effects) than currently available PDE4 inhibitors.

The structural determinants of the rolipram sensitivity of PDE4 isoenzymes have been mapped to a 109 amino acid region located at the carboxyl terminus of the PDE4 catalytic domain (4). This region of PDE4 is relatively well conserved between PDE4 and other PDE gene families. Both residues that are specific to PDE4 isoenzymes and also those that are conserved between PDE4 and, for instance, PDE3 were identified as being important determinants for inhibition by rolipram. In general, mutation of residues that are important for sensitivity to rolipram and that are also conserved in the PDE3 gene family resulted in the largest changes in the affinity of the enzyme for cAMP. This supports the hypothesis that the catalytic site of PDE4 is closely liked to the rolipram binding site and that changes in the conformation of the active site can markedly affect its interaction with rolipram.

1.4 Src family tyrosyl protein kinases

The Src family tyrosyl kinases are a family of non receptor protein tyrosine kinases. In mammals 8 Src family tyrosyl kinases have so far been identified: Src, Fyn, Yes, Lck, Hck, Lyn, Fyr and Blk. These proteins range between 52–62 kDa in size and certain of the family members occur as multiple forms due to alternative mRNA splicing (Fgr, Lyn and Hck) or to posttranslational modification (Lck) (*Table 1.3*). All of the Src family tyrosyl kinases share a common domain structure composed of a myristalated, amino terminal membrane localisation (SH4) domain; a unique domain that is between 45–85 amino acids and is not conserved between the various family members, an SH3 domain (see section 1.5.1.1); an SH2 domain (see section 1.5.1); a linker region; the tyrosine kinase catalytic region and a conserved carboxyl terminal region that contains a regulatory tyrosine residue (Y527 in chicken Src).

The crystal structures of human Src (247), chicken Src (244) and human Hck (206) have recently been determined and this has provided insights into the regulation of

these enzymes. The inactive conformation of Src family tyrosyl kinases is stabilised by multiple intramolecular interactions including an interaction between a phosphorylated regulatory tyrosine residue within the carboxyl terminal region of the kinase and its SH2 domain and an interaction between the SH3 domain and a region within the small lobe of the kinase domain. Full activation of Src family tyrosyl kinases therefore requires the disruption of both the intramolecular SH2 and SH3 domain interactions to allow the reorganisation of the kinase into its active conformation.

Src family tyrosyl kinases become activated following the stimulation of cells with a number of hormones and growth factors that activate receptors with intrinsic tyrosine kinase activity such as the platelet derived growth factor receptor (PDGFR) (49). Src family kinases are also activated downstream of antigen receptor complexes, that lack intrinsic tyrosine kinase activity, in lymphoid cells (88). The roles of the various Src family tyrosyl kinases in signalling downstream of activated receptors are not well understood and appear to vary between different cell types and even downstream of different receptors within a single cell type. Src, for instance, functions differently downsteram of activated α and β PDGFRs in several cell lines (49). Also, different family members appear able to substitute for one another in knockout cell lines. Stimulation of a Src^- murine fibroblast cell line by plalatelet derived growth factor (PDGF) was still able to innitate mitogenesis, however kinase inactive mutants of Src functioned as dominant negatives when expressed in these cells. This was presumably due to competition between the mutant Src and other endodgenous Src family tyrosyl kinases that were sufficient to support signalling in the Src^- cells (22). Despite these difficulties it is clear that Src family tyrosyl kinases are recruited to activated receptors by an interaction between their SH2 domain and phosphorylated tyrosine residues on the receptor and that, at least in the case of mitogenic signalling in murine fibroblasts, a functional SH3 domain on the Src family kinase is required for further signalling to downstream elements of the pathway (22, 49).

Src family tyrosyl kinase	Molecular mass of protein (kDa)
Src	60
Yes	62
Fyn	59
Fgr	55/53[a]
Lyn	56/53[a]
Lck	56 (58,60,62....)[b]
Hck	59/56[a]
Blk	55

Table 1.3: Molecular masses of the mammalian Src family tyrosyl kinases

Abbreviations:[a], two forms due to alternative mRNA splicing or alternative translational initiation sites

[b], Multiple forms due to posttranslational modification

Table adapted from (150)

1.5 Protein–protein interactions in signal transduction

Much of the signalling in eukaryotic cells is mediated by the actions of broad specificity kinases and phosphatases. Understanding how promiscuous enzymes such as these are organised into specific signal transduction pathways represents an essential step towards attaining a full knowledge of the control of cell function. Although, as with the control of metabolism, the physical separation of pathways into membrane-bound intracellular compartments undoubtedly plays an important role in the organisation of signalling, many distinct signal transduction pathways do exist within a single subcellular compartment. It is difficult to imagine how the integrity of these pathways, many of which consist of highly related enzymes exhibiting similar substrate specificities, could be maintained solely by variations in enzyme and substrate levels.

It is becoming increasingly apparent that regulated protein–protein interactions play an important role in the organisation of signalling pathways. The cytosolic compartment of a cell is not envisaged as a "soup" of proteins diffusing in free solution but, rather, as a highly organised environment where regulated protein–protein interactions localise signalling molecules to specific regions and so define the pool of substrates on which they can act (60, 168). This model presents the opportunity for controlled "crosstalk" between pathways as, depending on the juxtaposition of molecules within a given cell type, pathways sharing common elements could either interact or operate independently of one another. It also allows for differential activation of functionally distinct pathways by a single second messenger following the establishment of non-homogeneous distributions of that messenger within the cell (85) (see section 1.4.3).

1.5.1 Modular domains for protein–protein interaction

Modular domains for protein–protein interaction occur in a wide number of different types of protein. Transcription factors and signalling proteins are 2 important examples of proteins that frequently contain domains for protein–protein interaction. In transcription factors such domains function both to allow the dimerisation of DNA

binding proteins and also to allow the assembly of multi-protein complexes around the promoter regions of the genes that they control.

The concept of conserved, modular domains that mediate protein–protein interactions between signalling molecules arose with the identification of Src homology 2 (SH2) domains. These domains, which share homology with a region of approximately 100 amino acids towards the amino terminus of Src kinase (amino acids 143–244) (247), bind to specific phosphotyrosine containing motifs within their target proteins. A large number of other conserved domains for protein–protein interaction have now been identified (*Table 1.1.4*). Such domains form distinct modular units within proteins and seem to function independently of surrounding sequences. Each type of domain mediates protein–protein interactions by binding to a short, peptide-like core motif (74). These motifs are flanked by more variable sequences that also interact with the domain to increase the specificity and the affinity of interaction (167).

The domains for protein–protein interaction that occur in signalling proteins function as regulated docking sites that allow multiprotein complexes to dynamically assemble and disassemble during signalling. The recruitment of proteins into such complexes appears to be an essential feature of many signalling pathways (133). This may be because such complexes serve to enhance the efficiency of signal transduction by brining enzymes and their substrates into close proximity. Another function of these signalling complexes seems to be in maintaining the integrity of discrete signalling pathways by presenting only the appropriate substrates to activated enzymes (60).

1.5.1.1 Src homology 3 (SH3) domains

Src homology 3 (SH3) domains are a class of modular domain for protein–protein interaction that, as with SH2 domains, were first identified in Src kinase. SH3 domains share homology with a region of approximately 60 amino acids in the amino-terminal region of Src kinase (amino acids 83–142) (137). Studies in which expression libraries were screened for interacting proteins revealed that SH3 domains bind to regions of target proteins that are rich in proline residues and contain the core PxxP motif (1). Structural studies and peptide binding assays have revealed that SH3

binding sequences adopt a left handed polyproline type II (PPII) helical conformation and that residues flanking the PxxP motif are also important in stabilising the interaction (61).

It has been proposed that SH3 domain binding sequences may be divided into two distinct classes (class I and class II) (205).

Class I sequences conform to the consensus X_1 p X_2 P p X_3 P
Class II sequences conform to the consensus X_3 P p X_2 P p X_1

A lowercase p indicates a scaffolding residue, responsible for stabilising the PPII helix. This is often found to be a proline residue.
An uppercase P represents a proline residue that contacts the SH3 domain.
Subscripted Xs represent non-conserved residues that also contact the SH3 domain.

The residues represented by X_1 and X_1 are especially noteworthy as these positions are believed to make contact with a pocket on the SH3 domain that is distinct from the proline binding pockets (205). In SH3 domains such as that of Src, this pocket is acidic. The X_1 or X_1 positions of ligands for these SH3 domains are therefore usually occupied by arginine residues, which form a salt bridge with an acidic residue in the SH3 domain (D99 in Src kinase). Whereas the X_1 position of class I ligands lies on the amino-terminal side of the PXXP motif, the X_1 position of class II ligands is on the carboxyl-terminal side of the PXXP motif. This difference has been suggested to cause class I and class II sequences to bind to SH3 domains in opposite orientations (205).

In addition to its role in mediating intermolecular protein–protein interactions the SH3 domain of Src kinase engages in an intramolecular with another region in Src kinase. This interaction affects the conformation of the tyrosine kinase domain of Src in such a way as to constrain its catalytic activity. The intermolecular interaction of the SH3 domain of Src with another protein is therefore involved in the activation of Src tyrosine kinase activity (247).

1.5.1.2 WW domains

WW domains derive their name from the presence of 2 conserved tryptophan residues that are spaced at either end of these domains. These domains are relatively

small, compared to other domains that mediate protein–protein interactions, being only 35–40 residues in length. They fold into a compact, 3-stranded β-sheet structure that presents a flat surface formed from the conserved residues within the domain. This provides the site of protein–protein interactions. As with SH3 domains, WW domains bind to ligands that contain stretches of proline rich sequences. The sequences that bind to WW domains are, however, of a different form to those that bind to SH3 domains and conform to the consensus PPxY or PPLP (29, 168, 222, 223).

1.5.1.3 Phospho tyrosine binding (PTB) domains

Phospho tyrosine binding (PTB) domains are a class of protein–protein interaction domains that, although having low sequence homology with one another, all share a similar secondary structure. These domains are composed from between 100–150 residues that form 7-stranded β-sheeted structures, capped by a helix at the carboxyl terminal end of the domain (74). The PTB domains of Shc and of insulin receptor substrate-1 (IRS-1) bind to sequences that conform to the consensus motif NPxY in which the tyrosine residue is phosphorylated (257). Sequences that lie amino terminal to the phospho-tyrosine recognition motif also make contact with these domains and increase the affinity and specificity of the interaction. Despite their name, certain PTB domains can bind to motifs in which the tyrosine residue is not phosphorylated. Examples of this include the PTB domains of X11, Fe65 and Numb (19, 254).

1.5.1.4 PDZ domains

PDZ domains are structurally similar to PTB domains. This class of domain binds to sequence motifs at the extreme carboxyl terminal end of proteins that conform to the consensus xS/TxV (54). The target proteins that PDZ domains bind to are frequently transmembrane receptors or ion channels. All 3 classes of glutamate receptor, for example, are recognised by distinct PDZ domain containing proteins. Many PDZ proteins contain multiple PDZ domains that can often bind to different target proteins. PDZ domains can also frequently heterodimerise with PDZ domains in other proteins. This has lead to the speculation that PDZ domain containing proteins

may have an important role in mediating the clustering of transmembrane receptors and ion channels (168, 235).

1.5.1.5 Pleckstrin homology (PH) domains

Pleckstrin homology (PH) domains do not mediate protein–protein interactions but rather protein–phospholipid interactions. I have, nevertheless, included a brief description of PH domains in this section because these domains share a similar secondary structure to both PTB and PDZ domains. PH domains occur in a wide variety of signalling proteins including certain tyrosine kinases, protein kinase B (PKB/AKT) and phospholipase C. This class of protein domain binds to the charged headgroups of specific phosphoinositide phospholipids. PH domains may therefore function to target proteins to specific regions of cellular membranes that are enriched in a specific phospholipids. This would allow for the coupling of phospholipid signalling pathways to protein kinase and other signalling pathways within a cell (168). An example of this is provided by the PH domain of the Bruton's tyrosine kinase (Btk). This PH domain binds to phosphatidylinositol-3,4,5 triphosphate (PI-3,4,5-P_3) and so may serve to recruit Btk to areas of membrane where this phospholipid is being produced. In so doing it serves to facilitate the interactions of Btk with other signalling molecules already present. As Btk contains an SH2 and an SH3 domain, in addition to its PH domain, it is possible that Btk may itself then recruit other proteins to a forming complex (32).

Domain for protein–protein interaction	Reference
BTB domain/ POZ domain	(119)
PDZ domain	(54, 55, 189, 235)
PH domain	(3, 32)
PTB/ PI/ SAIN domain	(254) (19) (74) (257)
SH2 domain	(18, 183, 239, 247)
SH3 domain	(61, 86, 148, 149, 162, 176, 205, 247)
WD repeat/ beta-transducin repeat	(120, 156, 211, 252)
WW domain/ WWP motif/ RSP5 repeat	(29, 131, 222, 223)

Table 1.1.4: Modular domains for protein–protein interaction that occur in signalling proteins

1.5.2 Protein–protein interactions in cAMP signalling

The role of regulated protein–protein interactions in organising signalling through the cAMP, PKA pathway is now well established. A family of functionally related PKA anchoring proteins (AKAPs) target the inactive, holoenzyme form of protein kinase A (PKA) to specific intracellular locations. Protein serine/threonine phosphatases are targeted to substrates and regulated by a variety of binding proteins. Cyclic AMP phosphodiesterases also interact with binding proteins which may play a role in the targeting and regulation of these molecules.

1.5.2.1 Interaction of PKA with AKAPs

A family of AKAPs target the inactive, holoenzyme form of PKA to specific intracellular locations. At least 2 functional domains within AKAPs are involved in the targeting of PKA: a PKA regulatory (R) subunit binding region and a second region which anchors the AKAP–PKA complex to its specific intracellular location. Mutagenesis and deletion experiments have been used to map these domains in AKAPs and, on the basis of predictions from sequence data, it has been proposed that an acidic, amphipathic helical structure may be an important feature of the PKA binding region (184).

PKA holoenzymes are subdivided into type I (containing RIα or RIβ R subunit isoforms) and type II (containing RIIα or RIIβ R subunit isoforms) forms of the kinase (see section 1.1.1.6). Initially it was thought that only type II forms of PKA were targeted by interaction with AKAPs. Recent reports, however, suggest that certain AKAPs, such as D-AKAP1, may also target type I forms of PKA (89, 90). Although the interaction of RI subunits with most AKAPs is approximately 500 times weaker than with RII subunits, the Kd for interaction is still in the μM range. This is within the physiological concentration range of RI subunits and AKAPs in cells. There is evidence to suggest that, under conditions where RII subunit concentrations are limiting, RIα subunits may be capable of physiologically relevant interactions with AKAPs; for instance, although regulation of skeletal muscle L-type

Ca^{2+} channels by PKA is dependant on the anchoring of PKA by an AKAP, this regulation is unaffected in RIIα subunit knockout mice (26, 100).

In addition to PKA, certain AKAPs also bind to a variety of other signalling molecules. For instance AKAP 79 anchors PKA, the α, βI and βII isoforms of PKC and protein phosphatase 2B (PP-2B, or calcineurin) at the postsynaptic densities of neurones (36, 106); AKAP 250 (gravin) anchors both PKA and PKC to the cell periphery and filopodia of human erythroleukemia cells (153). Functionally distinct regions of these AKAPs mediate interaction with each class of ligand and simultaneous binding of different ligands can occur. This has lead to speculation that these AKAPs may function in a similar way to the scaffolding protein Sterile-5 that functions to organise a MAP kinase cascade that is required for mating in *S.cerevisiae* (35, 60). Unlike Sterile-5, however, enzymes targeted by AKAPs are in an inactive state when bound (106). Indeed the interaction of a constitutively active form of PP-2B with AKAP 79 is sufficient to inhibit this enzyme (36). Interaction with AKAPs may therefore serve to localise a pool of signalling molecules in close proximity to the process which they control and so facilitate rapid, specific signal transduction following activation by second messengers.

1.5.2.2 Protein–protein interactions of protein serine/threonine phosphatases

Protein serine/threonine phosphatases catalyse the removal of phosphate groups from serine and threonine residues in their substrate phosphoproteins. These enzymes are classified into 4 major families (PP1, PP2A, PP2B and PP2C) on the basis of differences in substrate specificity, dependence on divalent cations and susceptibility specific inhibitors and activators. Molecular cloning has revealed that each family consists of multiple isoforms. The PP1, PP2A and PP2B gene families are related to one another (40–50% homology) whereas the PP2C family is structurally distinct. In addition to the major families, other serine/threonine phosphatase families such as PP3 and PPX (which share homology with the PP1 and PP2 families) have been identified (73).

Protein phosphatases play important roles in signal transduction and can function as positive, as well as negative, regulators of cell function; for instance okadaic acid, an

inhibitor of PP2A, PP1 and of several other, more recently cloned, phosphatases including PP3 and PPX, blocks the expression of the cdc2 and cyclin A genes following serum stimulation of growth arrested cells. This shows that an okadaic acid sensitive protein phosphatase activity is necessary for this induction (190).

Compared to the large number of protein kinases that have been identified, many of which are extremely specific for the proteins that they can phosphorylate, relatively few protein phosphatases have been identified and those that have exhibit wide specificities for the phosphoproteins that they will dephosphorylate. This makes the problem of organising protein phosphatase activities into discrete pathways even more acute than with the organisation of protein kinase activities. Protein–protein interactions are an important feature of this organisation. The catalytic subunits of PP1, PP2A and PP2B can each interact with an array of distinct binding proteins (referred to as regulatory subunits) which serve to regulate and target the phosphatase. In the case of PP1, for instance, more that 12 regulatory subunits have been identified. The regulatory subunits of PP1 each contain a motif conforming to the consensus (R/K)(V/I)xF which interacts with a conserved regulatory subunit binding site on the catalytic subunit of PP1 (57).

1.5.3 Models for the compartmentalisation of cAMP signalling and potential roles for cAMP PDEs

The observation that each of the components of the cAMP signalling pathway can be specifically targeted to various subcellular locations has lead to the formulation of the hypothesis that a functional compartmentalisation of cAMP signalling occurs within cells (39, 60, 85, 184). That is to say, it is proposed that, localised increases in cAMP concentration at specific points within the 3 dimensional interior of a cell might be expected to activate the pool of PKA localised in that area without effecting another, functionally distinct pool of PKA that is localised to a different subcellular region (*Figure 1.7*). This hypothesis is broadly similar to the proposed compartmentalisation of Ca^{2+} signalling at the presynaptic junctions of neurones whereby Ca^{2+} entering the cell through voltage sensitive channels localised at the sites of neurotransmitter release is much more effective at stimulating rapid exocytosis than is Ca^{2+} released from intracellular stores or that enters the cell via an

ionophore (185). In the cases of both cAMP and of Ca^{2+} signalling non-uniform distributions of these second messengers have been directly visualised in cells following stimulation of these pathways (80). These observations lend considerable support to the hypothesis that signalling through these second messengers could be spatially organised into functionally distinct compartments.

A number of studies (34, 102) have used specific PDE inhibitors to investigate the possible role of these enzymes in maintaining the integrity of functionally distinct pools of cAMP. Jurevicius et al used the broad specificity PDE inhibitor IBMX to demonstrate that during β-adrenergic stimulation of a single frog ventricular myocyte, PDE activity limited the spread of localised pools of cAMP. They found that, in the absence of PDE inhibition, the selective stimulation of β-adrenergic receptors located in one region of the cell lead to a greater increase the local concentration of cAMP than it did in the cAMP concentration in distant regions of the cell. In the presence of the PDE inhibitor IBMX, however, a more uniform increase in the distribution of cAMP within the cell was observed (102).

In another study Chini et al used selective inhibitors of PDE3 and of PDE4 to investigate the involvement of these PDE classes in the regulation of cAMP signalling in primary cultures of rat kidney mesangial cells. In these cells 2 major responses to immunoinflammatory stimulation, accelerated proliferation and the generation of reactive oxygen metabolites (ROMs) are both inhibited by PKA activation downstream of increased cAMP levels.

The selective inhibition of either PDE3 or of PDE4 in these cells leads to an increased activation of PKA and the effect of the combined inhibition of both PDE3 and PDE4 is at least additive with the inhibition of either one alone. Inhibition of PDE3 suppressed the accelerated proliferation of these cells whereas inhibition of PDE4 did not affect the proliferation. Furthermore the combined inhibition of both PDE3 and PDE4, although more efficacious at activating PKA, was no more effective at inhibiting proliferation than was the inhibition of PDE3 alone. In contrast to this the inhibition of PDE4, but not of PDE3 in these cells suppressed the generation of ROMs and, again, the combined inhibition of both PDE3 and PDE4

was no more efficacious at suppressing ROM generation than was the inhibition of PDE4 alone (34).

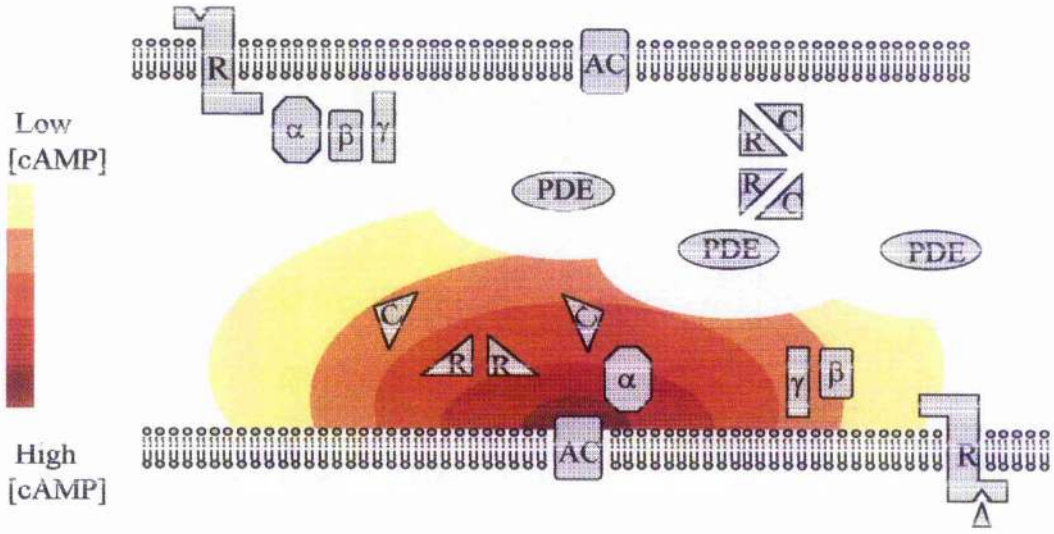

Figure 1.7: A model for the compartmentalisation of cAMP signalling

The figure is a diagram representing the hypothesised compartmentalisation of cAMP signalling within a polarised cell. Stimulation of receptors located at one face of the cell selectively activates adenylyl cyclases that are co-localised with the receptors. This creates a local increase in the concentration of cAMP that activates PKA anchored in that region of the cell (by interaction of RII subunits with AKAPs for instance). The localised increase in cAMP concentration is prevented from spreading throughout the cell and activating functionally distinct pools of PKA anchored in other regions of the cell interior by the action of specifically localised PDE.

2. Materials and methods

Except where stated otherwise, biochemicals were obtained either from Fisons or from Sigma-Aldrich and were of analytical grade.

2.1 Biochemical techniques

2.1.1 SDS polyacrylamide gel electrophoresis of proteins

2.1.1.1 Tris–glycine SDS PAGE

Tris–glycine SDS PAGE was performed following the discontinuous buffer system of Laemmli (188).

Acrylamide concentration* (%)	Protein size range (KD)
8	40–200
10	21–100
12	10–40

Table 2.2.1: Effective range of separation of SDS polyacrylamide gels.

** Molar ratio acrylamide:N,N'-methylenebisacrylamide of 29:1. Table adapted from (188).*

2.1.1.2 Buffers

Resolving gel (6–8%)

6–8%	29:1 acrylamide:N,N'-methylenebisacrylamide mix
0.375M	Tris/HCl (pH 8.8)
0.1%	SDS
0.1%	Ammonium persulfate
0.06%	N,N,N',N'-tetramethylethylenediamine (TEMED)

Resolving gel (10–15%)

10–15%	29:1 acrylamide:N,N'-methylenebisacrylamide mix
0.375M	Tris/HCl (pH 8.8)
0.1%	SDS
0.1%	Ammonium persulfate
0.04%	N,N,N',N'-tetramethylethylenediamine (TEMED)

Butanol saturated water

1:11	Butanol:deionised water (use the top phase)

Stacking gel

5%	29:1 acrylamide:N,N'-methylenebisacrylamide mix
0.125M	Tris/HCl (pH 6.8)
0.1%	SDS
0.1%	Ammonium persulfate
0.1%	N,N,N',N'-tetramethylethylenediamine (TEMED)

2X SDS loading buffer (Laemmli buffer)

0.125M	Tris/HCl (pH 6.8)
25%	Glycerol
4%	SDS
0.007%	bromophenol blue
5%	β-mercaptoethanol (added just prior to use)

5X SDS loading buffer (Hannah sample buffer)

0.26M	Tris/HCl (pH 6.7)
55.5%	Glycerol
8.8%	SDS
11.1%	β-mercaptoethanol

Tris–glycine running buffer

192mM	Glycine
25mM	Tris
0.15%	SDS

2.1.1.3 Preparation of samples

Samples were diluted either 1:2 with 2X SDS loading buffer or 1:5 with 5X SDS loading buffer and heated for 5 minutes at 100°C to denature the proteins.

2.1.1.4 Preparation of standards

Prestained protein molecular weight markers (Bio–Rad) contain the following proteins: myosin H chain (200kDa); phosphorylase B (97.4kDa); BSA (68kDa); ovalbumin (43kDa); carbonic anhydrase (29kDa); β-lactalbumin (18.4kDa) and lysozyme (14.3kDa). The apparent molecular weights varied from batch to batch and the precise sizes of the proteins were indicated on any particular figure.

2.1.1.5 Casting and running a tris–glycine gel

The gel apparatus was assembled in accordance with the manufactures instructions. A resolving gel of the appropiate percentage for size of proteins to be separated was prepared and poured between the plates of the gel kit (*Table 2.2.1*). Water saturated butanol was then layered on top of the resolving gel to produce a even surface and exclude oxygen during polymerisation. The gel was allowed to set and the water saturated butanol removed, a comb was inserted and the stacking gel poured. When the stacking gel had set, the comb was removed and the gel placed in a tank containing tris–glycine running buffer. Samples were loaded into the wells and the gel was run at a constant current until the dye front reached the bottom of the gel.

2.1.2 High resolution PAGE

Low molecular weight peptides were separated through high resolution gels consisting of a 16.5% separating gel, a 10% spacer gel and a stacking gel, each made with a 32:1 acrylamide:N,N'-methylenebisacrylamide ratio.

2.1.2.1 Buffers

Separating gel

16.5%	32:1 acrylamide:N,N'-methylenebisacrylamide mix
1M	Tris/HCl (pH 8.45)
0.1%	SDS
13.3%	Glycerol
0.05%	Ammonium persulfate
0.05%	N,N,N',N'-tetramethylethylenediamine (TEMED)

Spacer gel

10%	32:1 acrylamide:N,N'-methylenebisacrylamide mix
1M	Tris/HCl (pH 8.45)
0.1%	SDS
0.05%	Ammonium persulfate
0.05%	N,N,N',N'-tetramethylethylenediamine (TEMED)

Stacking gel

4%	32:1 acrylamide:N,N'-methylenebisacrylamide mix
0.75M	Tris/HCl (pH 8.45)
0.75%	SDS
0.08%	Ammonium persulfate
0.08%	N,N,N',N'-tetramethylethylenediamine (TEMED)

Anode buffer

0.2M	Tris/HCl (pH 8.9)

Cathode buffer

0.1M	Tris/HCl (pH 8.25)
0.1M	Tricine
0.1%	SDS

2.1.2.2 Protein low molecular weight markers

Pre-stained low molecular weight markers (Sigma) contained differently coloured ovalbumin (yellow, 45kD), carbonic anhydrase (orange, 29kD), trypsin inhibitor (green, 20kD), a-Lactalbumin (purple, 14kD), aprotinin (blue, 6.5kD)

2.1.2.3 Casting and running a high resolution gel

Mini-gel apparatus was assembled according to the manufacturers instructions. The separating gel was then poured 4.2cm high and the spacer gel was immediately poured on top 1cm high. Water saturated butanol was layered over the top of the separator gel. When the gels had set, the water saturated butanol was removed, a comb inserted and the stacking gel poured. When this had set, the comb was removed and the gel placed into the running tank. The anode and cathode chambers were filled with the appropriate buffers, samples (SDS loading buffer), were loaded into the wells and the gels were run at 100 volts until the dye front reached the bottom of the gel.

2.1.3 Staining of SDS polyacrylamide gels with Coomassie brilliant blue

Protein bands separated by SDS–PAGE were simultaneously fixed and stained. The limit of detection for protein on Coomassie stained gels is 0.3–1.0µg.

2.1.3.1 Buffers

Coomassie stain

0.025%	Coomassie brilliant blue R 250

40%	Methanol
7%	Acetic acid

Destain I

40%	Methanol
7%	Acetic acid

Destain II

7%	Acetic acid
5%	Methanol

2.1.3.2 Visualisation of proteins

Following separation by gel electrophoresis the gel was incubated in at least 5 volumes of Coomassie stain with gentle shaking at room temperature. The length of incubation was from 30 minutes to 4 hours, depending on the thickness of the gel.

Protein bands were then visualised by incubating the stained gel in destain I for 2–4 hours at room temperature with gentle shaking. Destaining was completed by exchanging the destain I for destain II and continuing the incubation for form several hours to overnight. After destaining, the gel was rehydrated by incubating in 1% glycerol for 30 minutes at room temperature with gentle shaking.

2.1.4 Staining of SDS polyacrylamide gels with silver salts

Greater sensitivity of detection than provided by Coomaissie staining was achieved by silver staining, the detection limit for which is 2–5ng protein.

2.1.4.1 Buffers

Destain I

40%	Methanol

7%	Acetic acid

Destain II

7%	Acetic acid
5%	Methanol

Cross-linking solution

10%	Glutaraldehyde

DTT (dithiothreitol) solution

0.0005%	Dithiothreitol

Silver nitrate solution

0.1%	Silver nitrate

Developing solution

3%	Sodium carbonate
0.019%	Formaldehyde

Stop solution

2.3M	Sodium citrate

2.1.4.2 Visualisation of proteins

Following separation by gel electrophoresis the gel was fixed by incubation in 100ml destain I for at least 30 minutes at room temperature with gentle shaking. The destain I was replaced with 100ml destain II and incubation was continued for 30 minutes. The destain II was exchanged for 100ml cross-linking solution and incubated for a further 30 minutes. The glutaraldehyde solution was discarded into a sink in a fume

cupboard and the gel washed with either several changes of deionised water over 2 hours or in 2l of deionised water overnight followed by a 30 minute wash in fresh deionised water the next day. After its final wash, the gel was incubated in 100ml DTT solution for 30 minutes at room temperature, with gentle shaking. The DTT solution was removed and the gel drained well but not rinsed before addition of 100ml silver nitrate solution. Incubation was continued for another 30 minutes then the gel was rinsed once under running deionised water and twice with 50ml of freshly prepared developing solution. The gel was then gently shaken in 100ml of the developing solution until protein bands appeared slightly lighter than desired. Development was then stopped by addition of 5ml stop solution.

Gloves were worn at all stages of the silver staining procedure and dedicated sandwich boxes were used for all incubations. This was to protect the gel from contaminating proteins.

2.1.5 Drying SDS polyacrylamide gels

Gels were dried on a Bio-Rad gel drier. The gel was placed on the drying surface of the drier, on top of a wetted piece of filter paper and covered with cellophane. The cover sheet of the drier was then laid over the gel and a vacuum applied so the cover sheet made a tight seal over the gel. The lid of the drier was then closed and the gel dried at 63°C for 1–2 hours, depending on the thickness of the gel.

2.1.6 Western (Immuno) Blotting

2.1.6.1 Buffers

Transfer Buffer

192mM	Glycine
25mM	Tris
20%	Methanol

Tris buffered saline (TBS)

137mM	NaCl
20mM	Tris pH 7.6

Blocking buffer

137mM	NaCl
20mM	Tris pH 7.6
5%	Skimmed milk powder

Ponceau S stain

0.1%	Ponceau S
3%	Trichloroacetic acid

2.1.6.2 Transfer of proteins onto nitrocellulose

Following separation by gel electrophoresis the gel was placed in a cassette on top of a piece of nitrocellulose paper, bound by two pieces of Whatman 3MM paper and two pieces of sponge. The cassette was assembled whilst submerged in a tray of blotting buffer, to exclude air bubbles. It was loaded into the transfer tank with the nitrocellulose side of the cassette towards the positive electrode. The tank was filled with blotting buffer and the proteins transferred for 1 hour at 1A or overnight at 0.05A.

2.1.6.3 Visualisation of transferred proteins

Following transfer the nitrocellulose was rinsed with deionised water and then incubated with Ponceau S stain untill the protein bands became visible. The filter was then washed with several changes of deionised water. The positions of lanes or significant bands such as unstained markers were marked. Ponceau S stain was then removed by washing with TBS containing 0.1% Tween-20 before proceeding with immunological detection.

2.1.6.4 Immuno-detection using ECL solution (AMERSHAM)

Any unoccupied protein binding sites on the nitrocellulose were blocked by incubation in blocking buffer for 1–2 hours at room temperature, with gentle shaking. The nitrocellulose was then washed four times with TBS containing 0.1% Tween-20 for 5 minutes each minutes each.

An antibody specific to the protein of interest (primary antibody), was diluted in 10ml TBS, 1% Skimmed milk powder. The nitrocellulose filter was sealed into a polythene bag with the primary antibody and incubated for at least 1 hour at room temperature with vigorous shaking. The nitrocellulose was then washed as described above.

A secondary, horse radish peroxidase (HRP) conjugated, anti-immunoglobulin, antibody (IgG) directed against the primary antibody was diluted in 10ml TBS, 1% Skimmed milk powder. The nitrocellulose was sealed into a polythene bag with the secondary antibody and incubated for at least 1 hour at room temperature with vigorous shaking. The nitrocelulose was then washed four times in TBS containing 0.1% Tween-20 for 5 minutes each.

The filter was incubated with ECL (Amersham) reagents according to the manufacturers instructions. X-ray film (Fuji) was exposed to the nitrocellulose for varying times depending on the intensity of the signal. The film was then developed using a Kodak X-omat.

2.1.7 Overlay assay

Purified GST fusion proteins were eluted from the glutathione-Sepharose beads by 3 incubations in 100µl elution buffer (10mM glutathione, 50mM Tris HCl (pH8.0)), for at least 10 min. each, end-over-end at 4°C. The 3 eluted fractions were pooled and assayed for protein concentration, diluted 1:2 with 2X SDS sample buffer and then boiled for 5 min.. The boiled samples were loaded onto a 10% SDS poly-acrylamide gel (10µg/lane) which was run at 40mA/gel until the dye front reached the bottom. The samples were then transferred from the gel onto a nitrocellulose

membrane. The membrane was incubated for 1h at room temperature with gentle shaking in 100ml blocking buffer (137mM NaCl, 20mM (Tris pH 7.6), 5% Skimmed milk powder). The blocked membrane was washed 4 times over a 20 min. period with T-TBS (137mM NaCl, 20mM (Tris pH 7.6), 0.1% Tween-20) and then incubated overnight at 4°C with rapid shaking in the presence of 1μg of either purified MBP or of MBP-HSPDE4D4 diluted in 10ml dilution buffer (buffer (137mM NaCl, 20mM (Tris pH 7.6), 1% Skimmed milk powder). The membrane was then washed as before and incubated for 1 h at room temperature with rapid shaking in the presence of an anti-MBP polyclonal antibody (New England Biolabs) diluted 1:10000 in dilution buffer. The membrane was then washed as before and incubated for 1 h at room temperature with rapid shaking in the presence of horseradish peroxidase conjugated anti-rabbit IgG (Sigma) diluted 1:20000 in dilution buffer. Finally the membrane was washed again as before and the labelled bands were detected according to the Amersham ECL western blotting visualisation protocol.

2.1.8 Immunoprecipitation

2.1.8.1 Buffers

Phosphate buffered saline (PBS)

2.7mM	KCl
137mM	NaCl
4mM	Na_2HPO_4
0.15mM	NaH_2PO_4, pH 7.4

Radio-immunoprecipitation assay buffer (RIPA buffer)

50mM	Tris/HCl (pH 8.0)
132mM	NaCl
0.1%	SDS
1%	Triton X-100
0.5%	Deoxycholate

22mM	NaF
11mM	Tetra-sodium pyrophosphate
1.1mM	EDTA
5.5mM	EGTA
	Complete protease inhibitor cocktail

2.1.8.2 Procedure

Cells were rinsed once with ice cold PBS and drained before being scraped into 500µl ice cold RIPA buffer and lysed with 8 strokes of a 26 ½ gauge needle attached to a disposable syringe. Cell debris were then removed by centrifugation at 12000xg for 10 min at 4°C. The cleared lysate was pre-cleared by incubation with 50µl bed volume protein-A sepharose 4B fast flow (Amersham) for 1 hour at 4°C with end-over-end mixing. The protein-A sepharose was removed by centrifugation at 12000xg for 10 sec at 4°C and an antibody specific for the species of interest was added at a concentration that has previously been established to be optimal for immunoprecipitation. The antibody and lysate were incubated together for 1 hour at 4°C with continual end-over-end mixing to allow immune complexes to form. The immune complexes were then precipitated by adding 50µl bed volume protein-A sepharose and incubating for a further 1 hour at 4°C with continual end-over-end mixing. The protein-A sepharose was harvested by centrifugation at 12000xg for 10 sec at 4°C, washed 3 times with 500µl ice cold RIPA buffer, a further 1 time with 500µl ice cold PBS and then transferred to a fresh Eppendorf tube before being resuspended in 1X SDS sample buffer and boiled for analysis by SDS–PAGE.

2.1.9 **Induction and Purification of GST Fusion Proteins**

Cultures of *Escherichia coli* (JM109), transformed either with the plasmid pGEX-2T (for the production of GST) or with recombinant pGEX-2T containing an SH3 domain (or another protein binding domain) as an in-frame fusion with GST were grown overnight at 37°C, with agitation, in Luria broth (L-broth) (170mM NaCl, 0.5% (w/v) Bacto-Yeast Extract 1 % (w/v) Bacto-Tryptone) containing 100µg/ml ampicillin. The overnight cultures were used to inoculate larger (400ml) cultures in the same medium. These were grown at 37°C, with agitation, until the OD. at

600nm reached 0.600 –1.000. Expression of the fusion protein was then induced by the addition of isopropyl ß-D-thiogalactoside (IPTG) to a final concentration of 0.1mM. Growth was continued for a further 4-6h, at 37°C, with agitation before the bacteria were harvested by centrifugation at 2500g for 5 min. in a refrigerated centrifuge. The bacteria were then resuspended in 20ml phosphate buffered saline (PBS) supplemented with 1mM dithiothreitol (DTT) and a cocktail of protease inhibitors (40mg/ml PMSF, 156mg/ml benzamidine, 1mg/ml apoprotinin, 1mg/ml antipain 1mg/ml leupeptin, 1mg/ml pepstatin, dissolved in DMSO). The resuspended bacteria were stored at -20°C in conveniently sized aliquots until needed.

Frozen aliquots were rapidly thawed at room temperature. The volume used was dependant on the level of expression achieved, which varied widely between constructs. In my hands 4ml of resuspended bacteria yielded between 0.4 and 3mg of most fusion proteins used. The defrosted bacteria were held on ice and sonicated in 20 sec. pulses, separated by 30 sec. intervals until cell lysis was complete. The sonicate was then subjected to centrifugation for 1 min. at high speed in a benchtop centrifuge and the supernatant was transferred to fresh tubes. Glutathione-sepharose beads equilibrated in PBS containing 1mM DTT and protease inhibitor cocktail were added to the sample which was then incubated end-over-end for 4–18h at 4°C. I routinely added 100µl bed volume of beads which was sufficient to bind up to about 3mg fusion protein. Following incubation, the beads were collected by centrifugation for 5 sec. at high speed in a benchtop centrifuge and the supernatant was discarded. The beads were then held on ice and washed three times with 1ml PBS containing 1mM DTT and protease inhibitor cocktail over a 15 min. period. The washed beads were resuspended as a 25% slurry and assayed for protein concentration.

2.1.10 Induction and Purification of MBP Fusion Proteins

The induction and purification of MBP fusion proteins was by a method based on that already described for the purification of GST fusion proteins but with the following differences:

The *Escherichia coli* (JM109) were transformed with pMAL-c2 (for the production

of MBP) or with pMAL-c2 containing the cDNA of interest as an in frame fusion protein with MBP.

The L-broth was supplemented with glucose (0.2% w/v) as well as with ampicillin (100μg/ml).

Expression of the fusion protein was induced by the addition of IPTG to a final concentration of 0.3mM. The culture was then shifted to 30°C for the expression of the fusion protein.

The sonicate was cleared by centrifugation at 9000g for 30min and the supernatant was incubated with amalose resin equilibrated in KHEM containing 1mM DTT and protease inhibitor cocktail.

The fusion protein was eluted from the washed amylose resin by 3 incubations in 1ml clution buffer (KHEM supplemented with 10mM maltose), for at least 10 min. each, end-over-end at 4°C. The 3 eluted fractions were pooled and dialysed at 4°C against 3 600ml batches of dialysis buffer (50mM NaCl, 20mM Tris pH8.0) before being snap frozen as aliquots. The aliquots were stored at -80°C until use.

2.1.11 Phosphodiesterase Assay

Phosphodiesterase activity was measured by a two step cAMP hydrolysis assay, based on the method developed by Thompson and Appleman [(1971) Biochemistry, 10, 2, 311-316]. In the first step ^{3}H-cyclic nucleotide (8 position of the adenine or guanine ring) was hydrolysed, by the phosphodiesterase activity, to form labelled nucleotide mono-phosphate. In the second step the nucleotide mono-phosphate ring was converted to the corresponding labelled nucleoside by incubation with snake venom (which has 5'-nucleotidase activity). Under the conditions used complete conversion of nucleotide mono-phosphate to nucleoside occurs within the incubation time. Separation of the remaining, unhydrolysed cyclic nucleotide from the nucleoside was achieved by a batch binding of the mixture to Dowex 1X8-400 anion exchange resin (Sigma): this binds the charged nucleotides, leaving only the

uncharged nucleosides in the soluble fraction.

2.1.11.1 Buffers

Assay buffer

10mM	$MgCl_2$
20mM	Tris/HCl, pH 7.4

Dilution buffer

20mM	Tris/HCl, pH7.4

2.1.11.2 Activation of Dowex 1X8-400 anion exchange resin

To activate the Dowex 1X8-400, 4l of NaOH (1M) was added to 400g of the resin and the mixture was incubated for 15 min at room temperature with gentle mixing. The resin was allowed to settle by gravity and the supernatant removed. The resin was then extensively washed with distilled water by resuspending the resin in 4l of distilled water then allowing it to settle by gravity before removing the supernatant (30 washes). After its last wash the resin was resuspended in 4l HCl (1M) and incubated for 15 min at room temperature with gentle mixing before being allowed to settle by gravity. The resin was then washed with distilled water, as described above, until the supernatant had a pH of 3 (approximately 4 washes). The activated resin was stored at 4°C as a 1:1 slurry with distilled water until required. Before use in phosphodiesterase assays ethanol was added to make a 1:1:1 slurry of Dowex:water:ethanol.

2.1.11.3 Assay procedure

The cyclic nucleotide substrate solution for phosphodiesterase activity assays was made up in assay buffer as a 2X stock (usually 2μM cAMP) supplemented with 8-^{3}H labelled cyclic nucleotide (0.003μCi μl^{-1}). Effectors were made up in dilution buffer

as a 4X stock. The first step of the assay was performed in a final volume of 100µl. This consisted of 50µl 2X substrate solution, 25µl 4Xeffector solution and 25µl sample. In assays where no effector was included 25µl dilution buffer was added in place of the 4X effector solution. Tubes were held on ice until all the additions had been made then rapidly mixed by vortexing before being incubated at 30°C (usually for 10 min). The reaction was stopped by boiling for 2 min to denature the phosphodiesterase. The tubes were then cooled on ice.

In stage 2 of the assay 25µl of 1mg ml^{-1} snake venom (either *Ophiophagus hannah* or *Crotalus atrox* venom) (Sigma) was added to the reaction mix from stage 1 of the assay. Tubes were then rapidly mixed by vortexing and incubated at 30°C for 10 min. Following incubation the tubes were held on ice and 400µl of a 1:1:1 slurry of Dowex:water:ethanol was added. The mixture was incubated on ice for 15 min with occasional vortexing and then separated by centrifugation at top speed in a bench top centrifuge for 3 min. A 150µl aliquot of the supernatant was then added to 1ml scintillation cocktail and counted on a Wallac 1409 liquid scintillation counter.

2.1.12 Kinetic analysis of enzyme activity data

I calculated the values of Km and Vmax by non-linear regression analysis using the computer program Hyper 1.02a (Shararewear. Author: J. S. Easterby). This program fits data to the hyperbolic form of the Michaelis-Menten equation by first obtaining estimates of the Km and Vmax, (using linear regression analysis to fit the data to a Hanes plot ([S]/v against [S])) and then using these estimates as starting values for a non-linear regression analysis which fits the data directly to a hyperbola.

I calculated values of IC_{50} for the inhibition of preparations of PDE4 by the inhibitor rolipram using the computer program KaleidaGraph. This program fits data to an equation describing a sigmoidal curve.

2.1.13 Pull down assay for protein–protein interaction

2.1.13.1 Pull down assays with GST–SH3 domain fusion protein as bait

Volumes of slurry containing 400µg immobilised fusion protein were pelleted and the supernatants discarded. The pellets were resuspended in crude cytosol from transfected COS-7 cells, diluted to a final volume of 200µl in KHEM buffer (50mM KCl, 50mM HEPES KOH (pH7.2), 10mM EGTA, 1.92mM $MgCl_2$) containing 1mM DTT and protease inhibitor cocktail. In pull down assays where the "bait" was a recombinant PDE overexpressed in COS-7 cells I routinely used cytosol containing 30 to 40 EU of PDE activity (pmol cAMP hydrolysed/min, with 1µM cAMP as substrate), this was typically 20µg cell protein. The immobilised fusion protein and cytosol were incubated together for 10 min. end-over-end at 4°C. The beads were then collected by centrifugation for 5 sec. at high speed in a benchtop centrifuge and the supernatant retained as the unbound fraction. The beads were then held on ice and washed three times with 400µl KHEM containing 1mM DTT and protease inhibitor cocktail over a 15 min. period. These washes were pooled along with the unbound fraction and aliquots were taken for PDE assay and immunoblotting. The bound PDE was eluted from the beads by 3 incubations with 100µl elution buffer (10mM glutathione, 50mM Tris HCl (pH8.0)), for at least 10 min. each, end-over-end at 4°C. The 3 eluted fractions were pooled and aliquots taken for PDE assay and immunoblotting.

2.1.13.2 Pull down assays with MBP–UCR1 fusion proteins as bait

50µg of MBP or MBP–UCR1 was incubated with sufficient crude cytosolic extract from COS-7 cells to contain 18–20 enzyme units of PDE enzyme activity (pmol cAMP hydrolysed/min, with 1µM cAMP as substrate), in a total volume of 350µl for 1 hour end-over-end at 4°C. 50µl (bed volume) of amylose resin, equilibrated in KHEM supplemented with DTT and complete protease inhibitor cocktail was then added and the incubation was continued for 1 hour more. The resin was then collected by centrifugation at 2500xg for 20 sec at room temperature and the supernatant was retained as the unbound fraction. The pelleted resin was held on ice and washed 3 times over 15 min, each time with 350µl KHEM supplemented with DTT and complete protease inhibitor cocktail. These washes were pooled along with

the unbound fraction and aliquots were taken for analysis by PDE enzyme assays an by immunoblotting. The bound PDE was eluted from the beads by 3 incubations end-over-end, for 10min each at 4°C with 100µl KHEM supplemented with 10mM maltose. The 3 eluted fractions were pooled and aliquots were taken for analysis by PDE enzyme assays and by immunoblotting.

2.1.14 ELISA assay for protein–protein interaction

2.1.14.1 Buffers

Tween tris buffered saline (T-TBS)

10mM	Tris HCl, pH 7.6
137mM	NaCl
0.05% (v/v)	Tween 20

Blocking buffer

1% (w/v)	Skimmed milk powder in T-TBS

Fixing Buffer

2.7mM	KCl
137mM	NaCl
4mM	Na_2HPO_4
0.15mM	NaH_2PO_4, pH 7.4
4% (v/v)	Paraformaldehyde

2.1.14.2 Procedure

1.5pmol of either MBP or of MBP–PDE fusion protein, diluted in 100µl T-TBS was incubated in each well of a 96 well microtiter plate for 1 hour at room temperature. This allowed the fusion protein to become adsorbed onto the plastic of the microtiter plate. The plate was then washed 3 times with 200µl T-TBS per well to remove any unbound fusion protein. 200µl blocking buffer was added to each well and the

plate was incubated at room temperature for 1 hour to block any unoccupied protein binding sites in the wells. The blocked wells were then washed 3 times with 200µl T-TBS per well and probed with varying concentrations of GST or of GST–SH3 domain fusion proteins diluted in 100µl blocking buffer, for 3 hours at room temperature. The plate was then cooled on ice for 2 min and the wells were rapidly washed 3 times with 200µl ice cold T-TBS per well. The bound GST fusion protein was then fixed by the addition of 100µl fixing buffer and incubation for 30 min at room temperature. The plate was washed 10 times with 200µl T-TBS per well. Bound GST fusion proteins were detected by the addition of 100µl per well anti-GST polyclonal antisera diluted 1:10000 in blocking buffer for 1 hour at room temperature. The plate was then washed 3 times with 200µl T-TBS per well and 100µl per well alkaline phosphatase conjugated anti-rabbit IgG (Sigma) diluted 1:2000 in blocking buffer was added for 1 hour at room temperature. The plate was then washed a further 3 times with 200µl T-TBS per well and the binding of second antibody was detected using the BCIP Microwell 2 Component Phosphatase Substrate System (KPL, Maryland, USA), following the manufactures instructions. The colour development was quantified using a MRX microtiter plate reader (Dynex Technologies) set to read at a wavelength of 630nM.

2.1.15 Quantification of protein (Bradford's assay)

Protein assays were conducted on 96 well microtiter plates. A spectrophotometric standard curve of protein concentration was constructed using 0-7µg bovine serum albumin (BSA). These amounts of protein were dissolved in 50µl distilled water. To this, 200µl Bio–Rad reagent diluted 1:5 with deionised water was added. The plate was incubated for 5 min at room temperature and then the absorbance was read at a wavelength of 590nm using a MRX microtiter plate reader (Dynex Technologies). Protein concentrations of the samples were determined on the same microtiter plate and simultaneously with the standard curve by diluting a known volume of the sample in 50µl distilled water, adding 200µl Bio–Rad reagent diluted 1:5 with distilled water and reading the absorbance in the plate reader. All samples were assayed in triplicate. Protein concentrations were determined by plotting the standard curve and using least squared regression analysis to determine the line of best fit. The

equation of the line was used to determine the protein concentration of the samples.

2.2 Cell Culture

2.2.1 The COS-7 cell line (ATCC Number: CRL-1651)

The COS cell lines (COS-1, COS-3 and COS-7) are simian (African green monkey) kidney cell lines derived from the CV-1 line by transfection with an origin-defective mutant of the Simian virus 40 (SV40) virus. The cells contain integrated copies of the early region of SV40 encoding the SV40 T antigen. This facilitates the overexpression of proteins in these lines by transient transfection as the presence of the SV40 T antigen allows plasmids that contain an SV40 origin of replication to be replicated in the COS cell lines (69).

2.2.1.1 Maintenance of COS-7 cells

COS-7 cells were maintained in continuous culture as a monolayer at 37°C in an atmosphere of 5% CO_2. The growth medium was a standard Dulbecco's modified Eagle's medium (DMEM) supplemented with 2mM L-glutamine, 10% (v/v) fetal calf serum, 1 unit/ml penicillin and 1mg/ml streptomycin. The COS cell lines have a fibroblast like morphology and will shed cells upon reaching confluency. The cells were passaged at approximately 90% confluency at which time they were split 1:3–1:6. Under this regime the cells needed to be passaged every 2–4 days. Due to the willingness of the COS cell lines to support the growth of viruses and the possibility of their containing a complete SV40 region these lines were regarded as being potentially biohazardous material.

2.2.2 Transient transfection with DAE-Dextran

2.2.2.1 Buffers

TE buffer

10mM Tris-HCl pH 7.2

1mM	EDTA

Transfection medium

DMEM supplemented with

2mM	Glutamine
10% (v/v)	Newborn calf serum
1unnit/ml	Penicillin
1mg/ml	Streptomycin
0.1mM	Chloroquine

PBS

2.7mM	KCl
137mM	NaCl
4mM	Na_2HPO_4
0.15mM	NaH_2PO_4, pH 7.4

Shock buffer

10% (v/v)	DMSO in PBS

2.2.2.2 Transfection procedure

The cells were passaged 24 hours before transfection and seeded onto new plates at approximately 50% confluency. The cells were transfected with 10µg plasmid DNA per 79cm^2 plated cells. Prior to transfection the DNA was diluted to 40ng/µl in sterile TE buffer, then further diluted 5:9 in sterile DEAE dextran solution (10mg/ml in PBS). This mixture was incubated for 15 min at room temperature to allow the formation of DNA–DEAE complexes. The growth medium was aspirated from the cells and replaced with transfection medium. 5ml transfection medium was added for every 79cm^2 plated cells. The DNA-DEAE dextran mixture was dropped onto the cells and mixed by swirling. The cells were then incubated at 37°C in an atmosphere

of 5% CO_2 for 3–4 hours. Following this incubation the cells were shocked with DMSO; the transfection medium was removed by aspiration or by pouring, replaced with an equal volume of shock buffer and then incubated for exactly 2 min at room temprature. The cells were then washed once in PBS, transferred to growth medium and incubated at 37°C for approximately 72 hours in an atmosphere of 5% CO_2. The cells were then harvested. Mock transfections were performed by treating the cells exactly as described above but omitting DNA from the mixtures.

2.2.3 Harvesting and subcellular fractionation

2.2.3.1 Buffers

KHEM

50mM	Hepes KOH, pH7.4
50mM	KCl
10mM	EGTA
1.92mM	$MgCl_2$

2.2.3.2 Harvesting and fractionation by differential centrifugation

Approximately 72 hours after transfection the growth medium was removed from the cells. The cells were then rinsed once with 5ml ice cold KHEM per 79cm^2 plated cells before being incubated for 10min at 4°C in 2ml ice cold KHEM supplemented with 1mM DTT and protease inhibitors, per 79cm^2 plated cells. The cells were then rinsed once more with 1ml ice cold KHEM supplemented with 1mM DTT and protease inhibitors, per 79cm^2 plated cells, drained and harvested by scraping. The harvested cells were made up to a known volume (usually 500µl/79cm^2 plated cells harvested) by the addition of ice cold KHEM supplemented with 1mM DTT and protease inhibitors and then disrupted by 20 strokes in a Dounce glass on glass homogenizer. Lactate dehydrogenase (a marker enzyme for cytosol) assays show that this method routinely achieves >96% cell breakage.

The cell homogenate was fractionated by differential centrifugation to produce a low

speed (850g) pellet fraction (P1) enriched in nuclear and cytoskeletal components; a high speed (100000g) pellet fraction (P2) enriched in plasma membranes, vesicles formed from the Golgi apparatus and the endoplasmic reticulum, lysosomes and endosomes; and a high speed (100000g) supernatant (S2) fraction enriched in cytosolic proteins (193).

The P1 pellet fraction was generated by centrifuging the cell homogenate for 5 min at 850g at 4°C. The P1 pellet was washed twice by being resuspended in ice cold KHEM supplemented with 1mM DTT and protease inhibitors and finally resuspended in an equal volume of ice cold KHEM supplemented with 1mM DTT and protease inhibitors to that of the S2 fraction. The P2 pellet fraction and the S2 fraction were generated by centrifuging the supernatant from the P1 pellet for 1 hour at 100000g at 4°C. The P2 pellet was washed twice by being resuspended in ice cold KHEM supplemented with 1mM DTT and protease inhibitors and finally resuspended in an equal volume of ice cold KHEM supplemented with 1mM DTT and protease inhibitors to that of the S2 fraction. Each of the cell fractions was aliquoted and snap frozen in liquid nitrogen then stored at -80°C until use.

2.2.4 Lactate Dehydrogenase Assay

Lactate dehydrogenase (LDH) activity was assayed by the reverse reaction:

Pyruvate + NADH → Lactate + NAD

The progress of this reaction was performed in a 96 well microtiter plate and the conversion of NADH to NAD was measured spectrophotometrically using a MRX microtiter plate reader (Dynex Technologies) set at a wavelength of 340nm.

For the measurement of free LDH activity the following reaction was set up:

186µl	0.15M Tris-HCl, pH7.4
7µl	10mM Na pyruvate
7µl	sample to be assayed

The reaction was started by the addition of 10µl 2mM β-NADH and readings were taken at 20sec intervals for 10min.

For the measurement of occluded LDH activity the following reaction was set up:

172µl	0.15M Tris-HCl, pH7.4
7µl	10mM Na pyruvate
14µl	30% Triton X-100
7µl	sample to be assayed

The reaction was started by the addition of 10µl 2mM β-NADH and readings were taken at 20sec intervals for 10min

In all cases the assays were performed in triplicate.

The initial rate of decrease in the absorbance at 340mM was taken to be directly proportional to the LDH activity present in the sample.

2.3 Molecular Techniques

2.3.1 Electrophoresis of DNA

2.3.1.1 Buffers

Tris acetate electrophoresis (TAE) buffer (50X stock)

2M	Tris base
1M	Acetic acid
0.05M	EDTA

2.3.1.2 Casting an agarose minigel

200 ml 1X TAE was prepared for each minigel. 20 ml of agarose suspension was made up in 1X TAE at the desired concentration (w/v) in a small conical flask and

the flask was weighed. This suspension was heated in a microwave until the agarose dissolved. Once this occurred, the flask was reweighed and made up to the original weight with distilled water. 1.7µl ethidium bromide was then added to the molten agarose and mixed by swirling before the agarose was poured into the casting tray of a minigel apparatus and allowed to set. The remaining TAE was then used to fill the tank. Samples were loaded into the wells of the gel after mixing with 6X loading dye (Promega) and the gel was run at 75V.

Range of Separation of linear DNA molecules according to agarose concentration.

Percentage gel	Size of fragment (kilobases)
0.9	0.5–7
1.2	0.4–6
1.5	0.2–3
2.0	0.1–2

2.3.1.3 Recovery of DNA from agarose gels

The recovery of DNA from agarose gels was achieved using the QIAquick gel extraction kit (QIAgen) according to the manufacturers instructions.

2.3.2 Large scale plasmid purification

The large scale purification of plasmid DNA was achieved using either the Promega Wizard™ maxiprep kit or the Qiagen QIAprep maxiprep kit according to the manufacturers instructions.

2.3.3 Small scale plasmid purification

The small scale purification of plasmid DNA was achieved using either the Promega Wizard™ miniprep kit or the Qiagen QIAprep spin miniprep kit according to the manufacturers instructions.

2.3.4 Quantification of DNA and RNA

Both DNA and RNA were quantified spectrophotometricly. A known volume of DNA or RNA solution was diluted to 1ml with distilled water and absorbance measurements were taken at 260nM and 280nM using a Shimadzu UV-1201 UV-VS spectrophotometer blanked on distilled water. The concentration of nucleic acid was then calculated using the following approximations:

An absorbance of 1 at 260nM corresponds to	50µg/ml double stranded DNA
	37µg/ml single stranded DNA
	40µg/ml single stranded RNA

The ratio between the absorbance measurements at 260nM and 280nM provided an indication of the purity of the nucleic acid. In solution, pure DNA and RNA typically have A_{260}:A_{280} ratios of 1.8 and 2.0, respectively. If the absorbance ratio is significantly less than this it indicates that the nucleic acid may be contaminated with either phenol or with protein.

2.3.5 Polymerase chain reaction (PCR)

2.3.5.1 PCR Reaction mix

50mM	KCl (Supplied 10X in Taq polymerase buffer)
10mM	Tris HCl (pH9) (Supplied 10X in Taq polymerase buffer)
200µM	dATP
200µM	dTTP
200µM	dGTP
200µM	dCTP
0.5µM	5' (sense) primer
0.5µM	3' (antisense) primer
1.5mM	$MgCl_2$
<1µg	Template cDNA
5 units	Taq DNA polymerase

2.3.5.2 Procedure

The PCR reaction mix was assembled in a sterile 0.5ml Eppendorf tube and cycled in a Techgene thermocycler PCR machine. The cycling conditions were optimised for each PCR reaction, typical conditions were:

Segment 1: 2 cycles

Denaturation	30 sec 94°C
Annealing	30 sec 37°C
Extension	30 sec 72°C

Segment 2: 28 cycles

Denaturation	30 sec 94°C
Annealing	30 sec at 8°C below the predicted melting temperature of the primers
Extension	30 sec 72°C

2.3.6 Site directed mutagenesis using the QuickChange™ kit

Site directed mutagenesis was performed using the QuickChange™ kit (Stratagene) according to the manufacturers instructions. Briefly, 2 complementary oligonucleotides each containing the desired mutation, flanked by unmodified sequence were generated and purified by high pressure liquid chromatography (HPLC). A series of 3 reactions was set up using various concentrations of template DNA (10ng, 25ng and 50ng). The concentration of the complementary primers was kept constant, at 125ng of each primer, in all 3 reactions. The components in the reactions were as follows:

5µl	10X reaction buffer (supplied with the kit)
xµl	template DNA plasmid
125ng	sense primer
125ng	antisense primer
1µ	dNTP mix (supplied with the kit)

sterile, deionised water to 50µl

2.5 units *Pfu* DNA ploymerase

The reaction mixes were assembled in sterile 0.5ml Eppendorf tubes and cycled in a Techgene thermocycler PCR machine. The cycling conditions were:

Segment 1: 1 cycle

Denaturation 30 sec 95°C

Segment 2: 12-18 cycles

Denaturation 30 sec 95°C
Annealing 1 min 55°C
Extension 2 min/kb of template plasmid 68°C

The number of cycles used in segment 2 depended upon the type of mutation desired: point mutations 12 cycles, single codon change 16 cycles, multiple codon deletions or insertions 18 cycles.

After the temperature cycling the reactions were cooled to below 37°C then 10 units DpnI restriction enzyme was added to each reaction and the tubes were incubated at 37°C for 1 hour. The DpnI restriction enzyme digests methylated but not non methylated DNA. Therefore this digestion serves to degrade the template DNA but not the newly synthesised DNA that includes the mutation. After this digestion the Dpn-I treated DNA from each of the reactions was used to transform *E.coli* XL1-Blue supercompetent cells (supplied with the kit).

2.3.7 RNA isolation

Pre-weighed tissue was homogenised in Tri-Reagent (1ml per 50-100mg tissue) using a sterilised glass homogeniser. Alternatively, one flask of a cell monolayer was scraped into 1ml of Tri-Reagent and resuspended with a pipette. The homogenate was stored at room temperature for 5 min. It was then transferred in 1ml aliquots to

sterile Eppendorf tubes. The homogenate was centrifuged at 12000g at 4°C to remove the cell membranes, polysaccharides and high molecular weight DNA. The supernatant was transferred to a fresh, sterile Eppendorf tube. The RNA and DNA were phase separated by the addition of 0.2ml RNAse-free chloroform per 1ml of Tri-Reagent. The solution was mixed by vortexing for 15 sec then stored at room temp for 3min. Phase partition was brought about by centrifugation at 12000g for 15 min at 4°C. The aqueous phase was transferred to a fresh, sterile Eppendorf tube and the RNA was precipitated by the addition of isopropanol (propan-2-ol): 0.5ml per 1ml of Tri-Reagent initially used. The precipitation was allowed to continue for 5–10 min at room temperature before the RNA was pelleted by centrifugation at 12000g for 10 min at 4°C. The supernatant was removed by aspiration and the pellet was washed in 1ml 75% ethanol. In this state the RNA can be stored for up to a year at -20°C.

2.3.8 First strand complementary DNA (cDNA) synthesis

2.3.8.1 buffers

cDNA synthesis reaction mixture

11µl	"Bulk 1st strand cDNA mix" (supplied with kit)
1µl	DTT solution (supplied with kit)
1µl	"Not1-d(T)18" (0.2 µg/µl) primer (supplied with kit) diluted 1:25 with distilled water
20µl	heat-denatured RNA from 1st tube

First strand cDNA was synthesised using the Pharmacia First-strand cDNA Synthesis Kit according the manufacturers instructions. Briefly 5µg of total RNA was made up to 20µl with DEPC treated distilled water. This was heated to 65°C in a thermal cycler for 10min then immediately chilled on ice. The "Bulk 1st strand cDNA mix" (supplied with the kit) was gently mixed by being pipetted up and down several times and was then collected with a brief centrifugation. The cDNA synthesis reaction mixture was assembled in a sterile 0.5ml Eppendorf tube that was chilled on ice. The cDNA

synthesis reaction was then incubated at 37°C for 1 hour.

2.3.9 DNA sequencing

DNA sequencing was performed using the ABI PRISM Dye Terminator Cycle Sequencing Ready Reaction Kit (Perkin-Elmer Corporation). Plasmid DNA samples were prepared for sequencing using the QIAprep spin miniprep kit (Qiagen) and resuspended in sterile, deionised water. The plasmid DNA (400ng) was mixed with 8µl of the Taq DyeDeoxy Terminator (ABI) reaction premix (supplied with the kit) and 3.2pmol of a sequencing primer. The reaction volume was made up to 20µl with sterile, deionised water. The sequencing reaction was then subjected to 25 rounds of thermal cycling using the following conditions:

Denaturation	96°C 30 sec
Annealing*	47°C 15 sec
Extension	60°C 4min

* This segment temperature was variable according to the primer used. The temperature shown was that used for the T7 sequencing primer (taatacgactcactataggg) and the pCR2.1 upstream primer (agctatgaccatgattacg)

After cycling the reaction products were concentrated by ethanol precipitation and the pellets sent to the Glasgow University Molecular Biology Support Unit for gel electrophoresis.

2.3.10 Sequence Aanalysis

Routine DNA and deduced amino acid sequence analysis was performed on the Gene Jockey II program. The GCG suite of software was used for similarity searching of the nucleotide and protein databases and also for sequence analyses that were not available in the Gene Jockey II program.

In all analyses of the deduced amino acid sequences of proteins the initiating methionine residue encoded by the cDNA was included in the analysis of the protein

sequence.

2.3.11 Restriction digestion of DNA

All restriction enzyme digest were performed on pure plasmid DNA using restriction enzymes supplied either by Promega, by New England Biolabs or by Boehringer Mannheim. The incubation conditions were 37°C for a minimum of 1 hour using the appropriate buffer supplied by the manufacturer.

2.3.12 Ethanol Precipitation of DNA

To the volume of DNA to be ethanol precipitated, 0.1 volume 3M sodium acetate and 2 volumes of 100% ethanol were added. The DNA mixed by vortexing and then incubated at -80°C for 30 min. The precipitated DNA was centrifuged at 12000g at 4°C for 10min to pellet the DNA. The supernatant was aspirated and 1ml of 70% ethanol added. The DNA was pelleted again by centrifugation at 12000g at room temperature for 5min. The supernatant was removed and the pellet allowed to air–dry for 5–10 minutes. The DNA was then resuspended in TE buffer or sterile, deionised water.

2.3.13 Ligation of DNA

Double stranded DNA was mixed with 100ng linearised vector DNA at 1:1 and 1:3 ratios (v/v) of vector:insert DNA and the mixture was made to 19.5µl 1X T4 DNA ligase buffer by the addition of 10X T4 DNA ligase buffer (supplied with the T4 DNA ligase. 10X T4 DNA ligase buffer is 30mM Tris-HCl, pH7.8. 100mM $MgCl_2$, 100mM DTT, 10mM ATP) and sterile, deionised water. The ligation reaction was then started by the addition of 1 unit of T4 DNA ligase (Promega). The reaction was incubated at 14°C overnight.

2.3.14 Preparation of competant cells

2.3.14.1 Buffers and media

L-broth

170mM	NaCl
0.5% (w/v)	Bacto-Yeast Extract
1 % (w/v)	Bacto-Tryptone

Transformation buffer Rf1

100mM	RbCl
50mM	$MnCl.4H_20$
30mM	Potassium acetate
10mM	$CaCl_2.2H_20$
15% (w/v)	glycerol
	pH adjusted to 5.8 with 0.2M acetic acid.
	Filter sterilised through a 0.22μ filter.

Transformation buffer Rf2

10mM	RbCl
10mM	3-(N-Morpholino)propane sulphonic acid (MOPS)
75mM	$CaCl_2.2H_2O$
15% (w/v)	glycerol
	pH adjusted to 6.8 with 0.2M NaOH.
	Filter sterilised through a 0.22μ filter.

2.3.14.2 Preparation of Competent JM109 or XL1-Blue E.coli

10ml of L-broth was inoculated with a stab from a glycerol stock of either JM109 or of XL1-Blue *E. coli* and grown overnight at 37°C with constant shaking. The next day 3ml of this culture was used to inoculate 400ml L-broth and this culture was grown at 37°C with constant shaking until the optical density at 550nm was between 0.5 and 0.55. The culture was divided equally between two sterile 250ml centrifuge bottles and cooled on ice for 30 minutes. The cooled culture was then centrifuged at 2500rpm (950g) at 4°C in a Beckman JA14 rotor for 15min and each pellet was

resuspended in 20ml of ice-cold transformation buffer Rf1. The cells were incubated on ice for a further 15min before being centrifuged at 2500rpm (950g) for 10 minutes in a Beckman JA14 rotor at 4°C. The supernatant was removed and the cell pellets were each gently resuspended in 3.5ml of transformation buffer Rf2. The resuspended cells were pooled and incubated on ice for 15 minutes. The competent cells were then snap-frozen in 250µl aliquots and stored at -80°C.

2.3.15 Transformation of *E.coli*

2.3.15.1 Media

L-broth

170mM	NaCl
0.5% (w/v)	Bacto-Yeast Extract
1 % (w/v)	Bacto-Tryptone

LB-Agar

170mM	NaCl
0.5% (w/v)	Bacto-Yeast Extract
1% (w/v)	Bacto-Tryptone
2% (w/v)	Agar

2.3.15.2 Transformation

An aliquot of frozen competent cells was thawed slowly on ice. For each transformation a 100µl aliquot of competent cells was transferred to a chilled, sterile, 17x100mm tube (Falcon 2059). To each 100µl aliquot of competent cells, approximately 100ng of DNA was added and this was incubated on ice for 30 min. The cells were then heat shocked for exactly 45 seconds at 42°C then incubated on ice for a further 2 min. 900µl of room temperature L-broth was then added and the transformed cells were incubated at 37°C for 30–60min with shaking. 100–500µl of the culture was plated on a 10cm agar plate containing a selection antibiotic. The

plate was incubated at 37°C overnight. The next morning transformed colonies were picked and glycerol stocks were made.

2.3.16 Glycerol stocks

A single colony was picked from an agar plate and used to inoculate10ml of L-broth supplemented with a selection antibiotic (usually 100μg/ml ampicillin). The culture was grown overnight at 37°C. The next morning 600μl of the overnight culture was transferred into a sterile Eppendorf tube and mixed with 300μl of sterile 45% glycerol. The glycerol stock was then stored at -80°C.

3. Interaction of type 4 phosphodiesterase with SH3 domains

3.1 Introduction

The rat PDE4A isoenzyme RNPDE4A5 and the human homologue of this protein, HSPDE4A4B can interact specifically with certain members of the Src homology 3 (SH3) class of domains for protein–protein interaction (141, 162).

SH 3 domains comprise a family of homologous, regions of sequence, approximately 60 residues in length, that occur in a wide variety of proteins (see section 1.4.1.1). SH3 domains represent genuine protein domains in that they form independently folding structures that appear to be able to fold correctly within a wide variety of different contexts and are little affected by the surrounding regions of the proteins in which they occur. These domains have a compact β-barrel structure that is formed from 5 anti-parallel β-strands. The amino and carboxyl termini of the folded domain are close together in 3 dimensional space. Thus SH3 domains can be thought of almost as distinct entities that are covalently linked to the proteins in which they are situated (148, 149, 247).

The functional role of SH3 domains is to mediate protein–protein interactions. An important role for these domains appears to be the recruitment of signalling proteins into multienzyme complexes. In this regard it is noteworthy that proteins which contain SH3 domains often also contain other classes of domain for protein-protein interactions. All members of the Src family of protein tyrosyl kinases, for instance, contain both an SH2 and an SH3 domain. This may serve to allow for the simultaneous association of a such a protein with 2 or more binding partners (168).

SH3 domains bind to regions of target proteins that are rich in proline and arginine residues. Peptide binding, phage display and crystallographic analyses have identified a consensus motif of the form PxxP as being an important determinant of binding to SH3 domains (see section 1.4.1) (1, 32, 205). Such sequences adopt a left

handed polyproline type II helical conformation that interacts with a highly conserved region, consisting mainly of aromatic residues on the surface of the SH3 domain (149, 205).

The long form PDE4A isoform RNPDE4A5 can interact specifically with certain SH3 domains, showing a preference for interaction with the SH3 domains of the Src family tyrosyl kinases Lyn and Fyn (162). The interaction of RNPDE4A5 with SH3 domains has an absolute requirement for the alternatively spliced amino terminal region of RNPDE4A5. This region of the protein is rich in proline and arginine residues and contains 3 regions of sequence that conform to the PxxP consensus motif that has been suggested to be important for binding to SH3 domains (*Figure 3.8*). It has been suggested that the 1 or more of the 3 proline rich motifs within the amino terminal region of RNPDE4A5 form the site of interaction between RNPDE4A5 and SH3 domains (162).

The human homologue of RNPDE4A5, namely HSPDE4A4B, has also recently been shown to interact with SH3 domains (141). In addition to the 3 putative SH3 domain binding motifs that are present in the alternatively spliced amino terminal region of this isoform, and that are conserved between the rat and the human proteins, there is an additional region of sequence that conforms to the motif PxxP present in the unspliced, Linker Region 2 (LR2) of human PDE4A. The LR2 of PDE4A appears to be hypervariable and is not conserved between the rat and the human sequences (see section 1.3.2.2) (141). Both an, as yet unidentified, site or sites within the alternatively spliced amino terminal region of HSPDE4A4B and also the proline and arginine rich region of sequence in the LR2 of human PDE4A can bind to SH3 domains (141).

In this chapter I will present evidence that a long splice variant of the PDE4D enzyme family, namely HSPDE4D4, can also interact with SH3 domains and that this interaction is dependent upon the alternatively spliced, amino terminal region of HSPDE4D4.

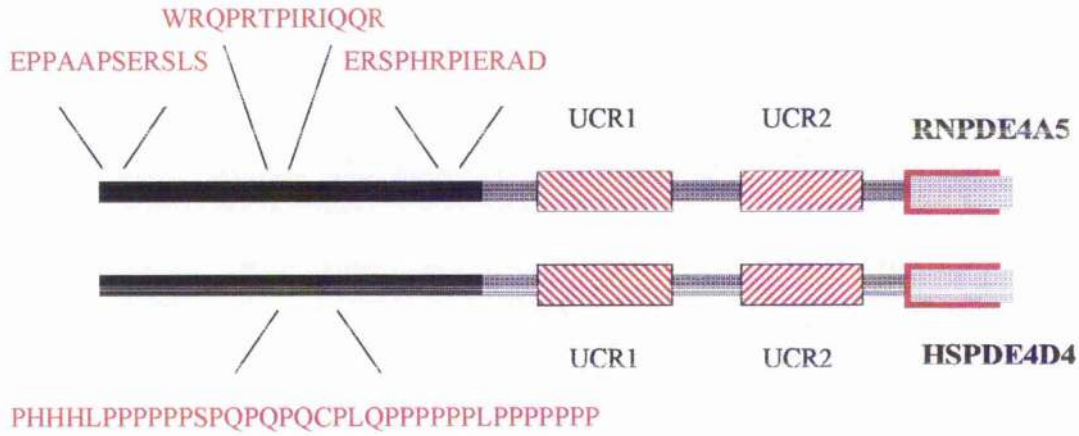

Figure 3.8: Isoforms of PDE4A and 4D contain consensus motifs for SH3 binding.

The figure shows diagrams representing the amino-terminal regions of RNPDE4A5 and HSPDE4D4. The alternatively spliced, extreme amino-terminal region of each isoform contains proline rich regions of sequence which conform to known consensus motifs for interaction with SH3 domains.

3.2 Results and discussion

It had previously been shown that both recombinant RNPDE4A5 (expressed in COS-7 cells) and rolipram sensitive, PDE4 activity from the cytosolic fraction of rat brain can specifically associate with the SH3 domains of Src and Fyn kinases (see section 3.1) (162). In this study GST fusion proteins of the SH3 domains from Src kinase and from Fyn kinase were immobilised on glutathione Sepharose resin and used as probes to identify PDEs in the cytosolic fraction of rat brain that could bind to these domains (see (162) for a description of the method used).

Immunoblots of the material from rat brain cytosol that bound to the GST–SH3 domain fusion proteins were performed using antisera specific for each of the PDE4 gene families. This revealed the presence of PDE4A (162) and PDE4D (*Figure 3.9*) but not of either PDE4B or PDE4C [J. O'Connell, personal communication]. A single isoform of PDE4A, namely RNPDE4A5, was detected in the cytosolic fraction of rat brain; this isoform was also present in the material that bound to the SH3 domain of Src kinase (162).

In these preliminary experiments 3 anti-PDE4D immunoreactive species were detected in the cytosolic fraction of rat brain. Each of these species co-migrated on SDS–PAGE with one of either recombinant HSPDE4D3, HSPDE4D4 or HSPDE4D5 (*Figure 3.9*). On this basis the 3 immunoreactive species were tentatively identified as being the rat homologues of the human HSPDE4D3, HSPDE4D4 and HSPDE4D5 isoforms, namely RNPDE4D3, RNPDE4D4 and RNPDE4D5. Only 1 of the 3 PDE4D species that were present in the rat brain cytosol was reproducibly detected in the material that bound to the SH3 domains of Src and Fyn kinases at levels above those in the material that bound to GST alone. This was the species that co-migrated, on SDS-PAGE, with recombinant HSPDE4D4 (*Figure* 3.9).

At the time this work was started the full length cDNA clone of human PDE4D4 had only just been isolated and the sequence for the rat homologue of this splice variant had not yet been cloned. Inspection of the deduced amino acid sequence of

HSPDE4D4 revealed that this protein contains proline rich sequences of a form that might be expected to interact with SH3 domains. This seemed to support the tentative identification of the PDE4D species present in rat brain cytosol and that bound to SH3 domains as being the rat homologue of HSPDE4D4.

Aberrant migration on SDS-PAGE is, however, a known feature of many PDE4 enzymes and at least 2 PDE4 isoforms are known to exhibit shifts in mobility on SDS-PAGE following stimulation of cells with various effectors (98, 132). I therefore felt that the immunoblot data alone was insufficient evidence to positively identify the rat PDE4D isoform as RNPDE4D4.

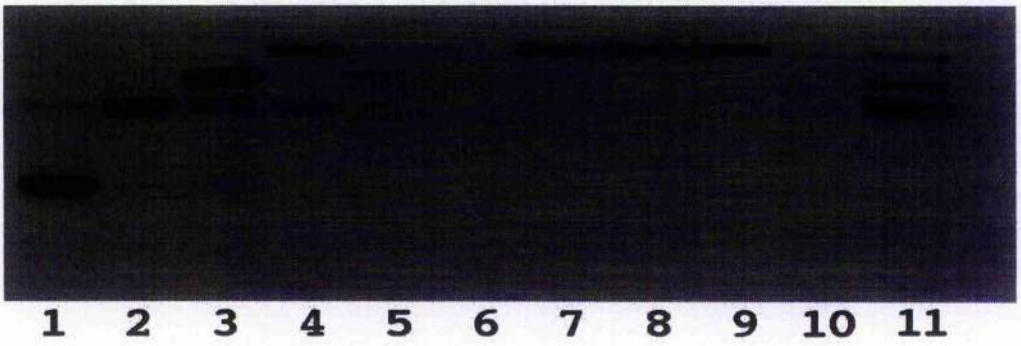

Figure 3.9: Endogenous PDE4D4 from Rat Brain Cytosol Binds to SH3 Domains

The figure shows an immunoblot of PDE4D species "pulled down" from rat brain cytosol by the SH3 domains of Src and Fyn, expressed as fusion proteins with GST and immobilised on glutathione Sepharose. Lanes 1–4 are cytosolic fractions from COS-7 cells overexpressing HSPDE4D1, HSPDE4D3, HSPDE4D5 and HSPDE4D4 respectively. Lanes 6–9 are the bound fractions from 100μg rat brain cytosol challenged with GST, GST-Src SH3, GST-Src SH2/3 and GST-Fyn SH3 respectively. Lane 11 is 25μg rat brain cytosol. The primary antibody used was the monoclonal antibody 61D10E (ICOS) that detects the common region of PDE4D isoforms. The secondary antibody was a horsradish peroxidase conjugated anti-mouse IgG, polyclonal antisera (Sigma).
Source: (161)

3.2.1 RT–PCR of RNPDE4D4 from rat brain

To support the hypothesis that the PDE4D isoform that is present in rat brain cytosol and that can interact with the SH3 domains of Src and Fyn kinases was RNPDE4D4, the rat homologue of HSPDE4D4, I decided to confirm the existence of this isoform using reverse transcriptase polymerase chain reaction (RT–PCR) analysis of RNA isolated from rat brain.

3.2.1.1 Optimisation of PCR conditions for amplification of PDE4D4

Primers AP10 and AP11, intended to amplify the entire alternatively spliced region of PDE4D4, were designed against the known human and, in the case of the antisense primer (AP11), rat sequences (*Figure 3.10, Table 3.3.1*). The plasmid pCMVPDE4D4, which contains the complete open reading frame for HSPDE4D4, was used as a source of template for the optimisation of PCR conditions.

Reactions were performed to test a range of Mg^{2+} and DMSO concentrations and various different cycling conditions. The 5' region of the cDNA encoding HSPDE4D4 is rich in guanine (G) and cytosine (C) residues (76% over the target region). It is possible the G–C rich character of this template could lead to incomplete melting of the DNA and hence poor amplification. In order to address this possibility, the melting temperature in these PCR reactions was set at 97°C (rather than 96°C, which is commonly used in PCR reactions). Further increases in melting temperature were found to cause a decreased signal in control reactions, presumably due to instability of Taq polymerase at temperatures in excess of 97°C. Conditions of 97°C melting temperature, 0.75mM $MgCl_2$ and 5% DMSO were found to amplify a single band of the predicted size (446 bp) (*Figure 3.11*). It has subsequently found that melting temperatures of 99°C and use of Deep Vent polymerase (New England Biolabs) can also improve amplification.

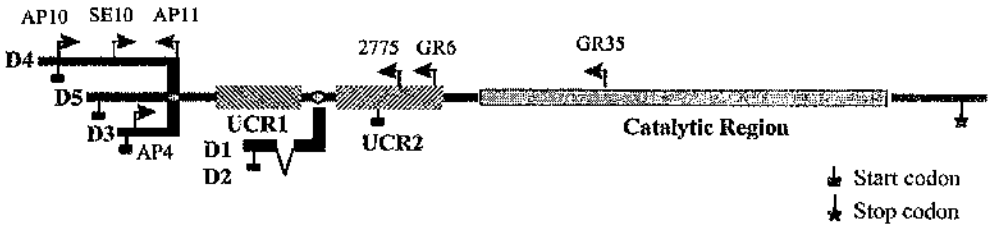

Figure 3.10: Annealing positions of primers designed against PDE4D isoforms.

The figure shows a diagram representing the known isoforms of PDE4D. The annealing positions of primers used in the RT–PCR analysis of these isoforms are indicated by arrows.

Primer	Sequence	Region of splice variant	Strand
AP10	GAGGCAGAGGGCAGCAGCG	HSPDE4D4 bp 426–444	Sense
AP11	CCTCGTTCCAGGGACTCAGGC	HSPDE4D4 bp 856–876	Antisense
SE10	AGCGCTACCTGTACTGTCG	HSPDE4D4 bp 760–778	Sense
2775	ACTTGTTGGAGGCCATCTCAC	HSPDE4D4 bp 1324–1344	Antisense
AP4	ATTTTCCGTTCAGAAGGCATTCCTGG	HSPDE4D3 bp 148–173	Sense
GR6	CCTGGTTGCCAGACCGACTCATTTCA	HSPDE4D4 bp 1382–1407	Antisense
GR35	GATC(CT)ACATCATGTATTGCACTGGC	HSPDE4D4 bp 1914–1938	Antisense

Table 3.3.1: Primers used in the RT–PCR analysis of PDE4D isoforms.

The table shows the sequences and annealing positions of the primers used in the RT–PCR analysis of PDE4D isoforms.

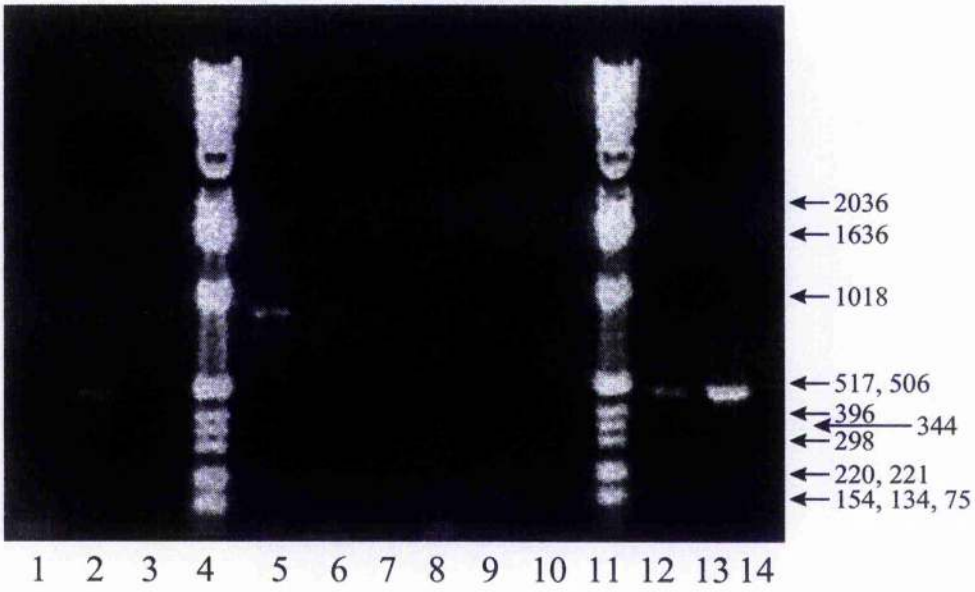

Figure 3.11: Optimisation of PCR conditions.

The figure shows products of PCR reactions performed with a range of Mg^{2+} and DMSO concentrations. Lanes 1–3 are 1.5μM $MgCl_2$ with 0, 2.5 and 5% DMSO respectively. Lanes 5–7 are 3μM $MgCl_2$ with 0, 2.5 and 5% DMSO respectively. Lanes 8–10 are 5μM $MgCl_2$ with 0, 2.5 and 5% DMSO respectively. Lanes 12–14 are 0.75μM $MgCl_2$ with 0, 2.5 and 5% DMSO respectively. Lanes 4 and 11 contain 1Kb ladder marker DNA (Gibco). The arrows indicate the molecular wetghts of the bands in the marker lanes.

3.2.1.2 RT–PCR of PDE4D4 from rat brain, total RNA

First strand cDNA was synthesised from rat brain, total RNA using MMLV reverse transcriptase (First-strand cDNA Synthesis Kit, Pharmacia) and the primer GR35, which is specific for PDE4D gene products (see Section 2.3.8). The cDNA was then probed for PDE4D4 by PCR, for 30 cycles under the optimised conditions. This reaction, however, failed to amplify the predicted 446 bp product.

There are several possible explanations for failing to obtain a signal in the above RT–PCR reaction. Amplification of the extreme 5' region of the PDE4D4 open reading frame is problematic even when using good quality plasmid DNA as the template; this is possibly due to the G–C rich character of the sequence. PDEs have a low abundance in native cells. The corresponding mRNA might also be present at low levels, making detection difficult. Furthermore, the sense primer AP10 was designed against the human sequence and was not degenerate; therefore regions of mismatch with the rat sequence were likely. In order to address at least some of these possibilities RT–PCR was attempted using the primers SE10 and 2775 (*Figure 3.10, Table 3.3.1*). These primers were designed to amplify a 585 bp region of PDE4D4 which overlaps the splice junction with PDE4D3 and does not include the G–C rich region of sequence at the extreme 5' end of the open reading frame. Amplification of RNPDE4D3 using primers AP4 and GR6 (*Figure 3.10, Table 3.3.1*) was performed in parallel to serve as a positive control for the cDNA synthesis reaction.

First strand cDNA was synthesised from rat brain total RNA using the primer GR35 (see section 2.3.8). This cDNA was probed for RNPDE4D4 and for RNPDE4D3 by PCR using the primers SE10 and 2775 (RNPDE4D4) and AP4 and GR6 (RNPDE4D3). Bands of the predicted sizes were amplified by both pairs of primers, corresponding to RNPDE4D4 (585 bp) and to RNPDE4D3 (561 bp) (*Figure 3.12*). The products from the RT–PCR amplification of PDE4D4 were then TA cloned into the plasmid pCR®2.1 (Invitrogen). The recombinant pCR®2.1 containing the RT–PCR reaction products was transformed into INVαF' One Shot™ Competent *E.coli* (Invitrogen). Several colonies containing recombinant plasmid (selected by blue–

white screening) were then picked and the inserts were sequenced (see section 2.3.9). Sequence alignment revealed 94.9% homology between HSPDE4D4 and the consensus sequence generated from the products of the RT–PCR reaction. Within the region of homology between PDE4D4 and PDE4D3, the amplified sequence aligned with the rat sequence at points of mismatch between rat and human sequences (*Figure 3.13*). The cDNA sequence of RNPDE4D4 was subsequently cloned by another group (accession number AF031373). The sequence of this cDNA matches that of the amplified fragment, providing further evidence to support the identification of the PDE4D isoform present in rat brain cytosol which can interact with SH3 domains as RNPDE4D4.

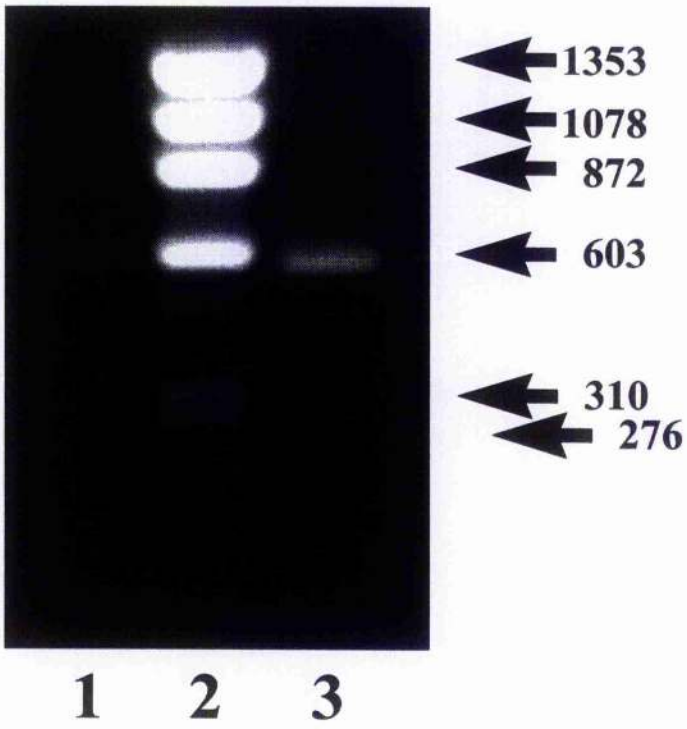

Figure 3.12: RT–PCR of PDE4D from Rat Brain

The figure shows the products of RT–PCR reactions (from rat brain, total RNA) run on a 1.5% agarose mini-gel and visualized under UV illumination by staining with ethidium bromide. Lane 1 contains the products using primers designed to amplify PDE4D4 (predicted size 585 bp), lane 2 contains Hae III phiX174 DNA markers (bands are 1353, 1078, 872, 603, 310 and 276 bp), lane 3 contains the products using primers designed to amplify PDE4D3 (predicted size 561 bp).

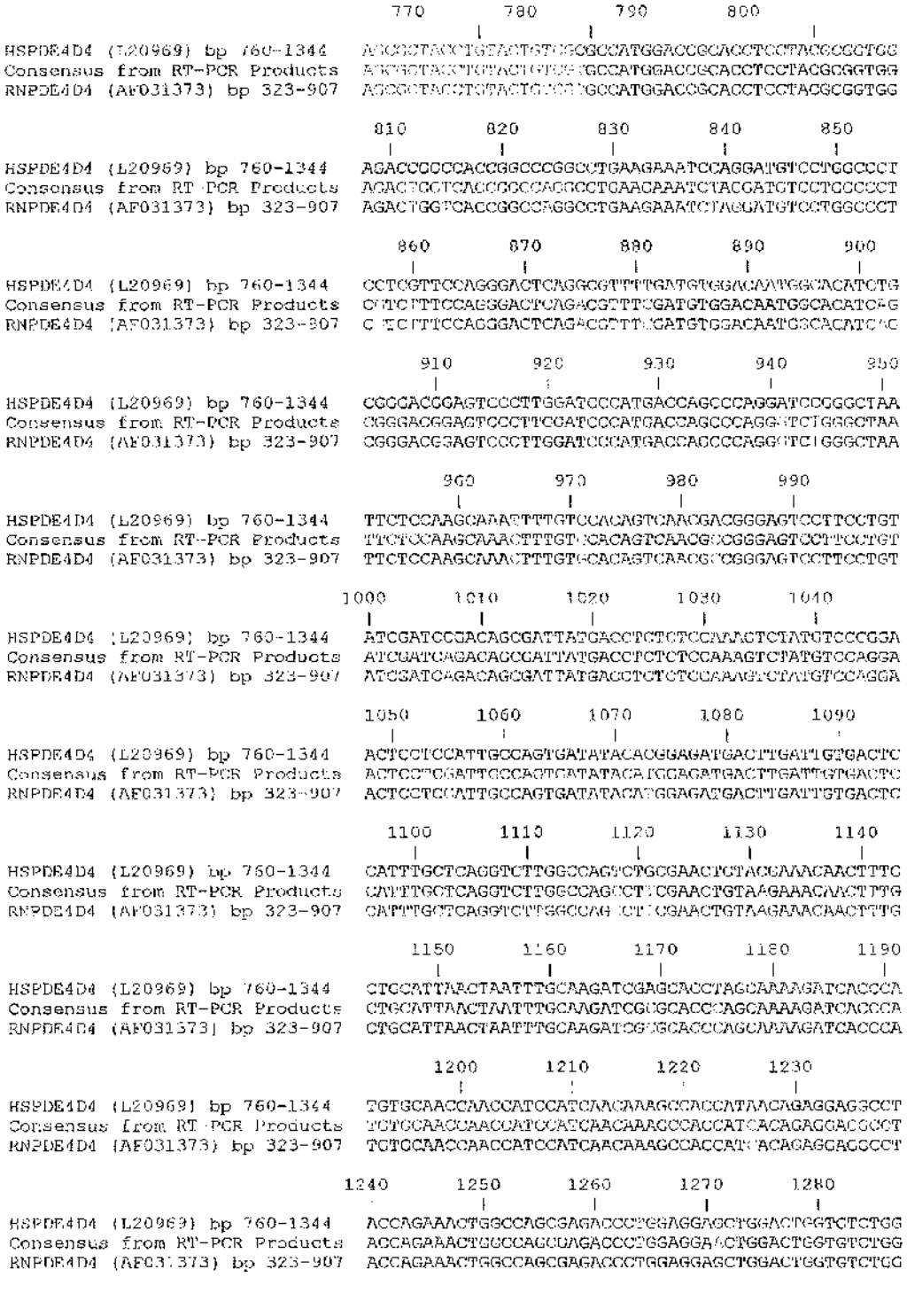
770 780 790 800
HSPDE4D4 (L20969) bp 760-1344
Consensus from RT-PCR Products
RNPDE4D4 (AF031373) bp 323-907
810 820 830 840 850
HSPDE4D4 (L20969) bp 760-1344 AGACCCCCCACCGGCCCGGCCTGAAGAAATCCAGGATGTCCTGGCCCT
Consensus from RT-PCR Products AGACTGGTCACCGGCCAGGCCTGAACAAATCTACGATGTCCTGCCCCT
RNPDE4D4 (AF031373) bp 323-907 AGACTGGTCACCGGCCAGGCCTGAAGAAATCTAGGATGTCCTGGCCCT
860 870 880 890 900
HSPDE4D4 (L20969) bp 760-1344 CCTCGTTCCAGGGACTCAGGCGTTTTGATGTGGACAATGGCACATCTG
Consensus from RT-PCR Products CCTCTTTCCAGGGACTCAGACGTTTCGATGTGGACAATGGCACATCTG
RNPDE4D4 (AF031373) bp 323-907 C TCTTTCCAGGGACTCAGACGTTTCGATGTGGACAATGGCACATCTG
910 920 930 940 950
HSPDE4D4 (L20969) bp 760-1344 CGCCACCGAGTCCCTTGGATCCCATGACCAGCCCAGGATCCGGGCTAA
Consensus from RT-PCR Products CGGGACGGAGTCCCTTCGATCCCATGACCAGCCCAGGATCTGGGCTAA
RNPDE4D4 (AF031373) bp 323-907 CGGGACGGAGTCCCTTGGATCCCATGACCAGCCCAGGATCTGGGCTAA
960 970 980 990
HSPDE4D4 (L20969) bp 760-1344 TTCTCCAAGCAAACTTTGTCCACAGTCAACGACGGGAGTCCTTCCTGT
Consensus from RT-PCR Products TTCTCCAAGCAAACTTTGTCCACAGTCAACGCCGGGAGTCCTTCCTGT
RNPDE4D4 (AF031373) bp 323-907 TTCTCCAAGCAAACTTTGTCCACAGTCAACGCCGGGAGTCCTTCCTGT
1000 1010 1020 1030 1040
HSPDE4D4 (L20969) bp 760-1344 ATCGATCCGACAGCGATTATGACCTCTCTCCAAAGTCTATGTCCCGGA
Consensus from RT-PCR Products ATCGATCAGACAGCGATTATGACCTCTCTCCAAAGTCTATGTCCAGGA
RNPDE4D4 (AF031373) bp 323-907 ATCGATCAGACAGCGATTATGACCTCTCTCCAAAGTCTATGTCCAGGA
1050 1060 1070 1080 1090
HSPDE4D4 (L20969) bp 760-1344 ACTCCTCCATTGCCAGTGATATACAGGAGATGACTTGATTGTGACTC
Consensus from RT-PCR Products ACTCCTCGATTGCCAGTGATATACATCGAGATGACTTGATTGTGACTC
RNPDE4D4 (AF031373) bp 323-907 ACTCCTCCATTGCCAGTGATATACATCGAGATGACTTGATTGTGACTC
1100 1110 1120 1130 1140
HSPDE4D4 (L20969) bp 760-1344 CATTTGCTCAGGTCTTGGCCAGCCTGCGAACTGTAAGAAACAACTTTC
Consensus from RT-PCR Products CATTTGCTCAGGTCTTGGCCAGCCTCCGAACTGTAAGAAACAACTTTG
RNPDE4D4 (AF031373) bp 323-907 CATTTGCTCAGGTCTTGGCCAGCCTCCGAACTGTAAGAAACAACTTTG
1150 1160 1170 1180 1190
HSPDE4D4 (L20969) bp 760-1344 CTCCATTAACTAATTTGCAAGATCGAGCACCTAGCAAAAGATCACCCA
Consensus from RT-PCR Products CTGCATTAACTAATTTGCAAGATCGCGCACCCAGCAAAAGATCACCCA
RNPDE4D4 (AF031373) bp 323-907 CTGCATTAACTAATTTGCAAGATCGCGCACCCAGCAAAAGATCACCCA
1200 1210 1220 1230
HSPDE4D4 (L20969) bp 760-1344 TGTGCAACCAACCATCCATCAACAAAGCCACCATAACAGAGGAGGCCT
Consensus from RT-PCR Products TGTGCAACCAACCATCCATCAACAAAGCCACCATCACAGAGGACGCCT
RNPDE4D4 (AF031373) bp 323-907 TGTGCAACCAACCATCCATCAACAAAGCCACCATCACAGAGGACGCCT
1240 1250 1260 1270 1280
HSPDE4D4 (L20969) bp 760-1344 ACCAGAAACTGGCCAGCGAGACCCTGGAGGAGCTGGACTGGTGTCTGG
Consensus from RT-PCR Products ACCAGAAACTGGCCAGCGAGACCCTGGAGGAGCTGGACTGGTGTCTGG
RNPDE4D4 (AF031373) bp 323-907 ACCAGAAACTGGCCAGCGAGACCCTGGAGGAGCTGGACTGGTGTCTGG

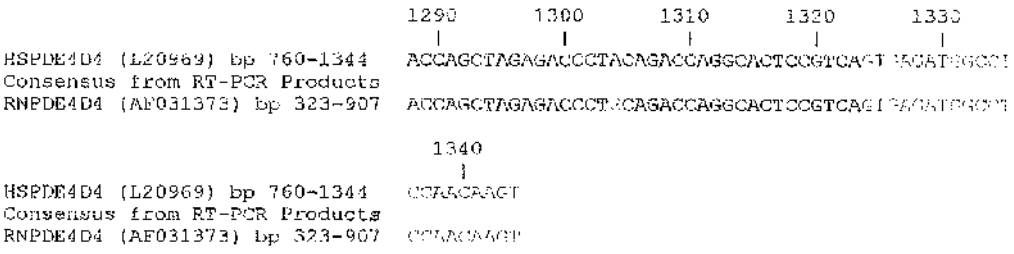

Figure 3.13: Alignment of the sequences of HSPDE4D4, RNPDE4D4 and the products of RT–PCR reactions from rat brain total RNA.

The figure shows a multiple alignment of the sequences of HSPDE4D4 and RNPDE4D4 with the consensus sequence from the products of RT–PCR reactions from rat brain total RNA using the primers SE10 and 2776. The sequences of the primers are coloured blue and regions of mismatch between the rat and human sequences are coloured red. Mismatch between the RT–PCR sequence and that of RNPDE4D4 is coloured green. This mismatch probably represents a point mutation which occurred during the PCR amplification step of the RT–PCR.

3.2.2 Optimisation of the pull down assay for protein–protein interaction

The RT–PCR data showed that RNPDE4D4, the rat homologue of HSPDE4D4, is expressed in rat brain. The immunoblot data showed that, of the 3 PDE4D immunoreactive species detected in rat brain cytosol, only 1 species, that co-migrated with HSPDE4D4 on SDS-PAGE, bound to the SH3 domains of Src and Fyn kinases. Taken together these data suggested that the PDE4D splice variant RNPDE4D4 is expressed in rat brain and that this species may be able to interact specifically with SH3 domains.

The model system of COS-7 cells transiently transfected to express recombinant PDEs has previously been used to investigate interactions between isoforms of PDE4A and SH3 domains. In these studies pull down assays were successfully used to assess the ability of transfected PDEs to interact with individual SH3 domains (141, 161, 162). I therefore decided to use this strategy to investigate further the interaction of PDE4D4 with SH3 domains.

I intended to use pull down assays to assess the ability of recombinant HSPDE4D4, expressed in COS-7 cells, to interact with a library of 22 GST fusion proteins so as to probe for possible protein–protein interactions with a variety of domains. Initially, however, I performed a series of control experiments to ensure that the pull down assay for protein–protein interaction was working in my hands.

3.2.2.1 Induction and purification of fusion proteins

Fusion proteins were expressed in JM109 *E.coli* and purified by a single step of affinity chromatography using glutathione Sepharose resin. The purifications were monitored on Coomassie stained SDS–PAGE gels (*Figure 3.14*). With 17 of the fusion proteins a strong band of the predicted molecular weight was observed on the Coomassie stained gels. This indicated that the affinity chromatography step resulted in a reasonable degree of purification for of each of these fusion proteins.

In the cases of the fusion proteins representing full length Src kinase, the 1st and 3rd WW domains of Nedd 4, the WW domain of FE65 and the WW domain of

dystrophin, a strong band of the predicted molecular weight was not observed on the Coomassie stained gels. In each of these cases, however, a band that co-migrated with GST was present. When the crude lysate from *E.coli* expressing these fusion proteins was visualised on a Coomassie stained gels strong, novel bands of the appropriate weights for these fusion proteins were present. This indicated that, under the conditions used, these fusion proteins were unstable and became degraded during the purification procedure. The reason that I was unable to purify these fusion proteins therefore was not due to premature termination or instability of the protein within the intact *E.coli*.

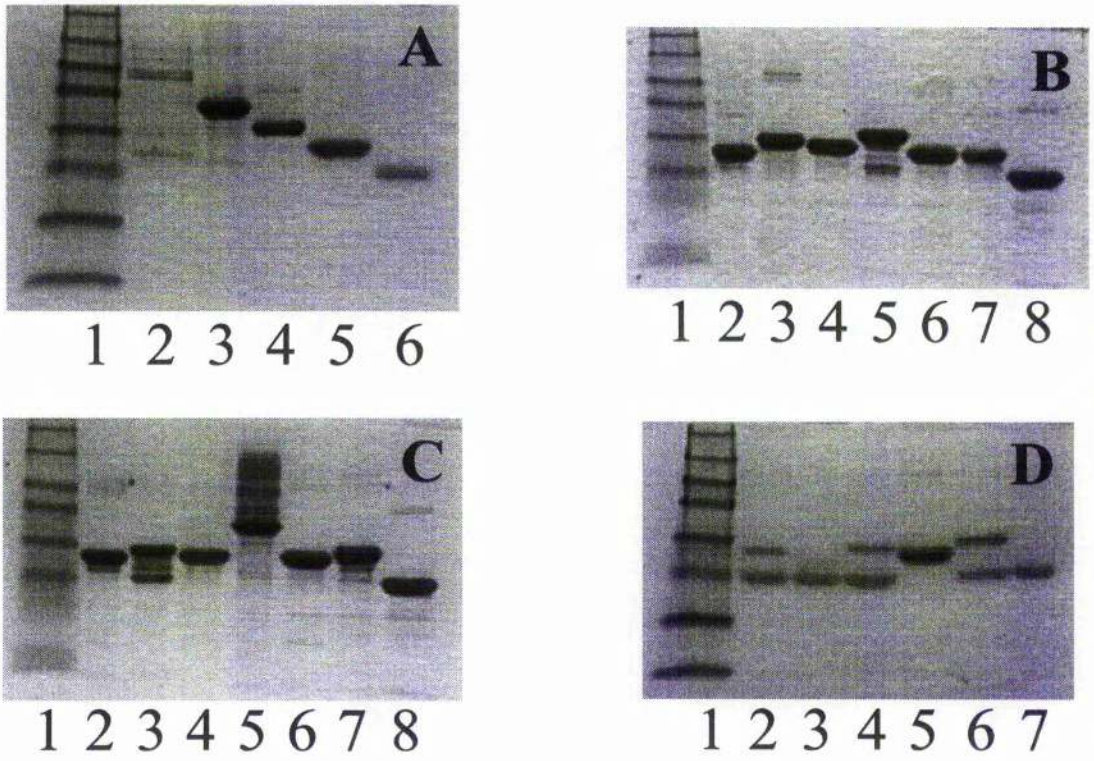

Figure 3.14: Purification of GST fusion proteins

The figure shows Coomassie stained gels of GST fusion proteins purified by a single step of affinity chromatography onto glutathione Sepharose resin. Panel A: lane 1 is molecular weight markers (New England Biolabs: MBP-b-galactosidase 175kDa, MBP-paramyosin 83kDa, Glutamic dehydrogenase 62kDa, Aldolase 47.5kDa, Triosephosphate isomerase 32.5kDa, b-Lactoglobulin A 25kDa, Lysozyme 16.5kDa); lanes 2–5 are GST fusions with full length Src, Src SH2/3, Src SH2 and Src SH3 respectively; lane 6 is GST. Panel B: lane 1 is molecular weight markers (New England Biolabs); lanes 2–7 are GST fusions with Abl SH3, Csk SH3, Lck SH3, Crk SH3, Fyn SH3 and Lyn SH3 respectively; lane 8 is GST. Panel C: lane 1 is molecular weight markers (New England Biolabs); lanes 2–7 are GST fusions with Grb-C SH3, Grb-N SH3, Cortactin SH3, Fodrin SH3, P53BP2 SH3 and PI3 Kinase SH3 respectively; lane 8 is GST. Panel D: lane 1 is molecular weight markers (New England Biolabs); lanes 2–6 are GST fusions with Dystrophin WW, FE65 WW, Nedd4 WW3, Nedd4 WW2 and Nedd4 WW1 respectively; lane 7 is GST.

3.2.2.2 Elution of fusion proteins from glutathione Sepharose resin

Incomplete elution of the fusion proteins from the glutathione Sepharose resin during a pull down assay would have resulted in an underestimation of the amount of bound material. To assess the efficiency with which these GST fusion proteins could be eluted I performed batch elutions of 400μg of GST and of 400μg of GST–Lyn SH3 from glutathione Sepharose resin (using 100μl batches of 10mM glutathione as the elution buffer). As in the pull down assays, I incubated each batch of elution buffer with the resin for 15 minutes at 4°C on an end over end mixer. The individual batches were kept separate and individually assayed.

Under the elution conditions used, more than 90% (assessed by digitally photographing Coomassie stained gels and counting pixels) of both GST and GST–Lyn SH3 was eluted in the first three 100μl batchs (*Figure 3.15*). This suggested that, under the conditions used in pull down assays, a good recovery of PDE–fusion protein complexes could be expected.

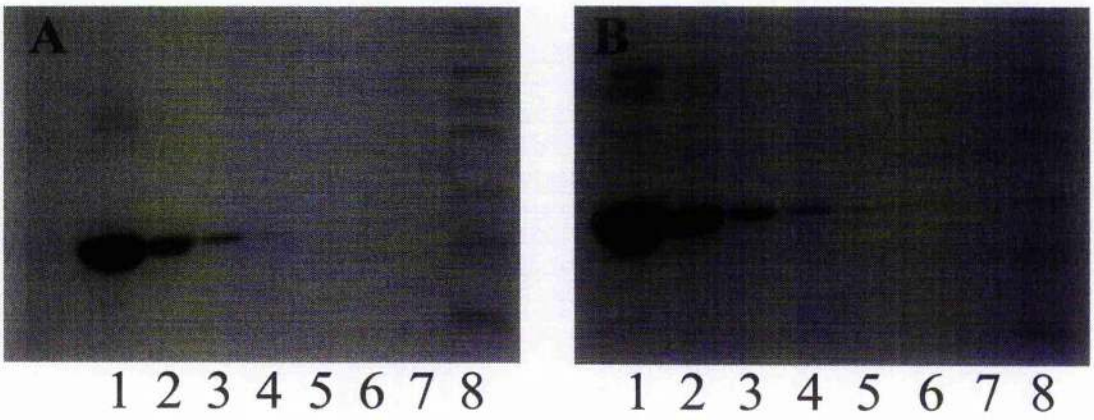

Figure 3.15: Elution of GST and GST–Lyn SH3 from glutathione Sepharose resin

The figure shows Coomassie stained gels of fusion proteins eluted from glutathione Sepharose resin in 100µl batches by 10mM glutathione. Panel A: lanes 1–7 are fractions 1–7 in the elution of GST, lane 8 is protein molecular weight markers (New England Biolabs: MBP-b-galactosidase 175kDa, MBP-paramyosin 83kDa, Glutamic dehydrogenase 62kDa, Aldolase 47.5kDa, Triosephosphate isomerase 32.5kDa, b-Lactoglobulin A 25kDa, Lysozyme 16.5kDa). Panel B: lanes 1–7 are fractions 1–7 in the elution of GST–Lyn SH3, lane 8 is protein molecular weight markers (New England Biolabs).

3.2.2.3 Separation of bound and unbound PDE

Incomplete separation of the bound from the unbound PDE would have increased the background noise and was therefore a potential source of error. To ensure that I could adequately remove the unbound PDE, I performed pull down assays between GST–Lyn SH3 and HSPDE4D4 expressed in the cytosol of transfected COS-7 cells. In these pull down assays I did not pool the wash fractions. Instead I individually probed each wash fraction for both PDE enzyme activity and immunoreactivity. This revealed that under the conditions used, more than 90% of both the activity and the immunoreactivity (assessed by digitally photographing immunoblots and counting pixels) that I was able to separate into the unbound fraction was released within the first two washing steps (*Figure 3.16*). This indicated that the washing regime employed in pull down assays was sufficient to achieve good separation of bound and unbound PDE.

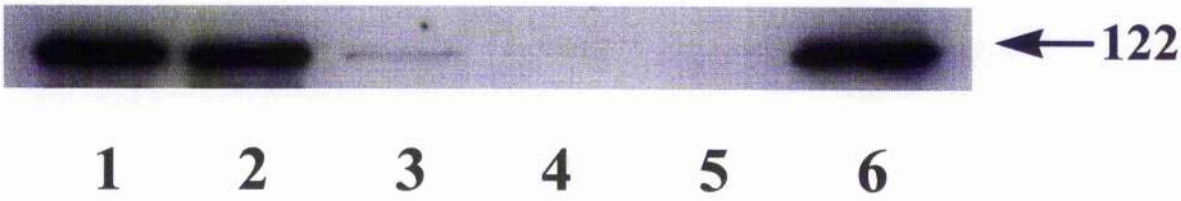

Figure 3.16: Separation of bound and unbound HSPDE4D4

The figure shows an immunoblot for PDE4D of fractions from a pull-down assay. Lane 1 is 4μg cytosol from COS-7 cells overexpressing HSPDE4D4, lane 2 is the unbound fraction from the pull down assay, lanes 3–5 are washes 1–3 respectively, lane 6 is the bound fraction. An equal proportion of each fraction (40%) was loaded onto each lane. The weight shown is the apparent molecular weight of the bands (kDa), calculated by plotting the Rf values of the bands and of prestained molecular weight markers run on the same gel.

3.2.2.4 Detection of PDE activity in bound and unbound fractions

In their investigation of the interactions between RNPDE4A5 and SH3 domains O'Connell and others monitored both the immunoreactivity and the enzyme activity in the bound and unbound fractions to assess the interaction of this PDE with each SH3 domain. To increase the sensitivity of the enzyme activity assay, the incubation time was extended from 10 to 25 minutes in these experiments (162). Phosphodiesterase activities are unstable *in vitro,* for instance RNPDE4A1 enzyme activity has a half life of approximately 11 min at 50°C and the truncated, human PDE4A h6.1 enzyme activity has a half life of approximately 2 minutes at this temperature (200, 245). These assays were, however, performed in the absence of substrate and it is possible that the interaction of the enzymes with their substrate may serve to stabilise them. To ensure that a 25 min assay accurately represented the initial rate of cAMP hydrolysis by HSPDE4D4 I performed time-course experiments (*Figure 3.17*).

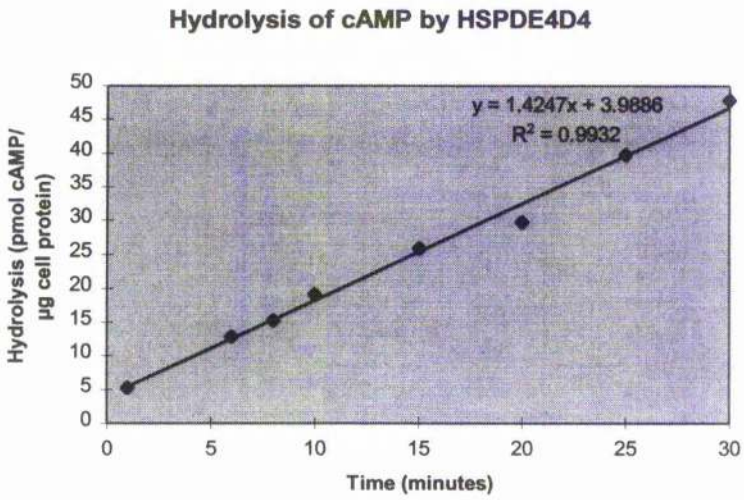

Figure 3.17:Phosphodiesterase activity assays:

The figure shows results from a representative time-course experiment assaying the hydrolysis of cAMP by HSPDE4D4. Assays were run under the conditions described in materials and methods (section 2.1.11). The experiment was performed three times using two separate preparations of PDE.

3.2.2.5 Percentage recovery of HSPDE4D4 in bound and unbound fractions

A marked loss of PDE activity occurred over the course of the pull down assays which I performed with HSPDE4D4. The total activity recovered in the bound and unbound fractions represented only 64% ± 2 of that which I initially added. Incomplete recovery of the PDE activity, from pull down assays, was also encountered by O'Connell and others in their investigation of the interactions of the PDE4A isoform RNPDE4A5 with SH3 domains (161). In the previous study, optimisation of the method suggested that the observed loss of PDE activity was due to an inhibition of the PDE, caused by it's immobilisation onto the glutathione Sepharose resin through interaction with an SH3 domain. Elution of the PDE–SH3 domain complexes was found to result in a complete recovery of PDE activity.

The observed loss of PDE activity in the pull down assays that I performed with HSPDE4D4 was not, however, due to an inhibition of the PDE caused by its immobilisation onto the glutathione Sepharose resin. In all of the pull down assays that I performed the PDE–SH3 domain complexes were eluted from the glutathione Sepharose resin prior to their assay for PDE enzyme activity.

A possible explanation for the observed loss of PDE enzyme activity is incomplete elution of the PDE–SH3 domain complexes from the glutathione Sepharose resin. Two lines of evidence, however, argue against this possibility. Firstly, under the conditions used in pull down assays, over 90% of the immobilised fusion protein was eluted from the glutathione Sepharose resin (*Figure 3.15*) therefore efficient recovery of PDE–fusion protein complexes can be expected. Secondly, control assays using either immobilised GST, washed resin alone or where no resin was included, were all subject to similar losses of activity. These results suggested that the observed loss of activity was neither due to incomplete elution of PDE–fusion protein complexes nor to the non-specific adsorption of PDE onto the glutathione Sepharose resin (*Figure 3.18*).

I do not believe the loss of activity was due to the degradation of the PDE by proteases present in the COS-7 cell cytosol as samples incubated on ice for the duration of the pull down assay were not subject to a similar loss of activity.

Indeed, the total activity added was calculated from assays of samples so treated. Neither do I believe that the loss was due to the action of proteases present in the preparations of fusion protein, as similar losses were observed in control assays where no fusion protein or resin were included (*Figure 3.18*). For similar reasons I do not believe that other enzymatic reactions (such as dephosphorylation by phosphatases) or that the dissociation of regulatory molecules from the PDE can account for the observed losses in PDE activity.

I suggest, therefore, that the observed loss of activity may be due to mechanical degradation of the PDE, or to it's non-specific adsorption onto the walls of the Eppendorf tubes, or to both. This conclusion is consistent with the observation that PDE4D immunoreactivity, which co-migrates with HSPDE4D4, can be stripped from the walls of washed Eppendorf tubes in which HSPDE4D4 has been incubated (*Figure 3.19*).

To minimise any mechanical damage to the PDE, during the pull down assays, I performed all mixing of samples by gentle agitation and not by vortexing. I also minimised all centrifugation times and attempted to keep the samples at low temperatures whenever possible.

I investigated the possibility of stabilising the PDE by inclusion of glycerol or protein in the assay mix . Neither the addition of glycerol nor of bovine serum albumin (BSA) prevented loss of activity over the course of pull down assays. Addition of BSA was, however, found to activate HSPDE4D4. This appeared to be a specific effect of BSA as neither casein nor soyabean trypsin inhibitor cause a similar activation.

I was not able to eliminate the losses in PDE enzyme activity over the course of pull down assays, however, the observed losses were reproducible and of equal magnitude in both control and test samples. To correct for these losses I have expressed the data generated in terms of the percentage of recovered activity present in the bound fraction (rather than as the percentage of the applied activity recovered in the bound fraction).

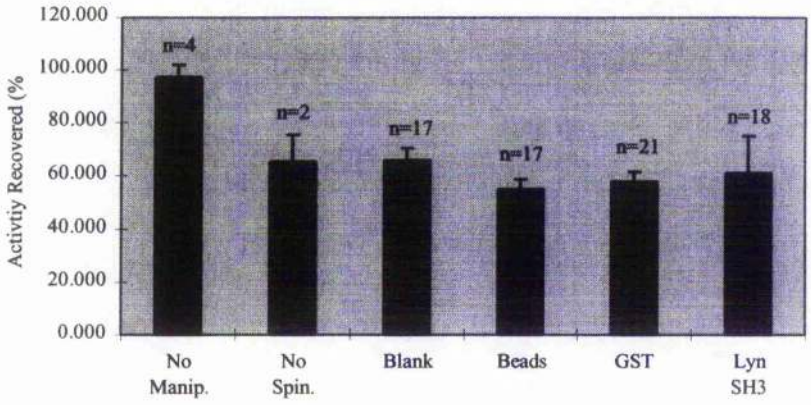

Figure 3.18: Activity recovered in pull-down assays:

The bar chart shows data from control assays where the sample has been subjected to: no manipulations, all manipulations except for centrifugation steps, all manipulations; and from pull-down assays where the sample has been challenged with: glutathione Sepharose resin alone, immobilised GST and immobilised GST–Lyn SH3. Values are means of n separate assays. Error bars show standard error of the means.

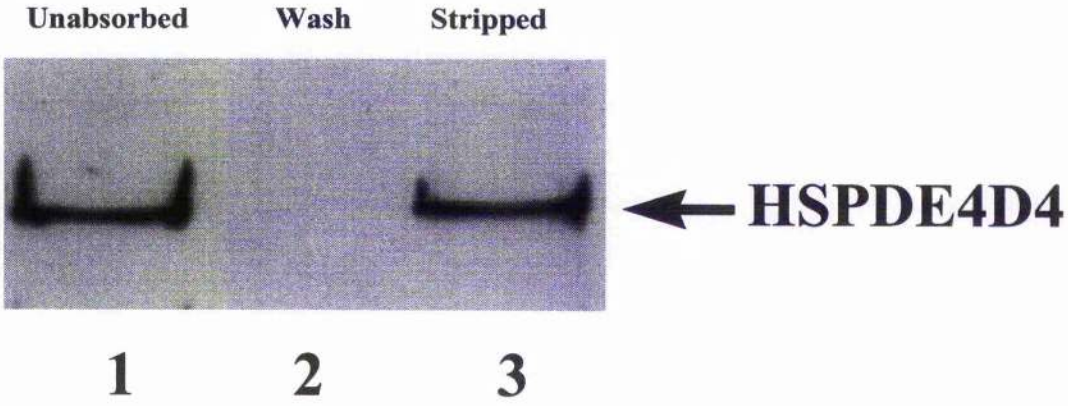

Figure 3.19: Stripping adsorbed HSPDE4D4 from the walls of an Eppendorf tube

To investigate the possibility that a significant amount of non-specific adsorption onto the walls of the Eppendorf tubes occurs, HSPDE4D4 was incubated, end over end for 15 minutes at 4°C. The tube was then washed as in a pull-down assay, sample buffer was added and the tube heated at 100°C for 5 minutes. The figure shows an immunoblot for PDE4D of the collected fractions. Lane 1 is unabsorbed HSPDE4D4, lane 2 is the pooled washes and lane 3 is sample buffer boiled in the washed tube. The immunoreactive bands migrated with apparent molecular weights of 108 kDa, calculated by plotting the Rf values of the bands and of prestained molecular weight markers run on the same gel.

3.2.3 Interaction of HSPDE4D4 with SH3 domains from various proteins

The long PDE4A isoform, RNPDE4A5 showed specificity for the SH3 domains with which it could interact; for example, it appeared to associate well with the SH3 domains of Src and of the related Src family protein kinases Lyn and Fyn, whereas little, if any, association was seen with the SH3 domains from the adapter proteins Grb2 and Crk (162). I therefore decided to investigate the ability of PDE4D4 to interact with the SH3 domains from a variety of different proteins.

I used recombinant HSPDE4D4, overexpressed in the cytosol of COS-7 cells as the source of enzyme for pull down assays with a variety of SH3 and other protein binding domains. I monitored both the immunoreactivity and the PDE enzyme activity in the bound and unbound fractions to assess the interaction of HSPDE4D4 with each fusion protein. In all cases the endogenous phosphodiesterase activity of the COS-7 cells, determined by assaying an equivalent mass of mock transfected COS-7 cell cytosol, was less than 5% of the total PDE enzyme activity in tranfected cells.

3.2.3.1 Analysis of enzyme activity data from pull-down assays

I needed some (semi) quantitative means of determining which of the fusion proteins interacted with HSPDE4D4 pull down assays. To do this I expressed PDE enzyme activity present in the bound fraction as a percentage of the total activity recovered in the assay. I then tested the data sets for significant differences in the mean percentage binding of HSPDE4D4 to each of the fusion proteins. The null hypothesis in each case was that the percentage binding of HSPDE4D4 to that fusion protein was equal to that of HSPDE4D4 to GST.

The two most commonly employed statistical tests for significant difference between sample means are Student's t-Test and Analysis of Variance. When comparing differences between the means of more than two samples, Analysis of Variance is the preferred test. This is because, when using t-Tests at (for instance) the 5% level of significance, there is a 1:20 chance of concluding the population means are different when in fact they are equal (a type I error). This probability of error applies to

each comparison made so, multiple comparisons greatly increase the risk of making type I errors. The problem is exaggerated if only those pairs of sample means which show the greatest differences are examined, as this selects for type I errors. With Analysis of Variance however, variation across the entire group of sample means is examined and steps can be taken which set the error level for the entire analysis.

An important assumption underlying both t-Tests and Analysis of Variance is that each sample represents a normally distributed population, which has a mean of μ and a standard deviation of σ. As the sample sizes of the pull-down assay data were small ($n<30$) I could not appeal to the central limit theorem to support an assumption of normality (56). Instead I selected the two largest samples (pull-down assays with GST and with GST–Lyn SH3) and used the Chi-squared test to assess each for goodness of fit to a normal distribution. The value of Chi-squared in each case corresponded to a probability greater than 0.05 (0.626 with GST and 0.853 with GST–Lyn SH3). I therefore accepted the hypothesis, that these samples represent normality distributed populations, at the 5% level.

Another assumption made in applying Analysis of Variance (and the most commonly used form of the t-Test) is that the normally distributed populations all have an equal variance. To test this assumption I have performed an F-Test for equality of variance on the data sets generated for the binding of HSPDE4D4 enzyme activity to GST and to GST-Lyn SH3 (144). The calculated value of F corresponded to a probability of much less than 0.5%; that is to say, two samples drawn from populations with an equal variance would be expected to show a difference in variance as large or larger than that observed less than 1 time in every 200 trials. I therefore rejected the hypothesis that these 2 samples represent normally distributed populations with an equal variance.

As Analysis of Variance is a more powerful method of analysis that Students t-Test, I also tested two transformations of the data ($\sqrt{(100-x)}$ and $\log(100-x)$) in an attempt to meet the assumptions made in applying Analysis of Variance. These transformations, however, also failed to satisfy the assumption of equal variance. This result means that an important assumption made when applying Analysis of

Variance is not safe for these data sets. Analysis of Variance should not, therefore, be used to analyse the enzyme activity data generated from these pull down assays.

I have used t-Tests to assess the data for significant differences between sample means. In t-Tests the ratio of the observed difference between 2 sample means and the estimated standard error of this difference is evaluated. Usually the standard error of the difference is estimated from the pooled sample data; estimating the standard error of the difference in this way, however, relies on the assumption that the 2 populations have a common variance. For these data sets such an assumption is not safe and the standard error of the difference must be estimated from the individual sample variances instead. The sample variances are themselves estimates of the true population variances and a drawback of using this method to estimate the standard error of the difference is that it reduces the number of degrees of freedom available with which to calculate the t-distribution.

As previously stated, performing multiple t-Tests leads to an increased risk of making type I errors. This problem can be somewhat alleviated by nominating, in advance of performing the experiments, a limited number of comparisons which will be made (166). Fortunately, when planning these experiments I had decided to run a negative control assay (with GST alone) in every experiment that I performed. I therefore felt justified in using t-Tests to compare the binding of HSPDE4D4 to each fusion protein with that of HSPDE4D4 to GST alone. To provide additional protection against type I errors I have also set the probability level at 1% (rather than 5%). This precaution is, however, at the expense of reduced sensitivity (increased risk of concluding that two means are equal when they are different, a type II error).

The association of phosphodiesterase activity with GST fusion proteins representing the SH3 domains of Src, Lyn, Fyn, Csk, Abl, Fodrin and with a fusion protein representing both the SH2 and SH3 domains of Src, was found to be significantly different from that with GST alone at the 1% level (*Figure 3.20*).

It is tempting to make comparisons of the relative amounts of binding of HSPDE4D4 to each of the various fusion proteins and then to compare the rank order of binding seen using HSPDE4D4 to that using RNPDE4A5. For these 2 PDE4 isoforms

have very different proline rich regions within their amino termini (*Figure 3.8*). Doing this would suggest that, although both HSPDE4D4 and RNPDE4A5 are able to specifically interact with SH3 domains *in vitro,* there seem to be differences in the rank order of preference for the domains tested. For instance RNPDE4A5 seems to be able to interact with the SH3 domain of Lyn kinase much more strongly (9.1±1.7 times the binding to the SH3 domain of Src kinase) than it can interact with the SH3 domain of Abl (0.48±0.09 times the binding to the SH3 domain of Src kinase) (162). The interaction of HSPDE4D4 with the SH3 domains of Lyn kinase and of Abl are not, however, significantly different (p=0.557). One must be circumspect about making comparisons such as these, however because of the increased risk of type I errors when multiple t-Tests are performed. Nevertheless the differences seem to be quite pronounced and, considering the differences between the putative SH3 domain binding sites in these 2 proteins are perhaps not unexpected.

In addition to their interaction with SH3 domains, I have examined the abilities of both HSPDE4D4 and RNPDE4A5 to interact with the second WW domain from the ubiquitin protein ligase Nedd4. I tested this domain because WW domains are another class of modular domains for protein–protein interaction which bind to proline rich regions within their target proteins (29). Neither HSPDE4D4 nor RNPDE4A5 were able to associate with this WW domain in pull down assays.

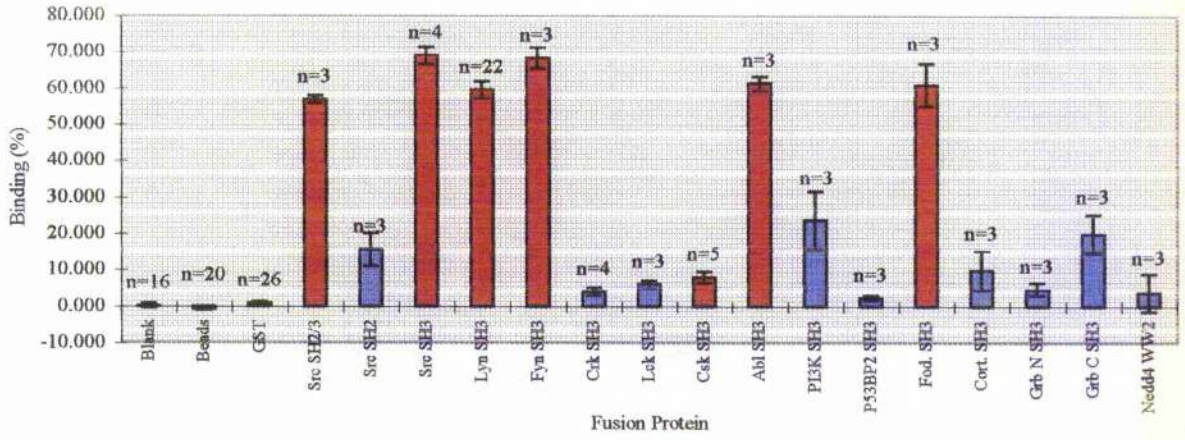

Figure 3.20: Binding of HSPDE4D4 enzyme activity to domains for protein–protein interaction

The bar chart shows data from pull-down assays to screen a library of SH3 and other protein–binding domains for interaction with HSPDE4D4. The data is expressed as percentage of recovered activity present in the bound fraction. Values are means of n separate experiments. Error bars show standard error of the means. Columns coloured in red are judged to be significantly different from GST by t-Tests performed at the 1% level.

3.2.3.2 Analysis of immunoblot data from pull down assays

Due to the large volume of data generated by screening against a library of 17 different fusion proteins and technical problems associated with performing quantitative immunoblots I have not performed a quantitative analysis of the immunoblot data generated from these pull-down assays. Instead I have used this data qualitatively to aid in the interpretation of the enzyme activity data.

With the exception of the fusion protein GST–Csk SH3, in all cases where the association of enzyme activity with a fusion protein was found to be significant, an immunoreactive band corresponding to HSPDE4D4 was readily detectable in the bound fraction from the pull down assay (*Figure 3.21*).

In pull down assays with fusion proteins representing the SH2 domain of Src, the SH3 domain of cortactin and the carboxyl-terminal SH3 domain of Grb, HSPDE4D4 immunoreactivity was readily detectable in the bound fractions, however, the PDE enzyme activity in these fractions was not significantly different from that in the bound fractions of pull down assays using GST alone (at the 1% level) (*Figure 3.20, Figure 3.21*).

Where the immunoblot and enzyme activity data agree (in pull down assays with the SH3 domains of Src, Lyn, Fyn, Abl, and Fodrin) this is good evidence that HSPDE4D4 can interact *in vitro* with these domains. I therefore consider these proteins to be potential *in vivo* binding partners of HSPDE4D4. In the cases where there is a discrepancy between the immunoblot and the enzyme activity data (pull down assays with the SH2 domain of Src, the carboxyl terminal SH3 domain of Grb and of the SH3 domains of Csk and Cortactin) this is less convincing evidence for an interaction and, although these domains may have some affinity for HSPDE4D4, I consider these proteins to be poor candidates for *in vivo* binding partners of HSPDE4D4.

3.2.3.3 Effects of binding to SH3 domains on PDE activity

Discrepancies between the enzyme activity and the immunoblot data from pull-down

assays performed with RNPDE4A5 and certain of the tested fusion proteins were also reported (162). At the time it was suggested that these discrepancies may have been due to changes in the catalytic activity of the PDE caused by it's interaction with the SH3 domains.

To address the possibility that interaction with certain SH3 domains can affect the catalytic activity of HSPDE4D4 and RNPDE4A5, I have assayed the cytosolic fraction of transiently transfected COS-7 cells, for PDE activity, in the presence of increasing concentrations of GST, GST–Lyn SH3 and GST–Crk SH3. I have also performed a similar experiment using purified, affinity tagged HSPDE4D4, expressed in *E.coli* as the source of phosphodiesterase activity. Neither of the tested SH3 domain fusion proteins were found to effect the catalytic activity of either RNPDE4A5 or HSPDE4D4. These data do not support the hypothesis that interaction with these SH3 domains has an effect on the enzymatic activity of the PDE (see also section 3.2.5.4).

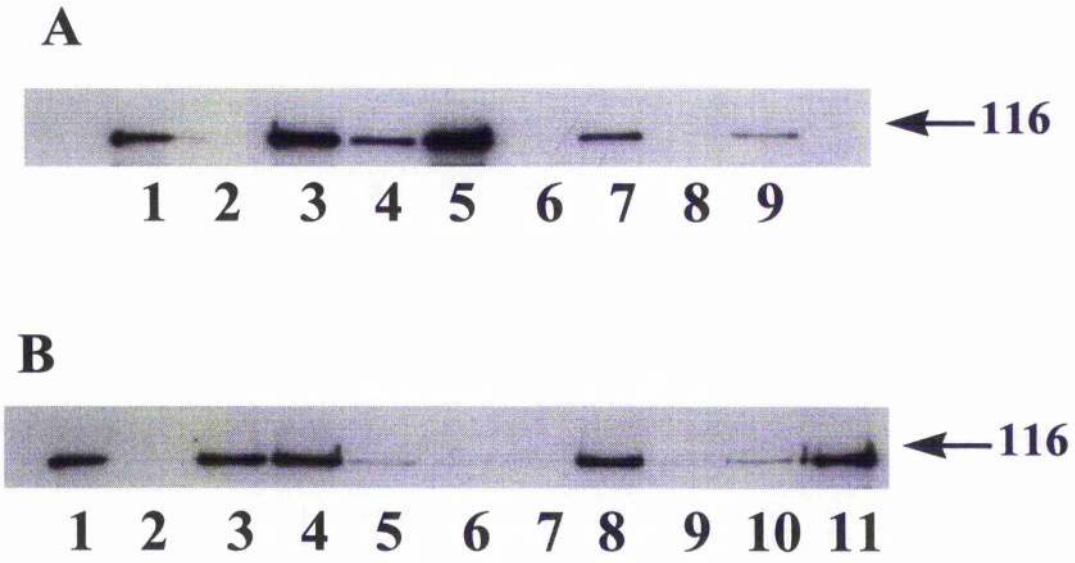

Figure 3.21: Binding of HSPDE4D4 to a library of domains for protein–protein interaction

The figure shows immunoblots of HSPDE4D4 overexpressed in COS-7 cells and "pulled down" with the SH3 domains from various proteins expressed as fusion proteins with GST and immobilised on glutathione Sepharose. Panel A: lane 1 is 4μg cytosol from COS-7 cells overexpressing HSPDE4D4, lanes 2–9 are bound fractions from 40μg cytosol challenged with GST, GST–Src SH3, GST–Src SH2, GST–Src SH2/3, GST–Nedd4 WW2, GST–GrbC SH3, GST–P53BP2 SH3 and GST–Cortactin SH3 respectively. Panel B: lane 1 is 4μg cytosol from COS-7 cells overexpressing HSPDE4D4, Lanes 2–11 are bound fractions from 40μg cytosol challenged with GST, GST–Lyn SH3, GST–Fyn SH3, GST–Crk SH3, GST–Lck–SH3, GST–Csk SH3, GST–Abl SH3, GST–GrbN SH3, GST–PI3K SH3 and GST–Fodrin SH3 respectively. The weights shown are the apparent molecular weight of the bands (kDa), calculated by plotting the Rf values of the bands and of prestained molecular weight markers run on the same gel.

3.2.4 Mapping the region of HSPDE4D4 responsible for interaction with SH3 domains

The putative sites of interaction between both HSPDE4D4 and RNPDE4A5 lie within the alternatively spliced, extreme amino-terminal regions of these isoforms (see section 3.1). This region of RNPDE4A5 is necessary for interaction with SH3 domains as other PDE4A isoforms (RNPDE4A8, RNPDE4A1) and an engineered, truncated species (Met^{26} RD1), all of which share identical sequence with RNPDE4A5 outside of the amino-terminal spliced region, do not interact with the SH3 domain of Src in pull-down assays (162).

To assess the importance of the amino-terminal domain of HSPDE4D4 for interaction with SH3 domains I have assayed the PDE4D isoforms HSPDE4D3 and HSPDE4D5 for interaction with the SH3 domains of Src and Lyn kinases.

3.2.4.1 Pull down assays with HSPDE4D3 and HSPDE4D5 implicate the alternative spliced amino terminal region of HSPDE4D4 in the interaction with SH3 domains

Outside of their, alternatively spliced, amino-terminal regions the isoforms HSPDE4D3, HSPDE4D4 and HSPDE4D5 all share an identical primary structure. Neither HSPDE4D3 nor HSPDE4D5, however, were able to interact with the SH3 domains of Src or Lyn kinases in pull down assays (*Figure 3.22*). This suggests that the alternatively spliced, amino-terminal region of HSPDE4D4 is necessary for it's interaction with SH3 domains.

I have also expressed the extreme amino-terminal region of HSPDE4D4 as a fusion protein with maltose binding protein (MBP) (see sections 4.2.5.3–4.2.5.4). Using this fusion protein I have demonstrated that the alternatively spliced region of HSPDE4D4 is sufficient for interaction with the SH3 domain of Lyn (*Figure 4.23, Figure 4.25*). These results are consistent with the hypothesis that the interaction between HSPDE4D4 and SH3 domains is mediated by the proline rich motifs present in it's extreme amino-terminal domain.

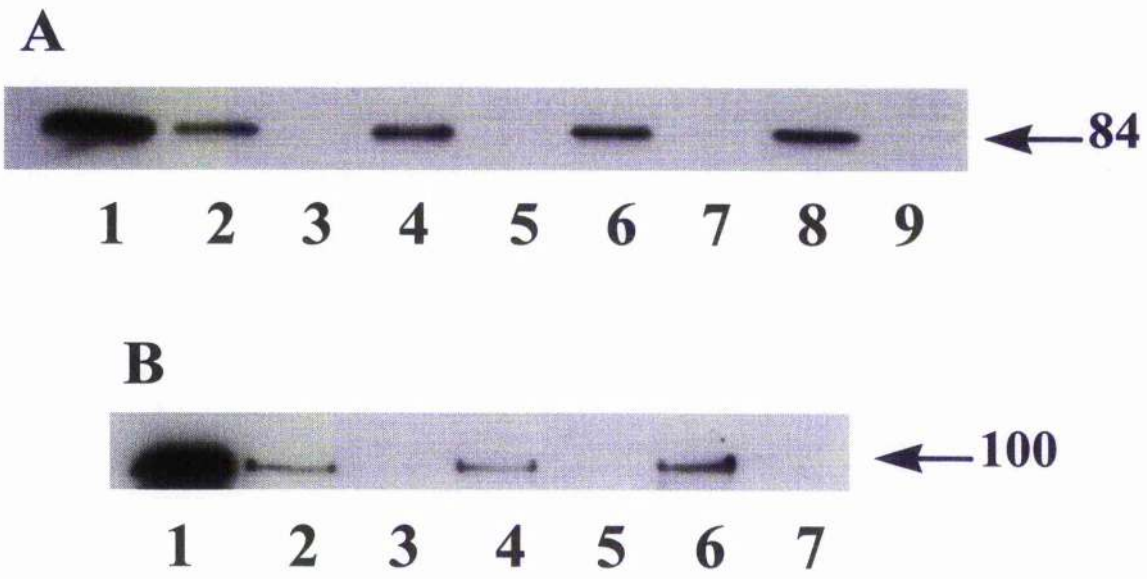

Figure 3.22: Recombinant HSPDE4D3 and HSPDE4D5 do not bind to the SH3 domains of Lyn or Src

The figure shows immunoblots of HSPDE4D3 and HSPDE4D5 overexpressed in COS-7 cells and "pulled down" with SH3 domains expressed as GST fusion proteins and immobilised on glutathione Sepharose resin. Panel A: lane 1 is 20μg cytosol from COS-7 cells overexpressing HSPDE4D3, lanes 2–3 are unbound and bound fractions from 40μg cytosol challenged with glutathione Sepharose resin alone, lanes 4–5 are unbound and bound fractions from 40μg cytosol challenged with GST, lanes 6–7 are bound and unbound fractions from 40μg cytosol challenged with GST–Lyn SH3, lanes 8–9 are unbound and bound fractions from 40μg cytosol challenged with GST–Src SH3. Panel B: lane 1 is 10μg cytosol from COS-7 cells overexpressing HSPDE4D5, lanes 2–3 are unbound and bound fractions from 30μg cytosol challenged with glutathione Sepharose resin alone, lanes 4–5 are unbound and bound fractions from 40μg cytosol challenged with GST, lanes 6–7 are unbound and bound fractions from 40μg cytosol challenged with GST–Lyn SH3. The weights shown are the apparent molecular weight of the bands (kDa), calculated by plotting the Rf values of the bands and of prestained molecular weight markers run on the same gel.

3.2.5 Characteristics of the association of HSPDE4D4 with SH3 domains

I decided to characterise the interaction of HSPDE4D4 with SH3 domains. As it was not practical to investigate the interactions of HSPDE4D4 with every SH3 domain which I had available I selected the SH3 domain of Lyn kinase to serve as an example of an SH3 domain from a Src family protein tyrosyl kinase. I chose this particular SH3 domain because both HSPDE4D4 and RNPDE4A5 interacted well with the GST–Lyn SH3 fusion protein in pull down assays, because both Lyn kinase and HSPDE4D4 are present in brain and because the GST-Lyn SH3 fusion protein was expressed well in *E.coli,* which allowed the straightforward purification of large amounts of this protein.

I have performed assays to assess the stability of the interaction with SH3 domains in the presence of high ionic strength and of detergent and also the effects of interaction on the enzymatic activity of HSPDE4D4. I have assayed for changes in the specific activity, the sensitivity to inhibition by rolipram and the affinity for magnesium ions of HSPDE4D4. Changes in one or more of these properties have previously been reported following modification (197) (82, 141) or truncation (95, 108, 187) of the amino-terminal domains of long-form splice variants of PDE4A, B and D

3.2.5.1 Effect of salt and detergent on the interaction between HSPDE4D4 and the SH3 domain of Lyn kinase

The interaction between HSPDE4D4 and the SH3 domain of Lyn kinase was not disrupted by repeated washing with buffer (50mM Tris/HCl, pH 8.0), salt (0.5M NaCl) nor with detergent (0.5% Triton X-100) (*Figure 3.23*). In this respect the interaction of HSPDE4D4 with the SH3 domain of Lyn is similar to those of RNPDE4A5 and HSPDE4A4B (162).

3.2.5.2 Effect of interaction with the SH3 domain of Lyn on the affinity of HSPDE4D4 for rolipram

Long isoforms of PDE4 can exist in at least 2 conformational states that can be

distinguished by changes in the enzymes sensitivity to the drug rolipram (see section 1.3.6). Interaction of the rat PDE4A isoform, RNPDE4A5 with the SH3 domain of Lyn kinase did not alter the enzymes sensitivity to inhibition by rolipram (162). In contrast to this, interaction of the human homologue of RNPDE4A5, namely HSPDE4A4B, with the SH3 domain of Lyn did cause a change in its sensitivity to inhibition by rolipram. This difference is linked to a hypervariable region of sequence called Linker Region 2 (LR2) that lies immediately amino terminal to the catalytic region in PDE4. The LR2 of human PDE4A contains a proline and arginine rich region of sequence that is not conserved in rat PDE4A (141). This region in HSPDE4A4B forms an additional site of interaction with SH3 domains. It is the binding of an SH3 domain to the LR2 region of HSPDE4A4B that causes the detected change in sensitivity to inhibition by rolipram (141).

I therefore decided to investigate whether the interaction of HSPDE4D4 with the SH3 domain of Lyn kinase caused a change in its sensitivity to inhibition by rolipram. To do this I performed PDE enzyme activity assays on the bound and the unbound fractions from pull down assays between HSPDE4D4 and GST-Lyn SH3 in the presence of a range of concentrations of rolipram. I then used the data from these assays to calculate the concentration of rolipram that caused a 50% inhibition of the PDE enzyme activity (IC_{50}) in each case. The IC_{50} values that I obtained in these assays were 0.08±0.02μM and 0.1±0.02μM for the bound and the unbound fractions respectively (*Figure 3.24*). These values are not significantly different from each other (t-Test 5% level).

I also performed similar experiments to determine the IC_{50} value of rolipram for the inhibition of HSPDE4D4 in the crude cytosolic fraction of transfected COS-7 cells. The IC50 value that I calculated from these assays was 0.16±0.03μM (*Figure 3.24*).

These results show that the interaction of HSPDE4D4 with the SH3 domain of Lyn kinase did not cause a change in the sensitivity of this isoform to inhibition by rolipram.

3.2.5.3 Effect of interaction with the SH3 domain of Lyn on the enzyme activity of

HSPDE4D4

To investigate whether interaction with SH3 domains affected the catalytic activity of PDE4 phosphodiesterase I have performed phosphodiesterase activity assays on the cytosolic fraction from COS-7 cells expressing either HSPDE4D4 or RNPDE4A5, in the presence of GST, GST-Lyn SH3 and of GST–Crk SH3. I examined the SH3 domain Crk as well as of Lyn kinase in these assays because there were discrepancies between the enzyme activity and immunoblot data generated in pull down assays with this SH3 domain for both HSPDE4D4 and RNPDE4A5 (see section 3.2.3.3). Assays were performed in the presence of 0, 12.5, 25, 50 and 100μg fusion protein. No change in phosphodiesterase activity was observed in the presence of either GST–Lyn SH3 or GST–Crk SH3 compared with that in the presence of GST (*Figure 3.25*).

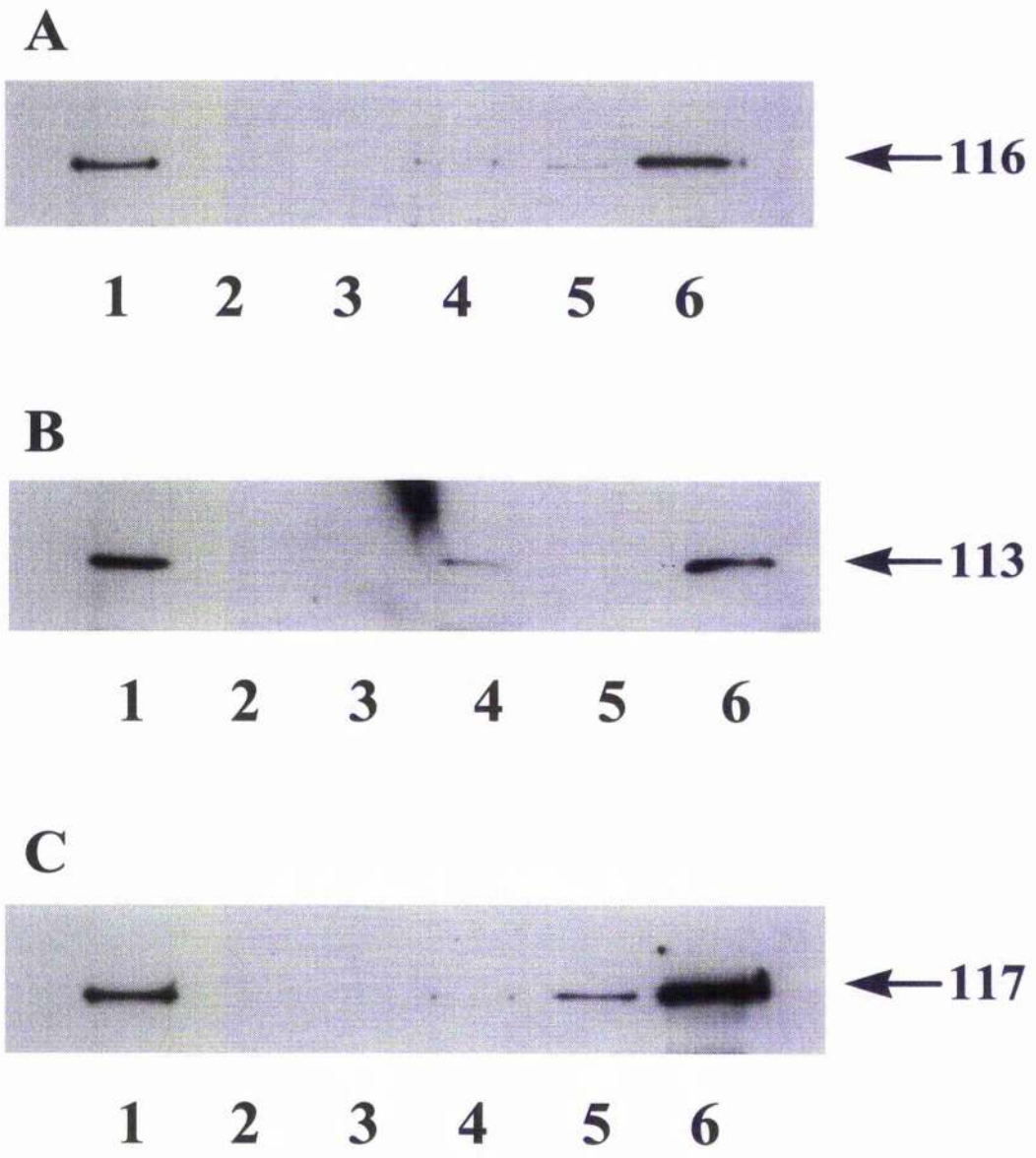

Figure 3.23: Binding of HSPDE4D4 to the SH3 domain of Lyn is neither disrupted by repeated washing nor by washing in the presence of salt or detergent

The figure shows immunoblots, for PDE4D, of fractions from pull-down assays performed with each of three different washing regimes. Panel A shows fractions from an assay where the washing buffer was 50mM Tris/HCl (pH 8.0); panel B shows fractions from an assay where the washing buffer was 0.5M NaCl, 50mM Tris/HCl (pH 8.0); panel C shows fractions from an assay where the washing buffer was 0.5% Triton-X100, 50mM Tris/HCl (pH 8.0). In each of the pannels: lanes 1–3 are the unbound, the wash and the bound fractions respectively, from a pull-down assay with GST; lanes 4–6 are the unbound, the wash and the bound fractions respectively, from a pull-down assay with GST–Lyn SH3. The weights shown are the apparent molecular weight of the bands (kDa), calculated by plotting the Rf values of the bands and of prestained molecular weight markers run on the same gel.

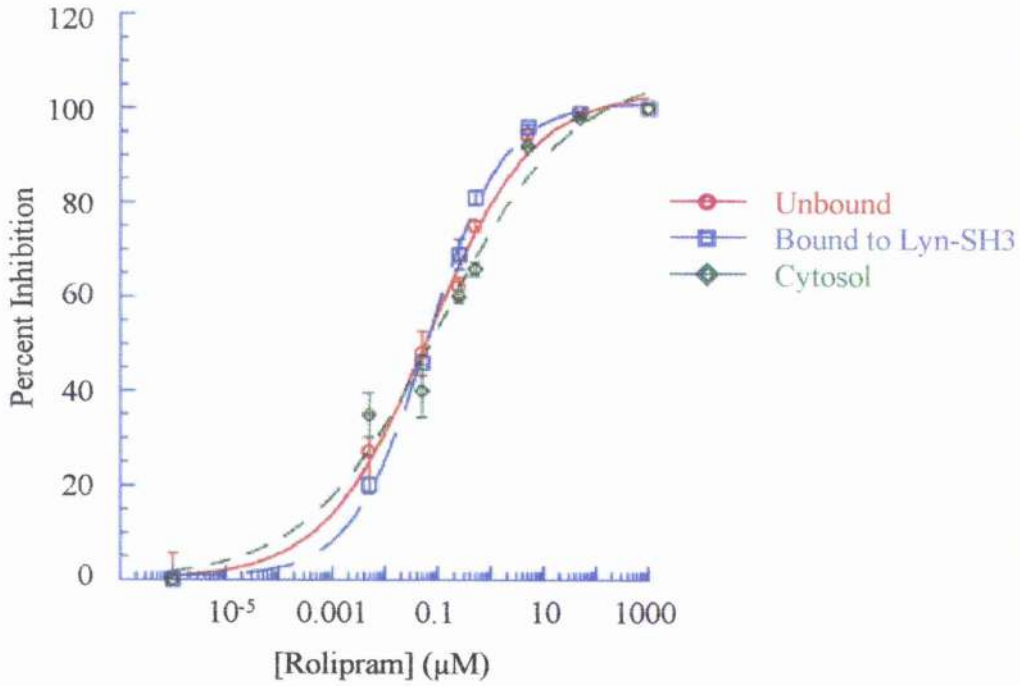

Figure 3.24: Inhibition of HSPDE4D4 by rolipram

The graph shows dose–response curves for the inhibition of PDE activity by rolipram in the presence of 1μM cAMP as substrate. Assays were performed on: the cytosolic fraction of COS-7 cells overexpressing HSPDE4D4 (◆)(IC50=0.16±0.03μM), the bound fraction from pull down assays with GST–Lyn SH3 (□)(IC50=0.08±0.02μM) and the unbound fraction from pull down assays with GST-Lyn SH3 (○)(IC50=0.10±0.02μM). 0% Inhibition is defined as the measured activity in the absence of inhibitor. The data shown are from 1 representative experiment of 3 performed. Error bars show the standard error of the mean for each data point in the shown experiment.

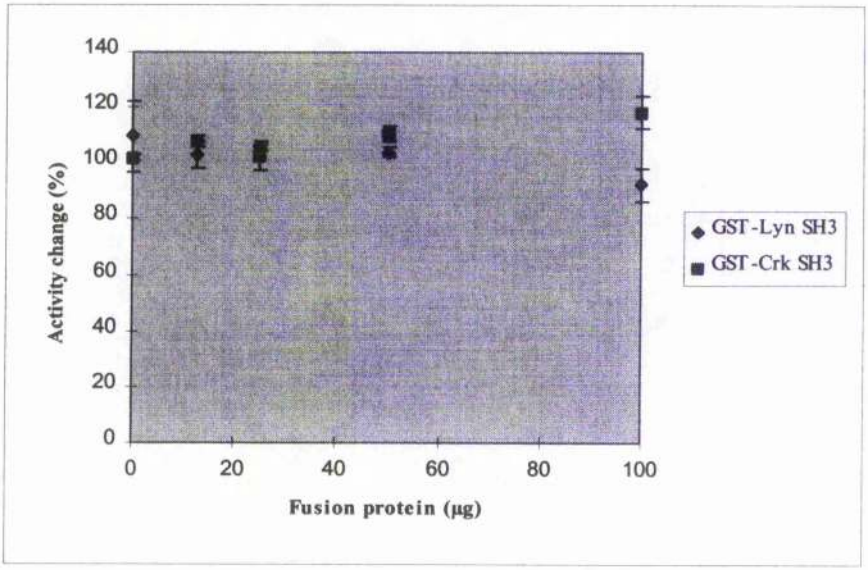

Figure 3.25: Effect of the SH3 domains of Lyn and Crk on the enzyme activity of HSPDE4D4

Phosphodiesterase enzyme activity assays were performed on the cytosolic fraction from COS-7 cells expressing HSPDE4D4, in the presence of GST, GST-Lyn SH3 and of GST–Crk SH3. Assays were performed in the presence of 0, 12.5, 25, 50 and 100µg fusion protein. The results are expressed as the percentage change in activity in the presence of each concentration of GST–SH3 domain fusion protein compared to the activity in the presence of the equal amount of GST. Each point represents the mean of 2 separate experiments with standard errors shown.

3.2.6 Subcellular distribution of HSPDE4D4

Both endogenously expressed PDE4D4 and recombinant HSPDE4D4 overexpressed in COS-7 cells occur partitioned between the soluble and particulate fractions of fractionated cells (P120±4%, P240±7%, S2 40±3%) (15, 98). The association of HSPDE4D4 with the particulate fraction requires is not disrupted by treatment with high ionic strength nor by washing with the non-ionic detergent triton X-100. These conditions also fail to disrupt the association of HSPDE4D4 with the SH3 domain of Lyn kinase *in vitro*. I therefore considered the possibility that HSPDE4D4 may be localised to some structure present in the particulate fraction of fractionated cells by interacting with SH3 domains present in one or more anchoring proteins.

3.2.6.1 Visualisation of HSPDE4D4 by immunoflourescent staining and confocal microscopy

Fractionation of cells by differential centrifugation is a low resolution method of determining the subcellular distribution of a protein. To gain more insight into the distribution of HSPDE4D4 immunoflourescent staining and confocal microscopy was used to visualise recombinant HSPDE4D4 overexpressed in COS-7 cells.

The confocal pictures show that, in this system, HSPDE4D4 is not randomly distributed within the cell; rather it appears to be enriched in the perinuclear region and within processes at the plasma membrane (*Figure 3.26*). This distribution is similar to that seen for HSPDE4A4B overexpressed in transiently transfected COS-7 cells (93). Unlike HSPDE4A4B, however, HSPDE4D4 did not appear to be enriched in the ruffles at the plasma membrane. I also noted that cells which had been transfected with HSPDE4D4 were extremely resistant to trypsin (used to dislodge the cells from the culture flask when preparing slides). Together with the enrichment of HSPDE4D4 within processes at the plasma membrane this may indicate that this isoform may have some involvement in regulating focal adhesions.

The antibody used for the immunoflourescent staining was raised against the carboxly-terminal region of PDE4D and can therefore detect all of the known splice variants of PDE4D. To show that the staining reflected the distribution of the

transfected HSPDE4D4 and not of endogenous PDE4D isoforms, mock transfected COS-7 cells were also fixed and stained using this antibody. No staining was observed in the mock transfected cells under these conditions. Indeed the low abundance of endogenous PDEs makes the immunoflourescent detection of these proteins very difficult in untransfected systems.

There must be concerns about the reliability of using an overexpressing, heterologous system to examine the distribution of a protein. To date, however, no cell lines that express endogenous PDE4D4 have been identified. Furthermore, a number of technical considerations suggest that the immunoflourescent detection of this isoform in untransfected cells is likely to be extremely technically challenging. These include (a) the low expression of endogenous PDEs in all cells thus far examined, (b) the only antibodies currently available that been successfully used for immunnfluorescent microscopy are not splice variant specific. I therefore feel that, as there is agreement between the fractionation data from transfected and natively expressed PDE4D4, these confocal pictures may give some useful information regarding the distribution of PDE4D4 in cells.

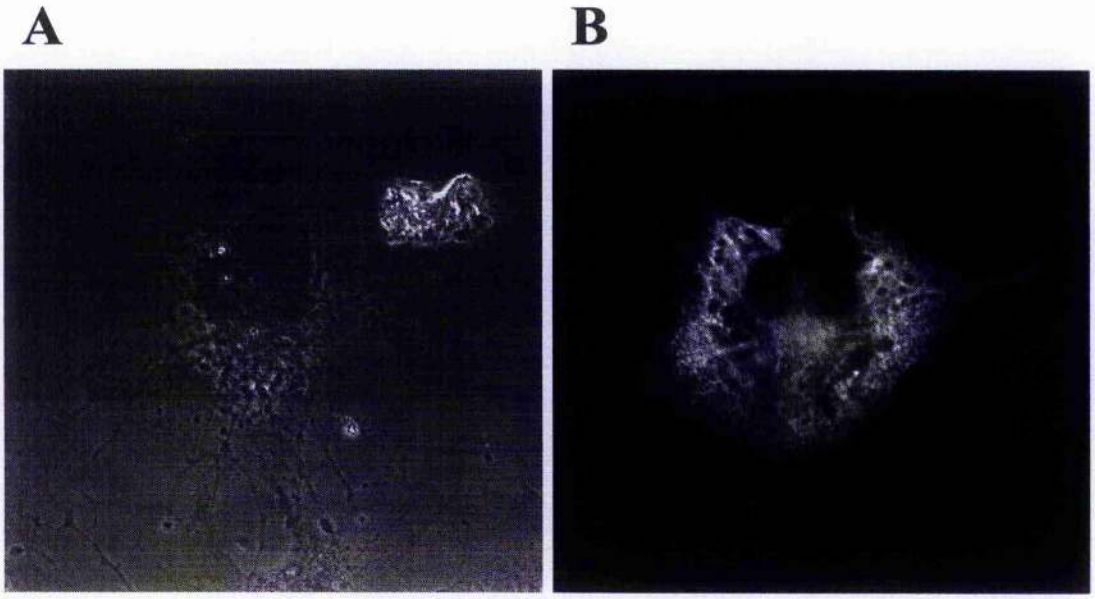

Figure 3.26: Subcellular distribution of HSPDE4D4

The figure shows confocal microscope pictures of a COS-7 cell transiently transfected to overexpress HSPDE4D4. Cells were fixed on coverslips 3 days after transfection then stained for immunofluorescence imaging. The primary antibody used was the monoclonal antibody 61D10E (Icos) which detects the common region of PDE4D isoforms. The staining was detected using an anti-mouse IgG conjugated to the fluorescent dye Rhodamine. The photographs were taken using a X60 lens. Panel A shows a transmission/phase contrast photograph of a typical cell overexpressing HSPDE4D4. Panel B shows a fluorescence image (taken by laser scanning confocal microscopy) of a 0.2μ section through the centre of the same cell.

The immunostaning and confocal imaging of these cells was performed by Dr E. Huston.

3.2.7 Interaction of HSPDE4D4 with SH3 domains *in vivo*

The pull down assays that I have performed with recombinant HSPDE4D4 overexpressed in COS-7 cells provide good evidence that this isoform can specifically interact with certain SH3 domains *in vitro*. I have also performed pull down assays, overlay assays and enzyme linked immunosorbent assays (ELISA) using a purified MBP fusion protein of HSPDE4D4 and GST–SH3 domain fusion proteins (see section 4.2.5). These assays support the hypothesis that HSPDE4D4 can directly bind to SH3 domains *in vitro*. In an attempt to address the question of whether HSPDE4D4 interacts with SH3 domains *in vivo* I have used the strategy of immunoprecipitating either HSPDE4D4 or candidate interacting proteins from cell lysates and probing the immunoprecipitated material for interacting proteins.

3.2.7.1 Immunoprecipitation of HSPDE4D4 and Lyn from transfected COS-7 cells

I performed immunoprecipitations from RIPA buffer extracts of COS-7 cells which had been transiently transfected to overexpress HSPDE4D4. I used RIPA buffer extracts because this buffer is able to solublise many membrane bound and cytoskeletal proteins which remain insoluble in less vigorous buffers (250). I immunoprecipitated from unsynchronised cells growing in the presence of 10% FCS, from cells which had been driven into stage G_0 of the cell cycle by overnight serum starvation; from cells which had been serum starved overnight and then stimulated with IBMX (100μM) for 25 minutes and forskolin (10μM) for 10 minutes prior to being harvested; from cells which had been serum starved overnight and then stimulated with epidermal growth factor (EGF) (50ng/ml) for 10 minutes prior to being harvested and from cells which had been serum starved overnight then stimulated with IBMX (100μM) for 25 minutes, forskolin (10μM) and epidermal growth factor (EGF) (50ng/ml) for 10 minutes prior to being harvested.

The stimulations with IBMX and forskolin were to raise intracellular cAMP and so activate pathways downstream of activated PKA. The stimulations with EGF were to activate tyrosine kinase signalling pathways downstream of the activated EGF receptor. I stimulated the cells in these ways to increase the chance of detecting

regulated protein–protein interactions which may only occur in certain activation states of the cell.

I decided to probe for *in vitro* interactions between HSPDE4D4 and Lyn kinase. I chose this protein as a potential binding partner of HSPDE4D4 because it is endogenously expressed in COS-7 cells and because I have shown that the fusion protein GST–Lyn SH3 interacts strongly with recombinant HSPDE4D4 *in vitro*.

I performed immunoprecipitations using antisera raised against Lyn kinase and also using antisera raised against the conserved, carboxyl-terminal region of PDE4D isoforms. I also performed negative control immunoprecipitations using pre-immune serum or with antisera raised against GST where no pre-immune serum was available. The immunoprecipitated material was separated by SDS–PAGE and immunoblotted using either a monoclonal antibody directed against PDE4D (anti-Lyn kinase immunoprecipitations) (*Figure 3.27*) or antisera raised against Lyn kinase (anti-PDE4D immunoprecipitations) (*Figure 3.28*). To ensure that the both Lyn kinase and HSPDE4D4 were immunoprecipitated by their respective antisera selected immunoblots were stripped and re-probed with antisera raised against the immunoprecipitated species.

Under these conditions HSPDE4D4 and Lyn kinase did not appear to co-immunoprecipitate. I have considered the possibility that an *in vivo* interaction between these proteins may exist but that it is disrupted by the detergents present in RIPA buffer. To address this possibility I performed pull down assays using samples prepared in RIPA buffer. In these assays recombinant HSPDE4D4 prepared in RIPA buffer was able to bind to the SH3 domain of Lyn kinase. This demonstrated that the interaction between HSPDE4D4 and the SH3 domain of Lyn kinase is not disrupted under the conditions similar to those in the immunoprecipitations.

That Lyn kinase and HSPDE4D4 did not appear to co-immunoprecipitate under any of the conditions that I tested tested suggests that these proteins do not interact in the RIPA buffer soluble fraction of transfected COS-7 cells. Although my immunoprecipitation data does not support an *in vivo* interaction between Lyn kinase and HSPDE4D4 I can not exclude the possibility that HSPDE4D4 might be able

to interact with a pool of Lyn that may be present in the RIPA buffer insoluble fraction of the COS-7 cells.

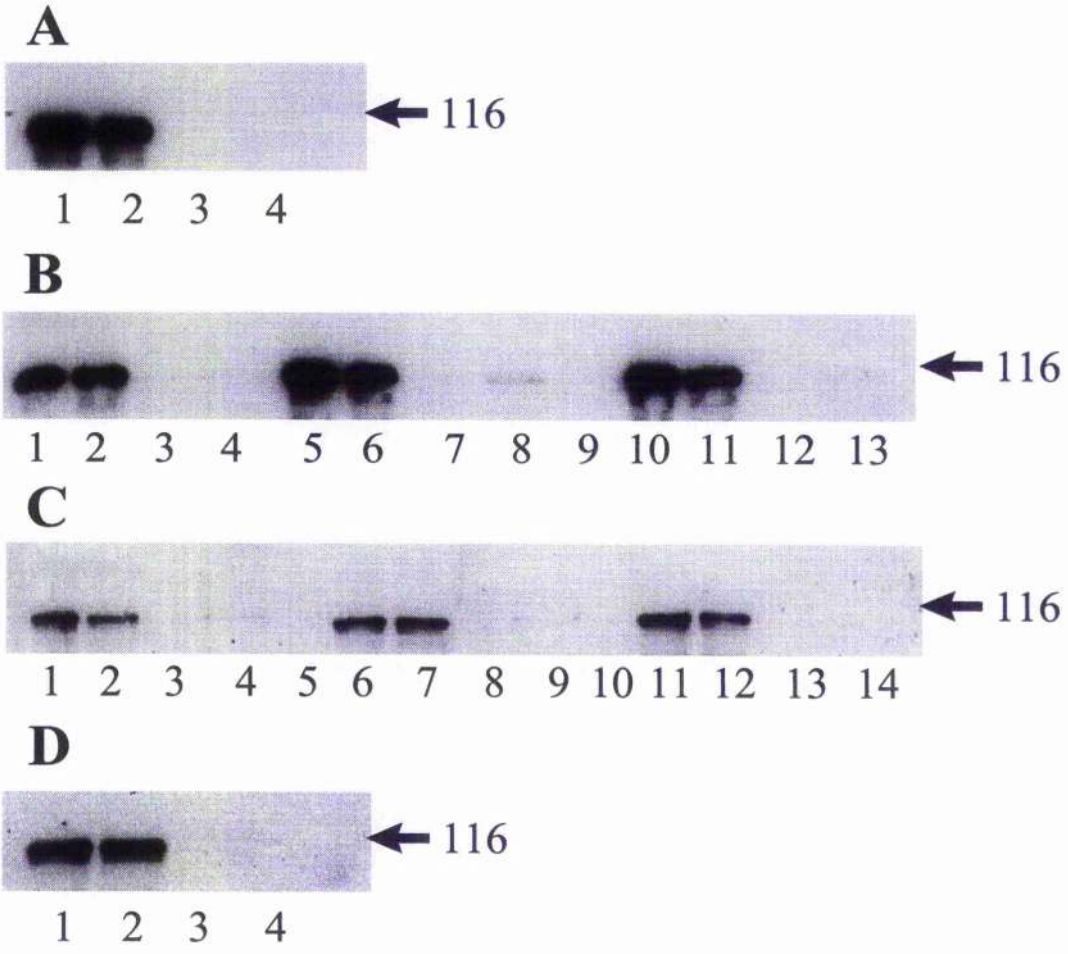
A
116
1 2 3 4
B
116
1 2 3 4 5 6 7 8 9 10 11 12 13
C
116
1 2 3 4 5 6 7 8 9 10 11 12 13 14
D
116
1 2 3 4

Figure 3.27: Immunoprecipitation of endogenous Lyn from COS-7 cells

The figure shows immunoblots of HSPDE4D4 in the RIPA buffer extracts, unbound fractions and bound fractions of immunoprecipitations using antisera raised against Lyn. Panel A: lane 1 is 20μg extract from unstimulated COS-7 cells, overexpressing HSPDE4D4; lanes 2 and 4 are the unbound and bound fractions respectively of an immunoprecipitation from unstimulated cells, using antisera raised against Lyn; lane 3 is empty. Panel B: lane 1 is 20μg extract from unstimulated COS-7 cells, overexpressing HSPDE4D4; lanes 2 and 4 are the unbound and bound fractions respectively of an immunoprecipitation from unstimulated, using antisera raised against GST; lanes 5 and 10 are 20μg extract from COS-7 cells, overexpressing HSPDE4D4 and stimulated with IBMX (100μM) and forskolin (10μM); lanes 6 and 8are the unbound and bound fractions respectively of an immunoprecipitation from cells stimulated with IBMX and forskolin, using antisera raised against Lyn; lanes 11 and 13 are the unbound and bound fractions respectively of an immunoprecipitation from cells stimulated with IBMX and forskolin, using antisera raised against GST; lanes 4, 7, 9 and 12 are empty. Panel C: lanes 1 and 6 are 20μg extract from COS-7 cells, overexpressing HSPDE4D4 and stimulated with EGF (50ng/ml); lanes 2 and 4 are the unbound and bound fractions respectively of an immunoprecipitation from cells stimulated with EGF, using antisera raised against Lyn; lanes 7 and 9 are the unbound and bound fractions respectively of an immunoprecipitation from cells stimulated with EGF, using antisera raised against GST; lane 11 is 20μg extract from COS-7 cells, overexpressing HSPDE4D4 and stimulated with EGF, IBMX and forskolin; lanes 12 and 14 are the unbound and bound fractions respectively of immunoprecipitations from cells stimulated with EGF, IBMX and forskolin, using antisera raised against Lyn; lanes 3, 5, 8, 10 and 13 are empty. Panel D: lane 1 is 20μg extract from COS-7 cells, overexpressing HSPDE4D4 and stimulated with EGF, IBMX and forskolin; lanes 2 and 4 are the unbound and bound fractions respectively of immunoprecipitations from cells stimulated with EGF, IBMX and forskolin, using antisera raised against GST; lane 4 is empty.

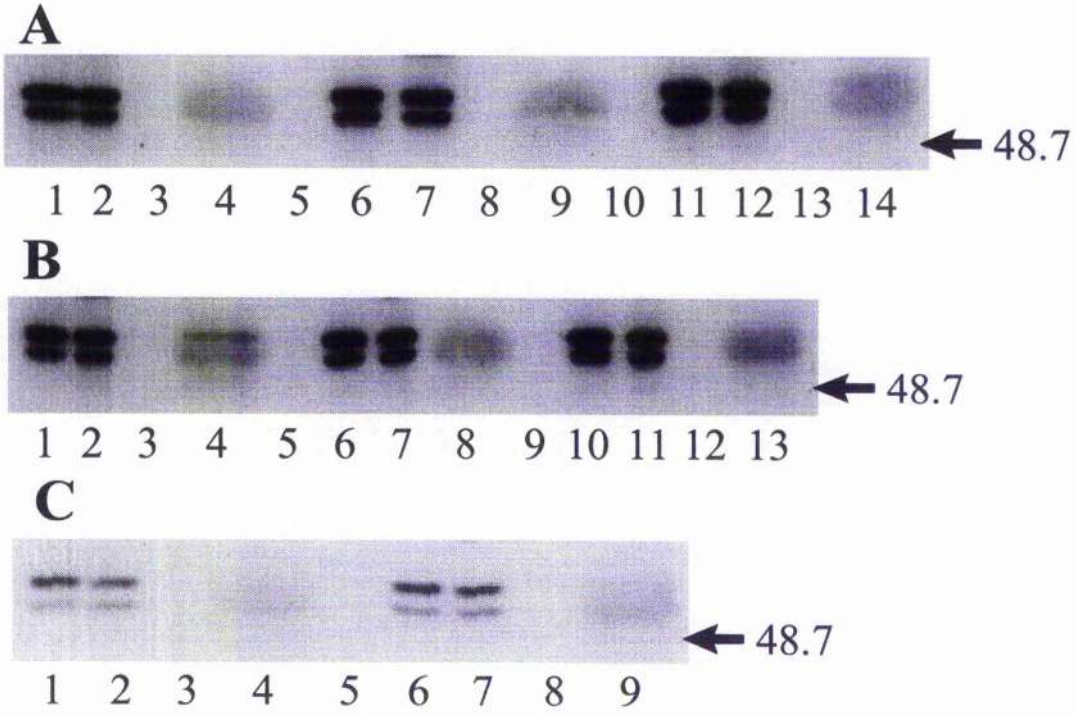
A
48.7
1 2 3 4 5 6 7 8 9 10 11 12 13 14
B
48.7
1 2 3 4 5 6 7 8 9 10 11 12 13
C
48.7
1 2 3 4 5 6 7 8 9

Figure 3.28: Immunoprecipitation of recombinant HSPDE4D4 from COS-7 cells

The figure shows immunoblots of Lyn in the RIPA buffer extracts, unbound fractions and bound fractions of immunoprecipitations using antisera raised against PDE4D Panel A: lanes 1 and 6 are 20μg extract from unstimulated COS-7 cells, overexpressing HSPDE4D4; lanes 2 and 4 are the unbound and bound fractions respectively of an immunoprecipitation from unstimulated cells, using antisera raised against PDE4D; lanes 7 and 9 are the unbound and bound fractions respectively of an immunoprecipitation from unstimulated cells, using pre-immune antisera; lane 11 is 20μg extract from COS-7 cells overexpressing HSPDE4D4 and stimulated with IBMX (100μM) and forskolin (10μM); lanes 12 and 14 are the unbound and bound fractions respectively of an immunoprecipitation from cells stimulated with IBMX and forskolin, using antisera raised against PDE4D; lanes 3, 5, 8, 10 and 13 are empty. Panel B: lane 1 is 20μg extract from COS-7 cells overexpressing HSPDE4D4 and stimulated with IBMX and forskolin; lanes 2 and 4 are the unbound and bound fractions respectively of an immunoprecipitation from cells stimulated with IBMX and forskolin, using pre-immune antisera; lanes 6 and 10 are 20μg extract from COS-7 cells overexpressing HSPDE4D4 and stimulated with EGF (50ng/ml); lanes 7 and 8 are the unbound and bound fractions respectively of an immunoprecipitation from cells stimulated with EGF, using antisera raised against PDE4D; lanes 11 and 13 are the unbound and bound fractions respectively of an immunoprecipitation from cells stimulated with EGF, using pre-immune antisera; lanes 3, 5, 9 and 12 are empty. Panel C: lanes 1 and 6 are 20μg extract from COS-7 cells, overexpressing HSPDE4D4 and stimulated with EGF, IBMX and forskolin; lanes 2 and 4 are the unbound and bound fractions respectively of an immunoprecipitation from cells stimulated with EGF, IBMX and forskolin, using antisrea raised against PDE4D; lanes 7 and 9 are the unbound and bound fractions respectively of an immunoprecipitation from cells stimulated with EGF, IBMX and forskolin, using pre-immune antisrea; lanes 3, 5 and 8 are empty.

3.2.7.2 Immunoprecipitation of HSPDE4D4 from metabolically labelled cells

I decided that attempting to co-immunoprecipitate HSPDE4D4 with every candidate interacting protein would be an inefficient strategy for identifying *in vivo* binding partners. Instead I performed immunoprecipitations from RIPA buffer extracts of ^{35}S methionine labelled COS-1 cells which I had transiently transfected to overexpress HSPDE4D4. I performed immunoprecipitations from unsynchronised cells growing in the presence of 10% FCS, using an antisera raised against the conserved carboxyl-terminus of PDE4D isoforms. I also performed immunoprecipitations using pre-immune serum as a negative control.

I separated the immunoprecipitated material by SDS-PAGE, transferred it onto a nitrocellulose membrane and imaged the precipitated proteins using a Fujix Bas 1000 phosphoimager (*Figure 3.29 panel A*). In a parallel experiment I performed similar immunoprecipitations from RIPA buffer extracts of unlabeled cells, separated the immunoprecipitated material by SDS-PAGE and then immunoblotted using a monoclonal antibody directed against the carboxyl-terminal region of PDE4D isoforms (*Figure 3.8 panel B*).

Two strong bands, corresponding to full length HSPDE4D4 and an amino-terminally truncated form of this enzyme were immunoprecipitated by the antisera raised against PDE4D. These bands were not precipitated by the pre-immune serum. Under these conditions, however, no bands which did not co-migrate with a PDE4D immunoreactive species and were not also precipitated by the pre-immune serum were clearly detected in the material immunoprecipitated by the anti PDE4D antisera.

It could be that HSPDE4D4 does interact with other proteins in COS-7 cells but that these proteins were poorly labelled by the regime employed and therefore below the limit of detection. I labelled the cells for 2 hours with a mixture of ^{35}S methionine and cystine before preparing the lysates. Alternatively it could be that proteins that interact with HSPDE4D4 are insoluble in RIPA buffer or that the interaction is disrupted by the RIPA buffer. Nevertheless a number of immunoprecipitation experiments have failed to provide evidence of an *in vivo* interaction between

HSPDE4D4 and other proteins present in the RIPA buffer soluble fraction of COS-7 cells.

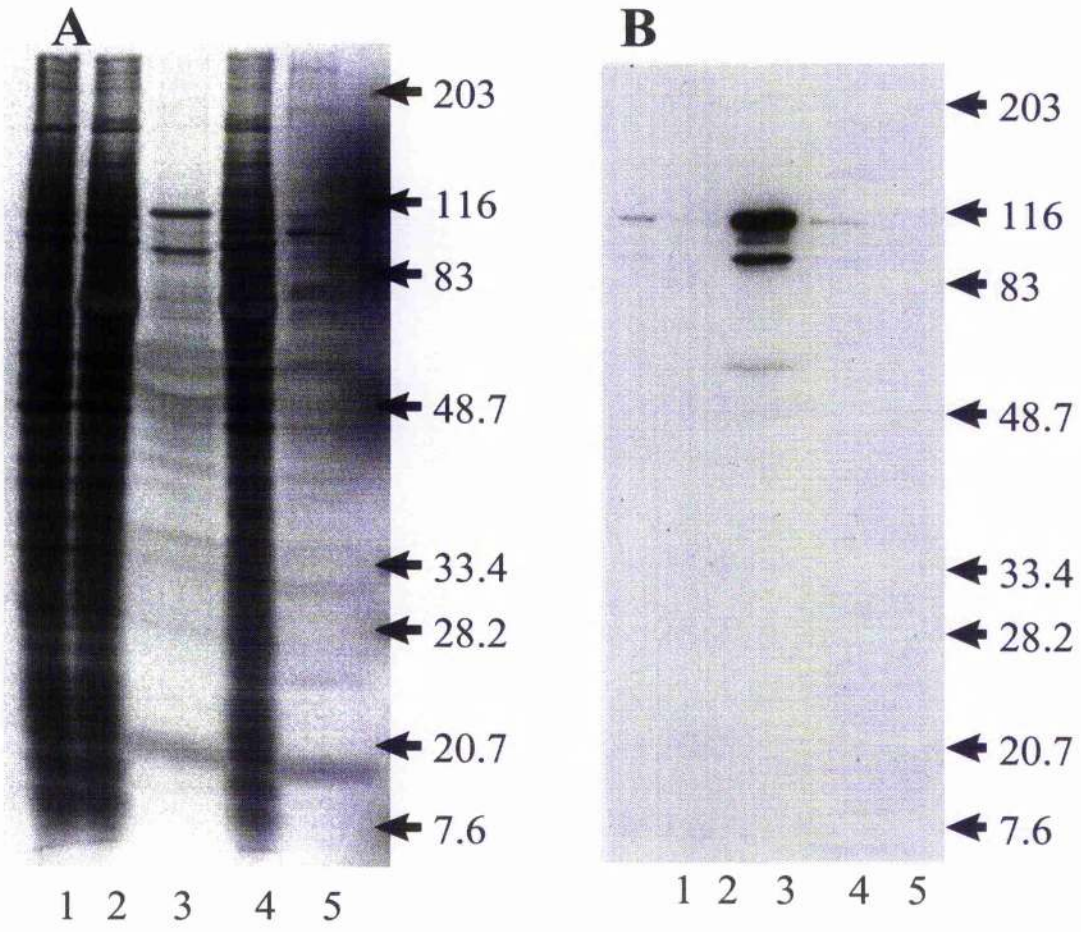

Figure 3.29: Immunoprecipitation of recombinant HSPDE4D4 from metabolically labeled COS-1 cells

Panel A is a phosphoimage of an immunoprecipitation from RIPA buffer extracts of metabolically labeled COS-1 cells, using antisera raised against PDE4D: lane 1 is 10μg extract from metabolically labeled COS-1 cells overexpressing HSPDE4D4; lanes 2 and 3 are the unbound and bound fractions respectively of an immunoprecipitation using antisera raised against PDE4D; lanes 4 and 5 are the unbound and bound fractions respectively of an immunoprecipitation using pre-immne antisera. Panel B is an immunoblot for PDE4D of an immunoprecipitation from RIPA buffer extracts of metabolically labeled COS-1 cells, using antisera raised against PDE4D: lane 1 is 10μg extract from metabolically labeled COS-1 cells overexpressing HSPDE4D4; lanes 2 and 3 are the unbound and bound fractions respectively of an immunoprecipitation using antisera raised against PDE4D; lanes 4 and 5 are the unbound and bound fractions respectively of an immunoprecipitation using pre-immne antisera.

3.3 Conclusions

In this chapter I have shown that both endogenous RNPDE4D4, expressed in rat brain, and HSPDE4D4 expressed in COS-7 cells can interact *in vitro* with SH3 domains. As is the case with the rat PDE4A isoform RNPDE4A5, HSPDE4D4 shows a distinct specificity for the SH3 domains with which it can interact. These PDE4A and PDE4D isoforms appear, however, to have a different rank order of preference for interaction with the various SH3 domains that have been tested. Neither the PDE4A (RNPDE4A5) nor the PDE4D (HSPDE4D4) isoforms were able to interact with a WW domain from the ubiquitin protein ligase Nedd4. WW domains are another class of modular domain for protein–protein interaction that binds to proline rich ligands. This supports the hypothesis that the interactions between these PDEs and SH3 domains are specific.

No changes in enzyme activity or in sensitivity to inhibition by the antidepressant drug rolipram were detected following the interaction of HSPDE4D4 with the SH3 domain of Lyn kinase. Therefore the interaction between HSPDE4D4 and the SH3 domain of Lyn kinase does not appear to cause any conformational change in the protein that is transmitted to the catalytic region.

The alternatively spliced, amino-terminal region of HSPDE4D4 is both necessary and sufficient for interaction with the SH3 domain of Lyn kinase. Furthermore, the purified fusion proteins GST–Lyn SH3 and MBP–HSPDE4D4 can interact with each other, as assessed by pull down assays, overlay assays and ELISA assays (see section 4.2.5). This shows that HSPDE4D4 can bind directly to the SH3 domain of Lyn kinase in *vitro*.

The amino-terminal region of HSPDE4D4 is extraordinarily rich in proline residues. A putative site of interaction between HSPDE4D4 and SH3 domains lies within the region of sequence between Pro^{53} and Pro^{88} of HSPDE4D4 (*Figure 3.8*). This region in HSPDE4D4 rich in proline residues (66.7%). The amino terminal region of HSPDE4D4, however, is not rich in arginine residues. Conserved arginine residues that flank the PxxP core motif are an important feature of the optimal sequences

for binding to several SH3 domains (1). I nevertheless feel that the proline rich region in the amino terminus of HSPDE4D4 is a good candidate for the site of interaction between HSPDE4D4 and certain SH3 domains. This is because the long stretches of proline residues present between Pro^{53} and Pro^{88} of HSPDE4D4 might be expected to form a left handed PPII helical structure such as is required for interaction with SH3 domains. There are also 3 (basic) histidine residues in this region, one of which could be considered to be a conservative substitution for arginine in the motif RxxPxxP that has been suggested to be optimal for binding to several SH3 domains (see section 1.4.1). Indeed, in one study the SH3 domain of Lyn kinase selected 2 peptide sequences with histidine in this position from a biased phage display library (176).

To directly assess the importance of the proline rich region of sequence between Pro^{53} and Pro^{88} of HSPDE4D4 in the interaction of this protein with SH3 domains it would be useful to construct deletion mutants and truncations of HSPDE4D4. The amino terminal region of the cDNA encoding HSPDE4D4 is, however, a poor template for PCR reactions and several attempts to construct such mutants have failed.

Using the strategy of immunoprecipitating HSPDE4D4 from transfected COS-7 cells I have not been able to demonstrate an *in vivo* interaction between HSPDE4D4 and another protein. Whether HSPDE4D4 does engage in physiologically relevant interactions with the SH3 domains of proteins *in vivo* remains to be determined.

Little is known about the tissue distribution and function of HSPDE4D4. It is therefore difficult to make predictions about which proteins are likely to interact with it *in vivo*. In the absence of a strong candidate interacting protein I feel that attempting to co-immunoprecipitate HSPDE4D4 with every protein containing an SH3 domain with which it can interact *in vitro* is likely to be an inefficient approach to identifying bona-fide HSPDE4D4 binding proteins. As more information regarding the tissue distribution and function of HSPDE4D4 becomes available this, together with the results of *in vitro* screens such as this one, will strengthen certain of the candidate interacting proteins. At that stage strategies such as immunoflourescent

confocal microscopy to examine the subcellular distributions of HSPDE4D4 and potential interacting proteins, co-immunoprecipitation experiments from cells that endogenously express PDE4D4 and the use of antisense to down-regulate the expression of putative targeting proteins could be attempted to show which if any of these potential interactions are physiologically relevant.

4. Purification of affinity tagged PDE4 expressed in *E.coli*

4.1 Strategies for the purification of PDE4

All cells and tissues thus far examined contain multiple forms of phosphodiesterase (PDE). A major obstacle to the study of the cyclic AMP (cAMP) specific, PDE4 enzymes has been obtaining homogeneous preparations of the various forms of this PDE to address questions such as, initially, whether the high affinity, cAMP specific PDE activity in a cell represented a number of different enzymes or a single core enzyme associated with variable regulatory subunits (147, 151, 157). Latterly, homogeneous preparations of PDE4 have been required to address questions regarding the regulation, function and pharmacology of individual PDE4 enzymes. Examples of such questions include the regulation by phosphorylation, the structure of and the binding of other molecules (such as rolipram) to PDE4s (179, 197).

4.1.1 Endogenous PDE4

Initial attempts to purify endogenous cAMP specific PDE isoforms from tissues and primary cell cultures met with only limited success. Apparently pure preparations of high affinity, cAMP specific PDEs were obtained by a number of groups, however, the purifications employed were laborious and frequently resulted in low yields. A major source of concern was that, despite having obtained an apparently purified enzyme, the fold purification and specific activity of these preparations were often low (*Table 4.4.1*). Coupled with the observation that cAMP specific PDE activities were extremely heat labile and sensitive to proteolysis, this led to speculation that the purified enzymes may have been denatured or proteolysed during their preparation (59, 147, 151).

		Specific Activity (nmol/min/mg)									
Isoform	**Source**	**Crude**	**Purified**	**Purification (fold)**	**Yield (%)**	**Km cAMP (μM)**	**Vmax (μmol/min/mg)**	**Inhibition by rolipram (μM)**	**Apparent Mw on SDS-PAGE (kDa)**	**Notes**	**Reference**
Probably PDE4	Dog kidney	0.18 (0.25μMcAMP)	22.4 (0.25μMcAMP)	124	5.3	2.2	0.095		60.6±2.2	Km for cGMP 312μM Inhibited by R20-1724: IC50 2.2μM, Ki 9.0μM Zn^{2+} does not support activity (not PDE4A)	(1, 2)
PDE4	Rat liver plasma membranes	0.04 (0.4μMcAMP)	380.2 (0.4μMcAMP)	9500	24	2-3 0.7±0.15	0.0091±0.0001		52.3±0.25	Km for cGMP 120μM Inhibited by R-1724: IC50 7.2μM	(3, 4, 5, 6)
PDE3,4,7or8	Rat skeletal muscle			50-60	25	2			92-94	Different amino acid composition that the dog kidney enzyme.	(7)
Probably PDE4	Human lung	3.3 (1μMcAMP)	100 (1μMcAMP)	303	6.2	0.7-0.8	0.2		58-62	Zn^{2+} does not support activity (not PDE4A) PDE assays performed at 24°C Mw determined by gel chromatography	(8)
Probably PDE3	Lukemic blast cells	0.045 (0.25μMcAMP)	1.2 (0.25μMcAMP)	30-50	5	0.6	0.0045		59±3	Km for cGMP 0.2μM Cross reacts with antisera raised against the dog kidney enzyme	(9)
PDE4,7or8	Lukemic blast cells	0.045 (0.25μMcAMP)	23 (0.25μMcAMP)		6	1.6	0.0095		30	Preparation was ~40% homogenity No cGMP PDE activity No cross reaction with antisera raised against the dog kidney enzyme	(9)
PDE4	Rat brain	0.657 (0.25μMcAMP)	30,245 (0.25μMcAMP)	46	4.6	3	0.36	Ki=0.9 IC_{50}=1.1	41-48	Mw determined by gel chromatography	(10)
PDE4	Postmeotic male mouse germ cells	0.21 (1μMcAMP)	2690 (1μMcAMP)	12990	1.8	3.3	10.5	Ki=0.77	43		(11)
PDE4D1 and or 4D2	Sertoli cells	0.71±0.38* (1μMcAMP)	1000-2000 (1μMcAMP)	>2000		1.97±0.26	9-10	IC_{50}=0.9	67-68	Preparation was 30-50% homogenicity *Homogenate from sertioli cells treated with 1mM Bt2 cAMP	(12)

Table 4.4.1: Purification of endogenous PDE4

The table summarises the published data on the purification of endogenous PDE4 isoforms.

References are: ***(1)*** *(232)* ***(2)*** *(59)* ***(3)*** *(136)* ***(4)*** *(135)* ***(5)*** *(173)* ***(6)*** *(172)* ***(7)*** *(151)* ***(8)*** *(147)* ***(9)*** *(164)* ***(10)*** *(157)* ***(11)*** *(68)* ***(12)*** *(40)*

4.1.2 Recombinant PDE4

In contrast to the slow progress made, during the 1980s, by groups using a biochemical approach to isolate and characterise cAMP specific PDE isoforms, a molecular biological approach to this problem proved extremely successful. In 1989 Ron Davis *et al* used a cDNA from the *Drosophila* dunce$^+$ gene to clone RNPDE4A1A (RD1), the first mammalian PDE4 cDNA to be reported. Additional PDE4 cDNAs were rapidly cloned and it soon became apparent that mammalian PDE4 activity represented a large enzyme family comprising the products of 4 related but distinct genes, with additional diversity arising from alternate mRNA splicing (38, 226)(see section 1.3).

The availability of cDNAs encoding mammalian PDE4 isoforms allowed researchers in the field to postpone the problem of PDE purification. Each newly cloned isoform was characterised in transiently transfected cell lines, such as COS-7, selected because of their low levels of endogenous PDE activity and the high efficiencies with which they could be transfected. In these systems enzyme purification was not necessary because of the relatively high levels of expression achieved. Indeed it was not uncommon for greater than 95% of the detectable PDE activity, present in the crude extracts of COS-7 cells transiently transfected with a recombinant PDE4 isoform, under the control of a strong promoter, to represent the transfected PDE (15, 16, 92, 93, 140, 194). The availability of sequence information from the cloned PDEs has also allowed for the generation of subtype specific antisera, which has greatly facilitated the study of PDE4 isoforms in crude extracts from both transfected and untransfected cells.

4.1.2.1 Purification of recombinant PDE4

The available immunological and molecular biological tools have allowed a great deal of progress to be made from the study of impure preparations of PDE4. There are, however, still a number of questions which will be very difficult to answer without first obtaining pure preparations of individual PDE4 isoforms. These include the 3 dimensional structure (108, 207), the interactions with inhibitors such as rolipram (179), the interactions with other proteins (252) and the acute

regulation by post-translational modification (for example by phosphorylation), of PDE4 isoforms (197).

Recent attempts to purify recombinant isoforms of PDE4, expressed in heterologous cells, have been more successful than the earlier purifications of native PDE4 (*Table 4.4.2*). This is probably due to the high levels of expression achieved in these artificial systems; although factors such as recent improvements in chromatography systems, improved protease inhibitors and the relative speed with which lysates can be prepared from cell lines compared to tissues may also be significant. It should be noted, however, that problems such as the low specific activity of many preparations persist and that there is no clear consensus on the criteria for acceptance of a preparation as being the correctly folded enzyme in a physiologically relevant state (186).

Isoform	Source	Specific Activity (nmol/min/mg)		Purification (fold)	Yield (%)	Km cAMP (μM)	Vmax (μmol/min/mg)	Inhibition by rolipram (μM)	Apparent Mw on SDS-PAGE (kDa)	Notes	Reference
		Crude	Purified								
HSPDE4A4C (h6.1) (Ac. No. U18087)	*S. cerevisiae*	0.005-0.009 (1μMcAMP)		53000	5-10	8±1	0.8±0.1	Ki=0.4±0.1	73±2	His_5 affinity tag at carboxyl terminus	(1)
HSPDE4A4B (aa201-886) (Ac. No. L20966)	Sf9 insect cells					5.2±0.3	0.0575±0.0015	IC_{50} = 0.0011±0.0003	90	~33 vector derived residues at amino terminus	(2)
HSPDE4A4B (Ac. No. L20965)	Sf9 insect cells	0.39 (0.1μMcAMP)	44.8 (0.1μMcAMP)	115	11	0.8±0.2	0.45	IC_{50} = 0.11			(3)
HSPDE4B2B (aa1-564) (Ac. No. L20971)	Sf9 insect cells					2-5	10-40	Ki=0.39±0.09* Ki=0.0056±0.0016**		*Postulated low affinity state (1h preincubation) **Postulated high affinity state (1h preincubation)	(4, 5)
HSPDE4B2B (aa 81-564) (Ac. No. L20971)	Sf9 insect cells	70 (0.5μMcAMP)	8900 (0.3μMcAMP)	127	10	4	40	Ki=0.6±0.2*** Ki=0.24±0.01* Ki=0.0086±0.0025**	55 (doublet)	***No preincubation with rolipram *Postulated low affinity state (1h preincubation) **Postulated high affinity state 1h preincubation)	(4, 5)
HSPDE4B2B (aa152-528) (Ac. No. L20971)	Sf9 insect cells					4	40	Ki=1*** Ki=0.36±0.04*	43	***No preincubation with rolipram *Postualted low affinity state (1h preincubation)	(4, 5)
HSPDE4B1A (Ac. No. L20966)[1]	Sf9 insect cells					4.7±0.0	0.1326±0.0033	IC_{50} = 0.0009±0.0	85	~33 vector derived residues at amino terminus	(2)
HSPDE4C1B (Ac. No. Z46632)[2]	Sf9 insect cells					1.7±0.1	0.3082±0.0091	IC_{50} = 0.3246±0.0274	80	~33 vector derived residues at amino terminus	(2)
HSPDE4D3 (Ac. No. L20970)	Sf9 insect cells					1.2±0.1	0.0279±0.0001	IC_{50} = 0.0611±0.0128	90	~33 vector derived residues at amino terminus	(2)

Isoform	Source	Specific Activity (µmol/min/mg) Crude	Purified	Purification (fold)	Yield (%)	Km cAMP (µM)	Vmax (µmol/min/mg)	Inhibition by rolipram (µM)	Apparent Mw on SDS-PAGE (kDa)	Notes	Reference
RNPDE4D1A (Ac. No. M25349)	RR1 *E.coli*	0.91 (5µMcAMP)	78.4 (5µMcAMP) 48.1±1.0 (1µMcAMP)	86	12.8	5.2±0.1	0.318±0.018	IC50 = 0.4	75	Mutation T556-S	(6)
RNPDE4D1A (96-584) (Ac. No. M25349)	RR1 *E.coli*		28.5±3.4 (1µMcAMP)			3.9±0.1	0.156±0.004		71	Mutations N98-T, I376-F and T556-S Mw calculated by plotting Rf values from the Coomassie stained gel shown in paper	(6)
RNPDE4D1A (aa121-584) (Ac. No. M25349)	RR1 *E.coli*		260±83			2.8±0.5	1.325±0.270		62		(6)
RNPDE4D1A (aa121-506) (Ac. No. M25349)	RR1 *E.coli*		334±102			1.8±0.3	1.360±0.020		49	Mw calculated by plotting Rf values from the Coomassie stained gel shown in paper	(6)
RNPDE4D1A (aa1-506) (Ac. No. M25349)	RR1 *E.coli*		14.9±0.4			3.2±0.5	0.146±0.018		64	Mw calculated by plotting Rf values from the Coomassie stained gel shown in paper	(6)
RNPDE4D1A (aa1-482) (Ac. No. M25349)	RR1 *E.coli*		3.7±1.2						57	Mw calculated by plotting Rf values from the Coomassie stained gel shown in paper	(6)
1 The author's RT-PCR products differed, at the amino acid level, from the genbank sequence as follows: Q171-R and Q202-L											
These differences were altered to match the genbank sequence by site-directed mutagenesis											
2 Sequence in genbank has cloning errors. The author's RT-PCR sequence differed, at the amino acid level, from the genbank sequence as follows: R81-P, Y261-C, D339-E, V340-L, D446-E and V447-L.											
These differences were altered to match the genbank sequence by site-directed mutagenesis											

Table 4.4.2: Purification of recombinant PDE4

The table summarises the published data on the purification of recombinant PDE4 isoforms expressed in heterologous cells.

References are: ***(1)*** *(245)* ***(2)*** *(241)* ***(3)*** *(169)* ***(4)*** *(178)* ***(5)*** *(179)* ***(6)*** *(108)*

4.2 Results and Discussion

I needed purified preparations of RNPDE4A5, HSPDE4A4 and HSPDE4D4 to investigate further the interactions of these isoforms with SH3 domains. I therefore decided to express the full length enzyme and truncated forms of each of these isoforms as fusion proteins. These were variously formed with maltose binding protein (MBP), with glutathione-S-transferase (GST) or as a 6 histidine motif (His_6) tagged species and expressed in *E.coli*. Such fusion proteins were then purified by affinity chromatography. This strategy has been successfully employed for the purification and characterisation of RNPDE4D1 (a short isoform of rat PDE4D) (108).

I chose to use *E.coli*, rather than mammalian cells, yeast or baculovirus, as the expression system because I was already experienced in the expression and purification of GST fusion proteins from *E.coli* (see sections 3.2.2.1–3.2.2.2). I was also attracted by the high levels of expression and the relative ease of purification which can often be achieved using this system.

4.2.1 Purification of affinity tagged PDE4A

I initially attempted to express the alternatively spliced, unique amino terminal regions from both the rat and the human PDE4A isoforms, RNPDE4A5 and HSPDE4A4B, as fusion proteins with carboxyl terminal, 6 histidine, zinc binding motifs (RNPDE4A5 His_6 and HSPDE4A4B His_6). These fusion proteins had been constructed in the plasmid pET5 (Promega) which carries a T7 promoter. I therefore chose to use the *E.coli* strain BL21(DE) as the host cells for expression of these fusion proteins. This strain contains the gene for T7 RNA polymerase under the control of a lac UV5 promoter. This promoter is inducible by isopropyl-β-D-thiogalactopyranoside (IPTG). Addition of IPTG to a growing culture of BL21(DE3) *E.coli* can be expected to induce T7 RNA polymerase expression and this will, in turn, transcribe any genes controlled by a T7 promoter.

Induction of BL21(DE3) *E.coli* transformed with either one of these plasmids

(pET5R6 for RNPDE4A5 His_6 and pET5H46 for HSPDE4A4B His_6) did not, however, result in the appearance of any novel bands in the induced lane when the crude lysates from induced and uninduced *E.coli* were visualised on a Coomassie stained gel.

To serve as a positive control for the induction conditions I transformed BL21(DE3) *E.coli* with the plasmid pET11TnC. This encodes the human heart muscle protein troponin C (TnC) under the control of an identical promoter to that which controlled the expression of the PDE His_6 fusion proteins in the plasmids pET5R6 and pET5H46. I induced cultures of these bacteria under identical conditions to those under which the bacteria transformed with the PDE His_6 fusion proteins in pET5 were induced. In these bacteria a novel band corresponding to TnC (predicted Mw 18.4kDa) was clearly visible in the induced lane when lysates of the bacteria were visualised on a Coomassie stained gel (*Figure 4.30*).

There are several possible explanations for having failed to achieve detectable levels of expression of the PDE isoforms from these plasmids. These included: secondary structures which may have been present in the DNA or the RNA and which may have hindered the progress of the polymerase or the transcriptase; also any toxic effects of the expressed protein which may have lead to plasmid instability (due to the cultures becoming overgrown by cells which had shed the plasmid). I tried a number of different conditions including varying the temperature (30–37°C), the concentration of IPTG (0.1–0.4mM) and the duration of the induction (0–14h) in an attempt to optimise the expression of these fusion proteins. I also addressed the possibility of plasmid instability by resuspending the bacteria in fresh growth medium containing ampicillin (100μ/μl) just prior to induction of the cultures. This last strategy was intended to counteract the effects of β-lactamase, which degrades ampicillin and is secreted into the medium by ampicillin resistant bacteria, and so to maintain selection for a longer period of time during the induction. I was, however, unable to identify conditions under which detectable expression of the PDE His_6 fusion proteins was achieved (*Figure 4.31*).

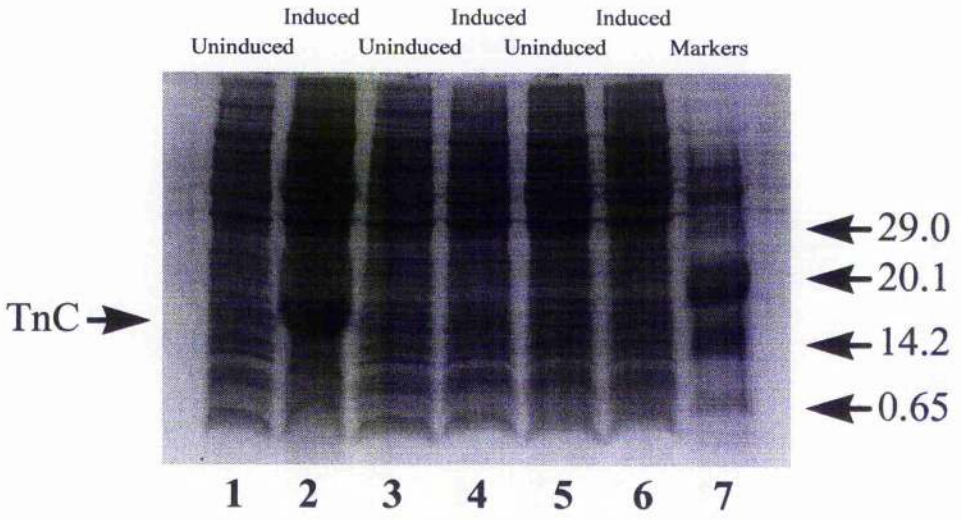

Figure 4.30: Expression of PDE4A in E.coli

The figure shows a Coomassie stained gel of lysates from BL21(DE3) E.coli transformed with plasmids encoding TnC (pET11TnC), the amino terminal of RNPDE4A5 (residues 1–76) as a fusion with a 6 His motif (pET5R6) and the amino terminal of HSPDE4A4B (residues 1–71) as a fusion with a 6 His motif (pET5H46). Lanes 1–2 are lysates prepared from growing cultures of cells transformed with pET11TnC before and 14h after induction with 0.1μM IPTG respectively, lanes 3–4 are lysates prepared from cells transformed with pET5R6 before and 14h after induction with 0.1μM IPTG respectively, lanes 5–6 are lysates prepared from cells transformed with pET5H46 before and 14h after induction with 0.1μM IPTG respectively, lane 7 is molecular weight markers (Sigma low range coloured markers). The arrows indicate the Mw (kDa) of each marker.

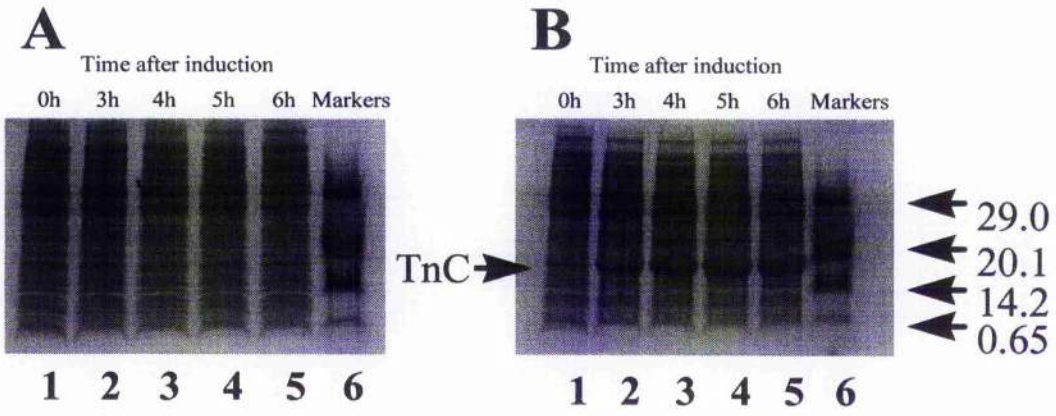

Figure 4.31: Time courses for the expression of proteins from pET plasmids in BL21(DE3) E.coli

The figure shows Coomassie stained gels of lysates prepared from BL21(DE3) E.coli, transformed with pET plasmids at various time points following induction with 0.1μM IPTG. Panel A: lanes 1–5 are lysates prepared from cells transformed with the plasmid pET5R6 at 0, 3, 4, 5 and 6h following induction respectively; lane 6 is molecular weight markers (Sigma low range coloured markers). Panel B: lanes 1–5 are lysates prepared from cells transformed with the plasmid pET11TnC at 0, 3, 4, 5 and 6h following induction respectively; lane 6 is molecular weight markers (Sigma low range coloured markers). The arrows indicate the Mw (kDa) of each marker.

4.2.1.1 Purification of RNPDE4A5 as a fusion protein with MBP

I considered the possibility that the difficulties I had experienced in expressing RNPDE4A5 His_6 and HSPDE4A4B His_6 may have been related, in some way, to the sequences at the extreme 5' ends of their open reading frames. I speculated that perhaps the bacterial transcription or translation machinery was inefficient at initiating either transcription or translation from these sequences and that a fusion protein, carrying an amino terminal tag which was known to be expressed well in bacteria, may be expressed at higher levels.

I decided to attempt to express and purify RNPDE4A5 as a fusion protein with MBP (MBP–RNPDE4A5). I chose to use MBP, rather than GST, as the affinity tag because I was intending to use this fusion protein in binding assays with GST SH3 domain fusion proteins. I therefore considered that it would be essential for the PDE to carry a different affinity tag to that carried by the SH3 domains unless I proteolytically removed the GST moiety from at least 1 of these species. This consideration was especially important because PDEs are extremely sensitive to proteolysis and I anticipated problems in proteolytically cleaving the affinity tag from the purified RNPDE4A5 fusion protein (see section 4.1.1 and references therein).

I chose to use the JM109 strain of *E.coli* for these experiments because they were, at the time, the most commonly used *E.coli* strain in the laboratory and had proved to be a good, general purpose strain suitable for the production of fusion proteins. I transformed these cells either with the plasmid pMALR6, which encodes full length RNPDE4A5 as a fusion protein with MBP or with the plasmid pMAL-c2, which encodes MBP alone. I then induced cultures of these cells to express the recombinant proteins. I used a lower temperature, 30°C rather than the more commonly used 37°C, for the induction and expression of these proteins because this can often reduce the proportion of the recombinant protein which becomes incorporated into inclusion bodies.

Induction of JM109 *E.coli*, transformed with the plasmid pMALR6, resulted in an approximately 10 fold increase in the PDE activity present in the soluble

fraction of the bacterial lysates over that observed in the lysates of bacteria transformed with pMAL-c2. A faint novel band which migrated with an apparent Mw of 176kDa on sodium dodecyl sulphate polyacrylamide gel electrophoresis (SDS–PAGE) was visible in the induced lane when lysates of these bacteria were visualised on a Coomassie stained gel (*Figure 4.32*). The predicted Mw for the MBP–RNPDE4A5 fusion protein, based on the primary structure, was 137.1kDa. The difference between the observed and predicted Mw for this fusion protein can be accounted for by the anomalous migration of PDE4 isoforms on SDS–PAGE (15, 16, 93, 108, 201).

I attempted to purify the MBP–RNPDE4A5 fusion protein by a single step of affinity chromatography using amylose resin (New England Biolabs). This resulted in a 27 fold purification of the PDE enzyme activity. I also monitored the purification by SDS–PAGE. This revealed that the eluted material, containing the PDE activity, did not migrate as a single band but gave a ladder of bands on Coomassie stained gels (*Figure 4.32*).

To investigate whether the multiple bands observed on Coomassie stained gels represented truncated forms of the MBP–RNPDE4A5 fusion protein, I performed immunoblots using a polyclonal antisera raised against the carboxyl terminal region of rat PDE4A and also using a polyclonal antisera raised against MBP. Both of these antisera detected an immunoreactive species which co-migrated with the 176kDa band observed on Coomassie stained gels. This species therefore contained epitopes that would be predicted to occur at the amino terminal, detected by the anti MBP antisera, and also at the carboxyl terminal, detected by the anti rat PDE4A antisera, of the MBP–RNPDE4A5 fusion protein. The 176kDa species was therefore, in all probability, full length MBP–RNPDE4A5 as it contained epitopes located within both the amino and the carboxyl termini of this fusion protein (*Figure 4.33*).

In addition to the 176kDa band, the anti MBP antisera, but not the anti-rat PDE4A antisera, detected 4 faster migrating bands. These bands most likely represented carboxyl terminal truncations of the MBP-RNPDE4A5 fusion protein, generated by proteolysis or premature termination, which retained their MBP tags and hence co-

purified with the full length fusion protein.

The PDE enzyme assay, and the immunological data supported the hypothesis that I had succeeded in expressing an active, full length, affinity-tagged PDE in the soluble fraction of JM109 *E.coli*. The affinity purification of this protein using amylose resin, however, resulted in a preparation with a low (1.84±0.11nmol/min/mg at 1μM cAMP) specific activity, compared to that estimated for RNPDE4A5 expressed in the cytosolic fraction of COS-7 cells and which ran as a ladder of bands on Coomassie stained gels. Several of the bands detected by Coomassie staining were neither detected by an anti-MBP antisera nor by an anti-rat PDE4A antisera. The identity of these contaminating bands is therefore unclear. As I did not have ready access to a liquid chromatography system with which to further purify this fusion protein I decided not to pursue the purification and analysis of this fusion protein.

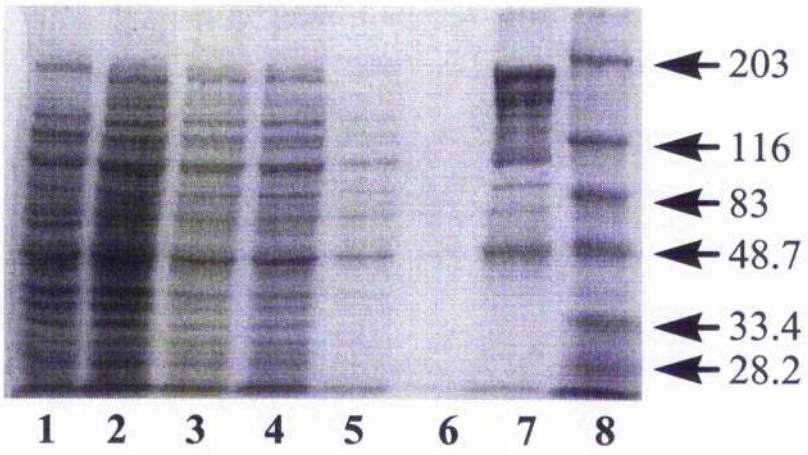

Figure 4.32: Purification of RNPDE4A5 as a fusion protein with MBP

The figure shows a Coomassie stained gel of fractions collected during the purification of MBP–RNPDE4A5. Lane 1 is whole cell lysate from uninduced bacteria transformed with the plasmid pMALR6; lane 2 is whole cell lysate from bacteria transformed with the plasmid pMALR6, which had been induced to express MBP–RNPDE4A5 by the addition of 0.3mM IPTG; lane 3 is the soluble fraction of the lysate from bacteria expressing MBP–RNPDE4A5 after incubation with amylose resin; lanes 4-6 are the material washed from the amylose resin by the 1st, 2nd and 3rd washing steps respectively; lane 7 is the material eluted from the amylose resin; lane 8 is molecular weight markers (Bio-Rad broad range prestained SDS–PAGE standards). The arrows indicate the Mw (kDa) of each marker.

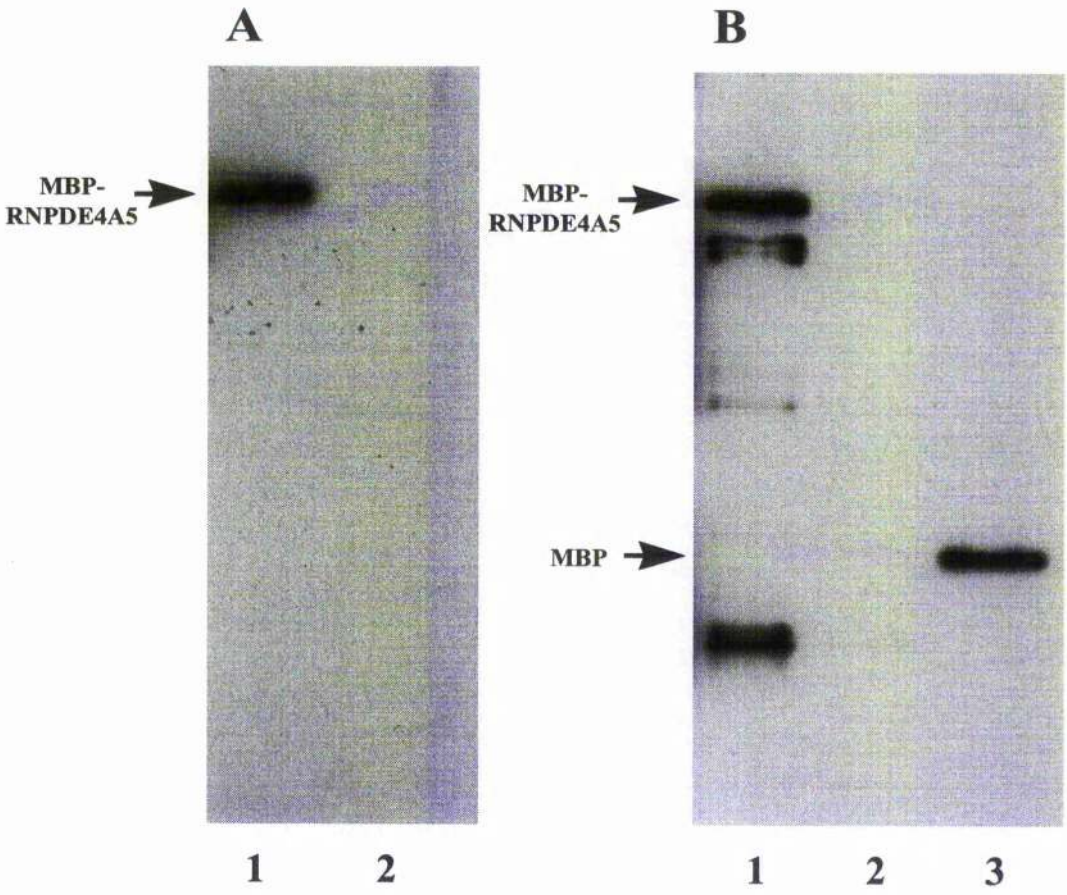

Figure 4.33: Immunological analysis of purified MBP and MBP–RNPDE4A5

The figure shows immunoblots of purified MBP and MBP–RNPDE4A5. Panel A shows an immunoblot that was probed with an antisera raised against the carboxyl terminal region of rat PDE4A: lane 1 is 0.02μg purified MBP–RNPDE4A5, lane 2 is 0.01μg purified MBP. Panel B shows an immunoblot that was probed with an antisera raised against MBP: lane 1 is 0.02μg purified MBP–RNPDE4A5, lane 2 is empty, lane 3 is 0.01μg purified MBP. The arrows indicate the positions of MBP–RNPDE4A5 and of MBP; these proteins ran with apparant molecular weights of 170 kDa and 50 kDa respectively, calculated by plotting the Rf values of markers run on the same gel.

4.2.2 Purification of affinity tagged PDE4D

At the same time that I was attempting to express and purify MBP–RNPDE4A5, I also attempted to express and purify MBP fusion proteins of full length HSPDE4D4 (MBP–HSPDE4D4) and also of the unique, amino terminal region (amino acids 1–166) of HSPDE4D4 (MBP–NT HSPDE4D4).

4.2.2.1 Purification of full length HSPDE4D4 as a fusion protein with MBP

I transformed JM109 *E.coli* with the plasmid pMALP39, which encodes full length HSPDE4D4 as a fusion protein with MBP. I then induced cultures of these cells to express the recombinant proteins. As with the MBP–RNPDE4A5 fusion protein I performed these inductions at 30°C in an attempt to maximise the proportion of the fusion protein expressed in the soluble fraction of the cells. This resulted in an approximately 75-fold increase in the PDE activity present in the soluble fraction of the bacterial lysates over that observed in the lysates of bacteria transformed with pMAL-c2. A faint novel band which migrated with an apparent Mw of 161±15.5kDa on SDS–PAGE was visible in the induced lane when lysates of the bacteria were visualised on a Coomassie stained gel (*Figure 4.34*). The predicted Mw for the MBP-RNPDE4D4 fusion protein, based on its primary structure, was 135kDa. As with the MBP–RNPDE4A5 fusion protein, the difference between predicted and the observed Mw for this fusion protein is likely to be accounted for by the anomalous migration of PDE4 isoforms on SDS–PAGE.

I attempted to purify MBP–HSPDE4D4 by a single step of affinity chromatography using amylose resin. This resulted in a 67-fold purification of the PDE enzyme activity. I also monitored the purification on Coomassie stained SDS–PAGE gels. The major band present in the eluted material migrated with an apparent Mw of 152±3.3kDa and represented >98% of the stained protein, as assessed by scanning the gel and counting pixels (*Figure 4.34*).

To investigate further the identity of the major protein band present in the eluted material I performed immunoblots using a monoclonal antibody against the carboxyl terminal region of HSPDE4D4 and also using a polyclonal antisera against

MBP. Both antibodies detected an immunoreactive band which co-migrated with the 152kDa band visible on the Coomassie stained gels (*Figure 4.35*). The immunological data therefore supported the hypothesis that the major protein species present in the eluted material was full length MBP–HSPDE4D4.

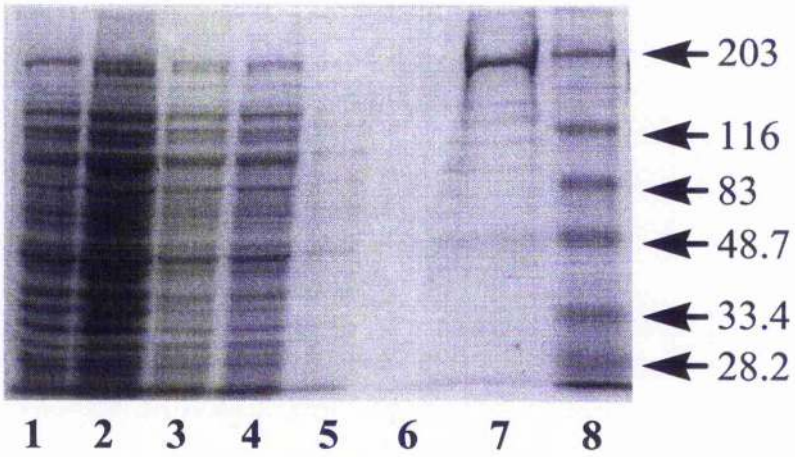

Figure 4.34 Purification of HSPDE4D4 as a fusion protein with MBP

The figure shows a Coomassie stained gel of fractions collected during the purification of MBP–HSPDE4D4. Lane 1 is whole cell lysate from uninduced bacteria transformed with the plasmid pMALP39; lane 2 is whole cell lysate from bacteria transformed with the plasmid pMALP39, which had been induced to express MBP–HSPDE4D4 by the addition of 0.3mM IPTG; lane 3 is the soluble fraction of the lysate from bacteria expressing MBP–HSPDE4D4 after incubation with amylose resin; lanes 4-6 are the material washed from the amylose resin by the 1st, 2nd and 3rd washing steps respectively; lane 7 is the material eluted from the amylose resin; lane 8 is molecular weight markers (Bio-Rad broad range prestained SDS–PAGE standards). The arrows indicate the Mw (kDa) of each marker.

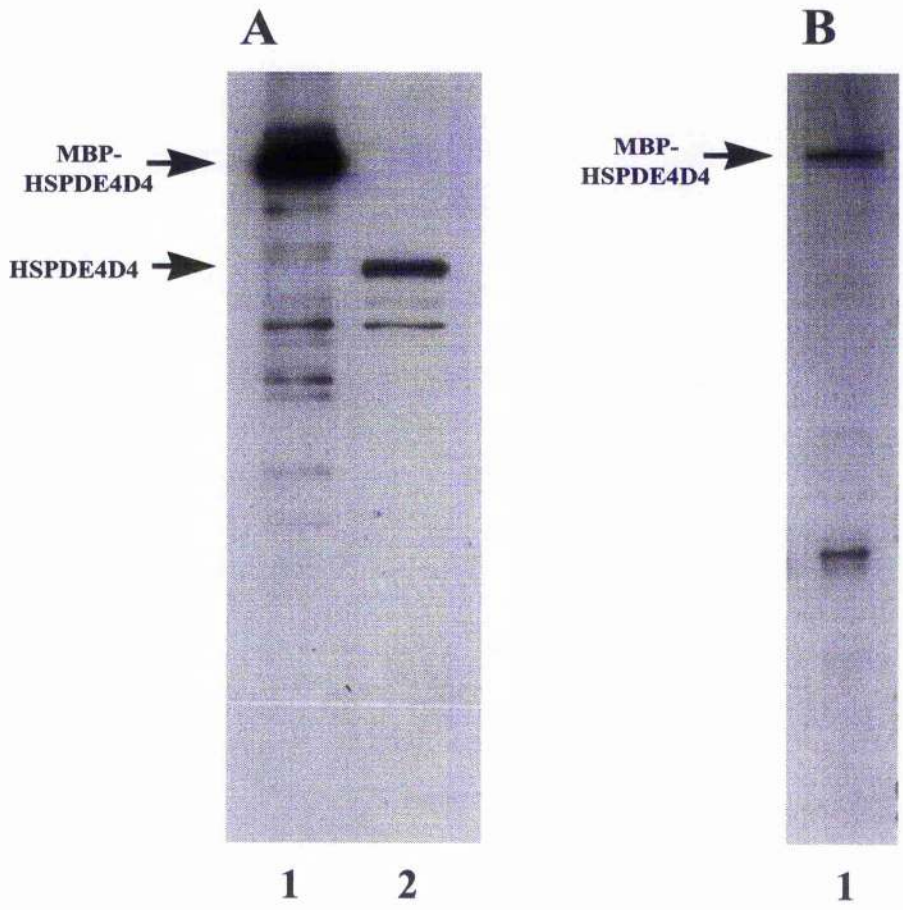

Figure 4.35 Immunological analysis of purified MBP–HSPDE4D4

The figure shows immunoblots of purified MBP–HSPDE4D4. Panel A shows an immunoblot that was probed with a monoclonal antibody against the carboxyl terminal region of human PDE4D: lane 1 is 0.2μg purified MBP–HSPDE4D4, lane 2 is 4μg cytosol from COS-7 cells overexpressing HSPDE4D4. Panel B shows an immunoblot that was probed with an antisera raised against MBP: lane 1 is 0.2μg purified MBP–HSPDE4D4. The arrows indicate the positions of MBP–HSPDE4D4 and of recombinant HSPDE4D4 expressed in the cytosol of transfected COS-7 cells; these proteins ran with apparant molecular weights of 153 kDa and 112 kDa respectively, calculated by plotting the Rf values of markers run on the same gel.

4.2.2.2 Purification of the amino terminal region of HSPDE4D4 as a fusion protein with MBP

The amino terminal region of HSPDE4D4 does not include the catalytic site of the enzyme. I was therefore unable to use PDE enzyme activity assays to monitor the purification of this fusion protein. I monitored the expression and purification of this fusion protein on Coomassie stained SDS–PAGE gels and also by immunoblotting using a polyclonal antisera against MBP.

Induction of JM109 *E.coli* transformed with the plasmid pMAL.P39A1, which encodes amino acids 1–166 of HSPDE4D4 as a fusion protein with MBP, did not result in the appearance of a detectable novel band in the induced lane of Coomassie stained SDS–PAGE gels. I did, however, detect a novel band of anti-MBP immunoreactive material in the induced lane of immunoblots. I therefore proceeded with the purification of this fusion protein, by affinity chromatography, using amylose resin.

By starting with 800ml of induced culture, which is double the amount used for the purification of MBP–HSPDE4D4, I was able to purify 108μg of material. The major band present in this eluted material migrated with an apparent Mw of 84±2.1kDa and represented >90% of the stained protein (assessed by scanning the gel and counting pixels) (*Figure 4.36*). The predicted Mw of this fusion protein was 61.8kDa.

Immunoblots of the eluted material, performed using a polyclonal antisera against MBP, revealed a major immunoreactive band which co-migrated with the 84kDa band visible on the Coomassie stained gel (*Figure 4.36*). The immunological data therefore supported the hypothesis that the major protein species present in the eluted material was a fusion protein between MBP and the amino terminal region of HSPDE4D4 (MBP–NT HSPDE4D4).

The difference between the predicted and the observed Mw of MBP–NT HSPDE4D4 was unexpected. The anomalous migration of PDE4 isoforms on SDS–PAGE has previously been attributed to the concentration of acidic amino acids in the carboxyl terminal regions of these proteins (15, 16, 93, 108, 201). Indeed, carboxyl

terminal deletion mutants of RNPDE4D1, expressed in and purified from *E.coli*, migrated as predicted on SDS–PAGE whereas full length and amino terminal deletion mutants of RNPDE4D1 migrated with apparent Mw 6–9kDa higher than predicted from their primary structures (108). The situation is, however, complicated by the finding that the human homologue of this splice variant, HSPDE4D1, expressed in COS-7 cells, does not exhibit anomalous migration on SDS–PAGE (15). In the same study, however, the splice variant HSPDE4D2, the primary sequence of which is entirely contained within that of HSPDE4D1, did show anomalous migration on SDS–PAGE. This suggests that the expression system used and also sequence contained in the amino terminal of certain isoforms, may also affect their migration on SDS–PAGE.

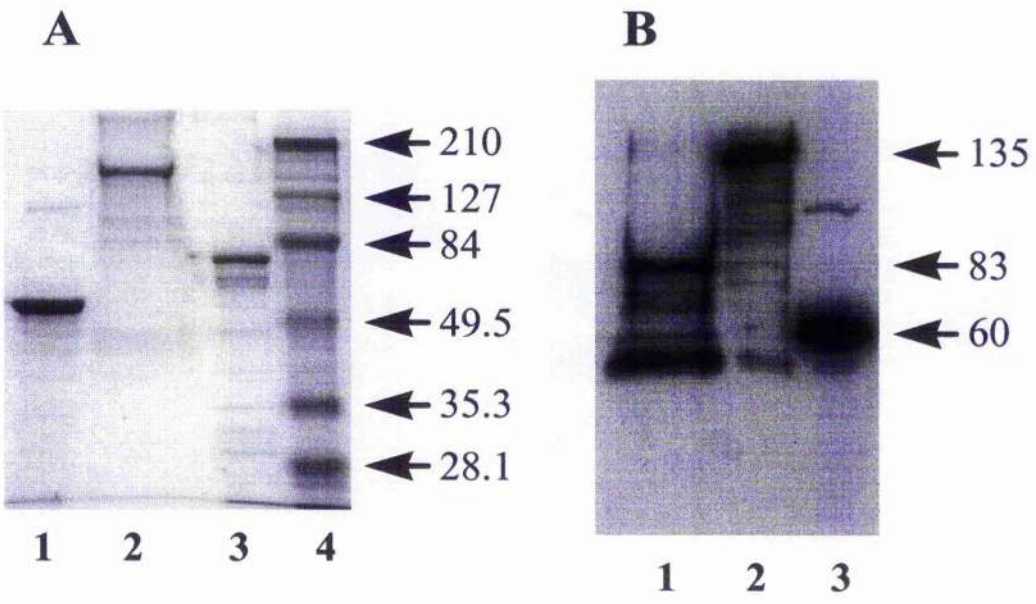

Figure 4.36: Purification of full length and truncated HSPDE4D4 as fusion proteins with MBP

The figure shows SDS–PAGE analysis of both full length and truncated HSPDE4D4 as fusion proteins with MBP. Panel A shows a Coomassie stained gel of purified MBP fusion proteins: lane 1 is 4μg purified MBP, lane 2 is 3μg purified MBP–HSPDE4D4, lane 3 is 3μg purified MBP–NT HSPDE4D4, lane 4 is molecular weight markers (Bio-Rad broad range prestained SDS–PAGE standards). The arrows indicate the Mw (kDa) of each marker. Panel B shows an immunoblot that was probed with an antisera raised against MBP: lane 1 is 0.05μg purified MBP–NT HSPDE4D4, lane 2 is 0.1μg purified MBP–HSPDE4D4, lane 3 is 0.1μg purified MBP. The arrows indicate the apparent Mw (kDa) each major band, calculated by plotting the Rf values of markers run on the same gel.

4.2.3 Characterisation of MBP–HSPDE4D4

On the basis of the immunological and the enzyme activity data, I had succeeded in purifying an intact fusion protein, between HSPDE4D4 and MBP, to apparent homogeneity. I next investigated whether this preparation accurately represented the correctly folded enzyme.

To address this question I performed a limited kinetic characterisation of MBP–HSPDE4D4. I decided to compare the kinetics of cAMP hydrolysis and the sensitivity to inhibition by rolipram, a specific inhibitor of PDE4, of MBP–HSPDE4D4 to those of recombinant HSPDE4D4, expressed in the cytosolic fraction of COS-7 cells. I also decided to compare the data to those obtained for other isoforms of PDE4D which have been expressed in *E.coli (Table 4.4.3)* and also in COS-7 cells (15). It would have been desirable to compare the properties of this fusion protein to those of endogenously expressed HSPDE4D4, unfortunately it was not possible to do so because this isoform has not yet been isolated from untransfected cells or from tissue (15).

Isoform	*E.coli* Strain	Specific Activity of Crude Extract (nmol/min/mg)	Km cAMP (μM)	Inhibition by rolipram (μM)	Apparant Mw on SDS-PAGE (kDa)	Notes	Reference
RNPDE4D1 (Ac. No. M25349)	DH5α	0.4 (1μMcAMP)	2.0±0.5	IC_{50}=0.56±0.1			(1)
RNPDE4D1 (Ac. No. M25349)	DH5α	0.1768±0.0049 (1μMcAMP)	2.84±0.62	IC_{50}=0.36±0.08	70-71	An additional doublet of 47-50kDa was also present in all experiments performed	(2)
RNPDE4D1 (aa1-485) (Ac. No. M25349)	DH5α	0.067±0.015 (1μMcAMP)	3.73±1.96	IC_{50}=0.50±0.10	53-55		(2)
RNPDE4D1 (Δaa49-145) (Ac. No. M25349)	DH5α	0.356* (1μMcAMP)	2.36±0.25	IC_{50}=0.94±0.16	60-61	An additional doublet of 47-50kDa was also present in all experiments performed *Specific activity estimated from bar chart presented in paper	(2)
RNPDE4D1 (Δaa49-179) (Ac. No. M25349)	DH5α	0.009* (1μMcAMP)			57-58	An additional doublet of 47-50kDa was also present in all experiments performed *Specific activity estimated from bar chart presented in paper	(2)
RNPDE4D1 (Δaa1-212) (Ac. No. M25349)	DH5α	0.009* (1μMcAMP)			54-55	An additional doublet of 47-50kDa was also present in all experiments performed *Specific activity estimated from bar chart presented in paper	(2)
HSPDE4D? (Ac. No. U02882)	SOLR	0.0053		IC_{50}=2.2		Fusion protein between residues 1-5 of β-galactosidase and residues 87-604 of the PDE	(3)
RNPDE4D1A (Ac. No. M25349)	RRI	0.91 (5μMcAMP)	5.2±0.1	IC_{50} = 0.4	73	Mutation T536-S	(4)

Isoform	*E.coli* Strain	Specific Activity of Crude Extract (nmol/min/mg)	Km cAMP (μM)	Inhibition by rolipram (μM)	Apparant Mw on SDS-PAGE (kDa)	Notes	Reference
RNPDE4D1A (aa96-584) (Ac. No. M25349)	RR1		3.9±0.1		71	Mutations N98-T, L376-P and T356-S Mw calculated by plotting Rf values from the Coomassie stained gel shown in paper	(4)
RNPDE4D1A (aa121-584) (Ac. No. M25349)	RR1		2.8±0.5		62		(4)
RNPDE4D1A (aa121-506) (Ac. No. M25349)	RR1		1.8±0.3		49	Mw calculated by plotting Rf values from the Coomassie stained gel shown in paper	(4)
RNPDE4D1A (aa1-506) (Ac. No. M25349)	RR1		3.2±0.5		64	Mw calculated by plotting Rf values from the Coomassie stained gel shown in paper	(4)
RNPDE4D1A (aa1-482) (Ac. No. M25349)	RR1				57	Mw calculated by plotting Rf values from the Coomassie stained gel shown in paper	(4)
HSPDE4D5 (Ac. No. S:1059276)	JM109	0.029±0.002 (1μMcAMP)	5.1±0.7	IC_{50} = 0.16±0.5		Fusion protein between maltose binding protein and HSPDE4D5	(5)

Table 4.4.3: Expression of recombinant PDE4 isoforms in E.coli

The table summarises the published data on the properties of recombinant PDE4 isoforms expressed in E.coli.

References are: ***(1)*** *(227)* ***(2)*** *(99)* ***(3)*** *(5)* ***(4)*** *(108)* ***(5)*** *(252)*

4.2.3.1 Kinetics of cAMP hydrolysis by MBP–HSPDE4D4

I performed a kinetic analysis of the purified MBP–HSPDE4D4 fusion protein and also of recombinant HSPDE4D4 expressed in the cytosolic fraction of transfected COS-7 cells. For these studies I assayed the initial velocity of cAMP hydrolysis at 16 different substrate concentrations over the range 0.1-50μM cAMP. I calculated values for the constants Km and Vmax for each preparation, by fitting the kinetic data to the hyperbolic form of the Michaelis-Menten equation using the computer program Hyper 1.02a (see section 2.2.12). This analysis revealed that both preparations of HSPDE4D4 catalysed the hydrolysis of cAMP with kinetics that conformed well to the Michaelis-Menten model and that were linear when plotted in accordance with several linear transformations of the Michaelis-Menten equation (*Figure 4.37, Figure 4.38*).

The purified MBP–HSPDE4D4 catalysed the hydrolysis of cAMP with a Km of 13.0±2.5μM and a Vmax of 1495±305μmol/min/mg. The unpurified preparation of recombinant HSPDE4D4, expressed in the cytosolic fraction of COS-7 cells, had a Km of 1.4±0.3μM for the hydrolysis of cAMP; the Vmax of this preparation was 5.3±0.6μmol/min/mg cytosolic protein. It should be noted that the Vmax of unpurified preparations of PDEs, expressed in COS-7 cells, can vary widely between preparations because of differences in the individual transfection efficiencies (see section 4.2.3.2).

The Km for cAMP of the purified MBP–HSPDE4D4 was approximately an order of magnitude higher than that of HSPDE4D4, expressed in the cytosolic fraction of COS-7 cells. The value for the Km that I obtained for HSPDE4D4, expressed in COS-7 cells, was in close agreement with that previously determined for this isoform in the same expression background and also with the published values of Km of several other isoforms of PDE4D, expressed in E.coli (*Table 4.4.3*) (15, 99, 108). This suggested that the cAMP binding site of the MBP–HSPDE4D4 fusion protein may have been in a different conformation to that of the other preparations of this enzyme.

It seemed likely that the difference in Km between these 2 preparations of HSPDE4D4 was due either to the MBP moiety of the fusion protein or to the prokaryotic expression system used for the production of MBP–HSPDE4D4. Other splice variants of PDE4D exhibit similar values of Km to themselves and to each other when expressed in either prokaryotic or eukaryotic cells. This shows that the observed difference in the Km of MBP–HSPDE4D4 is not simply because the cAMP binding site of PDE4D enzymes can not fold correctly in prokaryotes.

All of the active splice variants and truncations of PDE4D (with the exception of MBP–HSPDE4D4), thus far examined, exhibit a similar Km for cAMP. Indeed an MBP fusion protein of HSPDE4D5, expressed in and purified from *E.coli*, has a Km for cAMP of 5.1±0.4μM (252). This suggests that regions of the protein outside of the cAMP binding site have little influence on the conformation of this region. I therefore speculated that the MBP moiety of MBP–HSPDE4D4 may contact or sterically hinder the cAMP binding site of this protein. There were, however, various other possibilities that may have accounted for the difference in Km between HSPDE4D4 expressed in the cytosol of transfected COS-7 cells and MBP–HSPDE4D4 purified from *E.coli*. For example it could have been that the unique, alternatively spliced region of PDE4D4 does affect the binding of cAMP to this splice variant and that either some post-translational modification or the folding of this region is different when the protein is expressed in prokaryotic cells, as a fusion protein with MBP, compared to when the non-fusion protein is expressed in eukaryotic cells (see section 4.2.4.2).

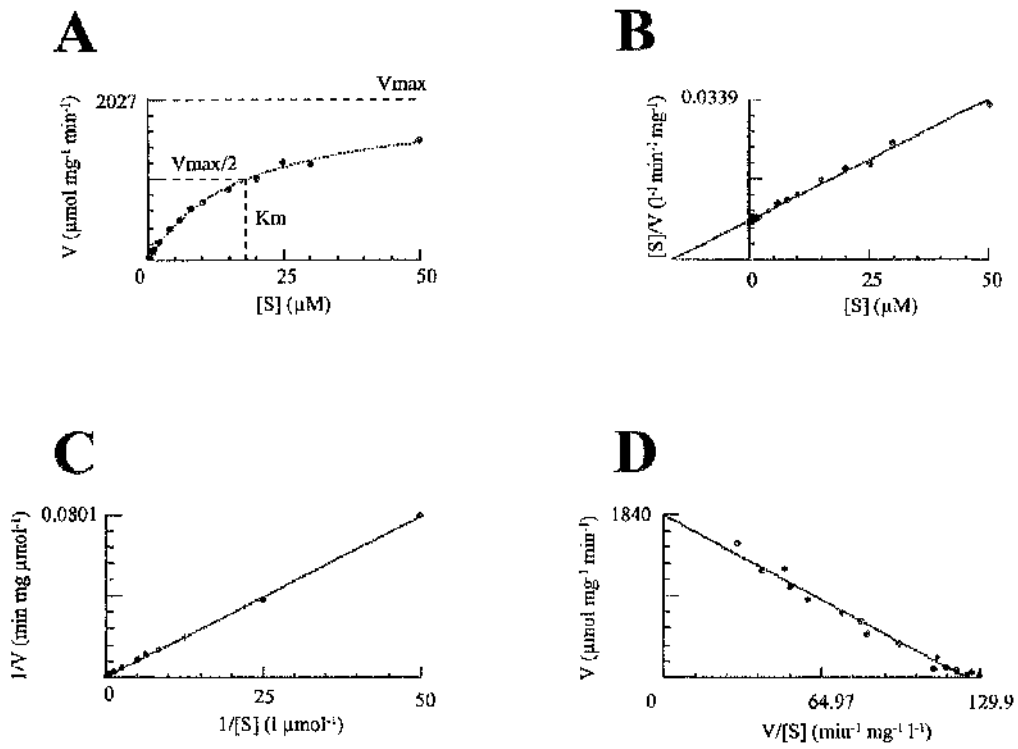

Figure 4.37: Kinetic analysis of purified MBP–HSPDE4D4

The figure shows graphical solutions of the Michaelis-Menten equation for the hydrolysis of cAMP by purified MBP–HSPDE4D4. The initial velocity of catalysis was assayed at 16 different substrate concentrations and the data were fitted to the Michaelis-Menten equation using the computer program Hyper 1.02a. Panel A shows a graph for the hyperbolic form of the equation. Panels B, C and D show a Hanes plot, a Lineweaver-Burk plot and an Eadie-Hofstee plot respectively. The graphs shown represent the results from a typical experiment of 3 performed. These analyses revealed a Km for cAMP of 13±2.5µM and a Vmax of 1495.5±304.7µmol/min/mg.

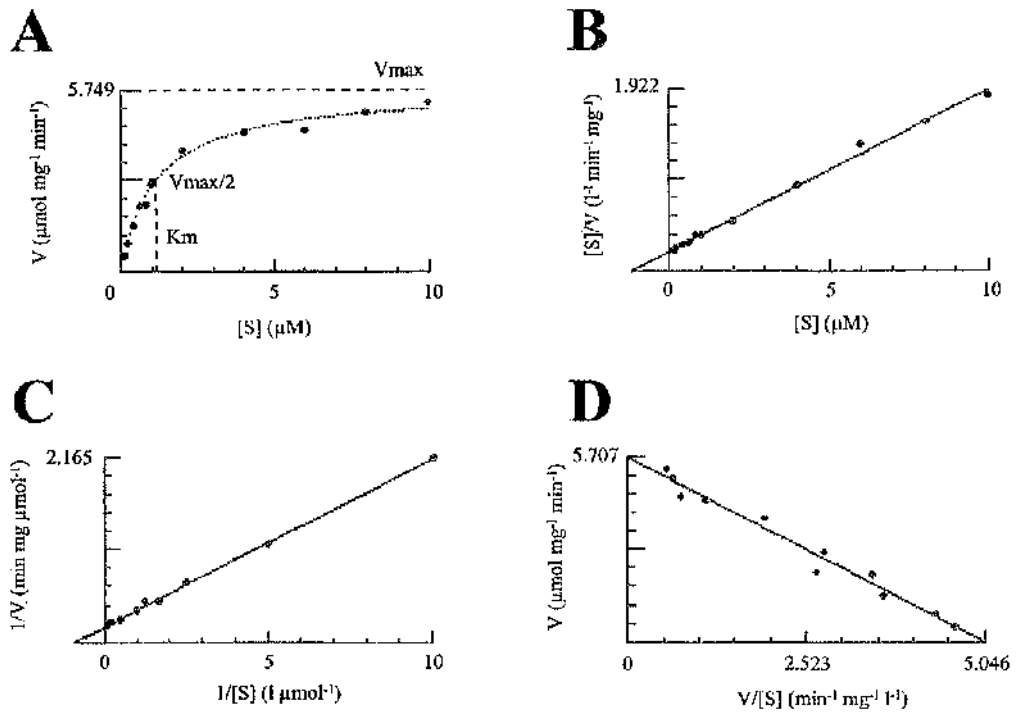

Figure 4.38: Kinetic analysis of unpurified HSPDE4D4 expressed in the cytosoluc fraction of COS-7 cells

The figure shows graphical solutions of the Michaelis-Menten equation for the hydrolysis of cAMP by unpurified HSPDE4D4 expressed in the cytosolic fraction of COS-7 cells. The initial velocity of catalysis was assayed at 11 different substrate concentrations and the data were fitted to the Michaelis-Menten equation using the computer program Hyper 1.02a. Panel A shows a graph for the hyperbolic form of the equation. Panels B, C and D show a Hanes plot, a Lineweaver-Burk plot and an Eadie-Hofstee plot respectively. The graphs shown represent the results from a typical experiment of 3 performed. These analyses revealed a Km for cAMP of 1.4±0.3µM and a Vmax of 5.3±0.6µmol/min/mg.

4.2.3.2 Estimated turnover number of HSPDE4D4 for cAMP hydrolysis

The value of Vmax which I have calculated for HSPDE4D4, expressed in the cytosolic fraction of COS-7 cells, is expressed in terms of activity per μg cytosolic protein. This value is therefore highly dependent upon the level of expression of HSPDE4D4 achieved in each particular transfection and should not be compared directly to the Vmax of other preparations.

To compare the activity of HSPDE4D4, expressed in the cytosolic fraction of COS-7 cells, with that of purified MBP–HSPDE4D4 I have performed quantitative immunoblots to estimate the molar concentration of HSPDE4D4 in the cytosolic fraction of a particular preparation of transfected COS-7 cells. I then calculated the turnover number (moles of cAMP hydrolysed per minute per mole of PDE) for cAMP hydrolysis by both MBP–HSPDE4D4 and of HSPDE4D4 expressed in the cytosolic fraction of COS-7 cells. This analysis revealed that MBP–HSPDE4D4 catalysed the hydrolysis of cAMP with a turnover number of 201±41.1min^{-1} and that HSPDE4D4, expressed in the cytosolic fraction of COS-7 cells, catalysed the hydrolysis of cAMP with a turnover number of 106±11.9min^{-1} (*Figure 4.39*). These values are not significantly different at the 5% level (Student's t-Test).

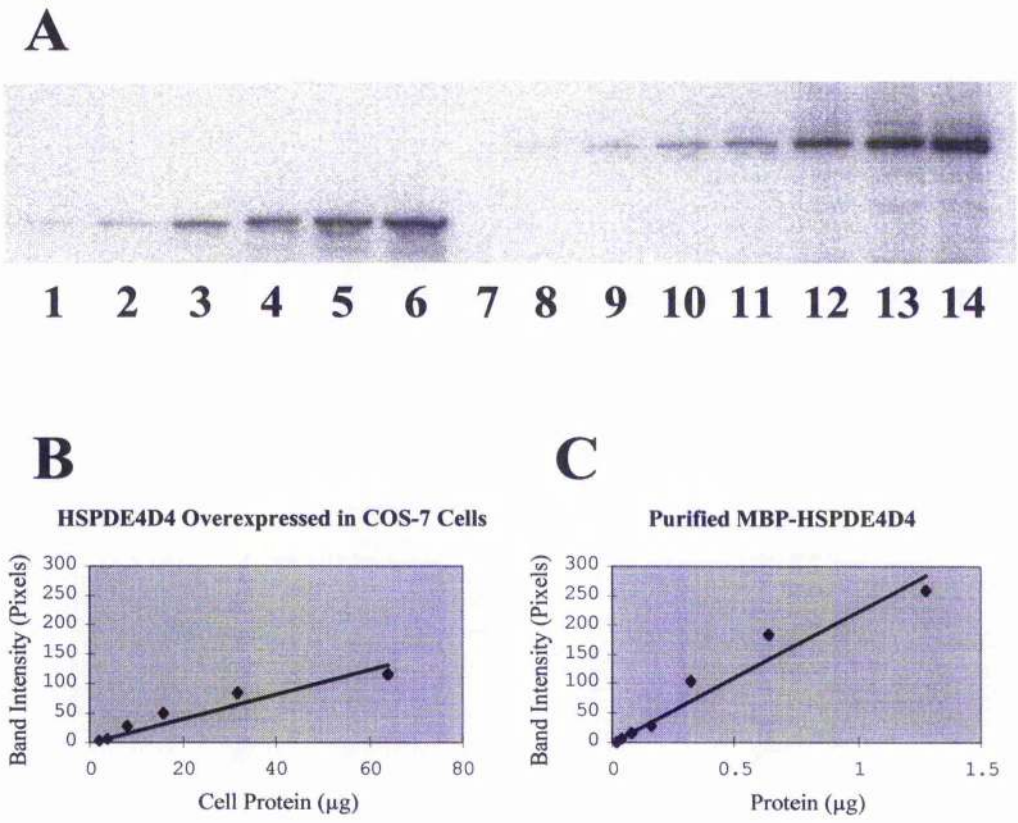

Figure 4.39: Determination of the concentration of HSPDE4D4 present in the cytosolic fraction of transfected COS-7 cells

The figure shows a quantitative immunoblot, for PDE4D, of the cytosolic fraction from COS-7 cells transiently transfected to overexpress HSPDE4D4 and of purified MBP–HSPDE4D4. Panel A shows a phosphoimage of the immunoblot. The primary antibody was the monoclonal antibody 61D10E (Icos) which binds to the carboxyl terminal region of PDE4D isoforms. The secondary antibody was an I^{125} conjugated anti-mouse IgG. Lanes 1–6 are 2, 4, 8, 16, 32 and 64µg cytosol from COS-7 cells overexpressing HSPDE4D4 respectively; lane 7 is empty; lanes 8–14 are 0.02, 0.04, 0.08, 0.16, 0.32, 0.64 and 1.28µg purified MBP–HSPDE4D4 respectively. Panels B and C are graphs showing band intensity against material loaded for HSPDE4D4 expressed in the cytosol of COS-7 cells and for purified MBP–HSPDE4D4 respectively. The data shown represent the results from a typical experiment of 3 performed.

4.2.3.3 Inhibition of MBP–HSPDE4D4 by rolipram

The antidepressant drug rolipram in a potent and specific inhibitor of PDE4 enzyme activity (87). Indeed, sensitivity to inhibition by rolipram is often used as a diagnostic test for the presence of PDE4. I therefore compared the sensitivity of purified MBP–HSPDE4D4 to inhibition by rolipram to that of HSPDE4D4 expressed in the cytosolic fraction of COS-7 cells.

I calculated values for the IC_{50} of rolipram on the hydrolysis of cAMP by both purified MBP–HSPDE4D4 and by unpurified HSPDE4D4, expressed in the cytosolic fraction of COS-7 cells. For these studies I assayed the initial rate of cAMP hydrolysis, at a substrate concentration close to the Km of the preparation, in the presence of 8 different concentrations of rolipram over the range 0–100μM. I used the computer program Kelidagraph to fit these data to an equation describing a sigmoidal curve and so derived the concentration of rolipram required to inhibit 50% of the activity observed in the absence of rolipram (see section 2.2.12) (*Figure 3.17 and Figure 4.40*). This analysis revealed that rolipram inhibited MBP–HSPDE4D4 with an IC_{50} of 0.215±0.001μM (at 10μM cAMP) and that it inhibited unpurified HSPDE4D4, expressed in the cytosolic fraction of COS-7 cells, with an IC_{50} of 0.160±0.029μM (at 1μM cAMP). These values are not significantly different at the 5% level (Student's t-Test).

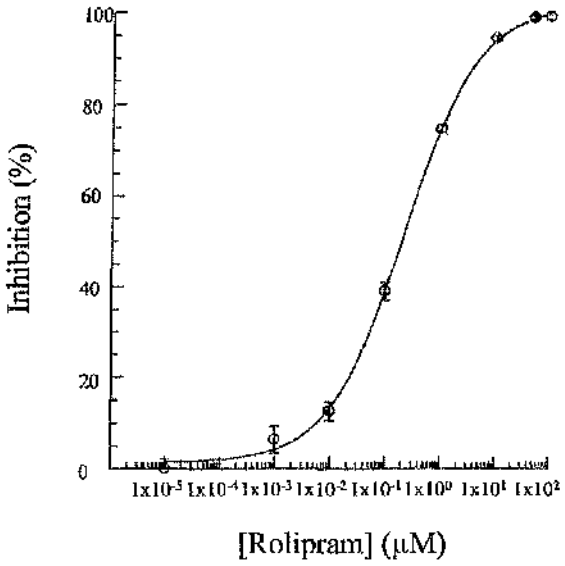

Figure 4.40: Inhibition of MBP–HSPDE4D4 by rolipram

The figure shows a dose-response curve for the inhibition of MBP–HSPDE4D4 PDE enzyme activity by rolipram in the presence of 10μM cAMP as substrate. The initial rate of cAMP hydrolysis was measured in the presence of 8 different concentrations of rolipram over the range 0–100μM and the percent inhibition was calculated with 0% inhibition defined as the measured activity in the absence of inhibitor. The data shown are from a representative experiment of 3 performed.

4.2.4 Proteolytic cleavage of MBP–HSPDE4D4

I have investigated the possibility of proteolytically cleaving the MBP moiety of MBP–HSPDE4D4 to produce a purified nonfusion protein of HSPDE4D4. The possibility of obtaining this species was especially attractive because of the difference in Km between the fusion protein and other preparations HSPDE4D (see section 4.2.3.1). If this difference was due to the MBP moiety contacting or sterically inhibiting the cAMP binding site of the PDE then cleavage of the fusion protein, to remove the MBP moiety, might be expected to yield a nonfusion HSPDE4D4 with a Km similar to that of other preparations of PDE4D enzymes.

4.2.4.1 Cleavage of MBP–HSPDE4D4 with factor Xa

The plasmid pMALN (derived from pMAL-c2), which was used to construct the MBP–HSPDE4D4 fusion protein, encodes a recognition site for the protease factor Xa that lies just upstream of the of the polylinker region of the plasmid. Cleavage of the MBP–HSPDE4D4 fusion protein with factor Xa at this site would be expected to produce free MBP (predicted Mw 42.5kDa) and an untagged HSPDE4D4 with only 10 vector derived amino acids at its extreme amino terminal (predicted Mw 92.3kDa, based on primary structure). Following cleavage a further step of affinity chromatography using amylose resin would be expected to remove the released MBP moiety and leave the purified, untagged HSPDE4D4 in the flow through.

I used the computer program Gene Jockey to search the peptide sequence of HSPDE4D4 for motifs which matched the recognition site of factor Xa (Ile-Glu-Gly-Arg). This search revealed no good matches for the recognition sequence. I therefore proceeded to treat 30µg MBP–HSPDE4D4 with 1µg factor Xa at 4°C. I monitored the digestion by taking 5µg aliquots at 0, 0.2, 0.5, 1.0, 3.8 and 20h time points, for analysis by SDS–PAGE. I also performed a mock digestion in which I incubated 5µg MBP–HSPDE4D4 in the absence of factor Xa for 20h at 4°C.

The digestion of MBP–HSPDE4D4 by factor Xa resulted in the gradual appearance of 5 major bands with apparent Mw 105.0±0.6, 91.7±0.7, 76.7±0.7, 65.7±0.3 and 47.0±0.0kDa on Coomassie stained gels. The appearance of these bands

coincided with the disappearance of the 152kDa MBP–HSPDE4D4 (*Figure 4.41*).

I investigated the identity of the novel bands produced by digesting MBP–HSPDE4D4 with factor Xa for 20 hours at 4°C by immunoblotting using a monoclonal antibody against the carboxyl terminal of HSPDE4D4 and also using a polyclonal antisera raised against MBP. The anti-MBP antisera detected a single major band of immunoreactivity in each lane. In the uncut and mock digested (no protease) lanes this immunoreactivity had an apparent Mw of 153kDa and co-migrated with the major protein bands visible in these lanes on Coomassie stained gels. In the factor Xa digested lane this immunoreactivity had an apparent Mw of 45kDa and co-migrated with the smallest of the 5 major novel bands visible on Coomassie stained gels (*Figure 4.42*).

The anti-PDE4D4 monoclonal antibody detected 2 major immunoreactive species with apparent Mw 223kDa and 156kDa in the uncut and in the mock digested lanes. The 223kDa species was not present in every experiment which I performed and probably represented an aggregated form of MBP–HSPDE4D4, which was not disrupted by the Laemmli's buffer. The 156kDa species was most likely monomeric MBP–HSPDE4D4. The factor Xa digested lane contained 3 major and several additional minor immunoreactive bands of anti PDE4D immubnoreactivity. The 3 major bands had apparent Mw of 106, 92 and 78kDa. These bands co-migrated with the 3 of the protein bands detected on Coomassie stained gels (*Figure 4.42*).

An important question was whether one of the bands, produced by the digestion of MBP–HSPDE4D4, represented full length, untagged HSPDE4D4. To address this question I ran factor Xa digested MBP–HSPDE4D4 on the same gel as HSPDE4D4, expressed in the cytosolic fraction of COS-7 cells, and detected these species by immunoblotting using an anti-PDE4D monoclonal antibody. This showed that the largest of the major immunoreactive bands, present in the digested lane, migrated with an apparent Mw which was lower than that of HSPDE4D4, expressed in the cytosolic fraction of COS-7 cells. A minor immunoreactive band which was present in the factor Xa digested lane but not in the mock digested lane, however, co-migrated with HSPDE4D4 expressed in the cytosolic fraction of COS-7 cells (*Figure*

4.43). This result suggested that full length, untagged HSPDE4D4 is not one of the major species produced by the digestion of MBP–HSPDE4D4 with factor Xa.

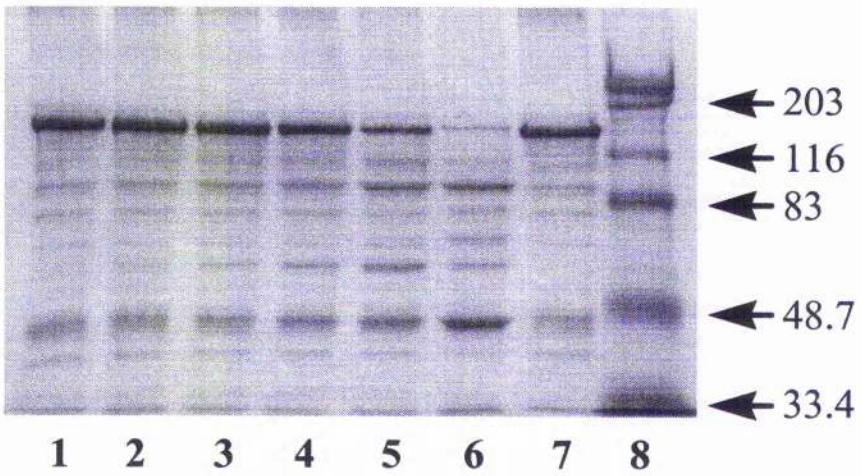

Figure 4.41: Clevage of MBP–HSPDE4D4 with factor Xa

The figure shows a Coomassie stained gel of the fractions collected during the proteolytic digestion of purified MBP–HSPDE4D4 by factor Xa. I incubated 30µg MBP–HSPDE4D4 with 1µg factor Xa at 4°C and collected 5µg aliquots at various time points. Lanes 1–6 are the aliquots collected at 0, 0.2, 0.5, 1.0, 3.8 and 20h time points respectively; lane 7 is a 20h mock digestion (no protease) of MBP-HSPDE4D4; lane 8 is molecular weight markers (Bio-Rad broad range prestained SDS–PAGE standards). The arrows indicate the Mw (kDa) of each marker.

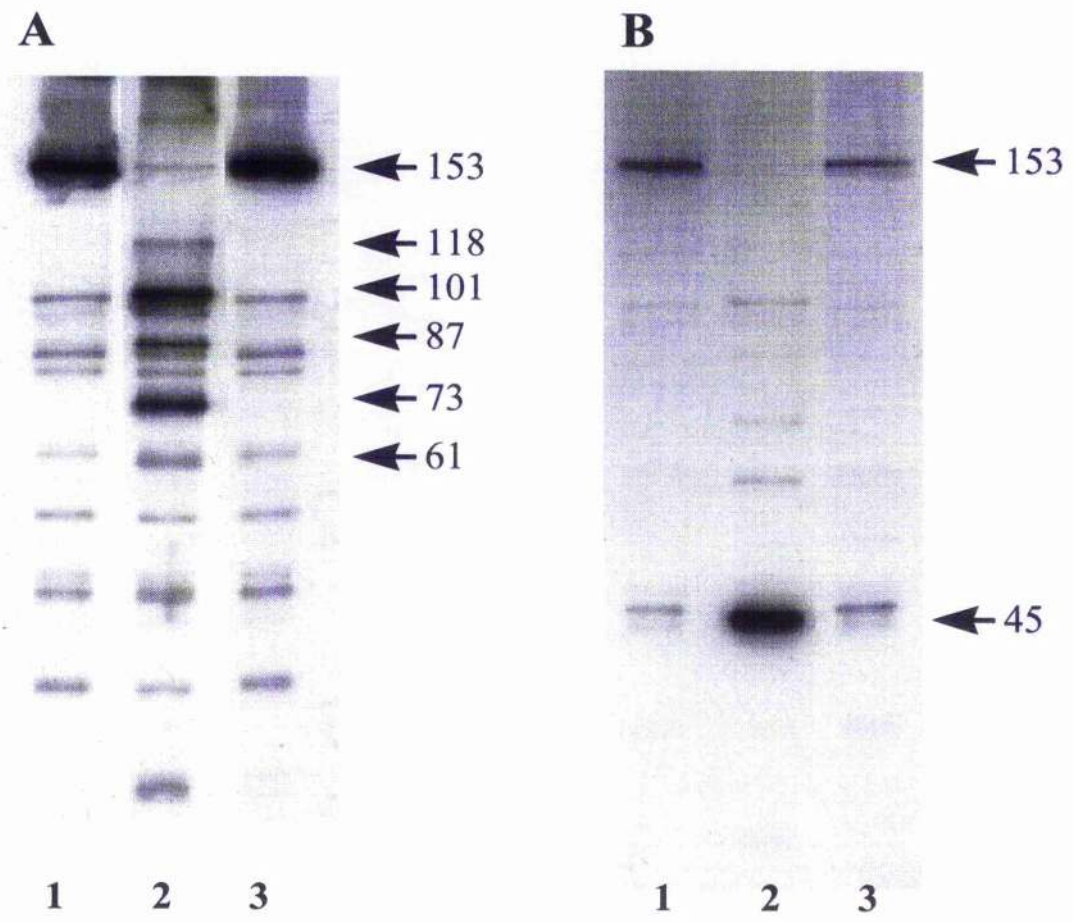

Figure 4.42: Immunological analysis of the digestion of MBP–HSPDE4D4 by factor Xa

The figure shows immunoblots of fractions collected during the proteolytic digestion of purified MBP–HSPDE4D4 by factor Xa. Panel A shows an immunoblot that was probed with a monoclonal antibody against the carboxyl terminal region of PDE4D: lanes 1 and 2 are 0.5µg aliquots collected at 0 and 20h time points respectively; lane 3 is a 0.5µg aliquot from a 20h mock digestion (no protease) of MBP–HSPDE4D4. Panel B shows the same immunoblot which has been stripped and re-probed using a polyclonal antisera raised against MBP. The arrows indicate the apparent Mw (kDa) of each major band, calculated by plotting the Rf values of markers run on the same gel.

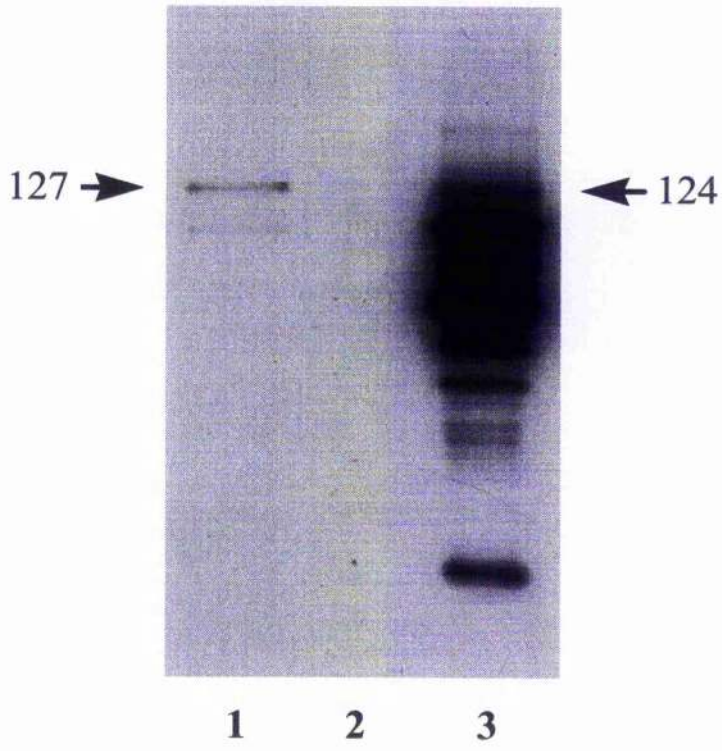

Figure 4.43: Comparison of the factor Xa digested MBP–HSPDE4D4 with HSPDE4D4 expressed in the cytosolic fraction of COS-7 cells

The figure shows an immunoblot of purified MBP–HSPDE4D4, which had been digested by factor Xa, and of HSPDE4D4 expressed in the cytosolic fraction of COS-7 cells. Lane 1 is 1.6μg cytosol from COS-7 cells transiently transfected to overexpress HSPDE4D4, lane 2 is empty and lane 3 is a 0.1μg aliquot collected after a 20h digestion of MBP–HSPDE4D4 by factor Xa at 4°C. Each arrow indicates the apparent Mw (kDa) of that band, calculated by plotting the Rf values of markers run on the same gel.

4.2.4.2 Cleavage of MBP–HSPDE4D4 with TEV protease

A potential solution to the problem presented by the apparent cleavage of HSPDE4D4 itself by factor Xa was provided by the tobacco mosaic virus protease (TEV) (Gibco BRL). The TEV protease is considered to exhibit higher fidelity than factor Xa (53, 237). I therefore investigated the possibility of engineering a sequence encoding a TEV protease recognition site (Glu-Asn-Leu-Tyr-Phe-Gln-Gly) into the plasmid pMALP39.

As a preliminary experiment I incubated 20μg MBP–HSPDE4D4 with 10 units TEV protease at 4°C. I monitored the digestion by taking 5μg aliquots at 0, 2.5, 4.5 and 12.5 hour time points for analysis by SDS–PAGE. Even at the longest time point examined there was no detectable digestion of MBP–HSPDE4D4 by TEV protease (*Figure 4.44*). This result suggested that the strategy of inserting a TEV protease site into the MBP–HSPDE4D4 fusion protein might provide a convenient way of removing the MBP tag from this fusion protein without also degrading the HDPDE4D4 moiety.

The plasmid pMALP39 had been constructed by cloning the open reading frame of HSPDE4D4 into the Not I site of the plasmid pMALN, which is itself a derivative of pMALc2 containing a Not I site inserted into the polylinker region of the plasmid. All 3 of these plasmids contain an Xmn I site which lies at the extreme 5' end of their polylinker regions. I was therefore able to engineer a TEV protease recognition site into pMALP39 immediately downstream of the factor Xa site already present.

I digested the plasmid pMALP39 with Xmn I to produce a blunt ended, linear molecule. I then used Taq polymerase to ligate adenosine overhangs onto the 3' end of each DNA strand. Next I annealed the complementary, synthetic oligonucleotides MB4 and MB5 together. This produced a double stranded DNA molecule which encoded a TEV protease recognition site and which had thymidine overhangs at the 3' end of each DNA strand (*Figure 4.45*). I ligated the annealed oligonucleotides with the linear, Taq polymerase treated pMALP39. I then transformed competent XL1 blue *E.coli* with the products of the ligation reaction and used PCR to screen for colonies which contained the recombinant plasmid ($pMALP39_{TEV}$). Finally I

sequenced across the inserted region to confirm the presence and the orientation of the inserted sequence.

I transformed JM109 *E.coli* with the plasmid pMALP39$_{TEV}$ then expressed and purified the fusion protein as before (see section 4.2.2.1). I then proceeded to treat 25µg MBP–HSPDE4D4$_{TEV}$ with 20 units TEV protease at 4°C. I monitored the digestion by taking 5µg aliquots at 0, 1, 2, 4.5 and 20h time points, for analysis by SDS–PAGE. I also performed a mock digestion in which I incubated 5µg MBP--HSPDE4D4$_{TEV}$ in the absence of TEV protease for 20h at 4°C. This digestion resulted in the gradual appearance of 2 bands with apparent Mw 120.7kDa and 47.8kDa on Coomassie stained gels. The appearance of these bands coincided with the gradual disappearance of the 152kDa MBP–HSPDE4D4$_{TEV}$ (*Figure 4.46*). The upper of these novel bands was probably untagged HSPDE4D4 with 11 vector derived amino acids remaining at it's amino terminus (Gly-Ile-Ser-Glu-Phe-Cys-Gly-Arg-Arg-Pro-Arg-). The lower novel band was probably the MBP moiety of the fusion protein.

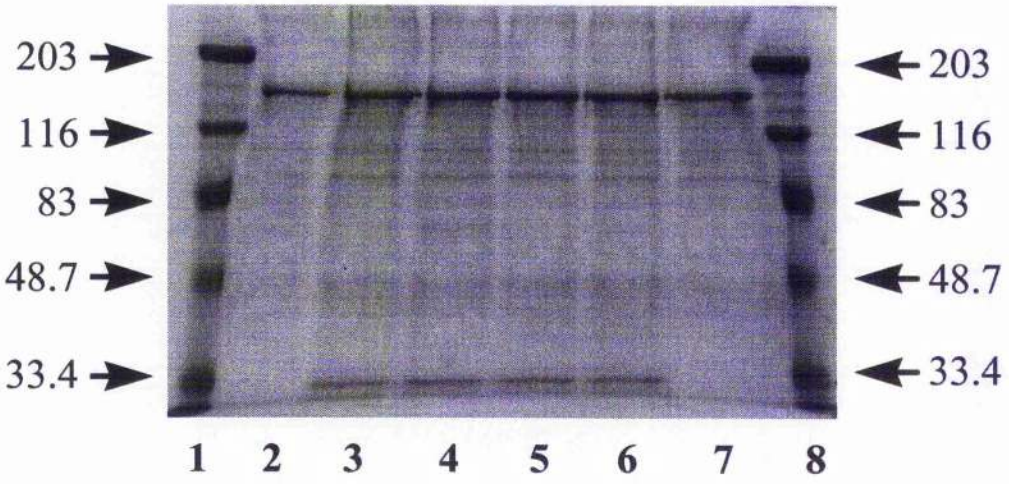

Figure 4.44: Treatment of MBP–HSPDE4D4 with TEV protease

The figure shows a Coomassie stained gel of the fractions collected during the treatment of purified MBP–HSPDE4D4 with TEV protease. I incubated 20μg MBP–HSPDE4D4 with 10 units TEV protease at 4°C and collected 5μg aliquots at various time points. Lanes 2–6 are the aliquots collected at 0, 2.5, 4.5 and 12.5h time points respectively; lane 7 is a 12.5h mock digestion (no protease) of MBP–HSPDE4D4; lanes 1 and 8 are molecular weight markers (Bio-Rad broad range prestained SDS-PAGE standards). The arrows indicate the Mw (kDa) of each marker.

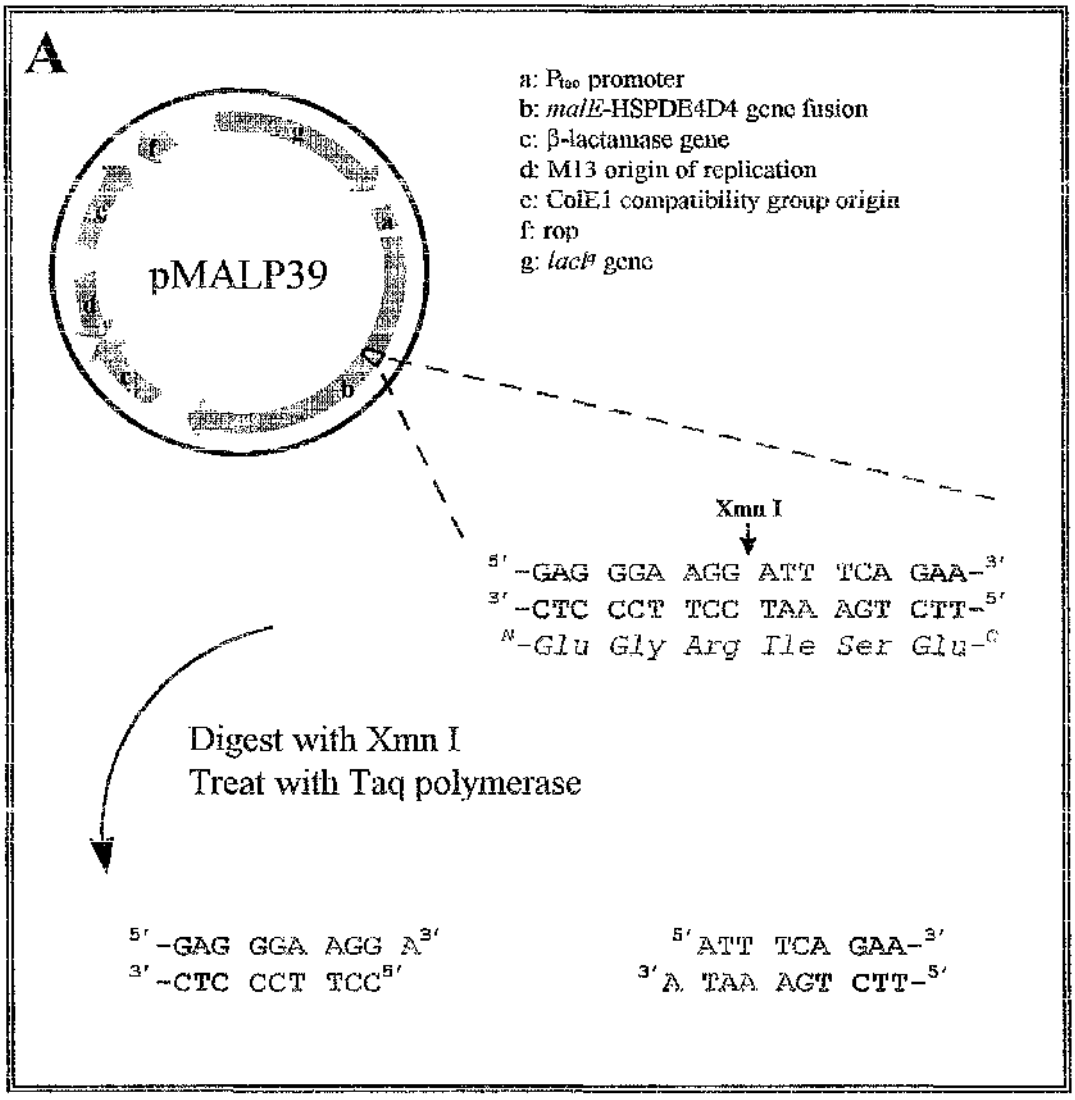
A
pMALP39
a: Ptac promoter
b: malE-HSPDE4D4 gene fusion
c: β-lactamase gene
d: M13 origin of replication
e: ColE1 compatibility group origin
f: rop
g: lacIq gene
Xmn I
5'-GAG GGA AGG ATT TCA GAA-3'
3'-CTC CCT TCC TAA AGT CTT-5'
N-Glu Gly Arg Ile Ser Glu-C
Digest with Xmn I
Treat with Taq polymerase
5'-GAG GGA AGG A3'
3'-CTC CCT TCC5'
5'ATT TCA GAA-3'
3'A TAA AGT CTT-5'

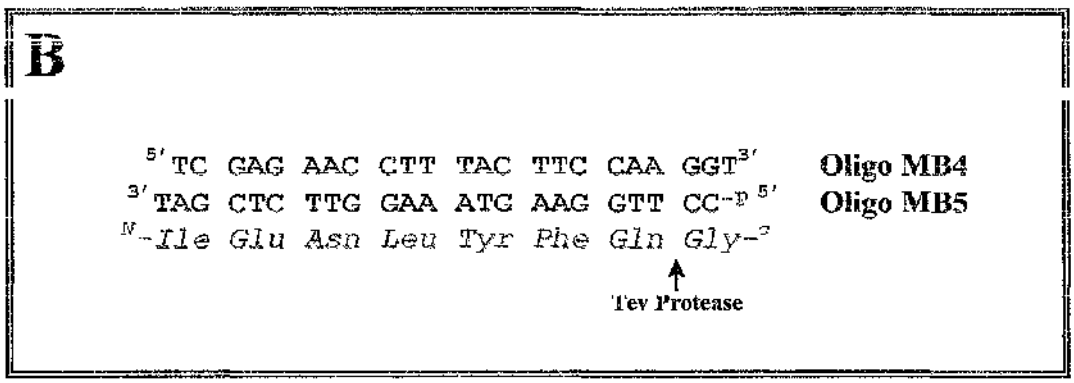
B
5'TC GAG AAC CTT TAC TTC CAA GGT3'
3'TAG CTC TTG GAA ATG AAG GTT CC-p 5'
N-Ile Glu Asn Leu Tyr Phe Gln Gly-C
Tev Protease
Oligo MB4
Oligo MB5

Figure 4.45: Insertion of a TEV protease site into MBP–HSPDE4D4

The figure shows the cloning strategy which I used to engineer a TEV protease site into MBP–HSPDE4D4. Panel A shows the preparation of the plasmid pMALP39, which encodes MBP–HSPDE4D4, for ligation with a DNA fragment encoding a TEV protease site. First I digested pMALP39 with the restriction endonuclease Xmn I. This cut the plasmid at a single site which lay within the open reading frame of MBP–HSPDE4D4 and was immediately downstream of the last codon of the factor Xa site. This produced a linear, blunt ended, double stranded molecule. I treated the digested plasmid with Taq polymerase to ligate adenosine overhangs onto the 3' end of each DNA strand. This was both to increase the efficiency of the subsequent ligation reaction and also to prevent the plasmid from re-circularising without incorporating the DNA fragment. Panel B shows the DNA fragment encoding a TEV protease site which I ligated into pMALP39. I generated this molecule by annealing 2 complementary oligonucleotides (MB4 and MB5). These oligonucleotides had been designed to produce a double stranded molecule with thymidine overhangs at the 3' end of each DNA strand. The oligonucleotide MB5 was phosphorylated at it's 5' end. This was to allow the formation of bonds between the 5' end of MB5 and the plasmid DNA in addition to bonds between the 3' ends of both MB4 and MB5 and the plasmid DNA during the ligation.

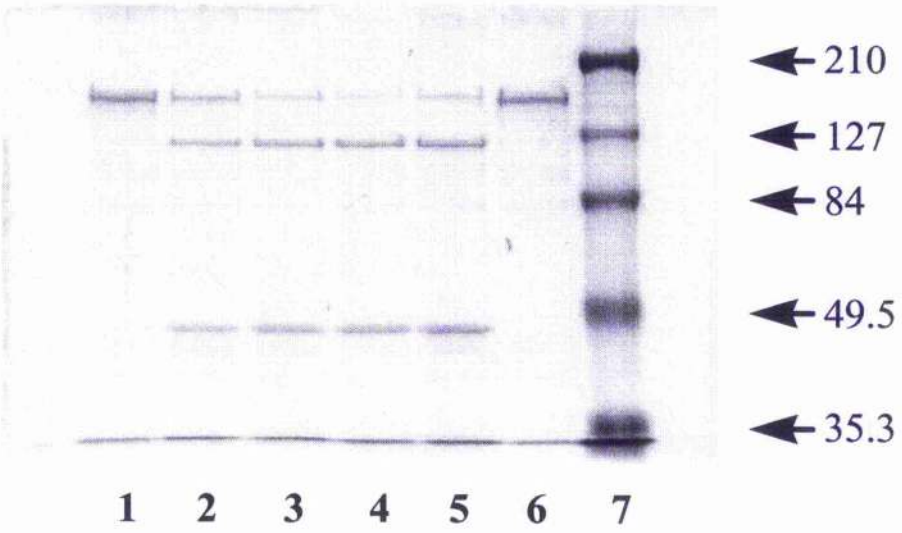

Figure 4.46: Cleavage of MBP–HSPDE4D4$_{TEV}$ with TEV protease

The figure shows a Coomassie stained gel of the fractions collected during the proteolytic digestion of purified MBP–HSPDE4D4$_{TEV}$ by factor Xa. I incubated 20µg MBP–HSPDE4D4$_{TEV}$ with 20 units TEV protease at 4°C and collected 5µg aliquots at various time points. Lanes 1–5 are the aliquots collected at 0, 1, 2, 4.5 and 20h time points respectively; lane 6 is a 20h mock digestion (no protease) of MBP-HSPDE4D4; lane 7 is molecular weight markers (Bio-Rad broad range prestained SDS–PAGE standards). The arrows indicate the Mw (kDa) of each marker.

4.2.4.3 Characterisation of purified, untagged HSPDE4D4$_{TEV}$

To test the hypothesis that the difference in Km between HSPDE4D4 expressed in the cytosol of COS-7 cells and purified MBP–HSPDE4D4 was due to some effect of the MBP moiety on the conformation of the protein, I digested purified MBP–HSPDE4D4$_{TEV}$ with TEV protease overnight at 4°C. I then removed both the released MBP moiety, using amylose resin, and the protease (which was His tagged), using a Ni^{+} chelate resin. I then assayed the initial velocity of cAMP hydrolysis by the untagged, purified enzyme at 13 different substrate concentrations over the range 0.1–20μM cAMP. I calculated values for the constants Km and Vmax for this preparation by fitting the kinetic data to the hyperbolic form of the Michaelis-Menten equation, using the computer program Hyper 1.02a. This analysis revealed that the untagged HSPDE4D4$_{TEV}$ catalysed the hydrolysis of cAMP with kinetics that conformed well to the Michaelis-Menten model and that were linear when plotted in accordance with several linear transformations of the Michaelis-Menten equation (*Figure 4.47*).

The purified, untagged HSPDE4D4$_{TEV}$ catalysed the hydrolysis of cAMP with a Km of 2.3μM and an apparent Vmax of 3490μmol/min/mg.

The Km for cAMP of the purified, untagged HSPDE4D4$_{TEV}$ was 6 fold lower that of purified MBP–HSPDE4D4. It was, however, in close agreement with the Km for cAMP of HSPDE4D4 expressed in the cytosolic fraction of COS-7 cells and with those of other preparations of PDE4D isoforms (see section 4.2.3.1).

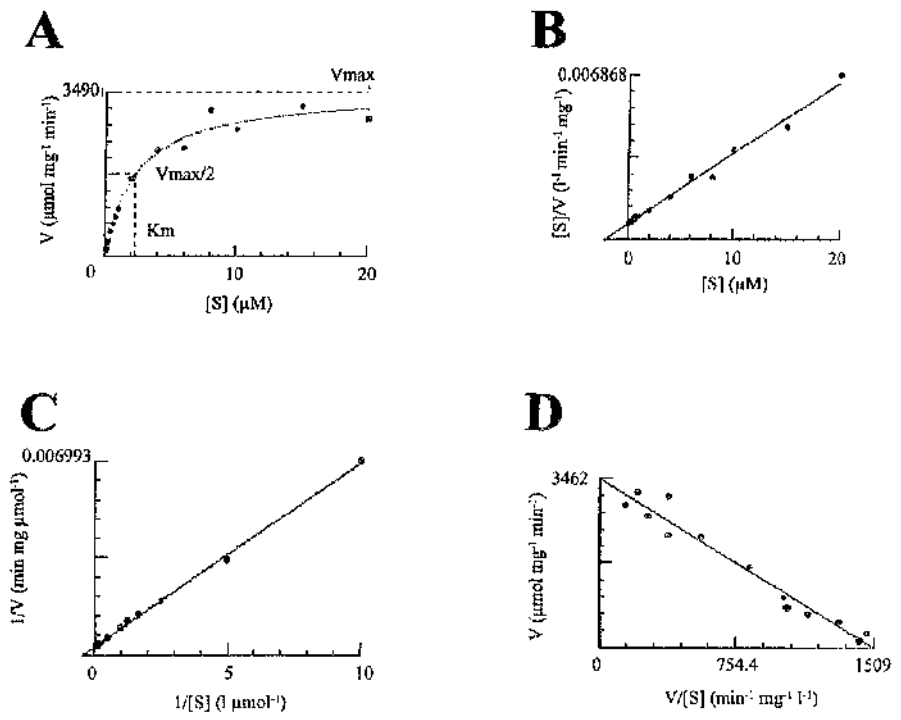

Figure 4.47: Kinetic analysis of purified, untagged HSPDE4D4$_{TEV}$

The figure shows graphical solutions of the Michaelis-Menten equation for the hydrolysis of cAMP by purified, untagged HSPDE4D4$_{TEV}$. The initial velocity of catalysis was assayed at 16 different substrate concentrations and the data were fitted to the Michaelis-Menten equation using the computer program Hyper 1.02a. Panel A shows a graph for the hyperbolic form of the equation. Panels B, C and D show a Hanes plot, a Lineweaver-Burk plot and an Eadie-Hofstee plot respectively. The graphs shown represent the results from a typical experiment of 3 performed. These analyses revealed a Km for cAMP of 2.3µM and a Vmax of 3490µmol/min/mg

4.2.5 Use of MBP–HSPDE4D4 fusion proteins to study protein–protein interactions

Both RNPDE4A5 (HSPDE4A4B) and HSPDE4D4 are able to interact with the SH3 domains of certain proteins (see chapters 3 and 5). I have used the purified MBP fusion proteins of full length HSPDE4D4 and also of the unique, amino terminal region (amino acids 1–166) of HSPDE4D4 to further characterise these interactions. I performed these experiments using a purified GST fusion protein of the SH3 domain of Lyn kinase, which I selected as an example of an SH3 domain from a Src family tyrosyl kinase (see section 3.2.5).

4.2.5.1 Pull down assays with full length HSPDE4D4 as a fusion protein with MBP

The pull down assays that I have described in chapter 3 of this thesis were performed using unpurified preparations of PDE. As such they did not address the question of whether the detected interactions between the PDEs and the SH3 domains represented direct interactions between these species. An equally likely possibility was that the PDEs and the SH3 domains each bound to a mutual, third species. To address this question I have performed pull down assays using purified preparations of MBP–HSPDE4D4 and of GST–Lyn SH3. In these assays I examined the binding of both MBP–HSPDE4D4 and of MBP alone to GST–Lyn SH3 and to GST alone.

In the pull down assays using MBP–HSPDE4D4 and either GST–Lyn SH3 or GST alone I was able to monitor the binding of both immunoreactivity and of PDE enzyme activity. In these assays, where GST–Lyn SH3 was used as the "bait", 49.3±7.6% of the recovered PDE enzyme activity was present in the bound fraction. This compared to only 3.2±1.1% of the recovered activity present in the bound fraction of pull down assays where the "bait" was GST alone. The binding of MBP–HSPDE4D4 enzyme activity to GST–Lyn SH3 was therefore significantly different from that to GST alone at the 1% level (Student's t-Test). As an additional control I also performed a pull down assay using purified MBP–HSPDE4D3 as the "prey" and either GST–Lyn SH3 or GST alone as the "bait". In this assay only 3.5% and 2.2% of the recovered activity was present in the bound fractions with GST–Lyn SH3 and with GST alone respectively. Although this is the result of only 1 trial and

should therefore be treated with caution it is in agreement with the data that I generated from pull down assays using the crude cytosolic fraction of COS-7 cells transiently transfected to overexpress HSPDE4D3 which suggested that HSPDE4D3 does not interact with this SH3 domain (see section 3.2.4).

The immunoblots that I generated from these pull down assays show an immunoreactive band corresponding to MBP–HSPDE4D4 in the bound fraction of the pull down assays using GST–Lyn SH3 but not of those using GST alone. This demonstrated that MBP–HSPDE4D4 immunoreactivity, as well as enzyme activity, bound to GST–Lyn SH3 (*Figure 4.48*).

In the pull down assays between MBP alone and either GST–Lyn SH3 or GST alone I was only able to monitor the binding of immunoreactivity. The immunoblots generated from these assays show that only trace amounts (>0.5%) of the recovered immunoreactivity was present in the bound fractions of pull down assays using either GST–Lyn SH3 or GST alone. This demonstrated that the detected interaction between MBP–HSPDE4D4 can not be attributed to the binding of MBP to the GST fusion protein (*Figure 4.51*).

These data show that MBP–HSPDE4D4, but not MBP alone, can bind directly to GST–Lyn SH3 but not to GST alone. This supports the hypothesis that HSPDE4D4 can bind directly to SH3 domains.

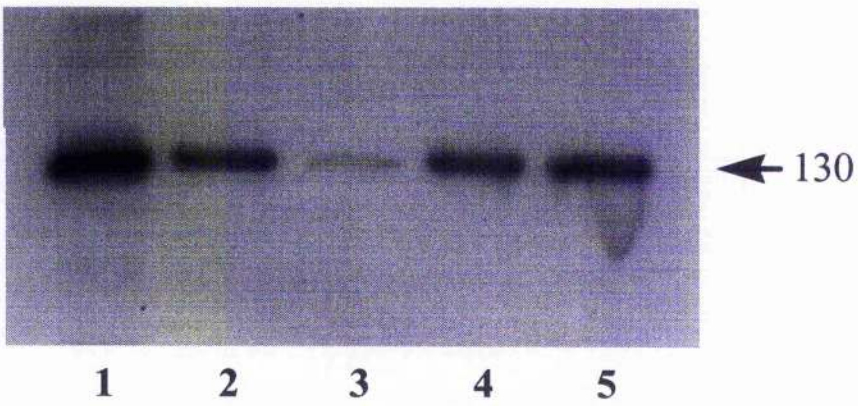

Figure 4.48: Binding of MBP–HSPDE4D4 to GST and GST–Lyn SH3

The figure shows an immunoblot for PDE4D of fractions from pull-down assays between purified MBP–HSPDE4D4 and GST and purified MBP–HSPDE4D4 and GST–Lyn SH3. Lane 1 is 0.2μg purified MBP–HSPDE4D4; lanes 2 and 4 each contain 11% of the total unbound fractions from 0.8μg MBP–HSPDE4D4 challenged with GST and with GST–Lyn SH3 respectively, 11%; lanes 3 and 5 each contain 53% of the bound fractions from these pull down assays with GST and GST–Lyn SH3 respectively. The arrow indicates the apparent Mw (kDa) of the bands, calculated by plotting the Rf values of markers run on the same gel.

4.2.5.2 Overlay assays

As an independent method to assess whether MBP–HSPDE4D4 could bind directly to SH3 domains I performed "overlay" assays, using a method based upon that commonly used to probe for protein kinase A anchoring proteins (AKAPs) (27, 28). In these experiments I subjected purified GST and GST fusion proteins of various SH3 domains to SDS–PAGE. I transferred these proteins from the gel onto a nitrocellulose membrane which I then blocked and probed with either purified MBP or MBP–HSPDE4D4. I washed the membrane, to remove any unbound probe, and then performed an immunoblot to detect the bound probe. Finally, I used Ponceau S stain to visualise the position of the GST fusion proteins on the nitrocellulose.

In these experiments MBP–HSPDE4D4, but not MBP alone, was able to interact with the SH3 domains of Src, Lyn and Fyn but not with those of Lck, Crk, Csk, Abl, P53BP2, Fodrin, PI3 Kinase, Cortactin, the SH2 domain of Src, GST alone nor with a fusion protein containing both the SH2 and the SH3 domains of Src. This supports the hypothesis that MBP–HSPDE4D4 can bind directly to the SH3 domains of Src, Lyn and Fyn kinases (*Figure 4.49, Figure 4.50*).

Recombinant HSPDE4D4, expressed in the cytosol of COS-7 cells, can interact with the SH3 domains of Abl and Fodrin, in pull down assays, to a similar extent as that to which it can interact with the SH3 domains of Src, Lyn and Fyn. It was therefore surprising to find that MBP–HSPDE4D4 did not interact with these domains in the overlay assays. Furthermore, although MBP–HSPDE4D4 did interact with GST–Src SH3, it was unable to interact with GST–Src SH2/3 in these overlay assays. A possible explanation for these results is that the overlay assay method relies on the "bait" proteins renatureing after being transferred from the SDS gel onto the nitrocellulose membrane. It may be the case that although certain proteins can renature under these conditions, others can not and that, with these proteins, no interaction is detected. An alternative explanation is that the interaction between HSPDE4D4 and certain SH3 domains depends upon the presence of other molecules that are present in the cytosolic fraction of COS-7 cells but not in the overlay assay. I therefore suggest that, although interactions detected in overlay assays can be

regarded as supporting evidence for a direct interaction between 2 species, the failure of 2 proteins to interact in an overlay assay should not be regarded as evidence that these species can not interact in solution.

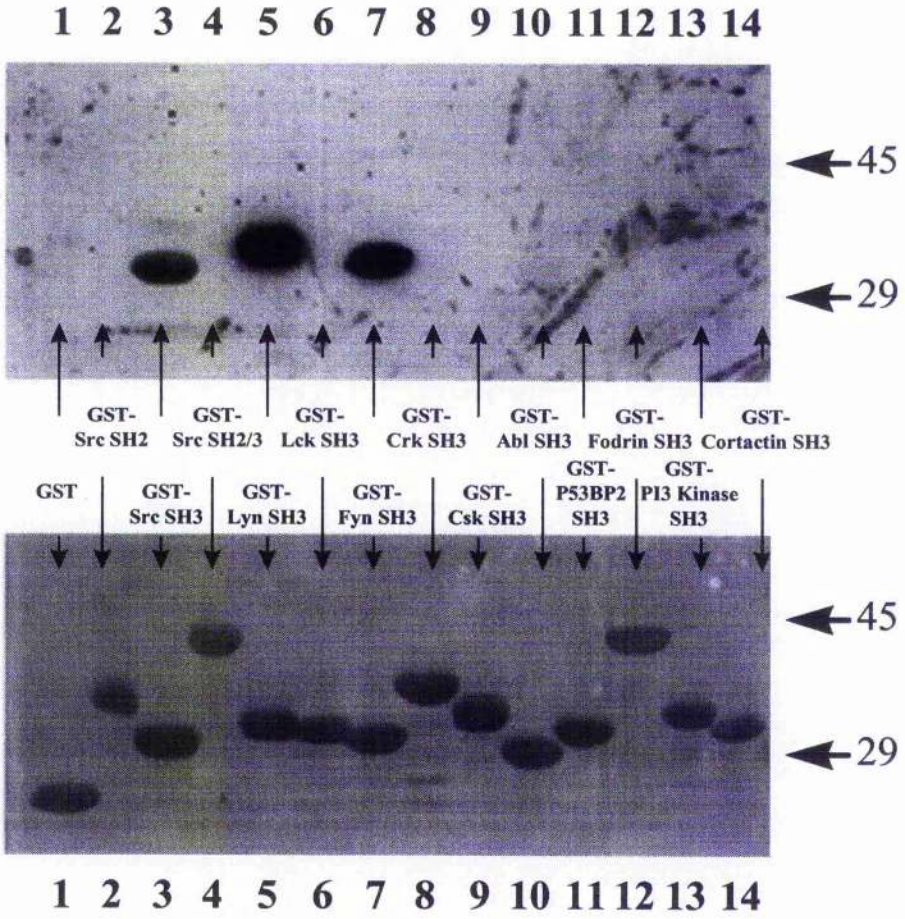

Figure 4.49: Direct interaction of MBP–HSPDE4D4 with SH3 domains

The figure shows an overlay assay for direct protein–protein interactions. GST and GST fusion proteins of various SH3 domains were subjected to SDS-PAGE, transferred to a nitrocellulose membrane and probed with MBP–HSPDE4D4. The bound probe was detected by immunoblotting and the fusion proteins were visualised using Ponecau S stain. Panel A is an immunoblot to detect the bound probe. Panel B is the nitrocellulose filter stained with Ponceau S: lanes 1–14 in both panels are GST, GST-Src SH2, GST-Src SH3, GST-Src SH2/3, GST-Lyn SH3, GST–Lck SH3, GST–Fyn SH3, GST–Crk SH3, GST–Csk SH3, GST–Abl SH3, GST–P53BP2 SH3, GST–Fodrin SH3, GST-PI3Kinase SH3 and GST-Cortactin SH3 respectively. The arrows indicate the position of molecular weight markers run on the same gel.

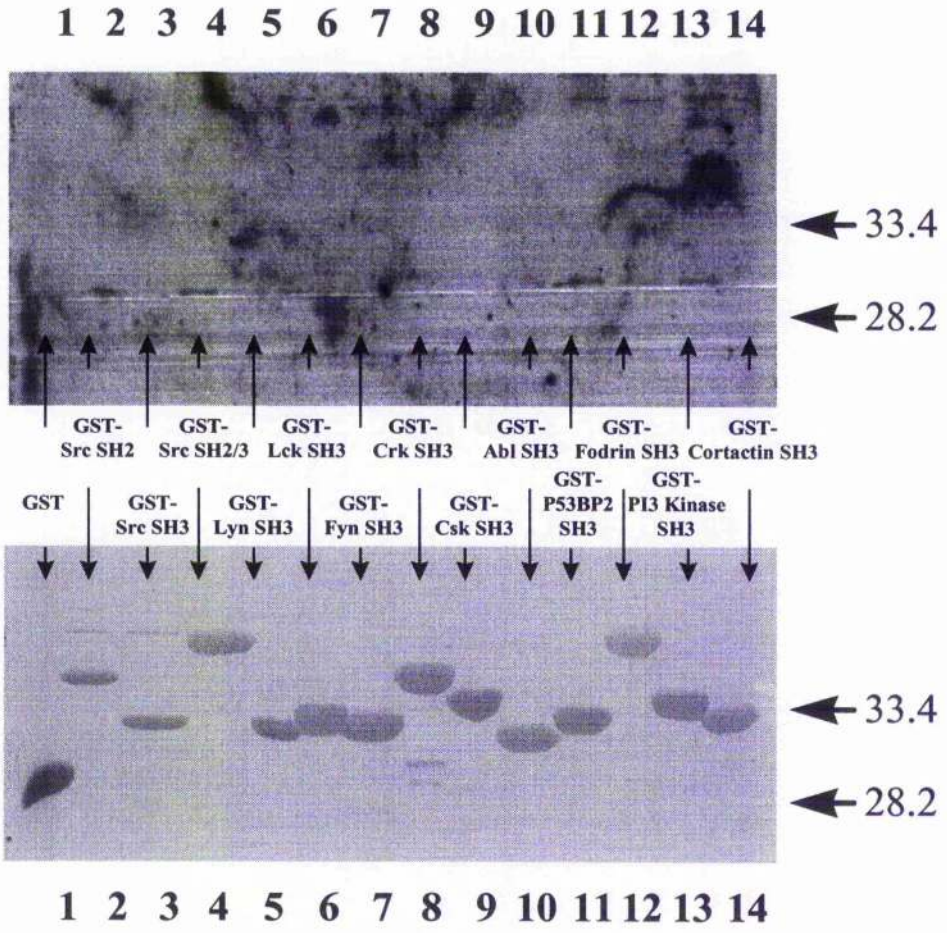

Figure 4.50: Direct interaction of MBP with SH3 domains

The figure shows an overlay assay for direct protein–protein interactions. GST and GST fusion proteins of various SH3 domains were subjected to SDS-PAGE, transferred to a nitrocellulose membrane and probed with MBP. The bound probe was detected by immunoblotting and the fusion proteins were visualised using Ponecau S stain. Panel A is an immunoblot to detect the bound probe. Panel B is the nitrocellulose filter stained with Ponceau S: lanes 1–14 in both panels are GST, GST-Src SH2, GST-Src SH3, GST-Src SH2/3, GST-Lyn SH3, GST–Lck SH3, GST–Fyn SH3, GST–Crk SH3, GST–Csk SH3, GST–Abl SH3, GST–P53BP2 SH3, GST–Fodrin SH3, GST-PI3Kinase SH3 and GST-Cortactin SH3 respectively. The arrows indicate the position of molecular weight markers run on the same gel.

4.2.5.3 Pull down assays with the amino terminal region of HSPDE4D4 as a fusion protein with MBP

The "long" PDE4D isoforms HSPDE4D3, HSPDE4D4 and HSPDE4D5 all share an identical primary structure outside of their alternatively spliced, amino terminal regions. Unlike HSPDE4D4, neither HSPDE4D3 nor HSPDE4D5 were able to interact with the SH3 domains of Src or Lyn kinase in pull down assays. This suggested that the unique, alternatively spliced, amino terminal region of HSPDE4D4 was necessary for it's interaction with these SH3 domains (see section 3.2.4.1).

To investigate whether the alternatively spliced, amino terminal region of HSPDE4D4 was also sufficient for interaction with SH3 domains I performed pull down assays using purified preparations of MBP–NT HSPDE4D4. In these assays I examined the binding of both MBP–NT HSPDE4D4 and of MBP alone to GST–Lyn SH3 and to GST alone.

The amino terminal region of HSPDE4D4 does not include the catalytic site of the enzyme, therefore I was not able to use PDE enzyme activity assays to monitor the binding of these species; instead I performed quantitative immunoblots, using a polyclonal antisera against MBP (*Figure 4.51*). In the pull down assays where MBP–NT HSPDE4D4 was the "prey" and GST–Lyn SH3 was the "bait", 18.2±8.6% of the recovered immunoreactivity was present in the bound fraction. This compared with 0.3±0.1% of the recovered immunoreactivity present in the bound fractions of assays where the "bait" was GST alone. In the pull down assays where MBP alone was the "prey", less than 0.2±0.2% of the recovered immunoreactivity was present in the bound fraction of assays with either GST–Lyn SH3 or GST alone as the "bait" (*fig.4.23*).

These results demonstrated that amino acids 1–166 of HSPDE4D4 can bind directly to the SH3 domain of Lyn kinase. This supports the hypothesis that the unique, alternatively spliced, amino terminal region of HSPDE4D4 is both necessary and sufficient for the interaction of HSPDE4D4 with SH3 domains.

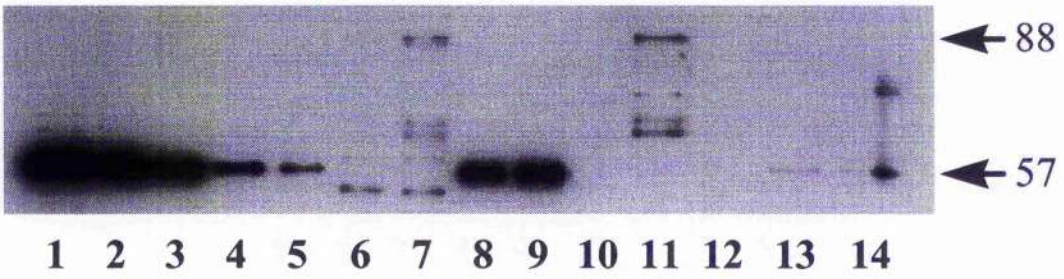

Figure 4.51: Binding of MBP–NT HSPDE4D4 to GST and GST–Lyn SH3

The figure shows a quantatative immunoblot for MBP of fractions from pull-down assays between purified MBP–NT HSPDE4D4, GST–Lyn SH3 and GST alone and between purified MBP GST–Lyn SH3 and GST alone. Lanes 1–5 are 0.5, 0.1, 0.05, 0.01 and 0.005μg purified MBP respectively; lanes 6 and 7 are the unbound fractions from 5μg MBP–NT HSPDE4D4 challenged with GST–Lyn SH3 and with GST respectively, 1% of each fraction was run; lanes 8 and 9 are the unbound fractions from 20μg MBP challenged with GST–Lyn SH3 and with GST respectively, 0.1% of each fraction was run; lane 10 is empty; lanes 11 and 12 are the bound fractions from the pull down assays of MBP–NT HSPDE4D4 with GST–Lyn SH3 and GST respectively, 13% of each fraction was run; lanes 13 and 14 are the bound fractions from the pull down assays of MBP with GST–Lyn SH3 and GST respectively, 27% of each fraction was run. The arrows indicates the apparent Mw (kDa) of the bands, calculated by plotting the Rf values of markers run on the same gel.

4.2.5.4 ELISA for protein–protein interaction

As a third, independent method of examining the interaction between HSPDE4D4 and SH3 domains I performed a series of ELISAs (enzyme linked immune adsorbant assays), using purified MBP and GST fusion proteins. A similar approach has previously been used to investigate the interaction between HSPDE4D5 and RACK1 (receptor for activated C kinase 1) (252).

I initially performed ELISAs in which either GST–Lyn SH3 or GST alone were immobilised on Reacti-Bind glutathione coated ELISA plates (Pierce) as the "bait" species. The immobilised GST fusion proteins were then challenged with either MBP–HSPDE4D4 or with MBP alone. These assays, however, resulted in an extremely high background due to the nonspecific binding of MBP–HSPDE4D4 to the wells of the ELISA plate.

I therefore decided to attempt ELISAs in which either MBP–HSPDE4D4 or MBP alone were immobilised as the "bait" species and challenged with either GST–Lyn SH3 or with GST alone. In these assays GST–Lyn SH3 bound both to MBP–HSPDE4D4 and to MBP–NT HSPDE4D4 in an apparent dose dependent fashion with EC_{50} values of 0.392±0.104μM and of 1179μM respectively. The binding of GST–Lyn SH3 to MBP alone and of GST alone to MBP–HSPDE4D4, to MBP–NT HSPDE4D4 or to MBP alone were typically about 5 fold lower than that of GST–Lyn SH3 to MBP–HSPDE4D4 or to MBP–NT HSPDE4D4 in these assays (*Figure 4.52Figure 4.53*). These data support the hypothesis that HSPDE4D4 can interact with SH3 domains and that the unique, amino terminal (amino acids 1–166) of the molecule are sufficient for this interaction.

If this system could be shown to be at equilibrium then, from modeling the kinetics of adsorption, it would follow that the measured EC_{50} for binding would be equal to the ratio between the dissociation and the association constants for this interaction (ie. the equilibrium constant (Ks)) (154).

I therefore performed time course experiments to measure the binding of GST–Lyn SH3 to MBP–HSPDE4D4 with time. This showed that, even after 20 hours, the

system had not reached equilibrium (*Figure 4.54*). The measured EC_{50} of binding for these ELISAs is therefore a non-equilibrium measurement and will depend not only upon the ratio between the dissociation constant and the association constant of the interaction but also upon the time of interaction (before separation of bound and unbound "prey").

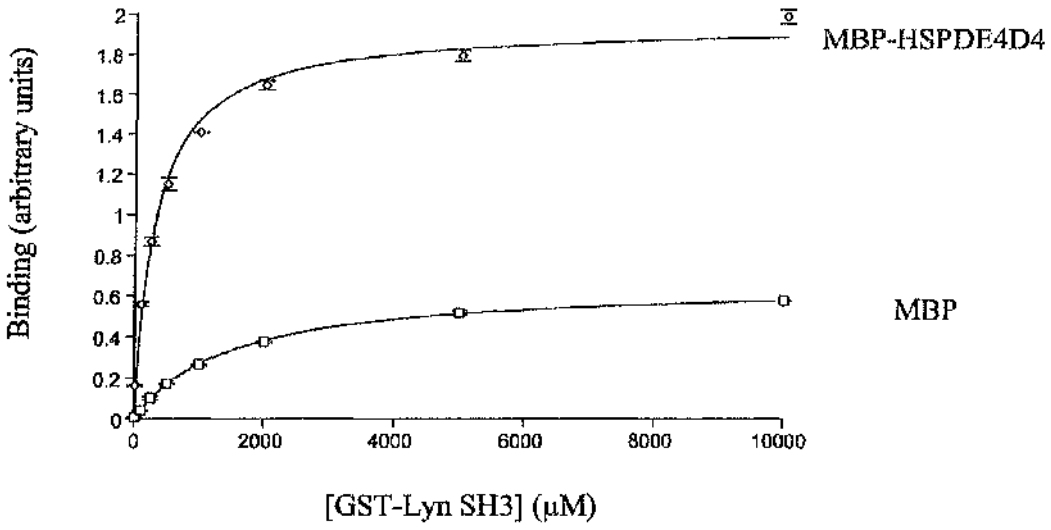

Figure 4.52: Binding of MBP–HSPDE4D4 and of MBP to GST–Lyn SH3

The figure shows results from an ELISA for interaction between MBP–HSPDE4D4 and GST–Lyn SH3. 1.5pmol MBP–HSPDE4D4 or MBP was immobilised in each well of a 96 well plate. The wells were then blocked and probed with a concentration range of either GST–Lyn SH3 or GST alone for 3 hours at room temperature. After rapid washing at 4°C the bound probe was fixed using paraformaldehyde and detected immunologically. The binding of GST alone at each concentration was used as the baseline value for the binding of GST–Lyn SH3 to the immobilised ligand.

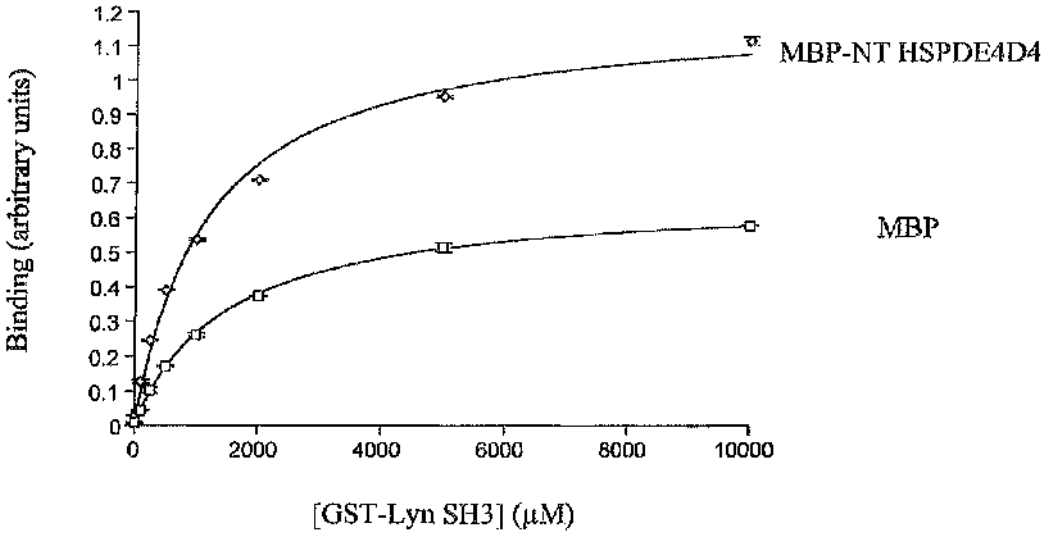

Figure 4.53: Binding of MBP–NT HSPDE4D4 and of MBP to GST–Lyn SH3

The figure shows results from an ELISA for interaction between MBP–NT HSPDE4D4 and GST–Lyn SH3. 1.5pmol MBP–NT HSPDE4D4 or MBP was immobilised in each well of a 96 well plate. The wells were then blocked and probed with a concentration range of either GST–Lyn SH3 or GST alone for 3 hours at room temprature. After rapid washing at 4°C the bound probe was fixed using paraformaldehyde and detected immunologically. The binding of GST alone at each concentration was used as the baseline value for the binding of GST–Lyn SH3 to the immobilised ligand.

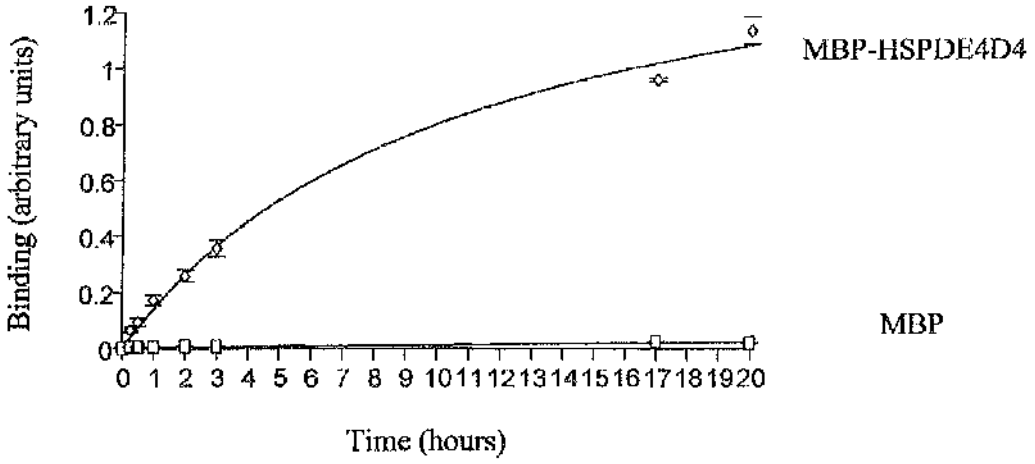

Figure 4.54: Time course for the binding of MBP–HSPDE4D4 and of MBP to GST–Lyn SH3

The figure shows results from an ELISA for interaction between MBP–HSPDE4D4 and GST–Lyn SH3. 1.5pmol MBP–HSPDE4D4 or MBP was immobilised in each well of a 96 well plate. The wells were then blocked and probed with either GST–Lyn SH3(300nM) or GST alone (300nM) for various periods of time. After rapid washing at 4°C the bound probe was fixed using paraformaldehyde and detected immunologically. The binding of GST alone at each time point was used as the baseline value for the binding of GST–Lyn SH3 to the immobilised ligand.

4.3 Conclusions

In this chapter I have shown that it is possible to express active, full length isoforms of PDE4 in *E.coli* as fusion proteins with MBP. Each of the "long" splice variants from the PDE4D gene can now be expressed, as an MBP fusion protein, and rapidly purified to near homogeneity, by a single step of affinity chromatography using amylose resin. I have demonstrated the purification of the HSPDE4D4 isoform in this chapter and the purification of the HSPDE4D3 and the HSPDE4D5 isoforms have been reported in a study by Yarwood and others (252).

I have also shown, at least in the case of MBP–HSPDE4D4, that by engineering a TEV protease site into the MBP–PDE fusion protein it is possible to separate the MBP and PDE moieties by limited proteolysis without degrading the PDE moiety. It seems likely that this strategy could now be used to produce purified, untagged preparations of each of the splice variants of PDE4D.

I have shown that the purified MBP–HSPDE4D4 is an active PDE4D enzyme, as judged by the criteria of PDE enzyme activity, immunoreactivity, and sensitivity to inhibition by the PDE4 selective inhibitor rolipram. This fusion protein catalyses the hydrolysis of cAMP with kinetics that conform well to the Michaelis-Menten model. The Km for cAMP of MBP–HSPDE4D4 is, however, approximately 10 fold higher than that of HSPDE4D4 expressed in the cytosolic fraction of COS-7 cells. This suggested that there were differences in the cAMP binding site of MBP–HSPDE4D4 compared to that of HSPDE4D4 expressed in the cytosolic fraction of COS-7 cells.

I determined the true Vmax of MBP–HSPDE4D4 to be 1496±305µmol/min/mg and also calculated the turnover number to be 201±41 min^{-1}. I then used quantitative immunoblots to calculate the molar concentration of HSPDE4D4 in the cytosolic fraction of transfected COS-7 cells (using purified MBP–HSPDE4D4 as a standard) and so estimated the turnover number for cAMP hydrolysis of this preparation of HSPDE4D4 to be 106±12 min^{-1}. These values were not significantly different at the 5% level (Student's t-Test). This suggested that although the affinity of MBP–HSPDE4D4 for cAMP was reduced compared to that of the wild type enzyme

the speed with which the active sites of the 2 enzymes were able to catalyse the hydrolysis of cAMP was similar. I therefore speculated that the elevated Km of the fusion protein may have been due to the MBP moiety either sterically hindering access of cAMP to the active site or altering the conformation of the active site in some way and so reducing it's affinity for cAMP. I therefore decided to pursue the proteolytic cleavage of the MBP tag from the fusion protein.

By engineering a TEV protease recognition site into the MBP–HSPDE4D4 fusion protein I was able to purify HSPDE4D4 as an untagged protein with just 11 vector derived amino acids remaining at its amino terminus. This protein was kinetically identical to recombinant HSPDE4D4 expressed in the cytosolic fraction of COS-7 cells.

I have used purified preparations of the MBP fusion proteins of HSPDE4D4 and also of the unique, amino terminal region of HSPDE4D4 (amino acids 1–166) to show that this isoform can bind directly to the SH3 domain of Lyn kinase and that the unique, amino terminal region of HSPDE4D4 is sufficient for this interaction. I demonstrated this interaction by 3 independent methods: pull down assays, overlay assays and ELISAs. Taken together with the data presented in chapter 3 of this thesis, which shows that HSPDE4D4 but neither the HSPDE4D3 nor HSPDE4D5 can interact with SH3 domains, this supports the hypothesis that the unique, amino terminal region of HSPDE4D4 is both necessary and sufficient for the interaction of HSPDE4D4 with the SH3 domain of Lyn kinase.

5. Mapping the sites within the amino terminal of RNPDE4A5 responsible for SH3 domain association and for targeting

5.1 Introduction

There are 3 distinct splice variants of rat PDE4A that have so far been characterised, RNPDE4A1, RNPDE4A5 and RNPDE4A8 (200) (16, 140, 201). In addition to these, another 2 splice variants, rPDE66 [G. Bolger and others, unpublished] and also the rat homologue of HSPDE4A10 [M. Houslay and others, unpublished] have been cloned but not yet characterised. The alternative splicing of rat PDE4A, as with all known active PDE4s, takes the form of 5' domain swaps such that all the members of this family share an identical primary structure outside of their alternatively spliced amino terminal regions.

5.1.1 Characteristics of RNPDE4A5

The splice variant RNPDE4A5, originally cloned from an adult rat brain cDNA library, is a long isoform of rat PDE4A (17). The alternatively spliced amino terminal region of this protein comprises 102 residues (including the initiating methionine) and does not share homology with any other known rat PDE. This region of RNPDE4A5 is, however 89% homologous with the spliced, amino terminal region of HSPDE4A4B, the human homologue of RNPDE4A5.

5.1.1.1 Interaction of RNPDE4A5 with SH3 domains

An isoform specific property of RNPDE4A5 is that it can selectively bind to the SH3 domains of certain proteins, namely those of the Src family tyrosyl kinases Src, Fyn, Lyn and of the cytoskeletal protein fodrin (see section 3.1.2.4). The alternatively spliced, amino terminal 102 residues of RNPDE4A5 are necessary for its interaction with these SH3 domains. This region of RNPDE4A5 contains 3 motifs that conform

to the PxxP consensus sequence that is proposed to confer an ability to interact with SH3 domains (see section 1.4.1). One or more of these motifs are likely to be the site of the interaction between RNPDE4A5 and SH3 domains. These PxxP motifs are also well conserved in HSPDE4A4B, the human homologue of RNPDE4A5 ().

5.1.1.2 Cleavage of RNPDE4A5 by caspase-3

The spliced amino terminal region of RNPDE4A5 contains a pair of motifs that conform to the consensus sequence for cleavage by the members of a family of cysteine proteases called caspases. This family of proteases, which are required for the initiation of apotosis, are synthesised as inactive zymogens and are proteolyticaly activated in a cascade similar to that of the immune complement system. RNPDE4A5 is a substrate for the ubiquitously expressed caspase-3 and is cleaved by this caspase at an early stage during the initiation of apotosis [Huston and others, manuscript in preparation].

The cleavage of RNPDE4A5 by caspase-3 does not result in a change in the catalytic activity of RNPDE4A5, nor does it cause any conformational change in the protein which can be detected by a change in its sensitivity to the PDE4 specific inhibitor rolipram (see section 1.3.6). The truncated form of RNPDE4A5, produced by cleavage with caspase-3 does, however, exhibit an altered intracellular distribution, as assessed by immunofluoresent staining and confocal microscopy, compared to the full length enzyme. The region of the RNPDE4A5 that is removed by caspase-3 cleavage is that which contains the 3 putative SH3 domain binding regions within the amino terminal of RNPDE4A5. The truncated RNPDE4A5 also shows a marked reduction in its ability to interact with SH3 domains and this has lead to speculation that the interaction of RNPDE4A5 with an SH3 domain may be involved in its subcellular targeting. It may be the case that the disruption of this targeting following the cleavage of RNPDE4A5 by caspase-3 is important in the progression of the apoptotic pathway of programmed death in cells where RNPDE4A5 is expressed [Huston and others, manuscript in preparation]

```
                3                                   10
RNPDE4A5        Pro Pro Ala Ala Pro Ser Glu Arg
HSPDE4A4B       Pro Pro Thr Val Pro Ser Glu Arg
                3                                   10


                35                                  42
RNPDE4A5        Arg Gln Pro Arg Thr Pro Ile Arg
HSPDE4A4B       Arg Gln Pro Arg Thr Pro Ile Arg
                35                                  42


                60                                  67
RNPDE4A5        Ser Pro His Arg Pro Ile Glu Arg
HSPDE4A4B       Gln Pro His Arg Pro Ile Glu Arg
                60                                  67
```

Figure 5.55: Alignments of the 3 proline and arginine rich regions of sequence contained within the alternatively spliced amino termini of RNPDE4A5 and of HSPDE4A4B

The figure shows alignments of the 3 regions of proline and arginine rich sequence, within the alternatively spliced amino termini of RNPDE4A5 and HSPDE4A4B, that conform to the consensus motif PxxP. The numbering above and below the sequences refer to the amino acid number in the deduced amino acid sequences of these proteins.

5.2 Results and Discussion

The only differences between the primary structures of RNPDE4A5 and of the other rat PDE4A isoforms are in their alternatively spliced, amino terminal regions. This suggests that sequences contained within the amino termini of these proteins are responsible for the splice variant specific properties and regulation of each isoform. To define in detail the regions within the amino terminal of RNPDE4A5 that are necessary for certain of its splice variant specific properties I decided to construct a series of amino terminal truncations in RNPDE4A5 and to investigate which of the RNPDE4A5 specific properties each truncation retained. The properties that I intended to characterise were: which regions (a) conferred interaction with SH3 domains, (b) conferred association with the particulate cell fractions and (c) might affect the enzyme activity.

5.2.1 Construction of amino-terminal truncations in RNPDE4A5

The plasmid pSPORTrPDE6 encodes RNPDE4A5 under the control of an SV40 promoter. This plasmid has previously been used to achieve high levels of expression of RNPDE4A5 in transiently transfected COS-7 cells (140, 162). I used the Quick Change method of mutagenesis (Stratagene) to construct a series of deletions and point mutations in pSPOTRrPDE6 that encoded a series of amino terminal truncations and also a point mutation of RNPDE4A5 (R6Δ1— R6Δ7 and R6P7-A) (*Figure 5.56, Figure 5.57*).

The Quick Change method of mutagenesis relies upon the polymerase chain reaction (PCR) to construct and amplify each mutated plasmid (see section 2.4.6). I performed these PCR reactions using Pfu polymerase (supplied with the Quick Change kit). This polymerase has proof reading activity and hence shows approximately 5 fold greater fidelity than the non proof reading polymerase Taq (Promega), however, even using Pfu polymerase, the possibility of unplanned mutations arising during the PCR amplification should not be ignored. I therefore sequenced the entire open reading

frame of the mutants to ensure that no unexpected mutations had been generated.

The plasmids pSPORTR6Δ1– pSPORTR6Δ3 were constructed to encode truncations of RNPDE4A5 which lacked each of the 3 putative SH3 domain binding motifs that occur within the amino terminal region of this protein (residues 1–10 (R6Δ1), 1–42 (R6Δ2) and 1–67 (R6Δ3) of the wild type protein respectively). The point mutation pSPORTR6P7-A was constructed to encode a mutation of RNPDE4A5 in which the residue Pro^7 of the wild type enzyme was mutated to Ala (R6P7-A). This mutation was intended to disrupt the first of the putative SH3 domain binding motifs (residues 4–10, PxxPxxR) by changing the second Pro in the motif to Ala (*Figure 5.56, Figure 5.57*).

The deletions pSPORTR6Δ4–pSPORTR6Δ7 were constructed to encode truncations of RNPDE4A5 which lacked putative functional domains within the amino terminal of this isoform. The truncation pSPORTR6Δ4 encoded a species in which the unique, spliced region of RNPDE4A5 was deleted (residues 1–103 (R6Δ4)). The truncation pSPORTR6Δ5 encoded a species that was truncated up to the beginning of upstream conserved region 1 (UCR1) (residues 1–134 (R6Δ5)). The truncation pSPORTR6Δ6 encoded a species that was truncated up to the end of UCR1 (residue s 1–197 (R6Δ6)). The truncation pSPORTR6Δ7 encoded a species that was truncated up to the beginning of upstream conserved region 2 (UCR2) (residues 1–219 (R6Δ7)) (*Figure 5.56, Figure 5.57*).

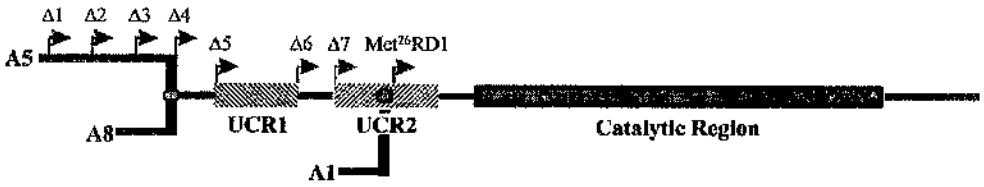

Figure 5.56: Truncation mutants in RNPDE4A5

The figure shows a diagram representing 3 of the splice variants from the rat PDE4A gene. The start sites of the engineered truncations R6Δ1 (residue 11 in RNPDE4A5), R6Δ2 (residue 43 in RNPDE4A5), R6Δ3 (residue 68 in RNPDE4A5), R6Δ4 (residue 103 in RNPDE4A5), R6Δ5 (residue 135 in RNPDE4A5), R6Δ6 (residue 197 in RNPDE4A5), R6Δ7 (residue 218 in RNPDE4A5) and Met^{26}RD1 (previously engineered by our group (200)) (residue 260 in RNPDE4A5) are indicated by arrows. The hashed boxes show the positions of UCR1 and of UCR2 and the grey box represents the conserved, catalytic region which is present in all known mammalian 3'5' phosphodiesterases.
NB. This figure is not drawn to scale.

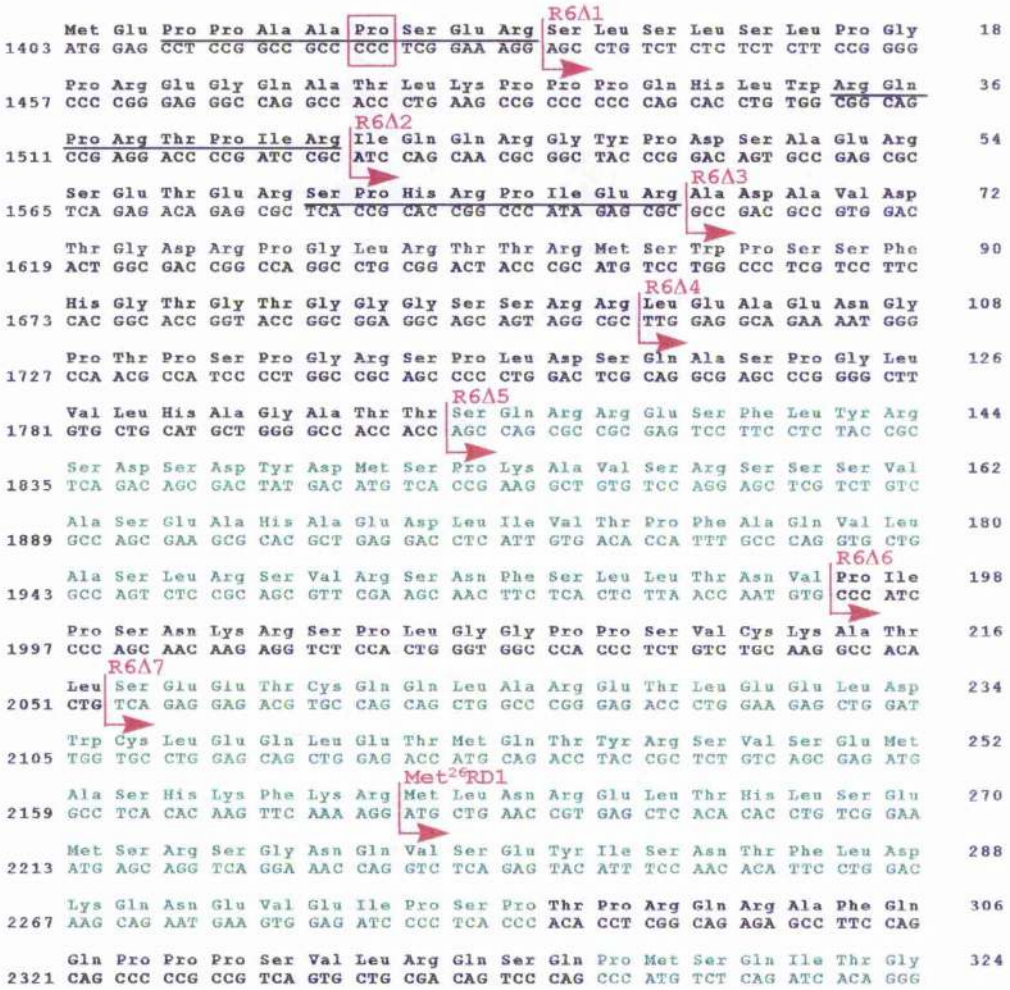

Figure 5.57: Positions of the truncations and point mutation in RNPDE4A5

The figure shows the amino acid and the nucleotide sequence of part of the open reading frame of RNPDE4A5. The positions of the truncations R6Δ1–R6Δ7and of Met[26]RD1 are shown by red arrows. These truncations were constructed in the plasmid pSPORTrPDE6 by deletion of the nucleotide sequence lying between the initiating ATG of RNPDE4A5 and the position indicated here by the red arrows. The position of the point mutation R6P7-A is shown by the red box. This mutation was constructed by mutation of the codon CCC to GCC. The regions of sequence coloured in green indicate regions conserved between all PDE4s. These are UCR1 (residues 135–196 in RNPDE4A5), UCR2 (residues 218–298 in RNPDE4A5) and the catalytic region (residues 318–674 in RNPDE4A5). The numbers along the right hand side of the figure indicate the codon number in the open reading frame of RNPDE4A5. The numbers along the left hand side of the figure indicate the nucleotide number in the genbank sequence for RNPDE4A5 (accession number L27057).

5.2.1.1 Expression of the engineered truncations in RNPDE4A5

To establish that each of the mutated plasmids did indeed encode for an active PDE, I transiently transfected COS-7 cells with each plasmid. I then performed both PDE enzyme activity assays and immunoblots, using a polyclonal antisera raised against the carboxyl terminal region of RNPDE4A5, on the crude cytosolic fraction of the transfected cells. In all cases the PDE enzyme activity in the cytosolic fraction of the transfected cells was 50–100 times that in the cytosolic fraction of mock transfected cells (no DNA). The immunoblots revealed a novel band of immunoreactivity present in the cytosolic fraction, of cells transfected with each plasmid, that migrated with an apparent Mw 9–16kDa higher, depending upon the deletion, than that calculated from the predicted primary structure of each mutant (see section 2.4.10) (*Figure 5.58 and Table 5.5.1*). This is consistent with the observed anomalous migration of RNPDE4A5 and other isoforms of PDE4 on sodium dodecyl sulphate polyacrylamide gel electrophroesis (SDS–PAGE) (15, 16, 93, 108, 140, 201).

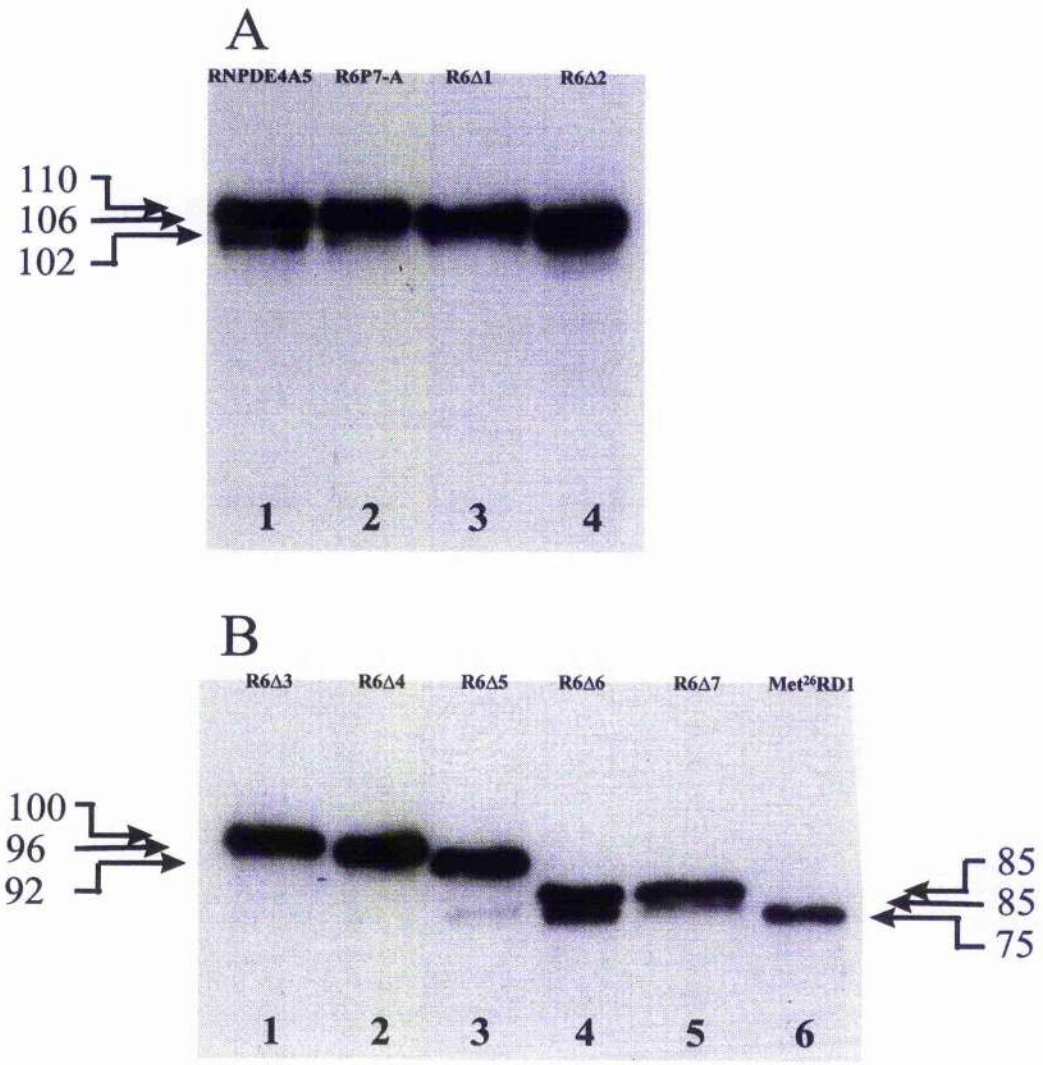

Figure 5.58:Expression of amino terminal truncated forms of RNPDE4A5 in COS-7 cells

The figure shows immunoblots of truncation mutants of RNPDE4A5 expressed in the cytosolic fraction of transiently transfected COS-7 cells. In panel A: lanes 1–4 are sufficient of the cytosolic fraction of transfected COS-7 cells to contain 8EU of RNPDE4A5, R6P7-A, R6Δ1 and R6Δ2 respectively. In panel B: lanes 1–6 are sufficient of the cytosolic fraction of transfected COS-7 cells to contain 8EU of R6Δ3, R6Δ4, R6Δ5, R6Δ6, R6Δ7 and Met^{26}RD1 respectively. The arrows indicate the apparent Mw (kDa) of that band, calculated by plotting the Rf values of markers run on the same gel.

Construct	Amino acids	Apparent Mw on SDS-PAGE	
		Calculated (kDa)	Observed (kDa)
RNPDE4A5	844	93	108±1
R6P7-A	844	93	108±1
R6Δ1	835	93	102±2
R6Δ2	803	89	98±3
R6Δ3	778	86	99±2
R6Δ4	743	82	98±1
R6Δ5	721	79	94±3
R6Δ6	649	72	86±1
R6Δ7	627	70	82±1
Met[26]RD1	585	65	81±1

Table 5.5.1: Molecular weights of truncations and a point mutation in RNPDE4A5

The table shows the predicted and the observed Mw of truncations and a point mutation in RNPDE4A5. The sequence analysis of these proteins was done using the computer program Gene Jockey and in all cases the initiating methionine of the peptide sequence has been included in the analysis. The observed Mw of each protein was determined by comparing the Rf value of the immunoreactive bands on immunoblots to those of molecular weight markers run on the same gels. Each reported value is the mean of at least 3 determinations and the reported errors are the standard error of each mean.

5.2.2 Mapping the regions of sequence within RNPDE4A5 necessary for interaction with SH3 domains

Unlike RNPDE4A5, neither RNPDE4A8 nor $Met^{26}RD1$ can interact with the SH3 domains of either Src or Lyn kinase in pull down assays (162). This suggested that the unique amino terminal region of RNPDE4A5 was necessary for its interaction with these SH3 domains. The extreme amino terminal region of RNPDE4A5 contains 3 motifs which conform to the PxxP consensus sequence for binding to SH3 domains. It has been suggested (162) that one or more of these motifs may be responsible for the detected interaction between RNPDE4A5 and SH3 domains (see sections 1.3.2.2). I therefore decided to use the amino terminal truncations in RNPDE4A5: R6Δ1, R6Δ2, R6Δ3, R6Δ4, $Met^{26}RD1$ (*Figure 5.56*) and also the point mutation R6P7–A (*Figure 5.55*) to define the sub-region within the amino terminal of RNPDE4A5 that is involved in binding to the SH3 domain of Lyn kinase.

I transiently transfected COS-7 cells to express either wild type (full length) RNPDE4A5 or one of the amino terminal truncations or the R6P7-A point mutation in this protein. I then used the cytosolic fraction from the transfected cells as the source of enzyme for pull down assays with either purified GST–Lyn SH3 or with GST alone. I used both PDE enzyme activity assays and immunoblots to monitor the binding of each construct to GST–Lyn SH3 and to GST alone (*Figure 5.59, Figure 5.60*).

In my previous study of the interactions between HSPDE4D4 and SH3 domains from various proteins, I had found that the data which I generated in those pull down assays was unsuitable for analysis by ANOVA (see section 3.2.3.1). I therefore designed this set of experiments in such a way that I was able to analyse the data using paired t-Tests (166).

I performed the pull down assays as a series of (tightly) paired determinations where, in each experiment, I measured the percentage binding of a construct to GST–Lyn SH3 and to GST alone. I then tested to see if the mean difference between these pairs

was significantly different from 0 at the 5% level.

This analysis revealed that, of the proteins examined, only R6Δ4 and Met^{26}RD1 failed to interact significantly with the SH3 domain of Lyn kinase (*Figure 5.59*). This was an unexpected result because the construct R6Δ3 does not contain any of the 3 putative SH3 domain binding PxxP motifs that are present in full length RNPDE4A5 yet it was still able to interact with the SH3 domain of Lyn kinase.

Inspection of the data showed that there appeared to be a large decrease in the mean percentage binding of R6Δ1 to GST–Lyn SH3 compared to that of full length RNPDE4A5. Further truncations in the unique, alternatively spliced region of RNPDE4A5 (R6Δ2 and R6Δ3) did not, however, appear to further reduce the binding to GST–Lyn SH3 in pull down assays (*Figure 5.59*).

That the truncated form R6Δ1 showed a large decrease in binding to GST–Lyn SH3 compared to that of full length RNPDE4A5 (48% and 19% respectively) suggested that the first 10 amino acids of RNPDE4A5 were important for the interaction of RNPDE4A5 with the SH3 domain of Lyn kinase (*Figure 5.57 and Figure 5.59*).

That the truncated forms R6Δ2 and R6Δ3 showed little further reduction in their binding to GST–Lyn SH3 (12% and 14% respectively) than did R6Δ1 suggested that the 2 PxxP motifs contained in the region between residues 11–68 of RNPDE4A5 are not important for the interaction of RNPDE4A5 with the SH3 domain of Lyn kinase (*Figure 5.57 and Figure 5.59*).

The truncated form R6Δ4 did not show significant binding to GST–Lyn SH3. This implicates the region between residues 68–102 of RNPDE4A5 as being involved in the interaction with the SH3 domain of Lyn kinase (*Figure 5.57 and Figure 5.59*).

I performed pull down assays using the point mutation R6P7-A to examine the effect of disrupting the putative SH3 domain binding motif that is present in the region of RNPDE4A5 deleted in the truncation mutant R6Δ1. The mean percentage binding of this point mutation to GST–Lyn SH3 appeared to be reduced compared to that of

RNPDE4A5. This is consistent with the hypothesis that the PxxP motif between residues 4–7 of RNPDE4A5 is involved in the interaction of this protein with SH3 domains (*Figure 5.57 and Figure 5.59*).

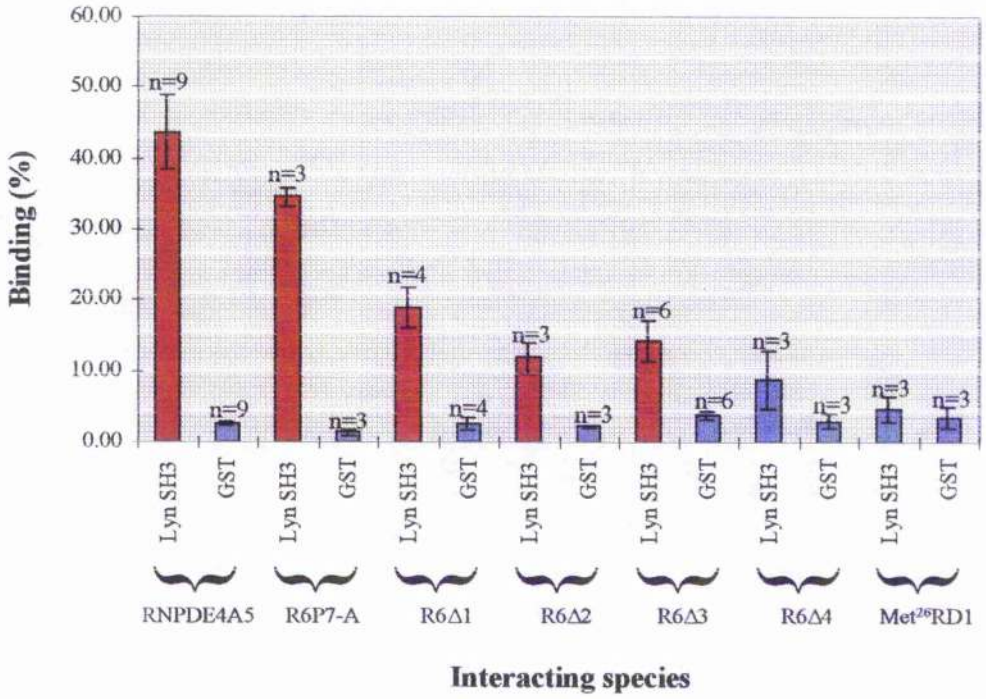

Figure 5.59: Binding of wild type, a point mutation of and truncations in RNPDE4A5 to the SH3 domain of Lyn kinase

The bar chart shows data from pull down assays to screen a point mutation of and a series of truncations in RNPDE4A5 for interaction with the SH3 domain of Lyn kinase. The data are expressed as the percentage of recovered PDE enzyme activity present in the bound fraction. The values are the means of n separate determinations with error bars showing the standard error of the means. Columns coloured in red indicate that the mean binding to GST-Lyn SH3 is significantly different from that to GST alone (paired t-Test, 5% level).

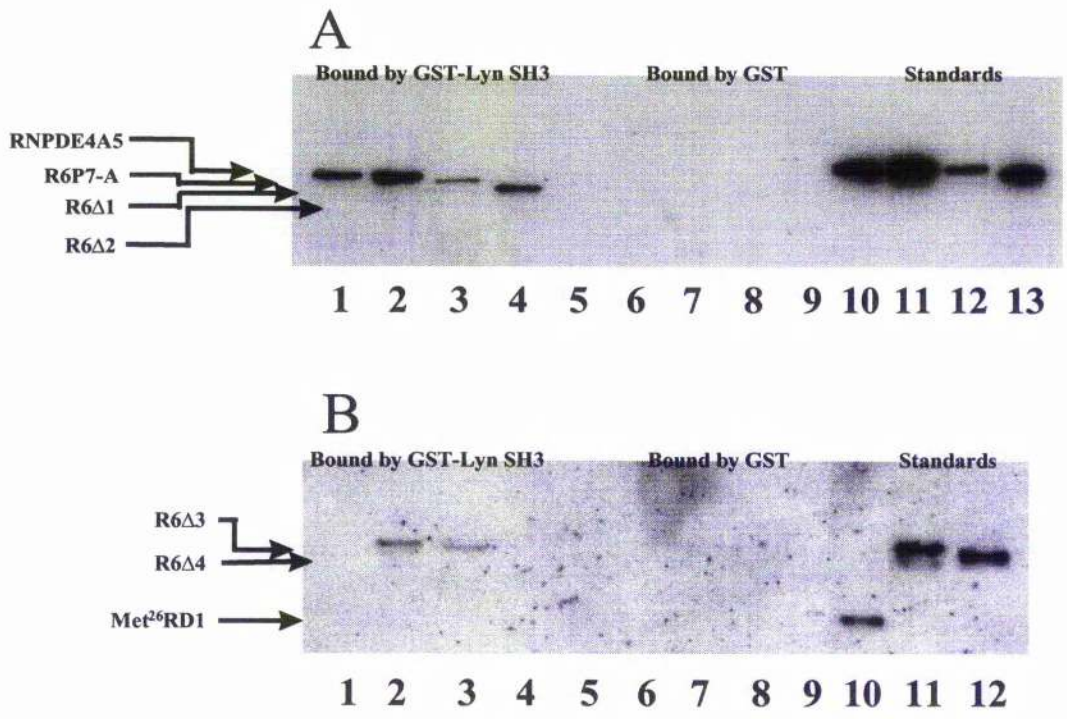

Figure 5.60: Binding of truncation mutants in RNPDE4A5 to the SH3 domain of Lyn kinase

The figure shows immunoblots for rat PDE4A of the bound fractions from pull-down assays between truncation mutants in RNPDE4A5 and either GST or GST–Lyn SH3. In panel A: lanes 1–4 are the bound fractions from pull down assays between GST–Lyn SH3 and RNPDE4A5, R6P7-A, R6Δ1 and R6Δ2 respectively; lane 5 is empty; lanes 6–9 are the bound fractions from pull down assays between GST and RNPDE4A5, R6P7-A, R6Δ1 and R6Δ2 respectively; lanes 10–13 are 20μg cytosolic fraction from transfected COS-7 cells expressing RNPDE4A5, R6P7-A, R6Δ1 and R6Δ2 respectively. In panel B: lanes 1–3 are the bound fractions from pull down assays between GST–Lyn SH3 and Met^{26}RD1, R6Δ3 and R6Δ4 respectively; lane 5 is empty; lanes 6–8 are the bound fractions from pull down assays between GST and Met^{26}RD1, R6Δ3 and R6Δ4 respectively; lane 9 is empty; lanes 10–12 are 20μg cytosolic fraction from transfected COS-7 cells expressing Met^{26}RD1, R6Δ3 and R6Δ4 respectively.

5.2.3 Mapping the regions of sequence within the amino terminal region of RNPDE4A5 that are necessary to targeting the protein to the particulate fraction of COS-7 cells

When expressed in transiently transfected COS-7 cells both RNPDE4A5 and RNPDE4A8 are found in both the soluble and the particulate cell fractions. This is also true for the RNPDE4A5 like species that is present in preparations of rat brain (16, 140). Another splice variant from the rat PDE4A gene, RNPDE4A1, is found associated exclusively with the particulate fraction of both transfected COS-7 cells and of rat brain preparations (140). This is in contrast to the truncated species Met^{26}RD1, which occurs as an exclusively cytosolic species when expressed in COS-7 cells (see section 1.3.2.1) (200). It therefore appears that the alternatively spliced, amino terminal regions of PDE4A splice variants are both necessary and, at least in the case of RNPDE4A1, sufficient for the association of these enzymes with the particulate fraction of cells (194).

Differences between the sub-cellular distributions of RNPDE4A5 and RNPDE4A8, as assessed by the fractionation of transfected COS-7 cells, have previously been reported (16). The primary structures of these 2 proteins, which are identical outside of their amino terminal regions, converge at residue 103 in RNPDE4A5 (residue 22 in RNPDE4A8). This suggested that sequences contained within the first 103 amino acids of RNPDE4A5 may be responsible for splice variant specific sub-cellular targeting of this isoform.

The association of RNPDE4A5 with the particulate fraction of COS-7 cells is not disrupted by washing with buffers containing high concentrations of salt, nor of the nonionic detergent Triton X-100. Neither is the association disrupted by washing with buffers containing both high concentrations of salt and of Triton X-100 (140). The interaction of RNPDE4A5 with SH3 domains in pull down assays is also not disrupted under these conditions. This has lead to speculation that the targeting of RNPDE4A5 into the salt and Triton X-100 insoluble pellet may involve its binding to an SH3 domain (162). The fraction of RNPDE4A8 which is found associated with the particulate fraction of transfected COS-7 cells is, however, also resistant to

solubilisation by salt and Triton X-100. This observation does not support the involvement of an SH3 interaction in the salt and Triton X-100 insolubility of RNPAE4A5. Rather it suggests that the region of sequence that is conserved between RNPDE4A5 and RNPDE4A8 may be, at least partly, responsible for the observed salt and detergent insolubility of these proteins (16).

I therefore decided to use the amino terminal truncation mutants in RNPDE4A5 to define the sub-regions of sequence within the amino terminal of RNPDE4A5 that are involved in mediating association with the particulate fractions of cells.

5.2.3.1 Assessment of the subcellular distribution of recombinant proteins by fractionation

I transiently transfected COS-7 cells to express either wild type (full length) RNPDE4A5 or one of the amino terminal truncations of this protein. I then fractionated the cells by differential centrifugation to produce a low speed (850g) pellet fraction (P1), a high speed (100000g) pellet fraction (P2) and a high speed (100000g) supernatant fraction (S2). This method of fractionation has been routinely used by members of our group as a rapid means of determining whether a protein has the propensity to interact with subcellular structures (15, 140, 193).

I used lactate dehydrogenase (a marker enzyme for cytosol) enzyme activity assays to monitor the efficiency of this fractionation procedure (see section 2.3.4). This analysis revealed that, under these conditions, I was able to achieve >96% cell breakage and <1% contamination of the pellet fractions by cytosolic proteins.

To assess the distribution of each recombinant PDE between the cell fractions I performed both PDE enzyme activity assays and semi-quantitative immunoblots on a known proportion of each fraction. This allowed me to calculate the percentage of both the total PDE enzyme activity and of the total anti-PDE4A immunoreactivity present in each fraction.

5.2.3.2 Distribution of RNPDE4A5, RNPDE4A8 and of Met^{26}RD1 in transfected COS-7 cells

Preliminary experiments indicated that, in my hands, the deletion mutant R6ΔP4 was present in the P1, as well as in the P2 and the S2 fractions of transfected COS-7 cells. This was a surprising result because R6ΔP4 is truncated up to the point at which the primary structures of RNPDE4A5 and RNPDE4A8 converge and it has previously been reported that only trace amounts of RNPDE4A8 were found associated with the P1 fraction of transfected COS-7 cells (16). I therefore decided to examine the distributions of RNPDE4A5, RNPDE4A8 and of Met26RD1 before proceeding with the analysis of the other truncation mutants.

I assayed the distributions of both the anti PDE4A immunoreactivity and of the PDE enzyme activity between the P1, the P2 and the S2 fractions of COS-7 cells transiently transfected with RNPDE4A5, with RNPDE4A8 and with Met^{26}RD1 (*Figure 5.61*). I then used ANOVA to compare the distributions of these PDEs (as determined by semi-quantitative immunoblotting and also by PDE enzyme activity assays).

First I compared the percentages of the total PDE that were present in each fraction of the cells. This revealed that there were significant differences (5% level) in the distributions of these species as determined both by semi-quantitative immunoblotting and by PDE enzyme activity assays. I then proceeded to partition the treatment sums of squares for each fraction and to compare the percentage of Met^{26}RD1 present in each fraction with the percentage of the other PDE species, taken together, present in that fraction. I did this because there is strong evidence that Met^{26}RD1 exists as an exclusively soluble species in transfected cells (140, 171, 200, 201). This comparison should therefore reveal any propensity of these species to associate with the particulate fractions of the cells.

The analysis revealed that the distribution of Met^{26}RD1, as assessed by semi-quantitative immunoblotting, was significantly different (5% level) from those of RNPDE4A5 and of RNPDE4A8 but that the distributions of these latter 2 species

were not significantly different from each other (5% level) (*Table 5.5.2, Table 5.5.3, Table 5.5.4*). I then applied this analysis to the distributions of these species as assessed by PDE enzyme activity assays. This revealed that whilst the distributions of $Met^{26}RD1$ and of the other 2 species were still judged to be significantly different (5% level), there was also a significantly (5% level) greater proportion of the RNPDE4A8 than of the RNPDE4A5 present in the S2 fraction and a significantly (5% level) smaller proportion of the RNPDE4A8 than of the RNPDE4A5 present in the P2 fraction (*Table 5.5.5, Table 5.5.6, Table 5.5.7*). It therefore appears that there are differences between the distributions of RNPDE4A5 and RNPDE4A8 in transfected COS-7 cell fractions but that, in my hands, both of these proteins are significantly associated with the P1, as well as with the P2, cell fraction.

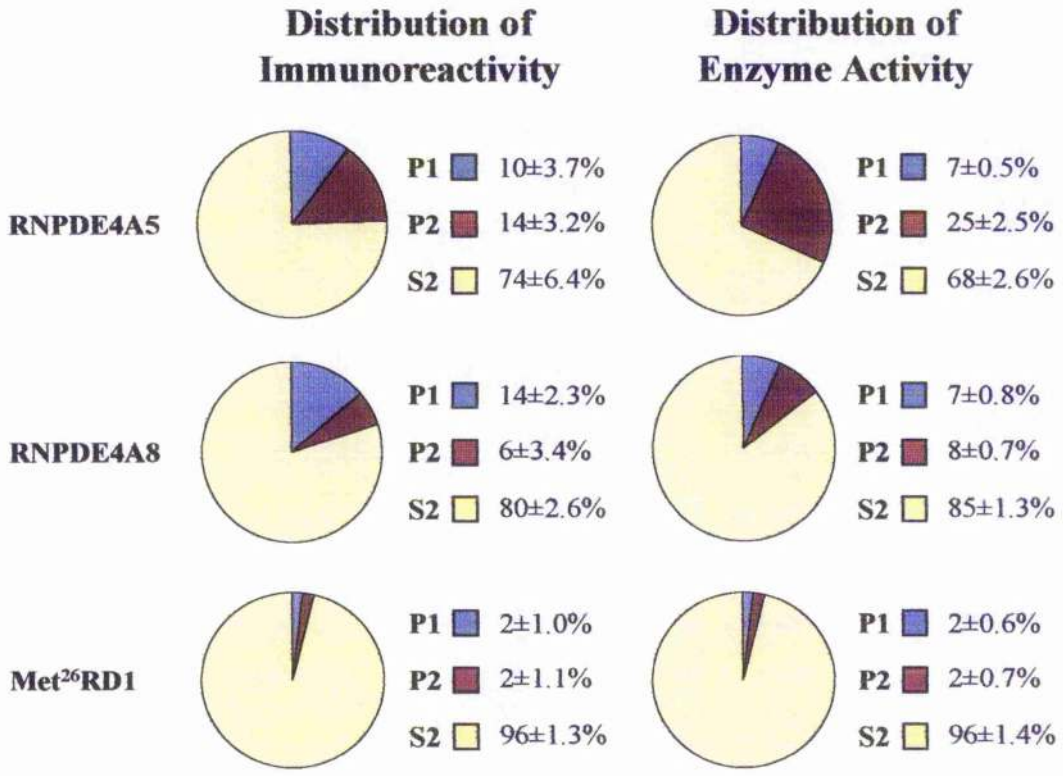

Figure 5.61: Distribution of PDE4A immunoreactivity and of PDE enzyme activity in transfected COS-7 cells

The figure shows the percentages of the total PDE4A immunoreactivity and of the total PDE enzyme activity that were present in the low speed pellet (P1), the high speed pellet (P2) and the high speed supernatant (S2) fractions of transfected COS-7 cells. The reported values are the means of at least 3 determinations with standard errors shown.

Table 5.5.2: ANOVA of percentage of anti PDE4A immunoreactivity in the P1 fraction of transfected COS-7 cells

Sources of variation	Sums of squares	Degrees of	Mean squares	F	Differen t p=0.05
All treatments:	269.23	2	134.62	3.00	No
Met^{26}RD1/others	243.84	1	243.84	5.43	Yes
Others	25.39	1	25.39	0.57	No
Error	448.78	10	44.88		
Total	718.01	12			

Table 5.5.3: ANOVA of percentage of anti PDE4A immunoreactivity in the P2 fraction of transfected COS-7 cells

Sources of variation	Sums of squares	Degrees of	Mean squares	F	Differen t p=0.05
All treatments:	373.46	2	186.73	4.84	Yes
Met^{26}RD1/others	259.30	1	259.30	6.72	Yes
Others	114.16	1	114.16	2.96	No
Error	386.00	10	38.60		
Total	759.45	12			

Table 5.5.4: ANOVA of percentage of anti PDE4A immunoreactivity in the S2 fraction of transfected COS-7 cells

Sources of variation	Sums of squares	Degrees of	Mean squares	F	Differen t p=0.05
All treatments:	1159.04	2	579.52	4.55	Yes
Met^{26}RD1/others	1102.44	1	1102.44	8.65	Yes
Others	56.60	1	56.60	0.44	No
Error	1274.74	10	127.47		
Total	2433.78	12			

Table 5.5.5: ANOVA of percentage of PDE enzyme activity in the P1 fraction of transfected COS-7 cells

Sources of variation	Sums of squares	Degrees of	Mean squares	F	Differen t p=0.05
All treatments:	78.77	2	39.38	17.84	Yes
Met^{26}RD1/others	77.80	1	77.80	35.24	Yes
Others	0.97	1	0.97	0.44	No
Error	19.87	9	2.21		
Total	98.63	11			

Table 5.5.6: ANOVA of percentage of PDE enzyme activity in the P2 fraction of transfected COS-7 cells

Sources of variation	Sums of squares	Degrees of	Mean squares	F	Differen t p=0.05
All treatments:	953.66	2	476.83	80.55	Yes
Met^{26}RD1/others	417.25	1	417.25	70.48	Yes
Others	536.41	1	536.41	90.61	Yes
Error	53.28	9	5.92		
Total	1006.93	11			

Table 5.5.7: ANOVA of percentage of PDE4 enzyme activity in the S2 fraction of transfected COS-7 cells

Sources of variation	Sums of squares	Degrees of	Mean squares	F	Differen t p=0.05
All treatments:	1438.61	2	719.30	66.34	Yes
Met^{26}RD1/others	855.74	1	855.74	78.92	Yes
Others	582.87	1	582.87	53.76	Yes
Error	97.58	9	10.84		
Total	1536.19	11			

5.2.3.3 Distribution of RNPDE4A truncation mutants in COS-7 cells

I then proceeded to use the amino terminal truncations in RNPDE4A5, namely R6Δ3, R6Δ4, R6Δ5, R6Δ6, R6Δ7 and Met^{26}RD1 to locate the regions, within the amino termini of long form PDE4A splice variants, that are involved in their association with the particulate fraction of COS-7 cells. For this analysis I needed to set criteria for a truncation to be regarded as retaining the ability to associate with particulate cell fractions. I set this as there being a significantly greater proportion of a species present in a particulate cell fraction than of Met^{26}RD1 in that fraction. I decided on this criteria because there is strong evidence that Met^{26}RD1 exists as an exclusively soluble species in transfected COS-7 cells (140, 171, 200, 201).

As with my previous analysis of the distributions of RNPDE4A5, RNPDE4A8 and Met^{26}RD1, I transfected COS-7 cells to express transiently each of the proteins. I then fractionated the cells by differential centrifugation to produce a P1, a P2 and an S2 fraction. I compared the distributions of each protein, as determined by semi-quantitative immunoblotting and also by PDE enzyme activity assays, by using the technique of ANOVA (*Figure 5.62, Table 5.5.8, Table 5.5.9, Table 5.5.10, Table 5.5.11, Table 5.5.12, Table 5.5.13*).

I first compared the percentages of the total PDE that were present in each cell fraction. After this I proceeded to partition the treatment sums of squares for each fraction and to compare the percentage of Met^{26}RD1 present in each fraction with the percentage of the other PDE species, taken together, present in that fraction *(Table 5.5.8, Table 5.5.9, Table 5.5.10, Table 5.5.11, Table 5.5.12, Table 5.5.13*). This analysis revealed that, although there were significant differences (5% level) between the distributions of the truncations R6Δ3, R6Δ4, R6Δ5, R6Δ6 and R6Δ7 (as judged by PDE enzyme activity assays) all of these species satisfied the criteria for being regarded as associated with the particulate fractions of the cells.

That the truncation R6Δ7 is found associated with the particulate fractions of COS-7 cells shows that amino acids 1–217 in RNPDE4A5 are not necessary for the association of this protein with the particulate cell fractions. Furthermore, taken

with the observation that $Met^{26}RD1$ does not associate with the particulate cell fractions, my analysis shows that the region between amino acids 218–259 in RNPDE4A5 is involved in targeting the protein to the particulate cell fractions.

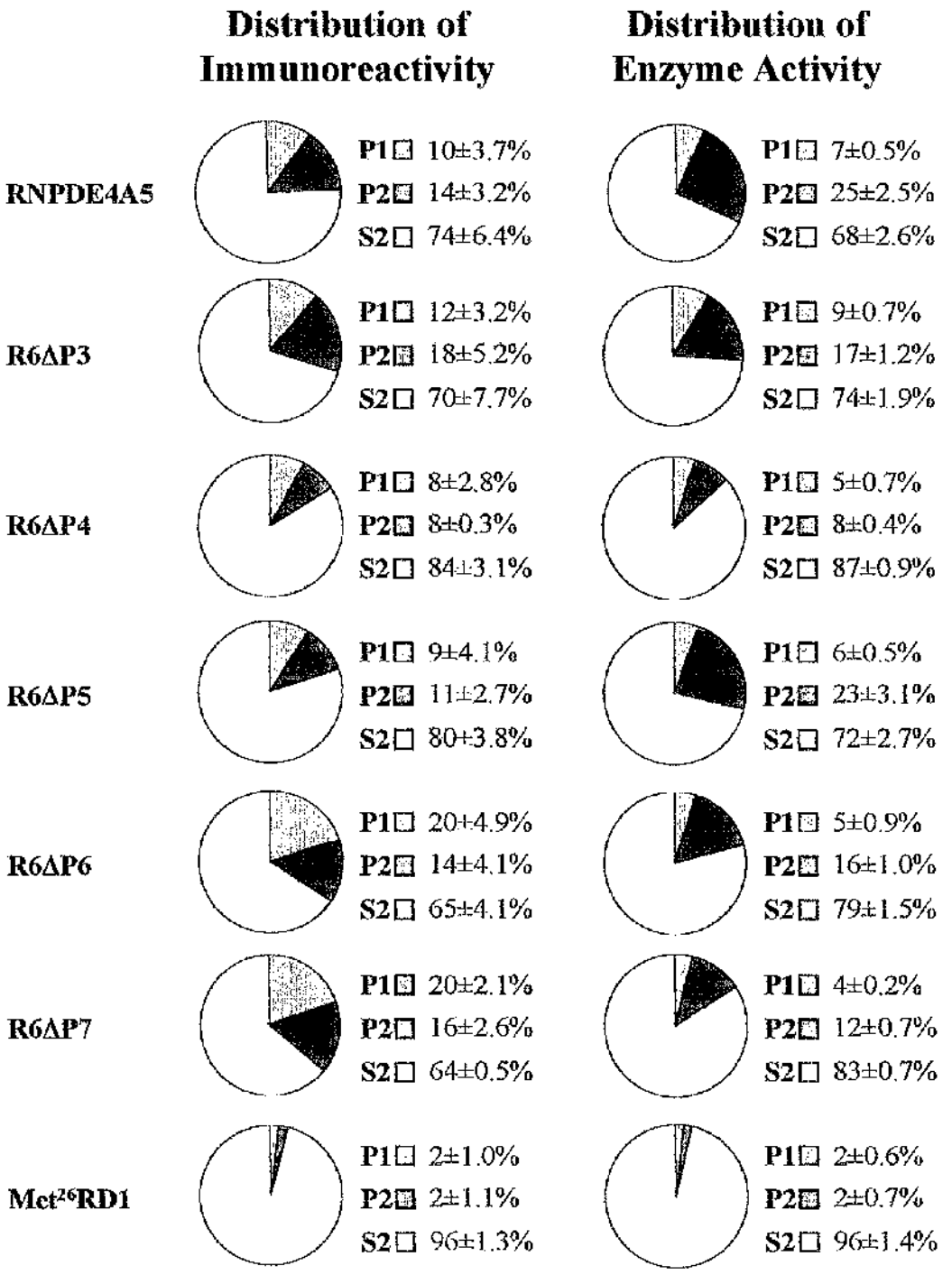
Distribution of Immunoreactivity
Distribution of Enzyme Activity
RNPDE4A5
P1 10±3.7%
P2 14±3.2%
S2 74±6.4%
P1 7±0.5%
P2 25±2.5%
S2 68±2.6%
R6ΔP3
P1 12±3.2%
P2 18±5.2%
S2 70±7.7%
P1 9±0.7%
P2 17±1.2%
S2 74±1.9%
R6ΔP4
P1 8±2.8%
P2 8±0.3%
S2 84±3.1%
P1 5±0.7%
P2 8±0.4%
S2 87±0.9%
R6ΔP5
P1 9±4.1%
P2 11±2.7%
S2 80±3.8%
P1 6±0.5%
P2 23±3.1%
S2 72±2.7%
R6ΔP6
P1 20±4.9%
P2 14±4.1%
S2 65±4.1%
P1 5±0.9%
P2 16±1.0%
S2 79±1.5%
R6ΔP7
P1 20±2.1%
P2 16±2.6%
S2 64±0.5%
P1 4±0.2%
P2 12±0.7%
S2 83±0.7%
Met[26]RD1
P1 2±1.0%
P2 2±1.1%
S2 96±1.3%
P1 2±0.6%
P2 2±0.7%
S2 96±1.4%

Figure 5.62: Distribution of PDE4A immunoreactivity and of PDE enzyme activity in transfected COS-7 cells

The figure shows the percentages of the total PDE4A immunoreactivity and of the total PDE enzyme activity that were present in the low speed pellet (P1), the high speed pellet (P2) and the high speed supernatant (S2) fractions of transfected COS-7 cells. The reported values are the means of at least 3 determinations with standard errors shown.

Table 5.5.8: ANOVA of percentage of anti PDE4A immunoreactivity in the P1 fraction of transfected COS-7 cells

Sources of variation	Sums of squares	Degrees of	Mean squares	F	Differen t p=0.05
All treatments:	1002.10	6	167.02	2.43	No
Met^{26}RD1/others	456.02	1	456.02	6.64	Yes
Others	546.08	5	109.22	1.59	No
Error	1373.63	20	68.68		
Total	2375.73	26			

Table 5.5.9: ANOVA of percentage of anti PDE4A immunoreactivity in the P2 fraction of transfected COS-7 cells

Sources of variation	Sums of squares	Degrees of	Mean squares	F	Differen t p=0.05
All treatments:	674.03	6	112.34	1.87	No
Met^{26}RD1/others	519.71	1	519.71	8.64	Yes
Others	154.33	5	30.87	0.51	No
Error	1203.27	20	60.16		
Total	1877.31	26			

Table 5.5.10: ANOVA of percentage of anti PDE4A immunoreactivity in the S2 fraction of transfected COS-7 cells

Sources of variation	Sums of squares	Degrees of	Mean squares	F	Differen t p=0.05
All treatments:	2914.313	6	485.72	3.80	Yes
Met^{26}RD1/others	2006.55	1	2006.55	15.71	Yes
Others	907.76	5	181.55	1.42	No
Error	2554.50	20	127.73		
Total	5468.82	26			

Table 5.5.11: ANOVA of percentage of PDE enzyme activity in the P1 fraction of transfected COS-7 cells

Sources of variation	Sums of squares	Degrees of	Mean squares	F	Differen t p=0.05
All treatments:	106.00	6	17.67	13.82	Yes
Met^{26}RD1/others	63.77	1	63.77	49.90	Yes
Others	42.22	5	8.44	6.61	Yes
Error	21.73	17	1.28		
Total	127.72	23			

Table 5.5.12: ANOVA of percentage of PDE enzyme activity in the P2 fraction of transfected COS-7 cells

Sources of variation	Sums of squares	Degrees of	Mean squares	F	Differen t p=0.05
All treatments:	1478.76	6	246.46	16.96	Yes
Met^{26}RD1/others	753.12	1	753.12	51.83	Yes
Others	725.64	5	145.13	9.99	Yes
Error	247.04	17	14.53		
Total	1725.8	23			

Table 5.5.13: ANOVA of percentage of PDE4 enzyme activity in the S2 fraction of transfected COS-7 cells

Sources of variation	Sums of squares	Degrees of	Mean squares	F	Differen t p=0.05
All treatments:	2209.19	6	368.20	25.75	Yes
Met^{26}RD1/others	1242.10	1	1242.10	86.88	Yes
Others	967.09	5	193.42	13.53	Yes
Error	243.06	17	14.30		
Total	2452.24	23			

5.2.4 Mapping the regions of sequence within the amino terminal of RNPDE4A5 which affect the PDE enzyme activity

Regions of sequence contained within the amino termini of PDE4 isoforms have been suggested as affecting the kinetic properties of these enzymes (16, 87). This implies that the amino terminal regions of these isoforms, although not necessary for catalysis, nevertheless, may influence the conformation of the active site. Truncation of both PDE4A and PDE4D isoforms at the amino terminal causes an increase in the Vmax of the enzyme which, in the case of rat PDE4A, appears not to be accompanied by any change in the Km for cAMP (84, 93, 95, 140, 200). I therefore decided to use the truncations R6Δ1–Met^{26} RD1 to define more precisely the regions within the amino terminus of RNPDE4A5 that affect the rate of cAMP hydrolysis.

I transfected COS-7 cells to express either wild type (full length) RNPDE4A5 or one of the amino terminal truncations of this protein. I then performed PDE enzyme activity assays on a known amount of the cytosolic fraction from each transfection. and used semi-quantitative immunoblots to correct for differences in the levels of expression of the various preparations (*Table 5.5.14*).

I used paired t-tests to determine whether the corrected specific activity of each of the truncated mutants was significantly different from that of wild type RNPDE4A5. This analysis revealed that, of the truncations that I examined, only Met^{26}RD1 was significantly more active than wild type RNPDE4A5. This finding agrees with previous studies in which the relative Vmax of Met^{26}RD1 was found to be 7 fold higher than that of RNPDE4A5 and with another study in which the relative Vmax of R6Δ3 was found not to be significantly different from that of RNPDE4A5 (16, 140)[Huston and others, manuscript in preparation].

These data suggest that the region of RNPDE4A5 between residues 218–259 is important in regulating both the catalytic activity and the sub-cellular targeting of the enzyme.

Construct	Relative specific activity (arbitrary units)	Different from RNPDE4A5 (5% level)
RNPDE4A5	1	No
R6Δ1	1.5±0.10	No
R6Δ2	1.6±0.09	No
R6Δ3	1.5±0.08	No
R6Δ4	1.4±0.14	No
R6Δ5	1.8±0.26	No
R6Δ6	1.3±0.20	No
R6Δ7	1.7±0.15	No
Met^{26}RD1	2.9±0.57	Yes

Table 5.5.14: Relative specific activities of truncations in RNPDE4A5

The table shows the relative specific activities of a series of truncations in RNPDE4A5. A known amount of the cytosolic fraction of transiently transfected COS-7 cells expressing either full length RNPDE4A5 or one of the truncations in this species was assayed for PDE enzyme activity. Semi quantitative immunoblots were then used to correct for differences in the levels of expression between preparations. The specific activity of each truncation is shown relative to that of full length RNPDE4A5 (arbitrarily set at 1). Paired t-tests were used to test whether the corrected specific activity of each truncation was significantly different from that to full length RNPDE4A5. The reported values of relative specific activity are the means of at least 2 determinations with standard errors shown.

5.3 Conclusions

In this chapter I have mapped regions of sequence within the amino terminal of RNPDE4A5 that are necessary for the interaction of this isoform with the SH3 domain of Lyn kinase, are involved in the targeting of RNPDE4A5 and of RNPDE4A8 to the particulate fractions of COS-7 cells and are involved in regulating the activity of rat PDE4A isoforms.

5.3.1 Interaction of RNPDE4A5 with SH3 domains

The extreme amino terminal region of RNPDE4A5 (residues 1–103) is necessary for its interaction with the SH3 domain of Lyn kinase. Within this region the first 10 residues seem to be especially important for the interaction. Deletion of residues 1–10 caused a large decrease in the degree of binding observed in pull down assays (44±5% binding of RNPDE4A5, 19±3% binding of R6Δ1). Deletion of these 10 residues removes the first of the 3 PxxP motifs that occur in the amino terminal region of RNPDE4A5. Two further truncations in the amino terminal region of RNPDE4A5 that remove the first 42 residues (R6Δ2) and the first 67 residues (R6Δ3), did not seem to produce much further reduction in binding to the SH3 domain of Lyn kinase. The deletion R6Δ2 removes the first 2 of the 3 PxxP motifs and the deletion R6Δ3 removes all 3 of the PxxP motifs that occur in the amino terminal region of RNPDE4A5.

The first 10 residues of RNPDE4A5 contain the motif **PAAPSER**. This conforms to the consensus PxxP that has been suggested as being able to confer binding to SH3 domains. It therefore seems plausible that this motif in RNPDE4A5 may represent the primary site of interaction between RNPDE4A5 and the SH3 domain of Lyn kinase in these assays. This region of sequence is well conserved in HSPDE4A4B, the human homologue of RNPDE4A5 (*Figure 5.55*). The results that I have obtained with R6Δ1 are in good agreement with the finding that a truncated form of HSPDE4A4B, in which residues 1–14 are deleted, called 10A, also shows a marked

reduction in binding to SH3 domains compared to full length HSPDE4A4B (87).

The lower but, nevertheless significant, degree of binding between the truncations R6Δ1 – R6Δ3 and the SH3 domain of Lyn kinase may be due to additional contacts between the PDE and the SH3 domain. Specific interactions between SH3 domains and regions outside of the core PxxP motif have been demonstrated using biased, dodecapeptide, phage display libraries and it is possible that regions of sequence even further removed from the core PxxP motif may also interact with an SH3 domain (61, 176).

The truncated form R6Δ4, in which the entire 102 residue, alternatively spliced region of RNPDE4A5 was deleted, did not interact significantly with the SH3 domain of Lyn kinase. This is consistent with the finding that another long form splice variant of PDE4A, namely RNPDE4A8, did not interact with the SH3 domain of Lyn kinase in pull down assays (162) as the amino acid sequence of R6Δ4 is entirely contained within that of RNPDE4A8. Taken together these findings implicate the region between residues 68–102 of RNPDE4A5, that is to say the region that is present in R6Δ3 but deleted in R6Δ4 (*Figure 5.56*), as being involved in the interaction between RNPDE4A5 and SH3 domains.

Another possibility that can not be excluded is that deletion of the first 10 residues of RNPDE4A5 may alter the structure of some other region within the protein that is the true site of the interaction with the SH3 domain of Lyn kinase. Under this model deletion of residues 1–10 in RNPDE4A5 would alter the structure of the SH3 domain binding region so as to reduce the strength of the interaction and the deletion of residues 1–103 would either further alter the structure of or delete this region so as to completely abolish the interaction.

5.3.2 Targeting of PDE4 isoforms

There has previously been speculation that the targeting of RNPDE4A5 to the particulate fractions of cells may involve its binding to an SH3 domain contained

within an anchoring protein that is itself located to those cell fractions.

In this study I have shown that the region of sequence that is necessary for the interaction of RNPDE4A5 with the SH3 domain of Lyn kinase is not also necessary for the targeting of RNPDE4A5 to particulate cell fractions. This shows that the ability of RNPDE4A5 to become associated with the particulate fractions of cells is not solely mediated by its binding to an SH3 domain. It is important to note, however, that these data do not exclude the possibility that an interaction between RNPDE4A5 and an SH3 domain may nevertheless be involved in the sub-cellular targeting of this enzyme.

Of all the truncations in RNPDE4A5 that I have examined, only Met^{26}RD1 did not become associated with the particulate cell fractions. This implicates residues 218–259 of RNPDE4A5 (*Figure 5.56*) as being involved targeting the protein to the particulate cell fractions. It does not, however, show that residues 218–259 are either necessary or sufficient for this targeting.

To address the question of whether the region between residues 218–259 is necessary to target RNPDE4A5 to the particulate cell fractions it will be necessary to construct a internal deletion mutant of RNPDE4A5 in which just these residues are deleted. To address the question of whether the region between residues 218–259 is sufficient to target RNPDE4A5 to the particulate cell fractions it will be necessary to construct chimeric proteins comprising this region of RNPDE4A5 and some heterologous, normally soluble protein such as GST or chloramphenicol acetyltransferase (CAT). This approach has been used previously to demonstrate that the alternatively spliced, amino terminal region of RNPDE4A1 is sufficient to target proteins to the particulate fractions of cells (194).

On the basis of the currently available evidence it remains entirely possible that more than one region within the amino terminal of RNPDE4A5 may be involved in the sub-cellular targeting of this isoenzyme. Indeed, analysis of the sub-cellular distributions of RNPDE4A5 and of R6Δ3 by immunoflourescent confocal microscopy has shown differences between the sub-cellular distributions of these

enzymes [Huston and others, manuscript in preparation]. This finding suggests that the extreme amino terminal region of RNPDE4A5, although not necessary for targeting to the particulate cell fractions, does have some effect on the sub-cellular targeting of RNPDE4A5.

5.3.2.1 The region implicated in the subcellular targeting of RNPDE4A5 corresponds to the amino terminal portion of UCR2

The amino termini of all long isoforms of PDE4 are characterised by the presence of 2 highly conserved regions of sequence, namely UCR1 and UCR2. Short isoforms of PDE4 do not contain UCR1 but do contain either the entire of or, in the cases of PDE4A1 and PDE4D2, just the carboxyl terminal portion of UCR2 (see sections 1.3.1 and 6.1). The region of sequence between residues 218–259 in RNPDE4A5, that my data has implicated as being involved subcellular targeting, corresponds to the amino terminal portion of UCR2. This region of sequence is therefore well conserved in other members of the PDE4 enzyme family. The only known, active PDE4 splice variants that do not contain this region of sequence are PDE4A1 and PDE4D2.

Examination of the subcellular distributions of other PDE4 splice variants makes it seem unlikely that the sequence between residues 218–259 of RNPDE4A5 can be sufficient for the targeting of a protein to the particulate fractions of cells (*Figure 5.63*). The short form PDE4B splice variant PDE4B2 contains an intact UCR2 and this species is able to associate with the particulate fractions of COS-7 cells (26%P1, 12%P2, 61%S2) (92). The short form PDE4D splice variant PDE4D2 does not contain the amino terminal portion of UCR2 and this species is entirely soluble in transfected COS-7 cells (15). The short form PDE4D splice variant PDE4D1, however, contains an intact UCR2 region and this species is also entirely soluble in COS-7 cells (15). This last example is not consistent with the amino terminal portion of UCR2 being sufficient for the association of PDE4 with the particulate fractions of cells.

A further complication arises because there appear to be species differences between

the sub-cellular targeting of rat and human PDE4A isoenzymes. The cDNA clone HSPDE4A4C (h6.1) encodes for an amino terminal truncation in human PDE4A that includes an intact UCR2, catalytic region and carboxyl terminal region of the enzyme (residues 210–886 in HSPDE4A4B). As such this species can be considered to be a human homologue approximating to the rat PDE4A species R6Δ7. The sub-cellular distribution of HSPDE4A4C is, however, markedly different from that of R6Δ7. HSPDE4A4C is present in the P1 and the S2 fractions (approximately 23% and 76% respectively) but only trace amounts are present in the P2 fraction (approximately 1%) of transfected COS-7 cells (141).

Although HSPDE4A4C is targeted to the P1 fraction of transfected COS-7 cells this targeting is not mediated by the amino terminal portion of UCR2. Rather, the association of HSPDE4A4C with the P1 fraction is dependent on a proline and arginine rich motif, that is located within LR2 (residues 305–331 in HSPDE4A4B) (141) but that is not conserved in rat PDE4A isoforms (see sections 1.3.1 and 1.3.2.2). In addition to its role in sub-cellular targeting, the proline and arginine rich motif in the LR2 region of human PDE4A is both necessary and sufficient for the interaction of HSPDE4A4C with SH3 domains such as those of Src and Lyn kinase. Internal deletions that delete this motif abolish the association of the HSPDE4A4C with both the P1 cell fraction and with SH3 domains (141). It therefore appears that, although the amino terminal portion of UCR2 in rat PDE4A has a role in targeting the enzyme to the particulate fractions of cells, the presence of this region in human PDE4A is not sufficient to target these enzymes to either the P1 or to the P2 cell fractions.

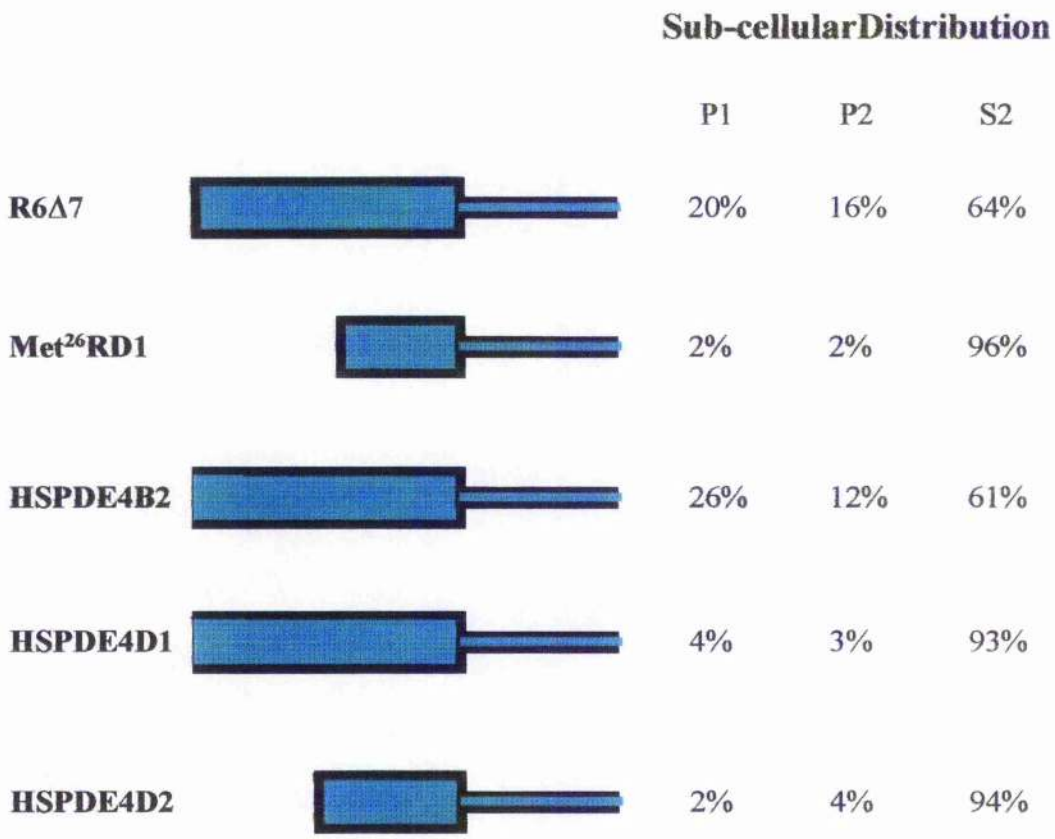

Figure 5.63: Comparison of the sub-cellular distributions of various PDE4 species

The figure shows a comparison of the sub-cellular distributions of various short form splice variants and amino terminally truncated forms of PDE4. The legends along the left hand side of the figure identify each protein. The green hieroglyphics represent the portion of UCR2 that is present in each of the proteins. In the cases of R6Δ7, HSPDE4B2 and HSPDE4D1 a large green box is drawn to indicate that these species each contain and intact UCR2. In the cases of Met[26]RD1 and HSPDE4D2 a smaller green box is drawn to indicate that these species each contain only the carboxyl terminal region of UCR2. None of the boxes representing these species are closed at the right hand sides; this is to indicate that these proteins all contain sequence that lies carboxyl terminal to UCR2. The boxes representing HSPDE4B2 and HSPDE4D1 are not closed at the left hand side; this is to indicate that these proteins contain sequence that lies amino terminal to UCR2. The numbers along the right hand side of the figure refer to the proportion of each species that fractionates with the P1, P2 and S2 cell fractions (as assessed by quantitative immunobloting).

5.3.3 Regulation of the catalytic activity of PDE4 isoforms

The observation that certain truncations and deletions within the amino termini of PDE4 isoforms led to an increase in the activity of certain of these enzymes has prompted the suggestion, by Conti and co workers, that UCR2 of PDE4 isoforms is an autoinhibitory region (41, 99, 122). This hypothesis is based largely on the results of work on the human PDE4D isoforms HSPDE4D1, HSPDE4D2 and HSPDE4D3. These studies located the region of sequence necessary for the inhibitory effect as that lying between amino acids 167–212 in HSPDE4D3 (99, 108, 122). This corresponds to the carboxyl terminal portion of UCR2 (amino acids 134–212 in HSPDE4D3).

The published data concerning the HSPDE4D isoforms support a relatively simple model in which a sub-domain within UCR2 is responsible for constraining the activity of the catalytic region. It is more difficult, however, to extend this model to accommodate the published data concerning the other PDE4 enzyme families (discussed below).

A study conducted on full length and truncated forms of HSPDE4A4A, expressed in yeast, supported (as do all relevant studies of which I am aware) the involvement of sequence, lying amino terminal to the catalytic region of PDE4 enzymes, in an inhibition of the catalytic activity (95). The location of the sequence necessary for the inhibition, in this case however, was not within UCR2 but it within the poorly conserved LR2, between UCR2 and the catalytic region. Indeed, truncation of HSPDE4A4A up to the end of UCR2 (amino acid 305) resulted in a marked inhibition of this truncation compared to full length protein.

It should be noted, however, that the clone HSPDE4A4A encodes a protein that differs at 9 amino acids from the clone, HSPDE4A4B. The clone HSPDE4A4B is widely accepted as representing the true, wild type sequence of this human PDE4A isoform. In contrast, HSPDE4A4A is thought to represent either a cloning artefact or a mutated enzyme (224). It should also be noted that the Km for cAMP of full length HAPDE4A4A, in this study, was determined to be 10μM (95). This value is rather

higher than the values of Km determined for the truncations of HSPDE4A4A examined in the same study (3μM). The value of 10μM for the Km of full length HSPDE4A4A is also higher than that reported by Livi and others (3μM) in the original report of this clone, where HSPDE4A4A was expressed in COS-1 cells (125).

The situation regarding human PDE4A is further complicated by the observation that the human PDE4A clone, HSPDE4A4C, has a relative Vmax that is 11 fold higher than that of HSPDE4A4B when each is expressed in COS-7 cells (224) (93). As HSPDE4A4C retains the entire of UCR2 this observation does not support a simple model in which part of UCR2 acts as the sole inhibitory domain contained in the amino terminal region of PDE4 (122).

Truncations within UCR2 of rat PDE4A do not appear to have the same effect on activity as do equivalent truncations in the human enzyme. In this regard the truncation in rat PDE4A, R6Δ7, that corresponds to the human species HSPDE4A4C, was not activated relative to full length RNPDE4A5 (*Table 5.5.14*).

The published data concerning isoforms of HSPDE4B (92) are also at variance with a simple model in which a subdomain within UCR2 is solely responsible for the inhibitory action of the amino termini of PDE4 isoforms (122). This is because the short form PDE4B splice variant HSPDE4B2 contains an intact UCR2 but nevertheless exhibits a Vmax that is approximately 4 fold higher than that of the long form splice variant HSPDE4B1 (92). This suggests that some region within the amino terminal of HSPDE4B1 other than UCR2 is involved in constraining the catalytic activity of this isoenzyme.

Therefore, although sequence lying amino terminal to the catalytic region of PDE4 isoforms seems to be able to influence the conformation of the active site and can cause a reduction in enzyme activity it is difficult, on the basis of the evidence currently available, to formulate a simple model to explain this effect.

In interpreting the available data it should be noted that comparing data from these

different studies is complicated by a number of potential problems. These include (a) the folding of the catalytic region of truncated enzymes may be altered compared to the full length species (b) differences in the expression backgrounds used between the various studies may have resulted in differences the post-translational modifications of the enzymes (c) differences in the expression backgrounds may have resulted in differences in the interaction of these enzymes with regulatory molecules.

If there is some common mechanism for constraining the activity of PDE4 isoforms that is associated with the amino termini of these proteins, then the sequence responsible for this must be located within the carboxyl terminal region of UCR2 as this is the only conserved region outside of the catalytic domain that is present in all known, active, PDE4 splice variants.

One possibility is that regions within the amino termini of individual PDE4 isoforms may regulate the interaction between an autoinhibitory region, located in the carboxyl terminal of UCR2, and the catalytic site of the enzyme. If this were the case then differences in the phosphorylation state, for instance, of a PDE4 that was examined in one of 2 different expression backgrounds might result in there being differences in the effects of truncating this species depending upon which expression background was used.

Another possibility is that more that one region within the amino termini of individual PDE4 isoforms may be able to interact directly with the catalytic unit to regulate its activity. If this were the case then a truncation in the enzyme that removed one of the regulatory regions might or might not result in a change in the enzyme activity, depending upon the interactions between the catalytic region and other regions of the protein. These, in turn, may vary depending upon the phosphorylation state and other regulatory influences on the PDE in the particular expression background used.

It is also possible that deletions and truncations may affect the quaternary structures of PDE4 isoforms that exist as dimers or as higher order oligomers. Such changes

could be, at least partially, responsible for the observed changes in activity. In this regard splice variants of PDE4D and of PDE4B have been found to form dimers or higher order oligomers in cells (40, 108, 178, 179). In contrast to this the human PDE4A clone HSPDE4A4C has been found to exist as a monomeric species (245).

It has been argued that effects on quaternary structure are unlikely to account for the effects of amino terminal truncations in PDEs on their catalytic activity because the regions important for dimerization of PDE4s have been putatively mapped to the carboxyl termini of the proteins (122). It seems to me, however, entirely plausible that a region within a multi subunit protein may affect its quaternary structure regardless of whether or not it is necessary for the oligmerization of that protein. Furthermore, although the carboxyl terminal regions of PDE4s are implicated in the formation of dimers and tetramers (108), regions in the amino terminal of both PDE4B and PDE4D have been implicated in the formation of higher order oligimers (108, 178, 179). This suggests that the amino termini of PDE4 isoforms can have an effect on the quaternary structures of these proteins.

6. Electrostatic interactions between UCR1 and UCR2

6.1 Introduction

The sequences of all known mammalian 3'5' cyclic nucleotide phosphodiesterases (PDEs) share homology with one another over a region of approximately 300 residues that are located towards the carboxyl terminal end of the proteins. This represents the only region of sequence that is conserved between all mammalian PDEs and there is good evidence that this is the location of the catalytic site of these enzymes (31, 95, 99). In addition to the catalytic region, the members of individual PDE enzyme families often share other conserved regions of sequence. In the case of the PDE4 enzyme family, that is encoded by 4 genes, there are 2 regions of sequence that are highly conserved. These are called Upstream Conserved Regions 1 and 2 (UCR1 and UCR2) and are present in the amino termini of these proteins (*Figure 6.64*) (13, 14).

These UCR1 and UCR2 of PDE4s appear to form distinct, modular entities as they are separated from each other by a region of poorly conserved sequence and they do not show homology to one another. Indeed, neither UCR1 nor UCR2 shares homology with any other sequence in the Swissprot database (last searched 28/9/99). The sequences of UCR1 and UCR2 show strong evolutionary conservation throughout the mammalian PDE4s and even between species as distantly related as *Drosophila* and humans. This suggests that UCR1 and UCR2 are important as sequences that are strongly conserved in evolution are often of functional significance.

Further evidence to suggest that UCR1 and UCR2 may have functional significance is that a major point of splicing in mammalian PDE4 genes, and in the *dunce* gene of *Drosophila,* lies between the exons that encode UCR1 and UCR2. Alternative splicing in this region leads to the production of either long PDE4 isoforms, that include UCR1, or short PDE4, isoforms that do not include UCR1, but that contain

all or a part of UCR2 (see section 1.3.1).

A

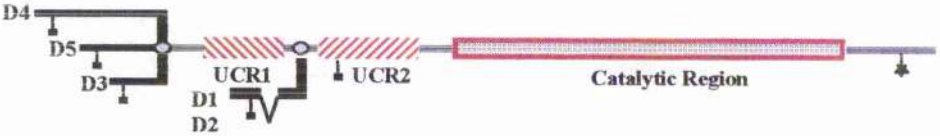

B

```
                                                                52
                                                              51|53 54
          17                                                  ↓↓↓  ↓              63
HSPDE4D   FDVDNG..TS AGRSPLDPMT SPGSGLILQA NF.VHSQRRE SFLYRSDSDY
HSPDE4C   FLDENGLSCG ..RRALDPQS SP.GLGRIMQ APVPHSQRRE SFLYRSDSDY
HSPDE4B   FDVENGP..S PGRSPLDPQA SSSAGLVLHA TFPGHSQRRE SFLYRSDSDY
HSPDE4A   FEAENGPTPS PGRSPLDSQA SP..GLVLHA GA.ATSQRRE SFLYRSDSDY
dunce     FDVENGQGA. ..RSPLEGG. SPSAGLVLQN LP....QRRE SFLYRSDSDY
                                                  UCR1 begins

                                83 84                 98  101
          64                     ↓ ↓                   ↓   ↓                     113
HSPDE4D   DLSPKSMSRN SSIASDIHGD DLIVTPFAQV LASLRTVRNN FAALTNLQDR
HSPDE4C   ELSPKAMSRN SSVASDLHGE DMIVTPFAQV LASLRTVRSN VAALARQQCL
HSPDE4B   DLSPKAMSRN SSLPSEQHGD DLIVTPFAQV LASLRSVRNN FTILTNLHGT
HSPDE4A   DMSPKTMSRN SSVTSEAHAE DLIVTPFAQV LASLRSVRSN FSLLTNVPVP
dunce     EMSPKSMSRN SSIASESHGE DLIVTPFAQI LASLRSVRNN LLSLTNVP..
                                                   UCR1 ends

                                                    143 146 147 149  153 156
          114                                         ↓   ↓  ↓  ↓    ↓   ↓
HSPDE4D   APSKRSPMCN QPSINKATIT .......EEA YQKLASETLE ELDWCLDQLE
HSPDE4C   GAAKQGPVGN PSSSNQLPPA .......EDT GQKLALETLD ELDWCLDQLE
HSPDE4B   .SNKRSPAAS QPPVSRVNPQ .......EES YQKLAMETLE ELDWCLDQLE
HSPDE4A   .SNKRSPLGG PTPVCKATLS .......EET CQQLARETLE ELDWCLEQLE
dunce     ASNKRRPNQS SSASRSGNPP GAPLSQGEEA YTRLATDTIE ELDWCLDQLE
                                UCR2 begins

          157                                                                    206
HSPDE4D   TIQTYRSVSE MASNKFKRML NRELTHLSEM SRSGNQVSEY ISNTFLDKQN
HSPDE4C   TLQTRHSVGE MASNKFKRIL NRELTHLSET SRSGNQVSEY ISRTFLDQQT
HSPDE4B   TIQTYRSVSE MASNKFKRML NRELTHLSEM SRSGNQVSEY ISNTFLDKQN
HSPDE4A   TMQTYRSVSE MASHKFKRML NRELTHLSEM SRSGNQVSEY ISTTFLDKQN
dunce     TIQTHRSVSD MASLKFKRML NKELSHFSES SRSGNQISEY ICSTFLDKQQ

          207                                                                    232
HSPDE4D   EVEIPSPTQK EKEKKKRP.. .......... .......... MSQISGVK..
HSPDE4C   EVELPKVTAE EAPQP..... .......... .......... MSRISGLH..
HSPDE4B   DVEIPSPTQK DREKKKKQQL .......... .......... MTQISGVK..
HSPDE4A   EVEIPSPTMK EREKQQAPRP RPSQPPPPPV PHLQP..... MSQITGLK..
dunce     EFDLPSLRVE DNPELVAANA AAGQQSAGQY ARSRSPRGPP MSQISGVK..
          UCR2 ends                                    Catalytic begins
```

Figure 6.64: Structures of UCR1 and UCR2

The figure shows the positions of conserved regions of sequence within PDE4 isoforms. Panel A shows a schematic diagram of the 5 mRNA transcripts from the human PDE4D gene. The grey bar indicates sequences homologous to those in other PDE4 families. The regions of strongest conservation, the catalytic region, UCR1 and UCR2 are indicated by the red box each of the 2 cross hatched areas respectively. The black bars represent the regions of sequence that are unique to each isoform. The black boxes represent the positions of the initiating ATG of each splice variant and the black star represents the termination codon of the open reading frames. Panel B shows an alignment of the amino acid sequences of the common amino terminal regions of the human PDE4 isoforms and of the dunce PDE of Drosophila melanogaster. The alignment begins at the point at which the sequences of HSPDE4D3, HSPDE4D4 and HSPDE4D5, in the human PDE4D family, converge and it extends to the beginning of catalytic region. The numbering of the alignment corresponds to the amino acid sequence of HSPDE4D3. Regions of sequence that are conserved between PDE4 isoforms and the dunce PDE are coloured green. Residues that have been mutated in various of the constructs used in this study are indicated by bold type and also by arrows. The regions of sequence that were included in the MBP–UCR1, the MBP–UCR1-C and the GST–UCR2 fusion proteins are underlined in red, blue and yellow respectively.

6.1.1 Sequence analysis of UCR1 and UCR2

Sequence analysis of the primary structures of UCR1 and of UCR2 reveals that these regions have very different predicted characteristics. UCR1 (residues 50–109 in HSPDE4D3) comprises a polar amino terminal region (residues 50–84 in HSPDE4D3) and an apolar carboxyl terminal region (residues 85–109 in HSPDE4D3). In contrast to this the entire of UCR2 (residues 134–212 in HSPDE4D3), is composed predominantly of residues with polar side chains. This region is predicted to be hydrophilic in nature.

Within the polar, amino terminal portion of UCR1, 37% of the residues have charged side chains. The occurrence of positive and negatively charged side chains in this region, however, is evenly balanced and the net charge is 1 positive. Secondary structure predictions indicate that this portion of UCR1 is likely to be highly flexible. In contrast, 63% of the residues within the carboxyl terminal portion of UCR1 have apolar side chains. Helical wheel analysis of this region suggests that it may be able to form an amphipathic helix with the few charged groups that do occur here focused on a discrete side of the molecule (87).

Secondary structure predictions of UCR2 indicate that it may form a series of 3 helical regions. The first and the third of these putative helical regions are predicted to be negatively charged (anionic) whilst the second of the putative helical regions is predicted to have a slightly positive net charge (cationic) (87).

6.1.2 Putative functions of UCR1 and UCR2

Although the functional significance of UCR1 and UCR2 has not yet been resolved putative functions for each of these regions have been proposed. These include possible roles for regions within UCR2 in the targeting of PDE4 isoforms and in constraining the catalytic activity of these enzymes, also a role for UCR1 as a site of regulation by protein kinase A (PKA) has been shown for PDE4D3. UCR1 is possibly a site for regulation by PKA in other long PDE4 isoforms as well (see sections 5.3.2–5.3.3) (122).

6.1.2.1 Regulation of HSPDE4D3 activity by phosphorylation within UCR1

A consensus motif, of the form RRxS, for phosphorylation by PKA is present at the amino terminal end of UCR1 (residues 51–54 in HSPDE4D3). There is strong evidence that PDE4D3 can be phosphorylated, in *vivo*, by PKA at this site and that this results in an activation of the enzyme (see section 1.3.5.3) (2, 82, 197, 198).

As the PKA recognition motif within UCR1 is conserved in all long isoforms of PDE4 one might expect that these enzymes would also be substrates for PKA. There are, however, no published reports to date that PKA can phosphorylate other PDE4 isoforms at this site. In the initial reports of the phosphorylation, by PKA, of PDE4D3 it was reported that splice variants of PDE4A and PDE4B that contain UCR1 were not significantly activated following treatment with PKA and Mg^{2+}ATP (2, 197). It has recently been shown, however, that long PDE4B, PDE4C and PDE4D isoforms can be phosphorylated on a serine residue (Ser^{579} in HSPDE4D3) by ERK2 and that this causes an inhibition of the enzyme activity of these isoforms. The subsequent phosphorylation of these proteins by PKA causes a recovery of their activities to basal levels [Baillie and MacKenzie personal communication]. As this effect of PKA on HSPDE4D3 is due to its phosphorylation of Ser^{54} (the PKA site in UCR1) this suggests that this site in other long PDE4 isoforms may also be a substrate for PKA (see section 1.3.5.4). To my knowledge, however, no study has directly examined the phosphorylation of this motif by PKA in any isoform other than PDE4D3.

6.2 Results and Discussion[1]

There is precedent for interactions between regions within the amino termini of PDE4 isoforms and other proteins. Examples of this include: the interaction of PDE1 isoforms with calmodulin; the interaction of the α and β subunits of PDE6 isoforms with their γ subunits; the interactions of the PDE4 isoforms HSPDE4A4B and HSPDE4D4 with SH3 domains and the interaction of HSPDE4D5 with RACK1 (7, 70, 141, 252). UCR1 and UCR2 seemed to be good candidates for forming regulatory regions of PDE4 enzymes as PKA regulates at least 1 PDE4 isoenzyme by phosphorylating a serine residue located within UCR1. It therefore seemed plausible that either one or both of UCR1 and UCR2 might interact with the catalytic region of the enzyme. It was speculated that UCR1 and UCR2 might even interact to create a regulatory module within the enzyme.

6.2.1 Isolation of UCR2 as and interaction partner for UCR1 in a two-hybrid screen

The two-hybrid screen is a powerful genetic approach for the isolation of cDNAs encoding proteins that can interact with a protein of interest. It was by this method that the interaction between PDE4D5 and RACK1 was first identified (252). In collaboration with our laboratory Prof. G. Bolger decided to use a two-hybrid method to screen for cDNAs encoding potential interacting partners for UCR1 or UCR2. Subsequently, mutated forms of UCR1 and UCR2 were also tested after discussions between myself, my supervisor and Prof. Bolger.

6.2.1.1 The carboxyl terminal half of UCR1 interacts with another region within PDE4D

Various portions of the HSPDE4D3 cDNA were cloned into the two-hybrid vector pLEXAN and such constructs were then used as baits in two-hybrid screens. All of the constructs that included the amino terminal half of UCR1 produced very high

[1] This project was conducted in collaboration with Prof. G. Bolger, University of Utah who constructed all of the plasmids used in this project and who also performed all of the yeast two-hybrid screens described in this chapter, subsequent to discussions with myself and my supervisor.

background "noise" (false positives) in these two-hybrid assays and therefore could not be used as baits in a screen. The reasons for the high background noise associated with these constructs were not established but it was speculated that the concentration of charged, acidic residues in the amino terminal region of UCR1 may have been sufficient to produce transcriptional transactivation activity when coupled to the LexA DNA binding domain, even in the absence of the normal activation domain.

To circumvent the problem of high background noise associated with baits containing the amino terminal portion of UCR1, the plasmid pLEXAU1D was constructed. This plasmid encoded just the carboxyl terminal portion of UCR1 (residues 80–116 in HSPDE4D3) as a fusion protein with the LexA DNA binding domain. This construct produced a sufficiently low background in control assays to be used as the bait in a two-hybrid screen.

A HeLa cell cDNA library was selected for the screen because several PDE4D species are present in HeLa cells. It was, therefore, considered likely that proteins which interact with UCR1 of PDE4D might also be present in this library (15). Of a total of $6x10^6$ recombinants that were screened, approximately 220 were HIS+, and of these, 82 were also LacZ+. Only 9 of the 82 LacZ+ recombinants were still positive after retrieval of the library from the yeast cells and the subsequent re-testing for interaction with pLEXAU1D. Five of these 9 remaining positives encoded non physiological fusion proteins, in which the open reading frame incorporated in the GAL4 fusion was different from that of the protein encoded naturally by the cDNA. All of these were discarded. All 4 of the remaining plasmids encoded an identical insert, consisting of a truncated PDE4D cDNA that encoded all of UCR2 and the catalytic region of the protein, but none of UCR1. This suggested that the carboxyl terminal region of UCR1 potentially interacted with other regions of the PDE4D protein located in UCR2, the catalytic region or the extreme carboxyl terminal of the protein.

To obtain supporting data that the interaction detected in this two-hybrid screen was specific, yeast two-hybrid β-galactosidase assays were used to test the two-hybrid

positive clone with a variety of baits expressed as LexA fusions. These included lamin, casein kinase II, Ras, Raf, several transcription factors and the DNA binding region of LexA itself (not fused to another protein). The plasmid pLEXAU1D was also tested with these proteins expressed as GAL4 fusions and with the GAL4 activation domain itself (not fused to another protein). No interactions were detected under conditions that demonstrated an interaction between pLEXAU1D and the positive from the screen. This suggested that the interaction detected in the screen was unlikely to be explained by non specific interactions between UCR1 and other proteins.

6.2.1.2 The carboxyl terminal half of UCR1 interacts with the amino terminal third of UCR2

To provide further evidence in support of the results from the two-hybrid screen and also to determine more precisely which regions of PDE4D3 interacted with the carboxyl terminal half of UCR1, various portions of the HSPDE4D3 cDNA were cloned into pGADN, to encode fusion proteins with the GAL4 activation domain. Yeast two-hybrid β-galactosidase assays were then used to test these constructs for interaction with the carboxyl terminal half of UCR1, called UCR1-C.

These assays were performed both with the pLEXAU1D construct encoding the carboxyl terminal portion of UCR1 (residues 80–116 in HSPDE4D3) and with another construct, pLEXAU1E that corresponded more closely to the carboxyl terminal portion of UCR1 (residues 80–109 in HSPDE4D3). The results of the assays using either one of these baits demonstrated that the carboxyl terminal portion of UCR1 interacted with a small portion of the PDE4D protein, located within the amino terminal half of UCR2 (residues 134–170 in HSPDE4D3).

It was also noticed that the carboxyl terminal half of UCR1 was unable to interact with any of the portions of HSPDE4D3 that contained UCR1, even if that portion also included UCR2. These results were interpreted as competition for the LexA-UCR1 binding site on the PDE4D-GAL4 fusion protein by the UCR1 already present in those constructs.

6.2.2 Biochemical analysis of the interaction between UCR1 and UCR2

Although positives from two-hybrid screens can be taken as indicative of a protein–protein interaction, it is crucial to be able to demonstrate such an interaction biochemically in order to provide strong evidence for the interaction. Furthermore biochemical analysis was requires to test full length UCR1 as a potential interacting partner for UCR2. To provide such biochemical evidence in support of the interaction between UCR1 and UCR2 that had been discovered by the two-hybrid method I decided to use fusion proteins of both full length and the carboxyl terminal portion of UCR1 with maltose binding protein (MBP). I decided to perform pull down assays with truncated forms of HSPDE4D3, expressed in the cytosolic fraction of transiently transfected COS-7 cells.

6.2.2.1 UCR1 and UCR2 interact in pull down assays

The fusion proteins that I used for these studies were MBP–UCR1, a fusion protein between MBP and residues 17–136 of HSPDE4D3, and MBP–UCR1-C, a fusion protein between MBP and residues 80–116 of HSPDE4D3. I expressed each of these fusion proteins, and also MBP alone, in JM109 *E.coli* then purified each one by affinity chromatography on amylose resin. I monitored the purification of these fusion proteins by sodium dodecyl sulphate polyacrylamide electrophoresis (SDS-PAGE). In neither the purified MBP–UCR1 nor the MBP–UCR1-C was a single band observed. This indicated that these preparations were not homogeneous. There was, however, a major band in each case that migrated more slowly than did MBP alone and this was presumed to be the chimeric MBP–UCR1 species. The uppermost band in each preparation migrated with an apparent Mw of 75kDa and of 70kDa for MBP–UCR1 and for MBP–UCR1-C respectively. These values compared to an apparent Mw of 60kDa for MBP itself. The faster migrating bands in these preparations probably represent carboxyl terminally truncated forms of these fusion proteins. These may have resulted either from premature termination or from proteolysis of the full length fusion protein during the purification (*Figure 6.65*).

I used these fusion proteins as the baits in pull down assays with either full length HSPDE4D3 or amino terminal truncations in this protein that were expressed in

the cytosolic fraction of transiently transfected COS-7 cells. I present here 2 typical immunoblots showing the bound and the unbound fractions from such pull down assays (*Figure 6.66*). These immunoblots show that the full length and the truncations in HSPDE4D3 were detected as single immunoreactive bands in both the bound and the unbound fractions of these pull down assays. I used both semi-quantitative immunoblots and PDE enzyme activity assays to assess the binding of these species (*Figure 6.67, Figure 6.68*). In all cases where I performed a semi-quantitative analysis of immunoblot data I also ran control lanes, on the same blot, that contained a known amount of HSPDE4D3. This was to show that, over the range of band intensities analysed, there was a linear relationship between band intensity and the amount of immunoreactive protein loaded. I analysed this data by performing t-tests to see if the mean difference between the binding of each of the truncations in HSPDE4D3 to each of the MBP–UCR1 fusion proteins was significantly different from the binding of that truncation to MBP alone. This analysis revealed that both MBP–UCR1 and MBP–UCR1-C were able to bind to UCR2+Cat, a truncation in HSPDE4D3 that lacked UCR1 but still contained UCR2. In contrast to this neither of the MBP–UCR1 fusion proteins were able to bind to full length HSPDE4D3 (NT+U1+U2+Cat+C) nor to a truncation in HSPDE4D3 that contained only the catalytic and the extreme carboxyl terminal regions of the protein (Cat+C).

In separate experiments I also examined the binding of a fusion protein between GST and UCR2 (residues 134–212 in HSPDE4D3), expressed in COS-7 cells, to the MBP–UCR1 fusion proteins. These experiments showed that the GST–UCR2 fusion protein, but not GST alone, was able to bind to both MBP–UCR1 and to MBP–UCR1-C but not to MBP alone in pull down assays (*Figure 6.69*)

Together theses data confirm the two-hybrid data that the carboxyl terminal portion of UCR1 can interact with UCR2. In particular they confirm that exogenous UCR1 can only interact with UCR2 when UCR1 is not present in the construct. In addition to this they demonstrate that full length, as well as just the carboxyl terminal portion of UCR1 can interact with UCR2.

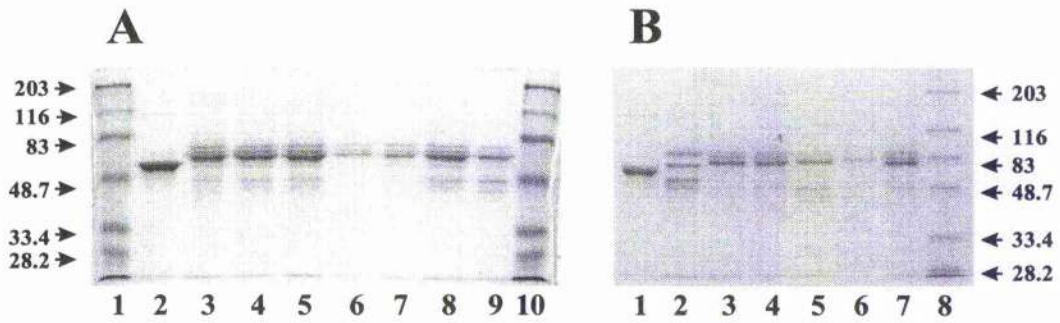

Figure 6.65: Fusion proteins on UCR1, UCR1-C and point mutations in UCR1 with MBP

The figure shows Coomassie stained gels of purified MBP fusion proteins. In panel A lanes 2–9 are 3μg purified MBP, MBP–UCR1, MBP–UCR1S54T, MBP–UCR1R51R52A, MBP–UCR1R98A, MBP–UCR1R101A, MBP–UCR1E53A, MBP–UCR1S54D respectively; lanes 1 and 10 are molecular weight markers (Bio-Rad broad range prestained SDS-PAGE standards). The arrows indicate the Mw (kDa) of each marker. In panel B lanes 1–7 are 3μg purified MBP, MBP–UCR1-C, MBP–UCR1R98A, MBP–UCR1R101A, MBP–UCR1S5A, MBP–UCR1R98R101A; lane 8 is molecular weight markers (New England Biolabs broad range prestained SDS-PAGE standards). The arrows indicate the Mw (kDa) of each marker. The apparent Mw of the slowest migrating band in each preparation was calculated by plotting Rf values; this was 60kDa, 70kDa, 75kDa and 75kDa for MBP, for MBP–UCR1-C, for MBP–UCR1 and for the point mutations in MBP–UCR1 respectively.

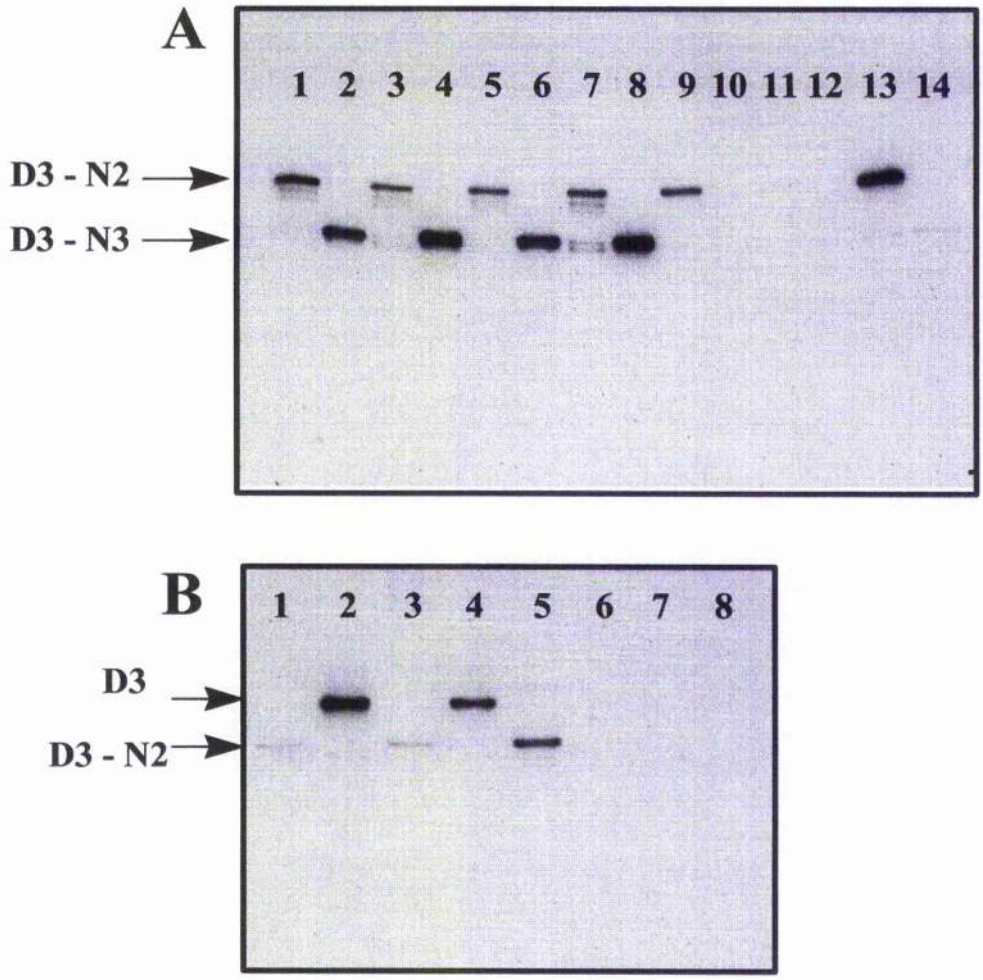

Figure 6.66: MBP–UCR1 interacts with the UCR2 of truncations in HSPDE4D3, in pull down assays

The figure shows immunoblots for PDE4D, of aliquots (8% and 16% respectively) from the bound and the unbound fractions from pull down assays of MBP–UCR1 and MBP–UCR1-C fusion proteins with truncations in HSPDE4D3 expressed in the cytosolic fraction of transiently transfected COS-7 cells. Panel A shows analysis of the truncation UCR2+Cat and of the Catalytic and carboxyl terminal region of HSPDE4D (Cat). Lanes 1 and 2 are standards for UCR2+Cat (D3-N2) and for Cat (D3-N3). Lanes 3–8 are unbound fractions and lanes 9–14 are bound fractions from pull down assays. The bait and prey pairs were: lanes 3 and 9, UCR2+Cat and MBP–UCR1; lanes 4 and 10, Cat and MBP–UCR1; lanes 5 and 11 UCR2+Cat and MBP; lanes 6 and 12 Cat and MBP; lanes 7 and 13 UCR2+Cat and MBP–UCR1-C; lanes 8 and 14 Cat and MBP–UCR1-C. Panel B shows analysis of full length HSPDE4D3 (D3) and of UCR2+Cat (D3-N2). Lanes 1–4 are unbound fractions and lanes 5–8 are bound fractions. The bait and prey pairs were: lanes 1 and 5 UCR2+Cat and MBP–UCR1; lanes 2 and 6, full length HSPDE4D3 and MBP–UCR1; lanes 3 and 7, UCR2+Cat and MBP; lanes 4 and 8, UCR2+Cat and MBP. Full length HSPDE4D3 migrated as a 98kDa species, UCR2+Cat as an 84kDa species and Cat as a 70kDa species in these experiments. These data are typical of those from experiments performed on 3 separate occasions.

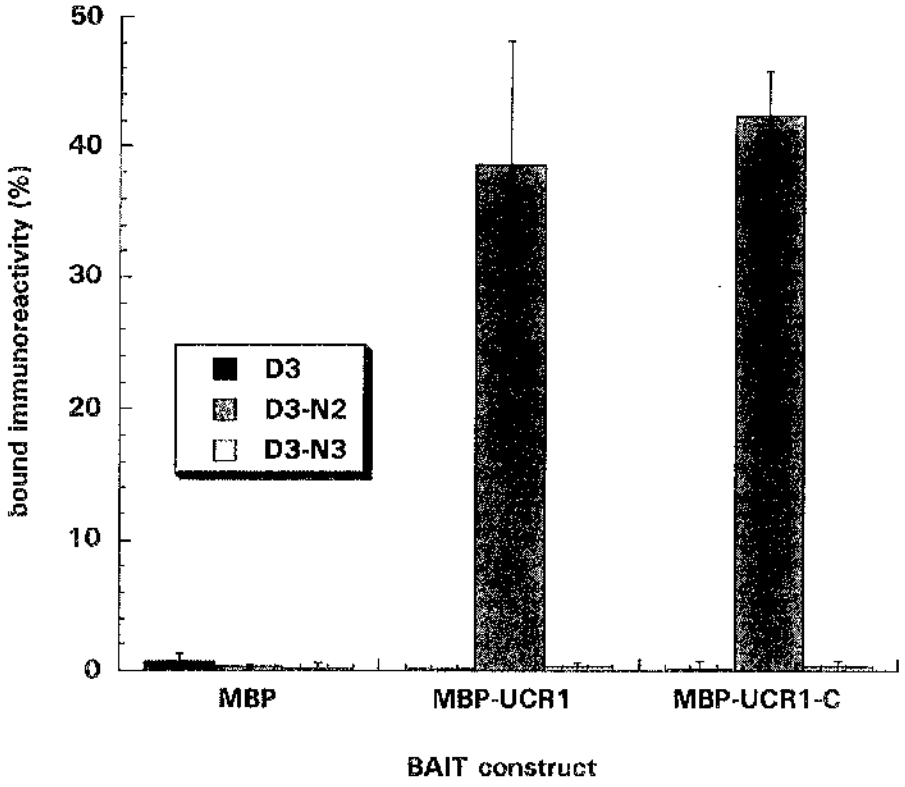

Figure 6.67: Semi quantitative analysis of bound immunoreactivity in pull down assays

The figure shows a histogram of the percentage binding in pull down assays between MBP, MBP–UCR1 and MBP–UCR1-C as the baits and full length HSPDE4D3, the truncations UCR2+Cat and Cat. The data show the proportion of the prey captured in the bound fraction as a percentage of total amount recovered. This was assessed by semi quantitative immunoblots for PDE4D. The figures represent the means of 3 separate experiments with standard errors shown.

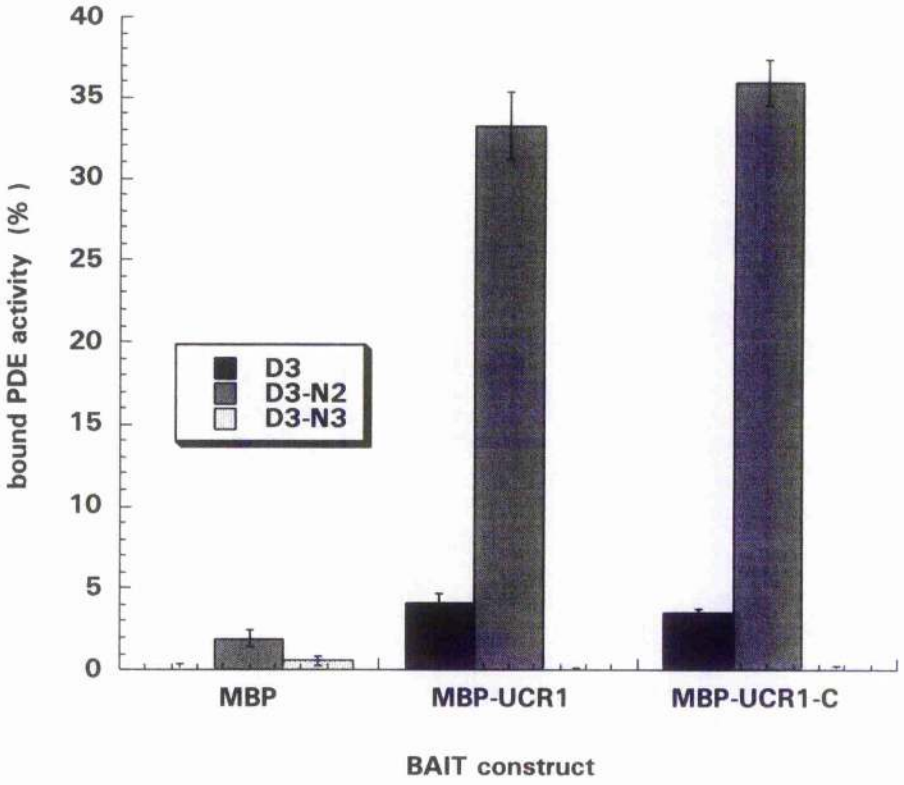

Figure 6.68: Analysis of bound PDE enzyme activity in pull down assays

The figure shows a histogram of the percentage binding in pull down assays between MBP, MBP–UCR1 and MBP–UCR1-C as the baits and full length HSPDE4D3, the truncations UCR2+Cat and Cat. The data show the proportion of the prey captured in the bound fraction as a percentage of total amount recovered. This was assessed by PDE enzyme activity assays. The figures represent the means of 3 separate experiments with standard errors shown.

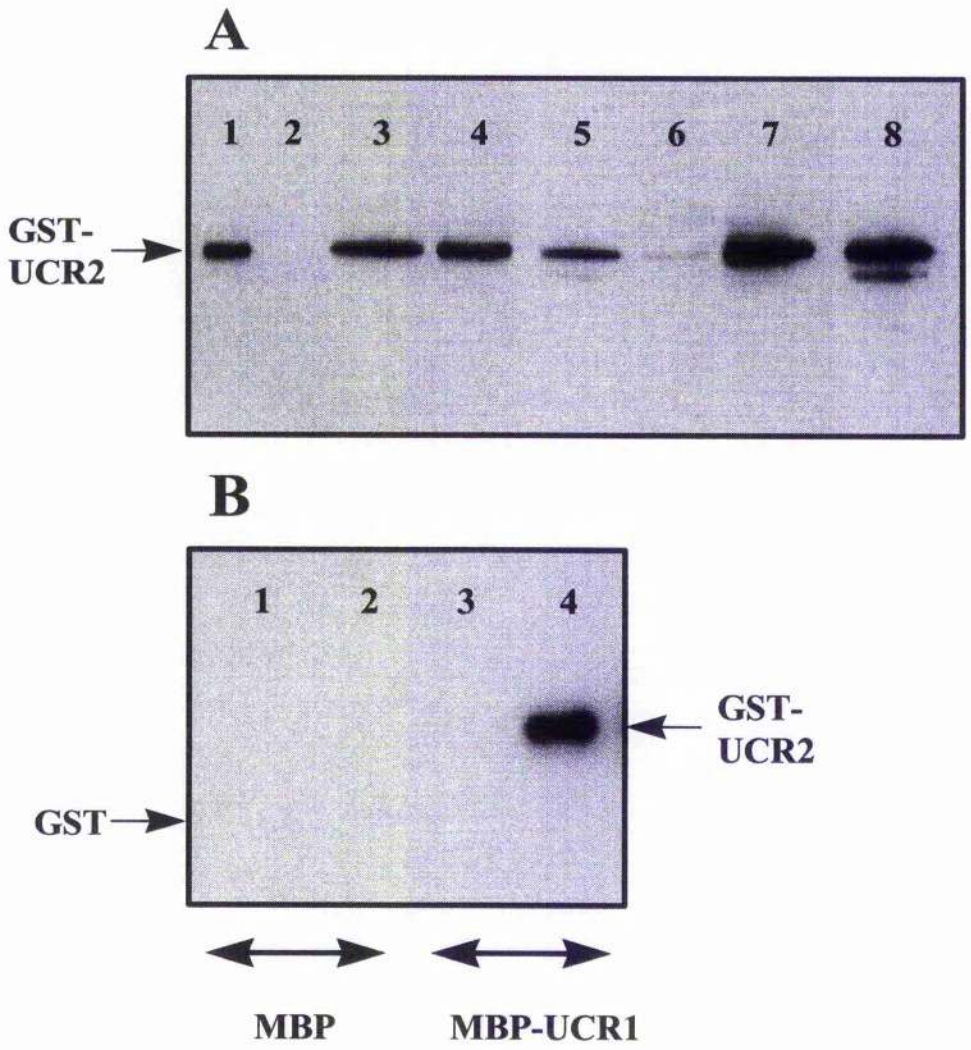

Figure 6.69: MBP–UCR1 interacts with GST–UCR2, in pull down assays

The figure shows immunoblots, with an antibody against GST, of aliquots (8% and 16% respectively) from the bound and the unbound fractions from pull down assays of MBP–UCR with GST–UCR2 expressed in the cytosolic fraction of transiently transfected COS-7 cells. In panel A is a standard for GST–UCR2, lane 2 is empty, lanes 3–5 are the unbound fractions and lanes 6–8 are the bound fractions. The bait and prey pairs were: lanes 3 and 6, MBP and GST–UCR2; lanes 4 and 7 MBP–UCR1 and GST–UCR2, lanes 5 and 8, MBP–UCR1-C and GST–UCR2. Panel B shows an experiment done to show that MBP–UCR1 did not bind to GST in these assays. The immunoblot shows the bound fractions only of pull down assays in which the bait and prey pairs were: lane 1, MBP and GST; lane 2, MBP and GST–UCR2; lane 3, MBP–UCR1 and GST; lane 4, MBP–UCR1 and GST–UCR2. These data are typical of those from experiments performed on 3 separate occasions.

6.2.3 Two charged amino acids within UCR1 are necessary for its interaction with UCR2

The carboxyl terminal of UCR1 is mainly composed of amino acids with apolar side chains. The few charged residues that occur within this region are D83, D84, R98 and R101 (numbers indicate the position of the residue in HSPDE4D3). These residues are highly conserved among all the mammalian PDE4 isoforms and in the *dunce* PDE of *Drosophila* (*Figure 6.64*). In contrast, the amino terminal portion of UCR2 (residues 134–179 in HSPDE4D3) is very hydrophilic and contains numerous amino acids with negatively charged side chains. It therefore seemed likely that the interaction between these 2 regions would involve the charged residues in the UCR1.

6.2.3.1 Yeast two-hybrid analysis of charged residues within UCR1

The involvement of the charged residues within the carboxyl terminal region of UCR1 was first investigated by the yeast two-hybrid method. The codon for each of the 4 charged residues in this region of UCR1 was mutated, separately and in various combinations, to encode alanine, in the plasmid pLEXAU1D. Two-hybrid assays were then used to test the mutants for their ability to interact with UCR2. The results of these assays demonstrated that both the R98 and the R101 individual mutants partially attenuated the interaction and that the R98,R101 double mutant completely blocked the interaction. In contrast to this neither the D83 nor the D84 mutations produced any detectable change in the interaction.

6.2.3.2 Biochemical analysis of charged residues within UCR1

To provide biochemical evidence in support of this two-hybrid data I expressed and purified 3 separate mutants of the MBP–UCR1 construct, in which the residues R98 and R101 had been mutated to alanine singly and in combination. I used these proteins as baits in pull down assays with the truncation in HSPDE4D3, UCR2+Cat, as the prey. I monitored binding in these experiments both by immunoblots and by PDE enzyme activity assays (*Figure 6.70, Figure 6.71*). I analysed this data by performing t-tests to see if the mean difference between the binding of UCR2+Cat to each of the MBP–UCR1 fusion proteins was significantly different from its

binding to MBP alone. This analysis revealed that mutation of either R98 or R101 to alanine partially attenuated the interaction and that the R98, R101 to alanine double mutation completely blocked the interaction.

Together with the results from the yeast two-hybrid experiments these data show that the positively charged arginine residues R98 and R101 are necessary for the interaction between UCR1 and UCR2 in these assays. This supports the hypothesis that the side chains of these residues project out from a generally hydrophobic region within UCR1 and that they are necessary for the binding of UCR1 to UCR2 in the full length PDE.

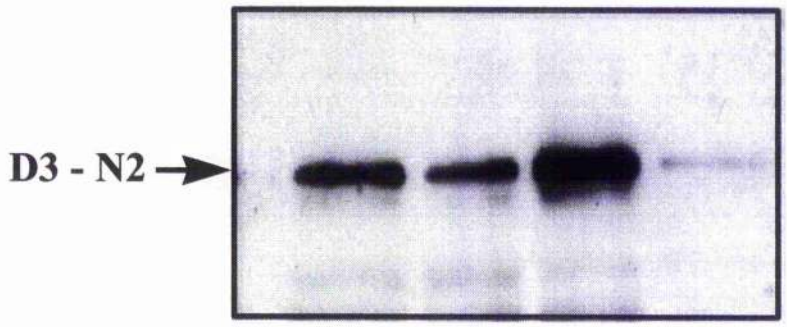

Figure 6.70: Specific amino acids (R98 and R101) in UCR1 mediate its interaction with UCR2

The figure shows an immunoblot, for PDE4D, of aliquots from the bound fractions of pull down assays between constructs of MBP–UCR1 with various mutations, as baits, and the cytosolic fraction from transiently transfected COS-7 cells expressing UCR2+Cat (D3-N2) as prey. The mutations in the MBP–UCR1 construct used in these pull down assays were: lane 1, R98A; lane 2, R101A, lane 3, wild type; lane 4, R98A,R101A. These data are typical of those from experiments performed on 3 separate occasions.

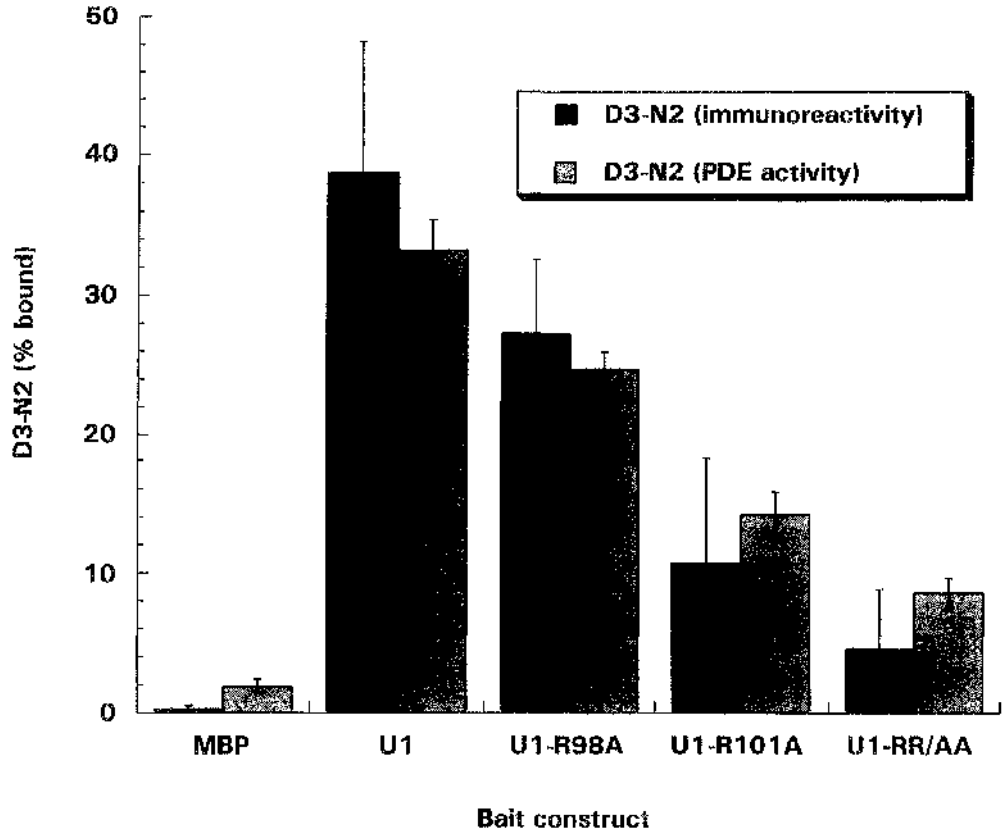

Figure 6.71: Analysis of bound PDE enzyme activity and of bound anti PDE4D immunoreactivity in pull down assays

The figure shows a histogram of the percentage binding in pull down assays between MBP, MBP–UCR1, MBP–UCR1R98A, MBP–UCR1R101A and MBP–UCR1R98R101A as the baits and full length UCR2+Cat as the prey. The data show the proportion of the prey captured in the bound fraction as a percentage of total amount recovered. This was assessed both by semi quantitative immunoblots (solid bars) and by PDE enzyme activity assays (cross hatched bars). The figures represent the means of 3 separate experiments with standard errors shown.

6.2.3.3 Yeast two-hybrid analysis of specific charged residues within UCR2

Further yeast two-hybrid analysis were then performed to determine which residues within UCR2 were necessary for the interaction with UCR1. Site directed mutagenesis was used to mutate various combinations of glutamic acids or aspartic acids within the amino terminal region of UCR2 to alanine. These mutants were then tested for their abilities to interact with pLEXAU1E in two-hybrid tests. The results of these assays demonstrated that the simultaneous mutation of 3 amino acids (E146, E147 and D149) to alanine significantly attenuated the interaction between UCR1 and UCR2. In contrast to this, the mutation of other combinations of charged amino acids, such as the double mutant pairs E143, E146 or D153, E156 to alanine had no detectable effect on the interaction.

To determine if the positively charged arginine residues R98 and R101 in UCR1 might specifically interact with the negatively charged glutamic and aspartic acids E146, E147 and D149 in UCR2 further two-hybrid assays were performed. These assays tested the ability of the single R98 to alanine and the R101 to alanine mutants in UCR1 to interact with various combinations of mutations that changed E146, E147 and D149 to alanine. These results showed that the combination of mutating R101 in UCR1 and D149 in UCR2 to alanines blocked the interaction, although each of these single mutants alone did not.

These data show that specific charged residues are important for the interaction between UCR1 and UCR2. This supports the hypothesis that UCR1 and UCR2 interact by electrostatic interactions between positively charged arginines within the carboxyl terminal portion of UCR1 and the negatively charged glutamic and aspartic acid residues in the amino terminal portion of UCR2. Indeed these data are consistent with, although do not prove, a putative direct interaction between residue R101 in UCR1 and one or both of the residues E146, E147. To further test this hypothesis it would be desireable to construct mutant proteins in which these residues were swaped and then to test whether these constructs could interact with each other.

6.2.4 Effect of phosphorylation at Ser54 on the interaction between UCR1 and

UCR2

The long PDE4D isoform PDE4D3 is activated upon phosphorylation by PKA (82, 197, 198). There are 2 distinct sites within PDE4D3 that conform to the consensus RRxS motif for phosphorylation by PKA (S13 and S54 in HSPDE4D3). Both of these sites in PDE4D3 are substrates for PKA in *vitro* and in *vivo* PKA (82, 197, 198). The phosphorylation of PDE4D3 at S54 leads both to activation of the enzyme and to a change in its sensitivity to inhibition by rolipram (197). The effects of phosphorylation at S54 on both the enzyme activity and its sensitivity to rolipram are completely mimicked by the mutation of S54 to aspartic acid (82). As the residue S54 in HSPDE4D3 lies within UCR1, I decided to investigate whether the phosphorylation of this residue affected the interaction between UCR1 and UCR2.

6.2.4.1 Effect of mutations in the PKA consensus phosphorylation motif in UCR1 on the interaction between UCR1 and UCR2

I decided to use mutations within the PKA phosphorylation motif in UCR1 as an initial strategy to investigate whether the phosphorylation of S54 was likely to affect the interaction of UCR1 with UCR2. This was because, by using mutations, rather than in *vitro* phosphorylated MBP–UCR-1, I could be confident that all of the bait fusion protein in the assays contained the modification. Another potential disadvantage associated with the alternative strategy of using in *vitro* phosphorylated MBP–UCR1 for the initial investigation was the possibility that residues other than S54 may have been modified under the conditions used for the in *vitro* phosphorylation of the fusion protein.

I expressed and purified 5 separate mutants of the MBP–UCR1 construct in which the residue S54 was mutated to an alanine, an aspartic acid, or a threonine residue (MBP–UCR1S54A, MBP–UCR1S54D and MBP–UCR1S54T respectively) or the residue E53 was mutated to an alanine (MBP–UCR1E53A) or the residues R51 and R52 were both mutated to alanines (MBP–UCR1R98R101A). I used these proteins as baits in pull down assays with UCR2+Cat, as the prey. I monitored binding in these experiments both by immunoblots and by PDE enzyme activity assays (*Figure 6.72, Figure 6.73*). I analysed this data by performing t-tests to see if the mean

difference between the binding of UCR2+Cat to each of the MBP–UCR1 fusion proteins was significantly different from its binding to MBP alone.

The effect of these mutations in full length HSPDE4D3 suggests that the phosphorylation of wild type HSPDE4D3 at S54 leads to at least 2 distinct conformational changes in the enzyme. One of these is suggested to result in activation and the other to yield a change in the enzymes sensitivity to inhibition by rolipram (82).

It has been proposed that the conformational change in HSPDE4D3 that is detected by a change in its sensitivity to inhibition by rolipram is caused by the disruption of a hydrogen bond involving the side chain hydroxyl group of S54. Consistent with this proposal, mutation of S54 in the full length enzyme to threonine, which preserves the hydrogen bonding potential at this site, does not cause a change in the enzymes sensitivity to rolipram. The conformational change in full length HSPDE4D3 that leads to enzyme activation was suggested to be due to the disruption of an ion pair interaction involving the negatively charged E53. Consistent with this proposal, mutation of E53 to alanine in the full length enzyme resulted in a species that was constitutively activated compared to the unphosphorylated, wild type enzyme but that did not display an altered sensitivity to inhibition by rolipram (82).

Mutation of S54 to either alanine or aspartic acid in MBP–UCR1 disrupted the interaction between UCR1 and UCR2 in pull down assays. These mutations in full length HSPDE4D3 both caused a change in the sensitivity of the enzyme to rolipram. In contrast to this, the effects of these mutations on the activity of HSPDE4D3 are different; with mutation of S54 to aspartic acid but not to alanine causing activation of the enzyme. Mutation of S54 to threonine in MBP–UCR1 did not disrupt the interaction between UCR1 and UCR2 in pull down assays. This mutation in full length HSPDE4D3 does not cause a change in sensitivity to rolipram (*Figure 6.72, Figure 6.73*) (82).

Mutation of E53 to alanine in MBP–UCR1 did not disrupt the interaction between UCR1 and UCR2 in pull down assays. This mutation in full length HSPDE4D3 does cause activation but does not affect the sensitivity of the enzyme to inhibition by

rolipram. The double mutation of R51 and R52 to alanines (which disrupts the phosphorylation motif for PKA) in MBP–UCR1 did not disrupt the interaction between UCR1 and UCR2 in pull down assays. This mutation in full length HSPDE4D3 did not affect either the sensitivity of the enzyme to inhibition by rolipram, nor did it cause activation compared to the unphosphorylated wild type enzyme (*Figure 6.72, Figure 6.73*) (82).

Together these data suggest that a change in the conformation in full length HSPDE4D3 that follows the phosphorylation of S54 by PKA and that results in a change in the sensitivity of this enzyme to inhibition by rolipram involves the disruption of an interaction between UCR1 and UCR2.

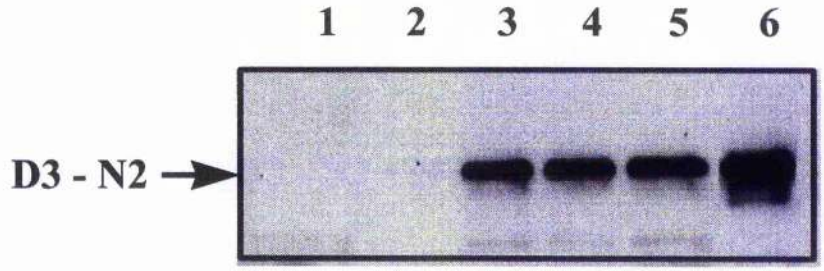

Figure 6.72: The effect of mutations within the PKA consensus phosphorylation motif in UCR1 on the interaction between UCR1 and UCR2 in pull down assays

The figure shows an immunoblot, for PDE4D, of aliquots from the bound fractions of pull down assays between constructs of MBP–UCR1 with various mutations, as baits, and the cytosolic fraction from transiently transfected COS-7 cells expressing UCR2+Cat (D3-N2) as prey. The mutations in the MBP–UCR1 construct used in these pull down assays were: lane 1, S54D; lane 2, S54A, lane 3, wild type; lane 4, S54T; lane 5, the double mutation R51R52A; lane 6, E53A. These data are typical of those from experiments performed on 3 separate occasions.

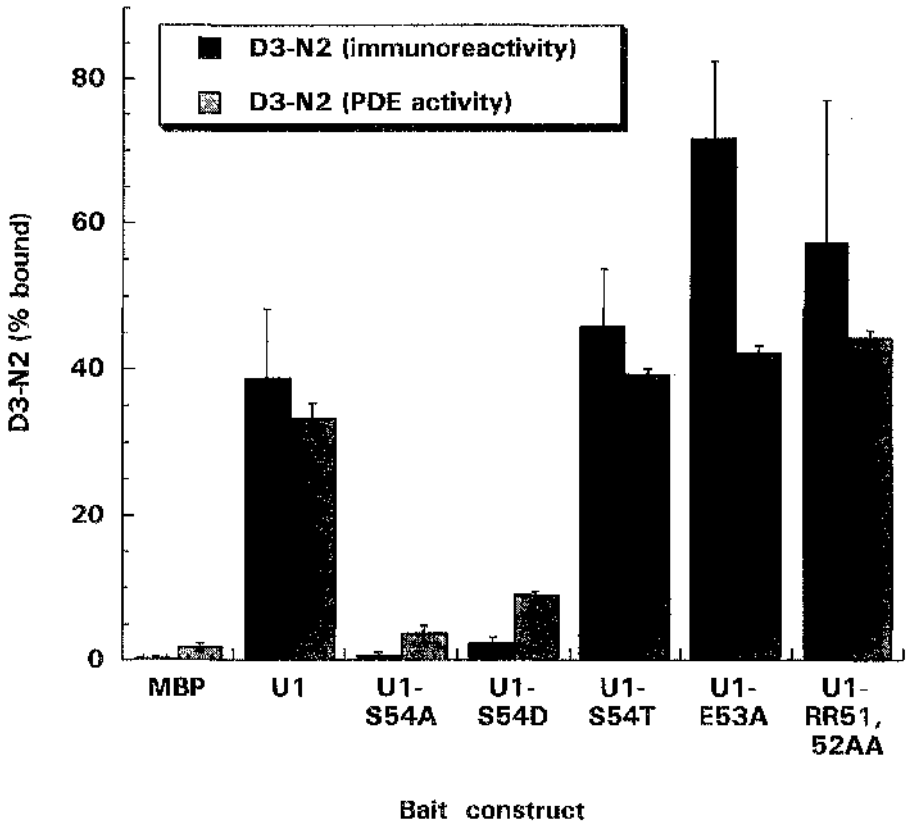

Figure 6.73: Analysis of bound PDE enzyme activity and of bound anti PDE4D immunoreactivity in pull down assays

The figure shows a histogram of the percentage binding in pull down assays between MBP, MBP–UCR1, MBP–UCRS54A, MBP–UCR1S54D, MBP–UCR1S54T, MBP–UCR1E53A and MBP–UCR1R51R52A as the baits and full length UCR2+Cat as the prey. The data show the proportion of the prey captured in the bound fraction as a percentage of total amount recovered. This was assessed both by semi quantitative immunoblots (solid bars) and by PDE enzyme activity assays (cross hatched bars). The figures represent the means of 3 separate experiments with standard errors shown.

6.3 Conclusion

In this chapter I have presented biochemical evidence to support the results of elegant yeast two-hybrid experiments performed in the laboratory of Prof. G. Bolger. Together these data suggest that UCR1 and UCR2 of PDE4 can interact and that this interaction is stabilised by electrostatic bonds between specific residues located in the carboxyl terminal portion of UCR1 and in the amino terminal portion of UCR2. I have also presented data which suggest that the interaction between UCR1 and UCR2 can be regulated by phosphorylation at a PKA consensus motif located within the amino terminal of UCR1.

6.3.1 UCR1 and UCR2 may form authentic domains within the amino termini of PDE4 isoforms

The sequences of UCR1 and UCR2 can be regarded as unique signatures of the PDE4, cAMP specific phosphodiesterase family. These conserved regions are located in the amino termini of PDE4s and are clearly separate from the catalytic regions of these enzymes. The data presented in this chapter are consistent with the hypothesis that both UCR1 and UCR2 act as authentic protein domains. That is to say that UCR1 and UCR2 each seem able to fold into independent modules that retain their structures in a variety of contexts. This is demonstrated by the data showing that UCR1 can interact with UCR2 when each is expressed as a fusion with one of several different proteins. These include the DNA binding domain of LexA and MBP for UCR1 and GST or the GAL4 activation domain for UCR2. This is reminiscent of SH2 and SH3 domains, that are also independently folding domains able to participate in protein–protein interactions (141, 162, 168).

6.3.2 Conformational change in PDE4D3 following phosphorylation on Ser^{54}

The data on the effect of mutations within the PKA phosphorylation site in UCR1 provide additional insight into the mechanism of the regulation of PDE4D3 by PKA. Conti and co-workers have demonstrated that PDE4D3 can be phosphorylated and activated by PKA in *vivo*. The critical phosphorylation site for this activation is S54

(197-199). This residue lies within the amino terminal portion of UCR1.

Phosphorylation of S54 in PDE4D3 produces both a change in the enzymatic activity (change in relative Vmax) and a change in the sensitivity of the enzyme to inhibition by rolipram. A study by Hoffmann and others that used mutants within the PKA phosphorylation sites in HSPDE4D3 showed that the changes in enzyme activity and in sensitivity to rolipram that followed modification of this region could be separated from one another. This study provided evidence to suggest that S54 and the adjacent E53 were each involved in forming bonds that influenced the structure of the catalytic site of the enzyme. The proposed model was one in which the side chain of E53 was involved in an ion pair that constrained the catalytic activity of the enzyme but that did not influence the sensitivity of the enzyme to inhibition by rolipram. The side chain hydroxyl group of S54 was suggested to be involved in a hydrogen bond that did not constrain the activity of the enzyme but that did influence the conformation of the catalytic site in a way that could be detected by a change in its sensitivity to inhibition by rolipram (82).

In this chapter I have shown that mutations in UCR1 that cause a change in the sensitivity of full length HSPDE4D3 to inhibition by rolipram also disrupt the interaction between UCR1 and UCR2 in pull down assays (MBP-UCR1S54A and MBP-UCR1S54D). Mutations in UCR1 that do not cause a change in the sensitivity of HSPDE4D3 to inhibition by rolipram do not, however, disrupt the interaction between UCR1 and UCR2 in pull down assays (MBP-UCR1S54T, MBP-UCR1E53A and MBP-UCR1R51R52A). This is regardless of whether or not they cause activation of full length HSPDE4D3.

These data support the hypothesis that the change in sensitivity to inhibition by rolipram but not the activation of PDE4D3, following phosphorylation by PKA on S54, is linked to the disruption of an interaction between UCR1 and UCR2 in the enzyme.

It would be desirable to perform pull down experiments using a wild type UCR1 fusion protein that was phosphorylated on S54 to support the results of these pull down assays using mutated fusion proteins. It would also be interesting to

further test the hypothesis, that the interaction between UCR1 and UCR2 affects the sensitivity of the enzyme to rolipram but not its activity, by characterising the effect of mutations in full length HSPDE4D3 that disrupt this interaction in pull down assays. Full length HSPDE4D3 in which R98 and R101 were mutated to alanines, for instance, would be predicted to show an altered sensitivity to inhibition by rolipram compared to the wild type enzyme.

The data presented in this chapter are consistent with a model for PDE4 structure where UCR1 and UCR2 in the full length protein each comprise 1 or more independently folding domains and that these domains interact with other regions of the enzyme. An important example of such an interaction is the electrostatic interaction between positively charged residues in the carboxyl terminal of UCR1 and negatively charged residues within the amino terminal of UCR2. It is proposed that this interaction is modulated by PKA phosphorylation of a serine residue in the extreme amino terminal region of UCR1. This portion of UCR1 is not necessary for the interaction with UCR2 in pull down or in two-hybrid assays. It might therefore not interact directly with UCR2. It is possible that the amino and the carboxyl terminal portions of UCR1 affect one another in such a way that the loss of hydrogen bonding capacity at S54 prevents the carboxyl terminal of UCR1 from interacting with UCR2. Under this model UCR1 and UCR2 can be thought of as forming a regulatory module that in turn regulates the catalytic site of long PDE4 isoforms. Structural analysis of PDE4 enzymes will, however, be needed to gain a full understanding of the molecular mechanisms of this regulation.

7. General discussion

The 3',5' cyclic adenosine monophosphate (cAMP) signalling pathway plays a central role in cellular signalling. As I have discussed, in detail, in the introduction of this thesis, signalling through cAMP is classically considered to involve the activation of protein kinase A (PKA) which then phosphorylates downstream proteins to bring about both acute changes in cellular physiology and also longer term changes in the transcription of cAMP responsive genes. In addition to causing activation of PKA, cAMP can also act to affect cell function by directly binding to certain ion channels and by binding to and activating the guanine nucleotide exchange factor Epac (exchange protein directly activated by cAMP). Once activated, Epac causes the activation of Rap-1 which can then feed into the mitogen activated kinase (MAPK/ERK) signalling pathways.

In addition to the direct actions of activated PKA on downstream proteins, every stage in the classical cAMP signalling pathway presents opportunities for crosstalk between the cAMP and other intracellular signalling pathways. Signalling through cAMP should therefore be thought of as an integrated part of the signal transduction potential of a cell. The cellular response to any single stimuli will depend not only upon the class of receptor that it activates and the signalling pathway that it couples to but also, in various and subtle ways, on the activation status of many, if not all, other signal transduction pathways within the cell.

An important aspect of the regulation of cAMP signalling within a cell is the spatial organisation of the components of this signalling pathway. Enzymes that catalyse each step of the cAMP signalling pathway are targeted to specific locations within the 3 dimensional interior of the cell. This creates a potential for the establishment of localised increases in cAMP concentration that could selectively activate PKA in that region but not affect other, functionally distinct, pools of PKA anchored in other regions of the cell.

In chapter 3 of this thesis I have shown that the type 4 phosphodiesterase (PDE4) splice variant PDE4D4 can specifically interact with Src homology 3 (SH3) domains

in *vitro* and that it appears to show a selectivity for interaction with the SH3 domains of the Src family tyrosyl protein kinases Src, Lyn and Fyn. This finding is significant because it raises the possibility that, in *vivo*, PDE4D4 may become recruited into signalling complexes by interacting with an SH3 domain and that this may serve to regulate local cAMP concentrations in the immediate vicinity of such complexes.

In chapter 4 of this thesis I have shown, for the first time, that recombinant, full length HSPDE4D4 can be expressed in *E.coli* as a fusion protein with maltose binding protein (MBP) and purified to near homogeneity by affinity chromatography. By using purified preparations of MBP–HSPDE4D4 and also of just the amino terminal region of HSPDE4D4 as a fusion protein with MBP I was able to demonstrate that both full length HSPDE4D4 and the alternatively spliced, amino terminal region of HSPDE4D4 alone can interact directly with SH3 domains.

By engineering a sequence encoding a recognition site for the viral protease TEV into the MBP–HSPDE4D4 fusion protein I was able to express and purify a fusion protein that included this protease recognition site. This enabled me to separate proteolytically the MBP moiety of the fusion protein from the HSPDE4D4 moiety. Doing this I obtained a purified recombinant HSPDE4D4 with only 11 vector derived amino acids remaining at its amino terminus.

The production of a bacterially expressed, highly purified, full length PDE is a significant advance as, in the past, the purification of these enzymes has proven to be extremely problematic. This has allowed me to perform a limited characterisation of purified HSPDE4D4. This was the first time that a purified preparation of HSPDE4D4 had been characterised. It is likely that the method I developed for the expression and the purification of untagged, full length, HSPDE4D4 will be generally applicable to the purification of other PDE4 isoforms. The ability to easily produce relatively large quantities of purified PDE4 isoenzymes will be of major importance to future investigations into the regulation and the structure of these proteins.

In chapter 5 of this thesis I investigated the interaction of another PDE4 isoform, RNPDE4A5, with SH3 domains. It had already been shown that RNPDE4A5

can specifically interact with SH3 domains and that the alternatively spliced, amino terminal region of the protein was necessary for this interaction. This region of RNPDE4A5 is characterised by 3 regions of proline and arginine rich sequence that each conform to the PxxP, minimal consensus sequence for binding to SH3 domains. By using a strategy of sequential amino terminal truncations in RNPDE4A5 I implicated the most amino terminal of these putative SH3 domain binding motifs as being of importance in the interaction between RNPDE4A5 and SH3 domains. I also used the truncation mutants in RNPDE4A5 to identify a region of sequence within the amino terminal region of this protein that is involved in the subcellular targeting of this enzyme. These findings will be important in planning further experiments to examine the roles of protein–protein interactions and of subcellular targeting in the regulation of cAMP signalling by RNPDE4A5.

In chapter 6 of this thesis I turned my attention from the intermolecular protein–protein interactions of PDE4s to investigate an intramolecular interaction between the UCR1 and UCR2 of long form PDE4 splice variants. I provided biochemical evidence to support preliminary yeast 2 hybrid data that demonstrated an interaction between the UCR1 and the UCR2 of HSPDE4D3. In a collaboration with Prof. G. Bolger I then proceeded to investigate the roles that specific residues within UCR1 and UCR2 play in regulating the interaction of these 2 regions. This investigation showed that specific charged residues located in the carboxyl terminal portion of UCR1 and the amino terminal portion of UCR2 were important for stabilising the interaction between UCR1 and UCR2. Furthermore, I showed that the interaction between UCR1 and UCR2 could be regulated by the phosphorylation of a serine residue located within a PKA recognition motif that lies within UCR1 (Ser^{54} in HSPDE4D3). This residue is found in all long PDE4 isoforms where it is an authentic substrate for modification by PKA in *vivo*.

UCR1 and UCR2 are unique "signature" regions of all long PDE4 isoforms. Phosphorylation of a serine residue within UCR1 can activate at lease one PDE4 isoform, namely HSPDE4D3. This modification also serves to disrupt the interaction between UCR1 and UCR2. I propose, therefore, that UCR1 and UCR2 may act as signal transducing modules within PDE4 enzymes that can interact with each other

and can also transmit the effects of regulatory post-translational modifications to the catalytic region of the enzyme (*Figure 7.74*).

Taken together the work presented in this thesis represents a significant contribution to the understanding of the role of regulated protein–protein interactions in the control of cAMP signalling by PDE4.

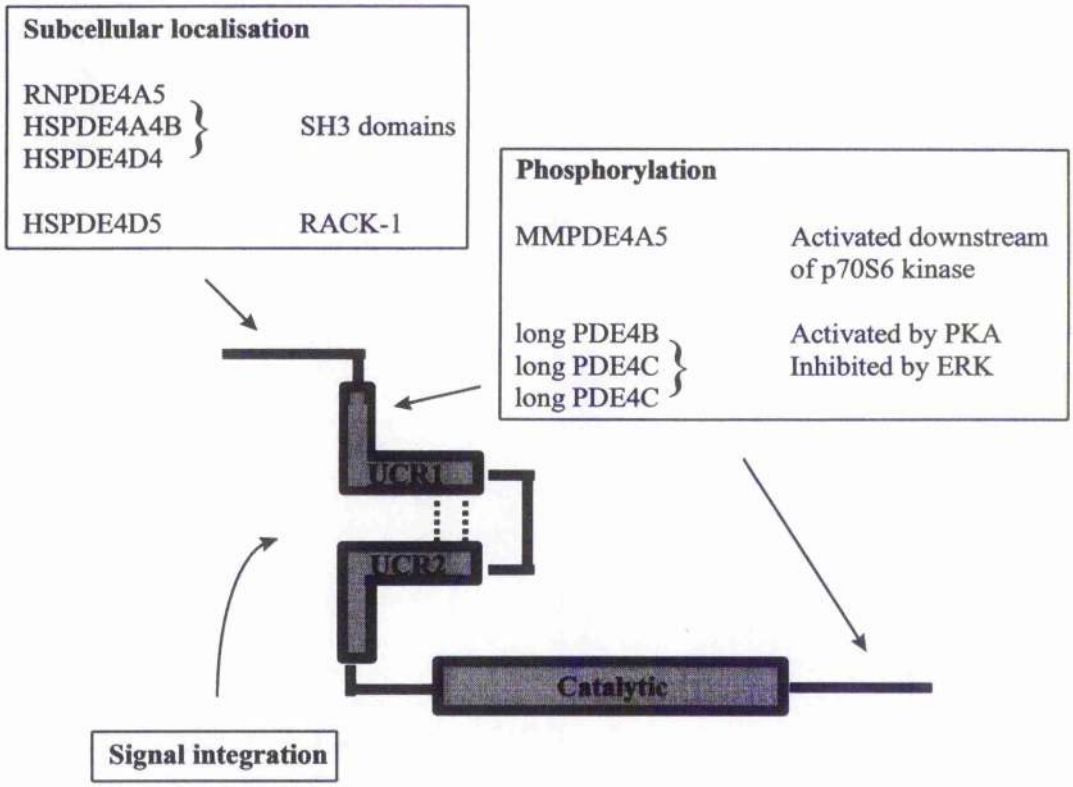

Figure 7.74: Proposed model for the regulation of PDE4

The figure shows a diagram representing the proposed roles for regions within long PDE4 isoforms. The green boxes represent regions that are conserved between all long isoforms of PDE4. These are Upstream Conserved Regions 1 and 2 (UCR1 and UCR2) and the catalytic region. It is suggested that the interactions of certain isoforms of PDE4A (162) and PDE4D (Chapter 3 of this thesis) with SH3 domains and the interaction of HSPDE4D5 with RACK-1 (252) may play a role in subcellular targeting. It is also suggested that UCR1 and UCR2 may interact to form a signal integration module that co-ordinates the effects of regulatory inputs and transmits these to the catalytic region. The phosphorylation of MMPDE4A5, downstream of p70S6 kinase (132) and of HSPDE4D3 by both PKA (197) and ERK2 (81) are shown as examples of regulatory inputs.

8. References

1. **Alexandropoulos, A., G. Cheng, and D. Baltimore.** 1995. Proline-rich sequences that bind to Src homology 3 domains with individual specificities. Proc. Natl. Acad. Sci. USA **92:**3110-3114.

2. **Alvarez, R., C. Sette, D. Yang, R. M. Eglen, R. Wilhelm, E. R. Shelton, and M. Conti.** 1995. Activation and selective inhibition of a cyclic AMP-specific phosphodiesterase, PDE-4D3. Molecular Pharmacology **48:**616-622.

3. **Andjelkovic, M., T. Jakubowicz, P. Cron, X. F. Ming, J. W. Han, and B. A. Hemmings.** 1996. Activation and phosphorylation of a pleckstrin homology domain containing protein kinase (RAC-PK/PKB) promoted by serum and protein phosphatase inhibitors. Proceedings of the National Academy of Sciences of the United States of America **93:**5699-704.

4. **Atienza, J. M., D. Susanto, C. Huang, A. S. McCarty, and J. Colicelli.** 1999. Identification of Inhibitor Specificity Determinants in a Mammalian Phosphodiesterase. The Journal of Biological Chemistry **274:**4839-4847.

5. **Baecker, P. A., R. Obernolte, C. Bach, C. Yee, and E. R. Shelton.** 1994. Isolation of a cDNA encoding a human rolipram-sensitive cyclic AMP phosphodiesterase (PDEIVD). Gene **138:**253-256.

6. **Barnette, M. S., J. O. Bartus, M. Burman, S. B. Christensen, L. B. Cieslinski, K. M. Esser, U. S. Prabhakar, J. A. Rush, and T. J. Torphy.** 1996. Association of the anti-inflammatory activity of phosphodiesterase 4 (PDE4) inhibitors with either inhibition of PDE4 catalytic activity or competition for [3H]rolipram binding. Biochemical Pharmacology **51:**949-56.

7. **Beavo, J. A.** 1995. Cyclic nucleotide phosphodiesterases: Functional implications of multiple isoforms. Physiological Reviews **75:**725-748.

8. **Beavo, J. A., M. Conti, and R. J. Heaslip.** 1994. Multiple cyclic nucleotide phosphodiesterases. Molecular Pharmacology **46:**399-405.

9. **Beebe, S. J., O. Oyen, M. Sandberg, A. Froyas, V. Namsson, and T. Jahnsen.** 1990. Molecular cloning of a tissue-specific protein kinase (C gamma) from human testis - representing a third isoform for the catalytic subunit of cAMP-dependent protein kinase. Mol. Endocrinol. **4:**465-475.

10. **Bentley, J. K., A. Kadlecek, C. H. Sherbert, D. Seger, W. K. Sonnenburg, H. Charbonneau, J. P. Novack, and J. A. Beavo.** 1992. Molecular cloning of cDNA encoding a '63'-kDa calmodulin-stimulated phosphodiesterase from bovine brain. Journal of Biological Chemistry **267:**18676-18682.

11. **Bigay, J., E. Faurobert, M. Franco, and M. Chabre.** 1994. Roles of lipid modifications of transducin subunits in their GDP-dependent association and membrane binding. Biochemistry **33:**14081-14090.

12. **Bloom, T. J., and J. A. Beavo.** 1996. Identification and tissue-specific expression of PDE7 phosphodiesterase splice variants. Proc. Natl. Acad. Sci. USA **93:**14188-14192.

13. **Bolger, G., T. Michaeli, T. Martins, T. St John, B. Steiner, L. Rodgers, M. Riggs, M. Wigler, and K. Fergurson.** 1993. A Family of Human Phosphodiesterases Homologous to the *dunce* Learning and Memory Gene Product of *Drosophila melanogaster* are Potential Targets for Antidepressant Drugs. Molecular and Cellular Biology **13:**6558-6571.

14. **Bolger, G. B.** 1994. Molecular Biology of the Cyclic AMP-specific Cyclic Nucleotide Phosphodiesterases: A Diverse Family of Regulatory Enzymes. Cellular Signalling **6:**851-859.

15. **Bolger, G. B., S. Erdogan, R. E. Jones, K. Loughney, G. Scotland, R. Hoffmann, I. Wilkinson, C. Farrell, and M. D. Houslay.** 1997. Characterization of five different proteins produced by alternatively spliced

mRNAs from the human cAMP-specific phosphodiesterase PDE4D gene. Biochem J **328:**539-48.

16. **Bolger, G. B., I. McPhee, and M. D. Houslay.** 1996. Alternative splicing of cAMP-specific phosphodiesterase mRNA transcripts. Characterization of a novel tissue-specific isoform, RNPDE4A8. Journal of Biological Chemistry **271:**1065-71.

17. **Bolger, G. B., L. Rodgers, and M. Riggs.** 1994. Differential CNS expression of alternative mRNA isoforms of the mammalian genes encoding cAMP-specific phosphodiesterases. Gene **149:**237-244.

18. **Booker, G. W., A. L. Breeze, A. K. Downing, G. Panayotou, I. Gout, M. D. Waterfield, and I. D. Campbell.** 1992. Structure of an SH2 domain of the p85 alpha subunit of phosphatidylinositol-3-OH kinase. Nature **358:**684-7.

19. **Borg, J. P., J. Ooi, E. Levy, and B. Margolis.** 1996. The phosphotyrosine interaction domains of X11 and FE65 bind to distinct sites on the YENPTY motif of amyloid precursor protein. Molecular & Cellular Biology **16:**6229-41.

20. **Bos, J. L.** 1998. All in the family? New insights and questions regarding interconnectivity of Ras, Rap1 and Ral. EMBO Journal **17:**6776-6782.

21. **Brechler, V., C. Pavoine, R. Hanf, E. Garbarz, R. Fischmeister, and F. Pecker.** 1992. Inhibition of glucagon of the cGMP-inhibited low-K(m) cAMP phosphodiesterase in heart is mediated by a pertussis toxin-sensitive G- protein. Journal of Biological Chemistry **267:**15496-15501.

22. **Broome, M. A., and T. Hunter.** 1996. Requirement for c-src Catalytic Activity and the SH3 Domain in Platelet-derived Growth Factor BB and Epidermal Growth Factor Mitogenic Signaling. J. Biol. Chem. **271:**16798-16806.

23. **Brunton, L. L., and S. E. Mayer.** 1979. Extrusion of Cyclic AMP from Pigeon Erythrocytes. The Journal of Biological Chemistry **254:**9714-9720.

24. **Burns, F., and N. J. Pyne.** 1992. Interaction of the catalytic subunit of protein kinase A with the lung type V cyclic GMP phosphodiesterase: Modulation of non-catalytic binding sites. Biochemical & Biophysical Research Communications **189:**1389-1396.

25. **Burns, F., I. W. Rodger, and N. J. Pyne.** 1992. The catalytic subunit of protein kinase A triggers activation of the type V cyclic GMP-specific phosphodiesterase from guinea-pig lung. Biochemical Journal **283:**487-491.

26. **Burton, K. A., B. D. Johnson, Z. E. Hausken, R. E. Westenbroek, R. L. Idzerda, T. Scheuer, J. D. Scott, W. A. Catterall, and G. S. McKnight.** 1997. Type II regulatory subunits are not required for the anchoring-dependent modulation of Ca2+ channel activity by cAMP-dependent protein kinase. Proceedings of the National Academy of Sciences of the United States of America **94:**11067-11072.

27. **Carr, D. W., and J. D. Scott.** 1992. Blotting and band-shifting: techniques for studying protein-protein interactions. TIBS **17:**246-249.

28. **Carr, D. W., R. E. Stofko-Hahn, I. D. C. Fraser, R. D. Cone, and J. D. Scott.** 1992. Localization of the cAMP-dependent Protein Kinase to the Postsynaptic Densities by A-Kinase Anchoring Proteins. The Journal of Biological Chemistry **267:**16816-16823.

29. **Chan, D. C., M. T. Bedford, and P. Leder.** 1996. Formin binding proteins bear WWP/WW domains that bind proline-rich peptides and functionally resemble SH3 domains. The EMBO Journal **15:**1045-1054.

30. **Chang, B. Y., K. B. Conroy, E. M. Machleder, and C. A. Cartwright.** 1998. RACK1, a Receptor for Activated C Kinase and a Homolog of the ß Subunit of G Proteins, Inhibits Activity of Src Tyrosine Kinases and Growth

of NIH 3T3 Cells. Mol. Cell. Biol. **18:**3245-3256.

31. **Charbonneau, H.** 1990. Structure-function relationships among cyclic nucleotide phosphodiesterases. *In* J. Beavo, and M. D. Houslay (ed.), Cyclic nucleotide phosphodiesterases, vol. 2. John Wiley, Chichester.

32. **Cheng, G., Z. Ye, and D. Baltimore.** 1994. Binding of Bruton's tyrosine kinase to Fyn, Lyn or Hck through a Src homology 3 domain-mediated interaction. Proc. Natl. Acad. Sci. USA **91:**8152-8155.

33. **Cheung, P. P., L. Yu, H. Zhang, and R. W. Colman.** 1998. Partial characterization of the active site human platelet cAMP phosphodiesterase, PDE3A, by site directed mutagenesis. Archives of Biochemistry and Biophysics **360:**99-104.

34. **Chini, C. C. S., J. P. Grande, E. N. Chini, and T. P. Dousa.** 1997. Compartmentalisation of cAMP Signalling in Mesangial Cells by Phosphodiesterase Isozymes PDE3 and PDE4. The Journal of Biological Chemistry **272:**9854-9859.

35. **Choi, K. Y., B. Satterberg, D. M. Lyons, and E. A. Elion.** 1994. Ste5 tethers multiple protein kinases in the MAP kinase cascade required for mating in S. cerevisiae. Cell **78:**499-512.

36. **Coghlan, V. M., B. A. Perrino, M. Howard, L. K. Langeberg, J. B. Hicks, W. M. Gallatin, and J. D. Scott.** 1995. Association of protein kinase A and protein phosphatase 2B with a common anchoring protein. Science **267:**108-111.

37. **Cohen, P.** 1992. Signal integration at the level of protein kinases, protein phosphatases and their substrates. Trends in Biochemical Sciences **17:**408-413.

38. **Colicelli, J., C. Birchmeier, T. Michaeli, K. O'Neill, M. Riggs, and M.**

Wigler. 1989. Isolation and characterization of a mammalian gene encoding a high-affinity cAMP phosphodiesterase. Proc. Natl. Acad. Sci. USA **86:**3599-3603.

39. **Colledge, M., and J. D. Scott.** 1999. AKAPs: From structure to function. Trends in Cell Biology **9:**216-221.

40. **Conti, M., S. Iona, M. Cnomo, J. V. Swinnen, J. Odeh, and M. E. Svoboda.** 1995. Characterization of a hormone-inducible, high affinity adenosine 3'-5'- cyclic monophosphate phosphodiesterase from the rat Sertoli cell. Biochemistry **34:**7979-7987.

41. **Conti, M., G. Nemoz, C. Sette, and E. Vicini.** 1995. Recent Progress in Understanding the Hormonal Regulation of Phosphodiesterases. Endocrine Reviews **16:**370-389.

42. **Corbin, J. D., and S. H. Francis.** 1999. Cyclic GMP phosphodiesterase-5: Target of sildenafil. Journal of Biological Chemistry **274:**13729-13732.

43. **Daaka, Y., L. M. Luttrell, and R. J. Lefkowitz.** 1997. Switching of the coupling of the beta2-adrenergic receptor to different g proteins by protein kinase A. Nature **390:**88-91.

44. **Daniel, P. B., W. H. Walker, and J. F. Habener.** 1998. Cyclic amp signaling and gene regulation. .

45. **Dauwalder, B., and R. L. Davis.** 1995. Conditional rescue of the dunce learning/memory and female fertility defects with Drosophila or rat transgenes. Journal of Neuroscience **15:**3490-3499.

46. **Davis, R. L.** 1996. Physiology and Biochemistry of Drosophila learning mutants. Physiology Reviews **76:**299-317.

47. **Davis, R. L., H. Takayasu, M. Eberwine, and J. Myres.** 1989. Cloning and

characterization of mammalian homologs of the *Drosophila* dunce+ gene. Proc. Natl. Acad. Sci. USA **86:**3604-3608.

48. **Degerman, E., P. Belfrage, and V. C. Manganiello.** 1997. Structure, Localization, and Regulation of cGMP-inhibited Phosphodiesterase (PDE3). The Journal of Biological Chemistry **272:**6823-6826.

49. **DeMali, K. A., S. L. Godwin, S. P. Soltoff, and A. Kazlauskas.** 1999. Multiple Roles for Src in a PDGF-Stimulated Cell. Experimental Cell Research **253:**271-279.

50. **Dickinson, N. T., E. K. Jang, and R. J. Haslam.** 1997. Activation of cGMP-stimulated phosphodiesterase by nitroprusside limits cAMP accumulation in human platelets: effects on platelet aggregation. Biochem. J. **323:**371-377.

51. **DiFrancesco, D., and P. Tortora.** 1991. Direct activation of cardiac pacemaker channels by intracellular cyclic AMP. Nature **351:**145-147.

52. **Dohlman, H. G., and J. Thorner.** 1997. RGS Proteins and Signaling by Heterotrimeric G Protiens. J. Bol. Chem. **272:**3871-3874.

53. **Dougherty, W. G., and T. D. Parks.** 1991. Post-translational processing of the tobacco etch virus 49-kDa small nuclear inclusion polyprotein: Identification of an internal cleavage site and delimitation of VPg and proteinase domains. Virology **183:**449-456.

54. **Doyle, D. A., A. Lee, J. Lewis, E. Kim, M. Sheng, and R. MacKinnon.** 1996. Crystal structures of a complexed and peptide-free membrane protein-binding domain: molecular basis of peptide recognition by PDZ. Cell **85:**1067-76.

55. **Dytrych, L., D. L. Sherman, C. S. Gillespie, and P. J. Brophy.** 1998. Two PDZ domain proteins encoded by the murine periaxin gene are the result of

alternative intron retention and are differentially targeted in Schwann cells. Journal of Biological Chemistry **273:**5794-800.

56. **Eason, G., C. W. Coles, and G. Gettinby.** 1980. Mathematics and Statistics for the Bio-Sciences, 1 ed. Ellis Hornwood Limited, Chichester.

57. **Egloff, M., D. F. Johnson, G. Moorhead, P. T. W. Cohen, P. Cohen, and D. Barford.** 1997. Structural basis for the recognition of regulatory subunits by the catalytic subunit of protein phosphatase 1. The EMBO Journal **16:**1876-1887.

58. **Engels, P., M. Sullivan, T. Muller, and H. Lubbert.** 1995. Molecular cloning and functional expression in yeast of a human cAMP-specific phosphodiesterase subtype (PDE IV-C). FEBS Letters **358:**305-310.

59. **Epstein, P. M., S. J. Strada, K. Sarada, and W. J. Thompson.** 1982. Catalytic and Kinetic Properties of Purified High-Affinity Cyclic AMP Phosphodiesterase from Dog Kidney. Archives of Biochemistry and Biophysics **218:**119-133.

60. **Faux, M. C., and J. D. Scott.** 1996. Molecular Glue: Kinase Anchoring and Scaffold Proteins. Cell **85:**9-12.

61. **Feng, S., C. Kasahara, R. J. Rickles, and S. L. Schreiber.** 1995. Specific interactions outside the proline-rich core of two classes of Src homology 3 ligands. Proc. Natl. Acad. Sci. U S A **92:**12408-12415.

62. **Fischer, D. A., J. F. Smith, J. S. Pillar, S. H. St Denis, and J. B. Cheng.** 1998. Isolation and Characterization of PDE9A, a Novel Human cGMP-specific Phosphodiesterase. J. Biol. Chem. **273:**15559-15564.

63. **Fisher, D. A., J. F. Smith, J. S. Pillar, S. H. St Denis, and J. B. Cheng.** 1998. Isolation and Characterization of PDE8A, a Novel Human cAMP-Specific Phosphodiesterase. Biochemical and Biophysical Research

Communications **246:**570-577.

64. **Florio, S. K., R. K. Prusti, and J. A. Beavo.** 1996. Solubilization of membrane-bound rod phosphodiesterase by the rod phosphodiesterase recombinant delta subunit. Journal of Biological Chemistry **271:**24036-24047.

65. **Fung, B. K. K., J. H. Young, H. K. Yamane, and I. Griswold-Prenner.** 1990. Subunit stoichiometry of retinal rod cGMP phosphodiesterase. Biochemistry **29:**2657-2664.

66. **Geoffroy, V., F. Fouque, V. Nivet, J. Clot, C. Lugnier, B. Desbuquois, and C. Benelli.** 1999. Activation of a cGMP-stimulated cAMP phosphodiesterase by protein kniase C in a liver Golgi-endosomal fraction. Eur. J. Biochem. **259:**892-900.

67. **Gether, U., and B. K. Kobilka.** 1998. G protein-coupled receptors. Journal of Biological Chemistry **273:**17979-17982.

68. **Giorgi, M., P. R. Piscitelli, and R. Geremia.** 1992. Purification and characterization of a low-Km 3':5'-cyclic adenosine phosphodiesterase from post-meiotic male mouse germ cells. Biochimica et Biophysica Acta **1121:**178-182.

69. **Gluzman, Y.** 1981. SV40-Transformed Simian Cells Support the Replication of Early SV40 Mutants. Cell **23:**175-182.

70. **Granovsky, A. E., M. Natochin, and N. O. Artemyev.** 1997. The gamma subunit of rod cGMP-phosphodiesterase blocks the enzyme catalytic site. Journal of Biological Chemistry **272:**11686-11689.

71. **Granovsky, A. E., M. Natochin, R. L. McEntaffer, T. L. Haik, S. H. Francis, J. D. Corbin, and N. O. Artemyev.** 1998. Probing domain functions of chimeric PDE6alpha'/PDE5 cGMP- phosphodiesterase. Journal

of Biological Chemistry **273:**24485-24490.

72. **Han, P., X. Zhu, and T. Michaeli.** 1997. Alternative Splicing of the High Affinity cAMP-Specific Phosphodiesterase (PD7A) mRNA in Human Skeletal Muscle and Heart. J. Biol. Chem. **272:**16152-16157.

73. **Hardie, D. G.** 1993. Protein Phosphorylation A Practical Approach, First ed. Oirl Press at Oxford University Press, Oxford.

74. **Harrison, S. C.** 1996. Peptide-Surface Association: The case of PDZ and PTB Domains. Cell **86:**341-343.

75. **Hashimoto, Y., R. K. Sharma, and T. R. Soderling.** 1989. Regulation of Ca2+/calmodulin-dependent cyclic nucleotide phosphodiesterase by the autophosphorylated form of Ca2+/calmodulin-dependent protein kinase II. Journal of Biological Chemistry **264:**10884-10887.

76. **Hayashi, M., K. Matsushima, H. Ohashi, H. Tsunoda, S. Murase, Y. Kawarada, and T. Tanaka.** 1998. Molecular Cloning and Characterization of Human PDE8B, a Novel Thyroid-Specific Isozyme of 3',5'-Cyclic Nucleotide Phosphodiesterase. Biochemical and Biophysical Research Communications **250:**751-756.

77. **Heasley, L. E., J. Azari, and L. L. Brunton.** 1984. Export of Cyclic AMP from Avian Red Cells: Independence from Major Membrane Transporters and Specific Inhibition by Prostaglandin A_1. Molecular Pharmacology **27:**60-66.

78. **Heasley, L. E., and L. L. Brunton.** 1985. Prostaglandin A_1 Metabolism and Inhibition of Cyclic AMP Extrusion by Avian Erythrocytes. The Journal of Biological Chemistry **260:**11514-11519.

79. **Heasley, L. E., M. J. Watson, and L. L. Brunton.** 1985. Appendix: Putative inhibitor of cyclic AMP efflux: chromatography, amino acid composition,

and identification as a prostaglandin A_1-glutathione adduct. The Journal of Biological Chemistry **260**:11520-11523.

80. **Hempel, C. M., V. P. Adams, S. R. Tsien, and A. I. Selverston.** 1996. Spatio-temporal dynamics of cyclic AMP signals in an intact neural circuit. Nature **384**:166-169.

81. **Hoffmann, R., G. S. Baillie, S. J. MacKenzie, S. J. Yarwood, and M. D. Houslay.** 1999. The MAP kinase ERK2 inhibits the cyclic AMP-specific phosphodiesterase HSPDE4D3 by phosphorylating it at Ser579. The EMBO Journal **18**:893-903.

82. **Hoffmann, R., I. R. Wilkinson, F. J. McCallum, P. Engels, and M. D. Houslay.** 1998. cAMP-specific phosphodiesterase HSPDE4D3 mutants which mimic activation and changes in rolipram inhibition triggered by protein kinase A phosphorylation of Ser-54: generation of a molecular model. Biochem. J. **333**:139-149.

83. **Horton, Y. M., M. Sullivan, and M. D. Houslay.** 1995. Molecular cloning of a novel splice variant of human type IVA (PDE-IVA) cyclic AMP phosphodiesterase and localization of the gene to the p13.2-q12 region of human chromosome 19 [corrected] [published erratum appears in Biochem J 1995 Dec 15;312(Pt 3):991]. Biochemical Journal **308**:683-91.

84. **Houslay, M. D.** 1996. The N-terminal alternately spliced regions of PDE4A cAMP-specific phosphodiesterases determine intracellular targeting and regulation of catalytic activity. Biochemical Society Transactions **24**:980-6.

85. **Houslay, M. D., and G. Milligan.** 1997. Tailoring cAMP-signalling responses through isoform multiplicity. Trends in Biochemical Sciences **22**:217-24.

86. **Houslay, M. D., G. Scotland, S. Erdogan, E. Huston, S. Mackenzie, J. F. McCallum, I. McPhee, L. Pooley, G. Rena, A. Ross, M. Beard, A. Peder,**

F. Begg, I. Wilkinson, S. Yarwood, C. Ackerman, E. S. Houslay, R. Hoffman, P. Engels, M. Sullivan, and G. Bolger. 1997. Intracellular targeting, interaction with Src homology 3 (SH3) domains and rolipram-detected conformational switches in cAMP-specific PDE4A phosphodiesterase. Biochemical Society Transactions **25:**374-81.

87. **Houslay, M. D., M. Sullivan, and G. B. Bolger.** 1998. The multienzyme PDE4 cyclic adenosine monophosphate-specific phosphodiesterase family: intracellular targeting, regulation, and selective inhibition by compounds exerting anti-inflammatory and antidepressant actions. Advances in Pharmacology **44:**225-342.

88. **Howe, L. R., and A. Weiss.** 1995. Multiple kinases mediate T-cell-receptor signaling. T.I.B.S. **20:**59-64.

89. **Huang, L. J. S., K. Durick, J. A. Weiner, J. Chun, and S. S. Taylor.** 1997. D-AKAP2, a novel protein kinase A anchoring protein with a putative RGS domain. Proceedings of the National Academy of Sciences of the United States of America **94:**11184-11189.

90. **Huang, L. J. S., K. Durick, J. A. Weiner, J. Chun, and S. S. Taylor.** 1997. Identification of a novel protein kinase A anchoring protein that binds both type I and type II regulatory subunits. Journal of Biological Chemistry **272:**8057-8064.

91. **Hurley, J. H.** 1999. Structure, Mechanism, and Regulation of Mammalian Adenylyl Cyclase. Journal of Biological Chemistry **274:**7599-7602.

92. **Huston, E., S. Lumb, A. Russell, C. Catterall, A. H. Ross, M. R. Steele, G. B. Bolger, M. J. Perry, R. J. Owens, and M. D. Houslay.** 1997. Molecular cloning and transient expression in COS7 cells of a novel human PDE4B cAMP-specific phosphodiesterase, HSPDE4B3. Biochemical Journal **328:**549-58.

93. **Huston, E., L. Pooley, P. Julien, G. Scotland, I. McPhee, M. Sullivan, G. Bolger, and M. D. Houslay.** 1996. The human cyclic AMP-specific phosphodiesterase PDE-46 (HSPDE4A4B) expressed in transfected COS7 cells occurs as both particulate and cytosolic species that exhibit distinct kinetics of inhibition by the antidepressant rolipram. Journal of Biological Chemistry **271:**31334-44.

94. **Imai, A., T. Nashida, and H. Shimomura.** 1996. Expression of mRNA encoding cAMP-specific phosphodiesterase isoforms in rat parotid glands. Biochemistry & Molecular Biology International **40:**1175-81.

95. **Jacobitz, S., M. M. McLaughlin, G. P. Livi, M. Burman, and T. J. Torphy.** 1996. Mapping the functional domains of human recombinant phosphodiesterase 4A: structural requirements for catalytic activity and rolipram binding. Molecular Pharmacology **50:**891-9.

96. **Janeway Jr, C. A., and K. Bottomly.** 1994. Signals and signs for lymphocyte responses. Cell **76:**275-285.

97. **Ji, T. H., M. Grossmann, and I. Ji.** 1998. G protein-coupled receptors I. Diversity of receptor-ligand interactions. Journal of Biological Chemistry **273:**17299-17302.

98. **Jin, S. C., T. Bushnik, L. Lan, and M. Conti.** 1998. Subcellular Localization of Rolipram-sensitive, cAMP-specific Phosphodiesterases. Differential targeting and activation of the splicing variants derived from the pde4d gene. J Biol Chem **273:**19672-8.

99. **Jin, S. L., J. V. Swinnen, and M. Conti.** 1992. Characterization of the structure of a low Km, rolipram-sensitive cAMP phosphodiesterase. Mapping of the catalytic domain. Journal of Biological Chemistry **267:**18929-39.

100. **Johnson, B. D., T. Scheuer, and W. A. Catterall.** 1994. Voltage-dependent potentiation of L-type Ca2+ channels in skeletal muscle cells requires

anchored cAMP-dependent protein kinase. Proceedings of the National Academy of Sciences of the United States of America **91:**11492-11496.

101. **Juilfs, D. M., H. J. Fulle, A. Z. Zhao, M. D. Houslay, D. L. Garbers, and J. A. Beavo.** 1997. A subset of olfactory neurons that selectively express cGMP-stimulated phosphodiesterase (PDE2) and guanylyl cyclase-D define a unique olfactory signal transduction pathway. Proceedings of the National Academy of Sciences of the United States of America **94:**3388-95.

102. **Jurevicius, J., and R. Fischmeister.** 1996. cAMP compartmentation is responsibel for a local activation of cardiac Ca^{2+} channels by β-adrenergic agonists. Proc. Natl. Acad. Sci. USA **93:**295-299.

103. **Kasuya, J., H. Goko, and Y. Fujita-Yamaguchi.** 1995. Multiple transcripts for the human cardiac form of the cGMP-inhibited cAMP phosphodiesterase. Journal of Biological Chemistry **270:**14305-14312.

104. **Kelly, J. J., P. J. Barnes, and M. A. Giembycz.** 1996. Phosphodiesterase 4 in macrophages: Relationship between cAMP accumulation, suppression of cAMP hydrolysis and inhibition of [3H]R-(-)-rolipram binding by selective inhibitors. Biochemical Journal **318:**425-436.

105. **Kilgour, E., N. G. Anderson, and M. D. Houslay.** 1989. Activation and phosphorylation of the 'dense-vesicle' high-affinity cyclic AMP phosphodiesterase by cyclic AMP-dependent protein kinase. Biochemical Journal **260:**27-36.

106. **Klauck, T. M., M. C. Faux, K. Labudda, L. K. Langeberg, S. Jaken, and J. D. Scott.** 1996. Coordination of three signaling enzymes by AKAP79, a mammalian scaffold protein. Science **271:**1589-1592.

107. **Kostic, M. M., S. Erdogan, G. Rena, G. Borchert, B. Hoch, S. Bartel, G. Scotland, E. Huston, M. D. Houslay, and E. G. Krause.** 1997. Altered expression of PDE1 and PDE4 cyclic nucleotide phosphodiesterase isoforms

in 7-oxo-prostacyclin-preconditioned rat heart. Journal of Molecular & Cellular Cardiology **29:**3135-46.

108. **Kovala, T., B. D. Sanwal, and E. H. Ball.** 1997. Recombinant expression of a type IV, cAMP-specific phosphodiesterase: characterization and structure-function studies of deletion mutants. Biochemistry **36:**2968-76.

109. **Krupinski, J., F. Coussen, H. A. Bakalyar, W. J. Tang, P. G. Feinstein, K. Orth, C. Slaughter, R. R. Reed, and A. G. Gilman.** 1989. Adenylyl cyclase amino acid sequence: Possible channel- or transporter-like structure. Science **244:**1558-1564.

110. **Kurahashi, T., and A. Menini.** 1997. Mechanism of odorant adaptation in the olfactory receptor cell. Nature **385:**725-729.

111. **Kurtz, A., K. H. Gotz, M. Hamann, and C. Wagner.** 1998. Stimulation of renin secretion by nitric oxide is mediated by phosphodiesterase 3. Proc. Natl. Acad. Sci. USA **95:**4743-4747.

112. **Lavan, B. E., T. Lakey, and M. D. Houslay.** 1989. Resolution of soluble cyclic nucleotide phosphodiesterase isoenzymes, from liver and hepatocytes, identifies a novel IBMX-insensitive form. Biochemical Pharmacology **38:**4123-4136.

113. **Lefkowitz, R. J.** 1998. G Protein-coupled Receptors: III. New roles for receptor kinases and β-arrestins in receptor signalling and desensitization. J. Biol. Chem. **273:**18677-18680.

114. **Lenhard, J. M., D. B. Kassel, W. J. Rocque, L. Hamacher, W. D. Holmes, I. Patel, C. Hoffman, and M. Luther.** 1996. Phosphorylation of a cAMP-specific phosphodiesterase (HSPDE4B2B) by mitogen-activated protein kinase. Biochem. J. **316:**751-758.

115. **Leroy, M. J., E. Degerman, M. Taira, T. Murata, W. Lu Hua, M. A.**

Movsesian, E. Meacci, and V. C. Manganiello. 1996. Characterization of two recombinant PDE3 (cGMP-inhibited cyclic nucleotide phosphodiesterase) isoforms, RcGIP1 and HcGIP2, expressed in NIH 3006 murine fibroblasts and Sf9 insect cells. Biochemistry **35:**10194-10202.

116. **Li, L., Y. Cassian, and J. A. Beavo.** 1999. CD3 and CD28-Dependent Induction of PDE7 Required for T Cell Activation. Science **283:**848-851.

117. **Li, N., S. K. Florio, M. J. Pettenati, R. Nagesh, J. A. Beavo, and W. Baehr.** 1998. Characterization of Human and Mouse Rod cGMP Phosphodiesterase d Subunit (PDE6D) and Chromosomal Localization of the Human Gene. Genomics **49:**76-82.

118. **Li, T., K. Volpp, and M. L. Applebury.** 1990. Bovine cone photoreceptor cGMP phosphodiesterase structure deduced from a cDNA clone. Proceedings of the National Academy of Sciences of the United States of America **87:**293-297.

119. **Li, X., J. M. Lopez-Guisa, N. Ninan, E. J. Weiner, F. J. Rauscher, 3rd, and R. Marmorstein.** 1997. Overexpression, purification, characterization, and crystallization of the BTB/POZ domain from the PLZF oncoprotein. Journal of Biological Chemistry **272:**27324-9.

120. **Liliental, J., and D. D. Chang.** 1998. Rack1, a receptor for activated protein kinase C, interacts with integrin beta subunit. Journal of Biological Chemistry **273:**2379-83.

121. **Liliental, J., and D. D. Chang.** 1998. Rack1, a Receptor for Activated Protein Kinase C, Interacts with Integrin ß Subunit. The Journal of Biological Chemistry **273:**2379-2383.

122. **Lim, J., G. Pahlke, and M. Conti.** 1999. Activation of the cAMP-specific Phosphodiesterase PDE4D3 by Phosphorylation. The Journal of Biological

Chemistry **274:**19677-19685.

123. **Lipkin, V. M., N. V. Khramtsov, I. A. Vasilevskaya, N. V. Atabekova, K. G. Muradov, V. V. Gubanov, T. Li, J. P. Johnston, K. J. Volpp, and M. L. Applebury.** 1990. beta-Subunit of bovine rod photoreceptor cGMP phosphodiesterase. Comparison with the phosphodiesterase family. Journal of Biological Chemistry **265:**12955-12959.

124. **Liu, H., and D. H. Maurice.** 1999. Phosphorylation-mediated Activation and Translocation of the Cyclic AMP-specific Phosphodiesterase PDE4D3 by Cyclic AMP-dependent Protein Kinase and Mitogen-activated Protein Kinases. The Journal of Biological Chemistry **274:**10557-10565.

125. **Livi, G. P., P. Kmetz, M. M. McHale, L. B. Cieslinski, G. M. Sathe, D. P. Taylor, R. L. Davis, T. J. Torphy, and J. M. Balcarek.** 1990. Cloning and expression of cDNA for a human low-Km, rolipram-sensitive cyclic AMP phosphodiesterase. Molecular & Cellular Biology **10:**2678-86.

126. **Lobban, M., Y. Shakur, J. Beattie, and M. D. Houslay.** 1994. Identification of two splice variant forms of type-IVB cyclic AMP phosphodiesterase, DPD (rPDE-IVB1) and PDE-4 (rPDE-IVB2) in brain: selective localization in membrane and cytosolic compartments and differential expression in various brain regions. Biochemical Journal **304:**399-406.

127. **Lopez-Aparicio, P., P. Belfrage, V. C. Manganiello, T. Kono, and E. Degerman.** 1993. Stimulation by insulin of a serine kinase in human platelets that phosphorylates and activates the cGMP-inhibited cAMP phosphodiesterase. Biochemical & Biophysical Research Communications **193:**1137-1144.

128. **Loughney, K., T. J. Martins, E. A. S. Harris, K. Sadhu, J. B. Hicks, W. K. Sonnenburg, J. A. Beavo, and K. Ferguson.** 1996. Isolation and characterization of cDNAs corresponding to two human calcium, calmodulin-

regulated, 3',5'-cyclic nucleotide phosphodiesterases. Journal of Biological Chemistry **271:**796-806.

129. **Luo, Z., B. Shafit-Zagardo, and J. Erlichman.** 1990. Identification of the MAP2- and P75-binding domain in the regulatory subunit (RIIbeta) of type II cAMP-dependent protein kinase. Cloning and expression of the cDNA for bovine brain RIIbe. Journal of Biological Chemistry **265:**21804-21810.

130. **Luttrell, L. M., S. S. G. Ferguson, Y. Daaka, W. E. Miller, S. Maudsley, G. J. Della Rocca, F. T. Lin, H. Kawakatsu, K. Owada, D. K. Luttrell, M. G. Caron, and R. J. Lefkowitz.** 1999. β-Arrestin-Depenenet Formation of β2 Adrenergic Receptor-Src Protein Kinase Complexes. Science **283:**655-661.

131. **Macias, M. J., M. Hyvonen, E. Baraldi, J. Schultz, M. Sudol, M. Saraste, and H. Oschkinat.** 1996. Structure of the WW domain of a kinase-associated protein complexed with a proline-rich peptide. Nature **382:**646-9.

132. **MacKenzie, S. J., S. J. Yarwood, A. H. Peden, G. B. Bolger, R. G. Vernon, and M. D. Houslay.** 1998. Stimulation of p70S6 kinase via a growth hormone-controlled phosphatidylinositol 3-kinase pathway leads to the activation of a PDE4A cyclic AMP-specific phosphodiesterase in 3T3-F442A preadipocytes. Proc Natl Acad Sci U S A **95:**3549-54.

133. **Maina, F., F. Casagranda, E. Audero, A. Simcone, P. M. Comoglio, R. Klein, and C. Ponzetto.** 1996. Uncoupling of Grb2 from the Met receptor in vivo reveals complex roles in muscle development. Cell **87:**531-42.

134. **Manganiello, V. C., M. Taira, E. Degerman, and P. Belfrage.** 1995. Type III cGMP-inhibited cyclic nucleotide phosphodiesterases (PDE3 gene family). Cellular Signalling **7:**445-455.

135. **Marchmont, R. J., S. R. Ayad, and M. D. Houslay.** 1981. Purification and properties of the insulin-stimulated cyclic AMP phosphodiesterase from rat

liver plasma membranes. Biochemical Journal **195:**645-52.

136. **Marchmont, R. J., and M. D. Houslay.** 1981. Characterization of the phosphorylated form of the insulin-stimulated cyclic AMP phosphodiesterase from rat liver plasma membranes. Biochemical Journal **195:**653-60.

137. **Mayer, B. J.** 1997. Clamping down on Src activity. Current Biology 7:R295-R298.

138. **McAllister-Lucas, L. M., W. K. Sonnenburg, A. Kadlecek, D. Seger, T. Hai Le, J. L. Colbran, M. K. Thomas, K. A. Walsh, S. H. Francis, J. D. Corbin, and J. A. Beavo.** 1993. The structure of a bovine lung cGMP-binding, cGMP-specific phosphodiesterase deduced from a cDNA clone. Journal of Biological Chemistry **268:**22863-22873.

139. **McLaughlin, M. M., L. B. Cieslinski, M. Burman, T. J. Torphy, and G. P. Livi.** 1993. A low-K(m), rolipram-sensitive, cAMP-specific phosphodiesterase from human brain. Cloning and expression of cDNA, biochemical characterization of recombinant protein, and tissue distribution of mRNA. Journal of Biological Chemistry **268:**6470-6476.

140. **McPhee, I., L. Pooley, M. Lobban, G. Bolger, and M. D. Houslay.** 1995. Identification, characterization and regional distribution in brain of RPDE-6 (RNPDE4A5), a novel splice variant of the PDE4A cyclic AMP phosphodiesterase family. Biochemical Journal **310:**965-74.

141. **McPhee, I., S. J. Yarwood, S. Scotland, E. Huston, M. B. Beard, A. H. Ross, E. S. Houslay, and M. D. Houslay.** 1999. Association with the SRC Family Tyrosyl Kinase LYN Triggers a Conformational Change in the Catalytic Region of Human cAMP-specific Phosphodiesterase HSPDE4A4B. Journal of Biological Chemistry **274:**11796-11810.

142. **Michaeli, T., T. J. Bloom, T. Martins, K. Loughney, K. Ferguson, M. Riggs, L. Rodgers, J. A. Beavo, and M. Wigler.** 1993. Isolation and

characterization of a previously undetected human cAMP phosphodiesterase by complementation of cAMP phosphodiesterase-deficient Saccharomyces cerevisiae. J. Biol. Chem. **268:**12925-12932.

143. **Miki, T., M. Taira, S. Hockman, F. Shimada, J. Lieman, M. Napolitano, D. Ward, M. Taira, H. Makino, and V. C. Manganiello.** 1996. Characterization of the cDNA and gene encoding human PDE3B, the cGIP1 isoform of the human cyclic GMP-inhibited cyclic nucleotide phosphodiesterase family. Genomics **36:**476-485.

144. **Miller, S.** 1989. Experimental Design and Statistics, Second ed. Routledge, London and New York.

145. **Mochly-Rosen, D., K. Hanita, and J. Lopez.** 1991. Identification of intracellular receptor proteins for activated protein kinase C. Proc. Natl. Acad. Sci. USA **88:**3997-4000.

146. **Monaco, L., E. Vicini, and M. Conti.** 1994. Structure of two rat genes coding for closely related rolipram-sensitive cAMP phosphodiesterases. Multiple mRNA variants originate from alternative splicing and multiple start sites. Journal of Biological Chemistry **269:**347-57.

147. **Moore, J. B., and D. E. Schroedter.** 1982. Purification and Characrerization of Human Lung Calmodulin-independent Cyclic AMP Phosphodiesterase. Archives of Biochemistry and Biophysics **213:**276-287.

148. **Morton, C. J., D. J. R. Pugh, E. L. J. Brown, J. D. Kahmann, D. A. C. Renzoni, and I. D. Campbell.** 1996. Solution structure and peptide binding of the SH3 domain from human Fyn. Structure **4:**705-714.

149. **Musacchio, A., M. Noble, R. Pauptit, R. Wierenga, and M. Saraste.** 1992. Crystal structure of a Src-homology 3 (SH3) domain. Nature **359:**851-855.

150. **Mustelin, T., and P. Burn.** 1993. Regulation of src family tyrosine kinases

in lymphocytes. T.B.B.S. **18:**215-220.

151. **Narindrasorasak, S., L. U. Tan, P. K. Seth, and B. D. Sanwal.** 1982. Regulation of Cyclic Adenosine 3':5'-Monophosphate Phosphodiesterase. J. Biol. Chem. **257:**4618-4626.

152. **Naro, F., R. Zhang, and M. Conti.** 1996. Developmental regulation of unique adenosine 3',5'-monophosphate-specific phosphodiesterase variants during rat spermatogenesis. Endocrinology **137:**2464-2472.

153. **Nauert, J. B., T. M. Klauck, L. K. Langeberg, and J. D. Scott.** 1997. Gravin, an autoantigen recognized by serum from myasthenia gravis patients, is a kinase scaffold protein. Current Biology **7:**52-62.

154. **Neame, K. D., and T. G. Richards.** Kinetic theory of carrier transport, p. 18-23, Elementary Kinetics of Membrane Carrier Transport. Blackwell Scientific Publications.

155. **Neer, E. J.** 1995. Heterotrimeric G proteins: Organizers of transmembrane signals. Cell **80:**249-257.

156. **Neer, E. J., C. J. Schmidt, R. Nambudripad, and T. F. Smith.** 1994. The ancient regulatory-protein family of WD-repeat proteins [published erratum appears in Nature 1994 Oct 27;371(6500):812]. Nature **371:**297-300.

157. **Nemoz, G., M. Moueqqit, A. Prigent, and H. Pacheco.** 1989. Isolation of similar rolipram-inhibitale cyclic-AMP-specific phosphodiesterases from rat brain and heart. Eur. J. Biochem. **184:**511-520.

158. **Nemoz, G., A. F. Prigent, M. Moueqqit, S. Fougier, O. Mascovschi, and H. Pacheco.** 1985. Selective inhibition of one of the cyclic AMP phosphodiesterases from rat brains by the neurotropic compound rolipram. Biochemical Pharmacology **34:**2997-3000.

159. **Nemoz, G., R. Zhang, C. Sette, and M. Conti.** 1996. Identification of cyclic AMP-phosphodiesterase variants from the PDE4D gene expressed in human peripheral mononuclear cells. FEBS Letters **384**:97-102.

160. **Obernolte, R., S. Bhakta, R. Alvarez, C. Bach, P. Zuppan, M. Mulkins, M. Jarnagin, and E. R. Shelton.** 1993. The cDNA of a human lymphocyte cyclic-AMP phosphodiesterase (PDEIV) reveals a multigene family. Gene **129**:239-247.

161. **O'Connell, J. C.** 1996. Ph.D. University of Glasgow, Glasgow.

162. **O'Connell, J. C., J. F. McCallum, I. McPhee, J. Wakefield, E. S. Houslay, W. Wishart, G. Bolger, M. Frame, and M. D. Houslay.** 1996. The SH3 domain of Src tyrosyl protein kinase interacts with the N-terminal splice region of the PDE4A cAMP-specific phosphodiesterase RPDE-6 (RNPDE4A5). Biochemical Journal **318**:255-61.

163. **O'Dowd, B. F., M. Huatowich, M. G. Caron, R. J. Lefkowitz, and M. Bouvier.** 1989. Palmitoylation of the human beta2-adrenergic receptor. Mutation of Cys341 in the carboxyl tail leads to an uncoupled nonpalmitoylated form of the receptor. Journal of Biological Chemistry **264**:7564-7569.

164. **Onali, P., S. J. Strada, L. Chang, P. M. Epstein, E. M. Hersh, and W. J. Thompson.** 1985. Purification and Characterization of High-Affinity Cyclic Adenosine 5'-Monophosphate Phosphodiesterases from Human Acute Myelogenous Leukemic Cells. Cancer Research **45**:1384-1391.

165. **Owens, R. J., S. Lumb, K. Rees-Milton, A. Russell, D. Baldock, V. Lang, T. Crabbe, M. Ballesteros, and M. J. Perry.** 1997. Molecular cloning and expression of a human phosphodiesterase 4C. Cell Signal **9**:575-85.

166. **Parker, R. E.** 1975. Introductory Statistics for Biology, 1 ed, vol. 43. The

Camelot Press Ltd, Southampton.

167. **Pawson, T.** 1995. Protein modules and signalling networks. Nature **373:**573-580.

168. **Pawson, T., and J. D. Scott.** 1997. Signalling Through Scaffold, Anchoring, and Adaptor Proteins. Science **278:**2075-2080.

169. **Percival, M. D., B. Yeh, and J. Falgueyret.** 1997. Zinc Dependent Activation of cAMP-Specific Phosphodiesterase (PDE4A). Biochemical and Biophysical Research Communications **241:**175-180.

170. **Piper, R. C., D. E. James, J. W. Slot, C. Puri, and J. C. Lawrence.** 1993. GLUT4 phosphorylation and inhibition of glucose transport by dibutyryl cAMP. J. Biol. Chem. **268:**16557-16563.

171. **Pooley, L., Y. Shakur, G. Rena, and M. D. Houslay.** 1997. Intracellular localization of the PDE4A cAMP-specific phosphodiesterase splice variant RD1 (RNPDE4A1A) in stably transfected human thyroid carcinoma FTC cell lines. Biochemical Journal **321:**177-85.

172. **Pyne, N. J., N. Anderson, B. E. Lavan, G. Milligan, H. G. Nimmo, and M. D. Houslay.** 1987. Specific antibodies and the selective inhibitor ICI 118233 demonstrate that the hormonally stimulated 'dense-vesicle' and peripheral-plasma-membrane cyclic AMP phosphodiesterases display distinct tissue distributions in the rat. Biochemical Journal **248:**897-901.

173. **Pyne, N. J., M. E. Cooper, and M. D. Houslay.** 1987. The insulin- and glucagon-stimulated 'dense-vesicle' high-affinity cyclic AMP phosphodiesterase from rat liver. Purification, characterization and inhibitor sensitivity. Biochemical Journal **242:**33-42.

174. **Rahn, T., L. Ronnstrand, M. J. Leroy, C. Wernstedt, H. Tornqvist, V. C. Manganiello, P. Belfrage, and E. Degerman.** 1996. Identification of the site

in the cGMP-inhibited phosphodiesterase phosphorylated in adipocytes in response to insulin and isoproterenol. Journal of Biological Chemistry **271:**11575-11580.

175. **Rascon, A., E. Degerman, M. Taira, E. Meacci, C. J. Smith, V. Manganiello, P. Belfrage, and H. Tornqvis.** 1994. Identification of the phosphorylation site in vitro for cAMP-dependent protein kinase on the rat adipocyte cGMP-inhibited cAMP phosphodiesterase. Journal of Biological Chemistry **269:**11962-11966.

176. **Rickles, R. J., M. C. Botfield, Z. Weng, J. A. Taylor, O. M. Green, J. S. Brugge, and M. J. Zoller.** 1994. Identification of Src, Fyn, Lyn, PI3K and Abl SH3 domain ligands using phage display libraries. The EMBO Journal **13:**5598-5604.

177. **RivetBastide, M., G. Vandecasteele, S. Hatem, I. Verde, A. Benardeau, J. J. Mercadier, and R. Fischmeister.** 1997. cGMP-stimulated cyclic nucleotide phosphodiesterase regulates the basal calcium current in human atrial myocytes. JOURNAL OF CLINICAL INVESTIGATION **99:**2710-2718.

178. **Rocque, W. J., W. D. Holmes, I. R. Patel, R. W. Dougherty, O. Ittoop, L. Overton, C. R. Hoffamn, G. B. Wisely, D. H. Willard, and M. A. Luther.** 1997. Detailed Characterization of a purified Type 4 Phosphodiesterase, HSPDE4B2B: Differentiation of High- and Low-Affinity (R)-Rolipram Binding. Protein Expression and Purification **9:**191-202.

179. **Rocque, W. J., G. Tian, J. S. Wiseman, W. D. Holmes, I. Zajac-Thompson, D. H. Willard, I. R. Patel, G. B. Wisely, W. C. Clay, S. H. Kadwell, C. R. Hoffamn, and M. A. Luther.** 1997. Human Recombinant Phosphodiesterase 4B2B Binds (R)-Rolipram at a Single Site with Two Affinities. Biochemistry **36:**14250-14261.

180. **Ron, D., C. Chen, J. Caldwell, L. Jamieson, E. Orr, and D. Mochly-**

Rosen. 1994. Cloning of an intracellular receptor for protein kinase C: A homologue of the ß subunit of G proteins. Proc. Natl. Acad. Sci. USA **91:**839-843.

181. **Rooij, J., F. J. T. Zwartkruis, M. H. G. Verheijen, R. H. Cool, S. M. B. Nijman, A. Wittinghofer, and J. L. Bos.** 1998. Epac is a Rap1 guanine-nucleotide-exchange factor directly activated by cyclic AMP. Nature **396:**474-477.

182. **Rosman, G. J., T. J. Martins, W. K. Sonnenburg, J. A. Beavo, K. Ferguson, and K. Loughney.** 1997. Isolation and characterization of human cDNAs encoding a cGMP-stimulated 3',5'-cyclic nucleotide phosphodiesterase. Gene **191:**89-95.

183. **Rozakis-Adcock, M., R. Fernley, J. Wade, T. Pawson, and D. Bowtell.** 1993. The SH2 and SH3 domains of mammalian Grb2 couple the EGF receptor to the Ras activator mSos1 [see comments]. Nature **363:**83-5.

184. **Rubin, C. S.** 1994. A kinase anchor proteins and the intracellular targeting of signals carried by cyclic AMP. Biochimica et Biophysica Acta - Molecular Cell Research **1224:**467-479.

185. **Sabatini, B. L., and W. G. Regehr.** 1995. Detecting changes in calcium influx which contribute to synaptic modulation in mammalian brain slice. Neuropharmacology **34:**1453-1467.

186. **Salanova, M., S. C. Jin, and M. Conti.** 1998. Heterologous expression and purification of recombinant rolipram-sensitive cyclic AMP-specific phosphodiesterases. Methods **14:**55-64.

187. **Saldou, N., R. Obernolte, A. Huber, P. A. Baecker, R. A. Wilhelm, R. Alvarez, B. Li, L. Xia, O. Callan, C. Su, K. Jarnagin, and E. R. Shelton.** 1998. Comparison of Recombinant Human PDE4 Isoforms: Interaction with

Substrate and Inhibitors. Cellular Signalling **10:**427-440.

188. **Sambrook, J., E. F. Fritsch, and T. Maniatis.** 1989. Molecular Cloning a Laboratory Manual, Second Edition ed, vol. 1. Cold Springs Harbor Laboratory Press, Cold Springs Harbor.

189. **Satoh, A., H. Nakanishi, H. Obaishi, M. Wada, K. Takahashi, K. Satoh, K. Hirao, H. Nishioka, Y. Hata, A. Mizoguchi, and Y. Takai.** 1998. Neurabin-II/spinophilin. An actin filament-binding protein with one pdz domain localized at cadherin-based cell-cell adhesion sites. Journal of Biological Chemistry **273:**3470-5.

190. **Schonthal, A., and J. R. Feramisco.** 1993. Inhibition of histone H1 kinase expression, retinoblastoma protein phosphorylation, and cell proliferation by the phosphatase inhibitor okadaic acid. Oncogene **8:**433-441.

191. **Schulman, H.** 1991. Serine/threonine kinases in the nervous system. Current Opinion in Neurobiology **1:**43-52.

192. **Schultz, J. E., S. Klumpp, R. Benz, W. J. C. Schurhoff-Goeters, and A. Schmid.** 1992. Regulation of adenylyl cyclase from Paramecium by an intrinsic potassium conductance. Science **255:**600-603.

193. **Scotland, G., M. Beard, S. Erdogan, E. Huston, F. McCallum, S. J. MacKenzie, A. H. Peden, L. Pooley, N. G. Rena, A. H. Ross, S. J. Yarwood, and M. D. Houslay.** 1998. Intracellular compartmentalization of PDE4 cyclic AMP-specific phosphodiesterases. Methods **14:**65-79.

194. **Scotland, G., and M. D. Houslay.** 1995. Chimeric constructs show that the unique N-terminal domain of the cyclic AMP phosphodiesterase RD1 (RNPDE4A1A; rPDE-IVA1) can confer membrane association upon the normally cytosolic protein chloramphenicol acetyltransferase. Biochemical Journal **308:**673-81.

195. **Seifert, R., U. Gether, K. Wenzel-Seifert, and B. K. Kobilka.** 1999. Effects of Guanine, Inosine, and Xanthine Nucleotides on β_2-Adrenergic Receptor/G_s Interactions: Evidence for Multiple Receptor Conformations. Molecular Pharmacology :348-358.

196. **Selbie, L. A., and S. J. Hill.** 1998. G protein-coupled-receptor cross-talk: The fine-tuning of multiple receptor-signalling pathways. Trends in Pharmacological Sciences **19:**87-93.

197. **Sette, C., and M. Conti.** 1996. Phosphorylation and activation of a cAMP-specific phosphodiesterase by the cAMP-dependent protein kinase. Involvement of serine 54 in the enzyme activation. Journal of Biological Chemistry **271:**16526-34.

198. **Sette, C., S. Iona, and M. Conti.** 1994. The short-term activation of a rolipram-sensitive, cAMP-specific phosphodiesterase by thyroid-stimulating hormone in thyroid FRTL-5 cells is mediated by a cAMP-dependent phosphorylation. Journal of Biological Chemistry **269:**9245-52.

199. **Sette, C., E. Vicini, and M. Conti.** 1994. The ratPDE3/IVd phosphodiesterase gene codes for multiple proteins differentially activated by cAMP-dependent protein kinase. Journal of Biological Chemistry **269:**18271-18274.

200. **Shakur, Y., J. G. Pryde, and M. D. Houslay.** 1993. Engineered deletion of the unique N-terminal domain of the cyclic AMP-specific phosphodiesterase RD1 prevents plasma membrane association and the attainment of enhanced thermostability without altering its sensitivity to inhibition by rolipram. Biochemical Journal **292:**677-86.

201. **Shakur, Y., M. Wilson, L. Pooley, M. Lobban, S. L. Griffiths, A. M. Campbell, J. Beattie, C. Daly, and M. D. Houslay.** 1995. Identification and characterization of the type-IVA cyclic AMP-specific phosphodiesterase RD1

as a membrane-bound protein expressed in cerebellum. Biochemical Journal **306:**801-9.

202. **Sharma, R. K.** 1991. Phosphorylation and characterization of bovine heart calmodulin-dependent phosphodiesterase. Biochemistry **30:**5963-5968.

203. **Shibata, H., and T. Kono.** 1990. Cell-free stimulation of the insulin-sensitive cAMP phosphodiesterase by the joint actions of ATP and the soluble fraction from insulin-treated rat liver. Biochemical & Biophysical Research Communications **170:**533-539.

204. **Shibata, H., and T. Kono.** 1990. Stimulation of the insulin-sensitive cAMP phosphodiesterase by an ATP-dependent soluble factor from insulin-treated rat adipocytes. Biochemical & Biophysical Research Communications **167:**614-620.

205. **Sibo, F., J. K. Chen, Y. Hongtao, J. A. Simon, and S. L. Schreiber.** 1994. Two Binding Orientations for Peptides to the Src SH3 Domain: Development of a General Model for SH3-Ligand Interactions. Science **266:**1241-1247.

206. **Sicheri, F., I. Moarefi, and J. Kuriyan.** 1997. Crystal structure of the Src family tyrosine kinase Hck. Nature **385:**602-609.

207. **Smith, K. J., G. Scotland, J. Beattie, I. P. Trayer, and M. D. Houslay.** 1996. Determination of the structure of the N-terminal splice region of the cyclic AMP-specific phosphodiesterase RD1 (RNPDE4A1) by 1H NMR and identification of the membrane association domain using chimeric constructs. Journal of Biological Chemistry **271:**16703-11.

208. **Soderling, S. H., S. J. Bayuga, and J. A. Beavo.** 1998. Cloning and characterization of a cAMP-specific cyclic nucleotide phosphodiesterase. Proc. Natl. Acad. Sci. USA **95:**8991-8996.

209. **Soderling, S. H., S. J. Bayuga, and J. A. Beavo.** 1998. Identification and

Characterization of a Novel Family of Cyclic Nucleotide Phosphodiesterases. J. Biol. Chem. **273:**15553-15558.

210. **Soderling, S. H., S. J. Bayuga, and J. A. Beavo.** 1999. Isolation and characterization of a dual-substrate phosphodiesterase gene family: PDE10A. Proc. Natl. Acad. Sci. USA **96:**7071-7076.

211. **Sondek, J., A. Bohm, D. G. Lambright, H. E. Hamm, and P. B. Sigler.** 1996. Crystal structure of a G-protein beta gamma dimer at 2.1A resolution [see comments] [corrected] [published erratum appears in Nature 1996 Feb 29;379(6568):847]. Nature **379:**369-74.

212. **Sonnenburg, W. K., P. J. Mullaney, and J. A. Beavo.** 1991. Molecular cloning of a cyclic GMP-stimulated cyclic nucleotide phosphodiesterase cDNA. Identification and distribution of isozyme variants. Journal of Biological Chemistry **266:**17655-17661.

213. **Sonnenburg, W. K., D. Seger, and J. A. Beavo.** 1993. Molecular cloning of a cDNA encoding the '61-kDa' calmodulin-stimulated cyclic nucleotide phosphodiesterase. Tissue-specific expression of structurally related isoforms. Journal of Biological Chemistry **268:**645-652.

214. **Sonnenburg, W. K., D. Seger, K. S. Kwak, J. Huang, H. Charbonneau, and J. A. Beavo.** 1995. Identification of inhibitory and calmodulin-binding domains of the PDE1A1 and PDE1A2 calmodulin-stimulated cyclic nucleotide phosphodiesterases. Journal of Biological Chemistry **270:**30989-31000.

215. **Souness, J. E., and S. Rao.** 1997. Proposal for pharmacologically distinct conformers of PDE4 cyclic AMP phosphodiesterases. Cellular Signalling **9:**227-236.

216. **Souness, J. E., and L. C. Scott.** 1993. Stereospecificity of rolipram actions on eosinophil cyclic AMP-specific phosphodiesterase. Biochemical Journal

291:389-395.

217. **Spence, S., G. Rena, M. Sullivan, S. Erdogan, and M. D. Houslay.** 1997. Receptor-mediated stimulation of lipid signalling pathways in CHO cells elicits the rapid transient induction of the PDE1B isoform of Ca2+/calmodulin-stimulated cAMP phosphodiesterase. Biochemical Journal **321:**157-63.

218. **Spence, S., G. Rena, G. Sweeney, and M. D. Houslay.** 1995. Induction of Ca2+/calmodulin-stimulated cyclic AMP phosphodiesterase (PDE1) activity in Chinese hamster ovary cells (CHO) by phorbol 12-myristate 13-acetate and by the selective overexpression of protein kinase C isoforms. Biochemical Journal **310:**975-82.

219. **Srivastava, R. K., Y. N. Lee, K. Noguchi, Y. G. Park, M. J. C. Ellis, J. Jeong, S. N. Kim, and Y. S. Cho-Chung.** 1998. The RIIβ regulatory subunit of protein kinase A binds to cAMP response element: An alternative cAMP signalling pathway. Proc. Natl. Acad. Sci. USA **95:**6687-6692.

220. **Stroop, S. D., H. Charbonneau, and J. A. Beavo.** 1989. Direct photolabeling of the cGMP-stimulated cyclic nucleotide phosphodiesterase. Journal of Biological Chemistry **264:**13718-13725.

221. **Stryer, L.** 1988. Biochemistry, Third Edition ed. W. H. Freeman and Company, New York.

222. **Sudol, M.** 1996. Structure and function of the WW domain. Progress in Biophysics & Molecular Biology **65:**113-32.

223. **Sudol, M., P. Bork, A. Einbond, K. Kastury, T. Druck, M. Negrini, K. Huebner, and D. Lehman.** 1995. Characterization of the Mammalian YAP (Yes-associated Protein) Gene and Its Role in Defining a Novel Protein Module, the WW Domain. The Journal of Biological Chemistry **270:**14733-

14741.

224. **Sullivan, M., M. Egerton, Y. Shakur, A. Marquardsen, and M. D. Houslay.** 1994. Molecular cloning and expression, in both COS-1 cells and S. cerevisiae, of a human cytosolic type-IVA, cyclic AMP specific phosphodiesterase (hPDE-IVA-h6.1). Cellular Signalling **6:**793-812.

225. **Sullivan, M., G. Rena, F. Begg, L. Gordon, A. S. Olsen, and M. D. Houslay.** 1998. Identification and characterization of the human homologue of the short PDE4A cAMP-specific phosphodiesterase RD1 (PDE4A1) by analysis of the human HSPDE4A gene locus located at chromosome 19p13.2. Biochem. J. **333:**693-703.

226. **Swinnen, J. V., D. R. Joseph, and M. Conti.** 1989. Molecular cloning of rat homologues of the Drosophila melanogaster dunce cAMP phosphodiesterase: Evidence for a family of genes. Proc. Natl. Acad. Sci. USA **86:**5325-5329.

227. **Swinnen, J. V., D. R. Joseph, and M. Conti.** 1989. The mRNA encoding a high-affinity cAMP phosphodiesterase is regulated by hormones and cAMP. Proc. Natl. Acad. Sci. USA **86:**8197-8201.

228. **Swinnen, J. V., K. E. Tsikalas, and M. Conti.** 1991. Properties and hormonal regulation of two structurally related cAMP phosphodiesterases from the rat Sertoli cell. Journal of Biological Chemistry **266:**18370-7.

229. **Tang, K. M., E. K. Jang, and R. J. Haslam.** 1997. Expression and mutagenesis of the catalytic domain of cGMP-inhibited phosphodiesterase (PDE3) cloned from human platelets. Biochemical Journal **323:**217-224.

230. **Tesmer, J. J. G., R. K. Sunahara, A. G. Gilman, and S. R. Sprang.** 1997. Crystal structure of the catalytic domains of adenylyl cyclase in a complex with G(salpha).GTPgammaSigma. Science **278:**1907-1916.

231. **Thomas, M. K., S. H. Francis, and J. D. Corbin.** 1990. Characterization of

a purified bovine lung cGMP-binding cGMP phosphodiesterase. Journal of Biological Chemistry **265:**14964-14970.

232. **Thompson, W. J., P. M. Epstein, and S. J. Strada.** 1979. Purification and Characterization of High-Affinity Cyclic Adenosine Monophosphate Phosphodiesterase from Dog Kidney. Biochemistry **18:**5228-5237.

233. **Torphy, T. J.** 1998. Phosphodiesterase isozymes: molecular targets for novel antiasthma agents. American Journal of Respiratory & Critical Care Medicine **157:**351-70.

234. **Torphy, T. J., J. M. Stadel, M. Burman, L. B. Cieslinski, M. M. McLaughlin, J. R. White, and G. P. Livi.** 1992. Coexpression of human cAMP-specific phosphodiesterase activity and high affinity rolipram binding in yeast. Journal of Biological Chemistry **267:**1798-804.

235. **Tsunoda, S., J. Sierralta, Y. Sun, R. Bodner, E. Suzuki, A. Becker, M. Socolich, and C. S. Zuker.** 1997. A multivalent PDZ-domain protein assembles signalling complexes in a G-protein-coupled cascade. Nature **388:**243-9.

236. **Turko, I. V., S. A. Ballard, S. H. Francis, and J. D. Corbin.** 1999. Inhibition of cyclic GMP-binding cyclic GMP-specific phosphodiesterase (type 5) by sildenafil and related compounds. Molecular Pharmacology **56:**124-130.

237. **Van Hoy, M., K. K. Leuther, T. Kodadek, and S. A. Johnston.** 1993. The acidic activation domains of the GCN4 and GAL4 proteins are not alpha helical but form beta she. Cell **72:**587-594.

238. **Vicini, E., and M. Conti.** 1997. Characterization of an intronic promoter of a cyclic adenosine 3',5'-monophosphate (cAMP)-specific phosphodiesterase gene that confers hormone and cAMP inducibility. Molecular Endocrinology

11:839-50.

239. **Waksman, G., D. Kominos, S. C. Robertson, N. Pant, D. Baltimore, R. B. Birge, D. Cowburn, H. Hanafusa, B. J. Mayer, and M. Overduin.** 1992. Crystal structure of the phosphotyrosine recognition domain SH2 of v-src complexed with tyrosine-phosphorylated peptides [see comments]. Nature **358:**646-53.

240. **Walsh, D. A., and S. M. Van Patten.** 1994. Multiple pathway signal transduction by the cAMP-dependent ptotein kinase. The FASEB Journal **8:**1227-1236.

241. **Wang, P., J. G. Myers, P. Wu, B. Cheewatrakoolpong, R. W. Egan, and M. M. Billah.** 1997. Expression, Purification, and Characterization of Human cAMP-Specific Phosphodiesterase (PDE4) Subtypes A, B, C, and D. Biochemical and Biophysical Research Communications **234:**320-324.

242. **Watson, S., and S. Arkinstall.** 1994. The G-protein Linked Receptor Facts Book, First ed. Academic Press Limited, London.

243. **Wess, J.** 1997. G-protein-coupled receptors: molecular mechanisms involved in receptor activation and selectivity of G-protein recognition. FASEB Journal **11:**346-354.

244. **Williams, J. C., A. Weijland, S. Gonfloni, A. Thompson, S. Courtneidge, G. Superti-Furga, and R. K. Wierenga.** 1997. The 2.35 crystal structure of the inactivated form of chicken Src: A dynamic molecule with multiple regulatory interactions. J. Mol. Biol. **274:**757-775.

245. **Wilson, M., M. Sullivan, N. Brown, and M. D. Houslay.** 1994. Purification, characterization and analysis of rolipram inhibition of a human type-IVA cyclic AMP-specific phosphodiesterase expressed in yeast. Biochemical Journal **304:**407-15.

246. **Woods, M., and M. D. Houslay.** 1991. Desensitization of atriopeptin stimulated accumulation and extrusion of cyclic GMP from a kidney epithelial cell line (MDCK). Biochemical Pharmacology **41**:385-94.

247. **Xu, W., S. C. Harrison, and M. J. Eck.** 1997. Three-dimensional structure of the tyrosine kinase c-Src. Nature **385**:595-602.

248. **Yan, C., A. Z. Zhao, J. K. Bentley, and J. A. Beavo.** 1996. The calmodulin-dependent phosphodiesterase gene PDE1C encodes several functionally different splice variants in a tissue-specific manner. Journal of Biological Chemistry **271**:25699-25706.

249. **Yan, C., A. Z. Zhao, J. K. Bentley, K. Loughney, K. Ferguson, and J. A. Beavo.** 1995. Molecular cloning and characterization of a calmodulin-dependent phosphodiesterase enriched in olfactory sensory neurons. Proceedings of the National Academy of Sciences of the United States of America **92**:9677-9681.

250. **Yan, S. R., L. Fumagalli, and G. Berton.** 1996. Activation of SRC family kinases in human neutrophils. Evidence that p58C-FGR and p53/56LYN redistributed to a Triton X-100-insoluble cytoskeletal fraction, also enriched in the caveolar protein caveolin, display an enhanced kinase activity. FEBS Letters **380**:198-203.

251. **Yanaka, N., J. Kotera, A. Ohtsuka, H. Akatsuka, Y. Imai, H. Michibata, K. Fujishige, E. Kawai, S. I. Takebayashi, K. Okumura, and K. Omori.** 1998. Expression, structure and chromosomal localization of the human cGMP-binding cGMP-specific phosphodiesterase PDE5A gene. European Journal of Biochemistry **255**:391-399.

252. **Yarwood, S. J., M. R. Steele, G. Scotland, M. D. Houslay, and G. B. Bolger.** 1999. The RACK1 signaling scaffold protein selectively interacts with the cAMP-specific phosphodiesterase PDE4D5 isoform. Journal of

Biological Chemistry **274:**14909-17.

253. **Zhang, G., Y. Liu, A. E. Ruoho, and J. H. Hurley.** 1997. Structure of the adenylyl cyclase catalytic core. Nature **386:**247-253.

254. **Zhang, Z., C. H. Lee, V. Mandiyan, J. P. Borg, B. Margolis, J. Schlessinger, and J. Kuriyan.** 1997. Sequence-specific recognition of the internalization motif of the Alzheimer's amyloid precursor protein by the X11 PTB domain. EMBO Journal **16:**6141-50.

255. **Zhao, A. J., H. Zhao, J. Teague, W. Fujimoto, and J. H. Beavo.** 1997. Attenuation of insulin secretion by insulin-like growth factor 1 is mediated through activation of phosphodieserase 3B. Proc. Natl. Acad. Sci. USA **94:**3223-3228.

256. **Zhong, H., H. S. Yang, H. Erdjument-Bromage, P. Tempst, and S. Ghosh.** 1997. The Transcriptional Activity of NF-κB is Regulated by the IκB-Associated PKAc Subunit through a Cyclic AMP-Independent Mechanism. Cell **89:**413-424.

257. **Zhou, M. M., B. Huang, E. T. Olejniczak, R. P. Meadows, S. B. Shuker, M. Miyazaki, T. Trub, S. E. Shoelson, and S. W. Fesik.** 1996. Structural basis for IL-4 receptor phosphopeptide recognition by the IRS-1 PTB domain. Nature Structural Biology **3:**388-93.